Expedition UT-GOM2-2
Methods

Terrebonne Basin (Walker Ridge Block 313)

WR313 H002 (API 608124014800) and WR313 H003 (API 608124014900)

30 July–28 September 2023

Expedition UT-GOM2-2 Scientists

Publisher's notes

This work was supported by the U.S. Department of Energy (DOE), National Energy Technology Laboratory (NETL), under Contract No. DE-FE00223919.

This work was the result of scientific collaboration between the following institutions The University of Texas at Austin (UT), DOE, NETL, the United States Geological Survey (USGS), the Bureau of Ocean Energy Management (BOEM), The Ohio State University, Columbia University, University of New Hampshire, Oregon State University, University of Washington, Tufts University, Colorado School of Mines, and Geotek Ltd.

Disclaimer

Authorship and citation

Peter B. Flemings, Carla Thomas, Stephen C. Phillips, Timothy S. Collett, Ann E. Cook, Evan Solomon, Frederick S. Colwell, Joel E. Johnson, David Awwiller, Irita Aylward, Athma R. Bhandari, Donald Brooks, Jessica Z. Buser-Young, Alejandro Cardona, Michael A. Casso, Rachel Coyte, Tom Darrah, Marcy Davis, Brandon Dugan, Dan Duncan, John T. Germaine, Melanie Holland, Jesse Houghton, Saffron Martin, N. Tanner Mills, Michael Mimitz, Daniel Minarich, Yuki Morono, Zachary Murphy, Joshua O'Connell, Ethan Petrou, Tom Pettigrew, John W. Pohlman, Alexey Portnov, Marcie Purkey Phillips, Thomas Redd, Derek E. Sawyer, Peter Schultheiss, Kelly Shannon, Camille Sullivan, Cathal Small, Kayla Tozier, Man-Yin Tsang, Camila Van Der Maal, William F. Waite, Taylor Walton, 2025, Expedition UT-GOM2-2 Methods. In Flemings et. al., Proceedings of the UT-GOM2-2 Deepwater Hydrate Coring Expedition, University of Texas Institute for Geophysics, **https://doi.org/10.5281/zenodo.13971228**.

Copies of these proceedings can be found on OSTI.gov (**Search for UT-GOM2-2 | OSTI.GOV**), Zenodo.org (**Search Terrebonne Basin Deepwater Hydrate Coring**), and the UT-GOM2-2 website (**UT-GOM2-2: Deepwater Hydrate Coring Expedition - UT Institute for Geophysics**).

Cover photos

Left: University of Texas at Austin (UT) team member Carla Thomas conducting split core sampling in Salt Lake City. Photo credit: William F. Waite

Right: The Helix *Q4000* deepwater well intervention vessel and the 290-foot *Harvey Hermes* supply boat, carrying UT-GOM2-2 labs, pipe, fluids, and equipment, during a rendezvous on site. Photo credit: Peter B. Flemings

Table of Contents

 https://doi.org/10.5281/zenodo.13971228

List of figures

List of tables

List of equations

List of acronyms

List of all acronyms, abbreviations, symbols, units, and sample codes used in these proceedings.

Term	Definition
2D	Two-dimensional
3D	Three-dimensional
4HE	4He residence times discrete sample
χ	Mass-normalized magnetic susceptibility
χ_{fd}	Frequency dependence of magnetic susceptibility
K	Effective Stress Ratio
κ	Volume-normalized magnetic susceptibility
µA	microamps
µL	microliter
µm	micrometer
σ_v	Overburden Stress
σ_{hmin}	Least Principal Stress
u_h	Hydrostatic Pore Pressure
ϕ	Porosity
ρ_b	Gamma density
ρ_f	Fluid density
ρ_{gr}	Grain density
ρ_h	Density of methane hydrate
Ωm or ohm m	ohm meter
AOM	Anaerobic Oxidation of Methane
APCT-3	Advanced Piston Coring Tool Temperature Sensor
API	American Petroleum Institute
ARM	Anomaly of Magnetic Susceptibility discrete split core sample

Term	Definition
ASTM	American Society for Testing and Materials
B	Static shift applied during calculations to project stratigraphic surfaces between holes
bbl or bbls	Barrels, US oilfield
BHA	Bottom Hole Assembly
BHSZ	Base of Hydrate-Stability Zone
BOEM	U.S. Bureau of Ocean Energy Management
BPM	Barrels per minute
BSI	Biogenic Silica discrete split core sample
BSF	Below the seafloor
BSEE	U.S. Bureau of Safety and Environmental Enforcement
BSL	Below sea level
BSR	Bottom Simulating Reflection
C	Depth-dependent correction used during calculations to project stratigraphic surfaces between holes
CAR	Authigenic Carbonate discrete split core sample
CC	Core Catcher whole-round sample
cc or cm^3	cubic centimeter, 1 mL
CCD	Charge-Coupled Device
ccSTP	cubic centimeter at standard temperature and pressure
CD	Compressed Depth
CD_{core}	Compressed depth in core
CEL	Cell Counts
CF	Compression Factor or Coarse Fraction discrete spit core sample, depending on the context
CFR	United States Code of Federal Regulation
CL	Computed Laminography
CMT	Cement
CNS	Total Carbon, Total Nitrogen, and Total Sulfur discrete split core sample
CRDS	Cavity Ring-Down Spectrometer
CRS	Constant Rate of Strain
CRYO	Cryogenically frozen and depressurized whole-round samples
CT	Computed tomography
D	Depth or diameter, depending on the context
d	Penetration depth of the fall cone (mm)
D_{core}	Depth in core
DIC	Dissolved Inorganic Carbon
D_{mbsf}	Depth below the seafloor in meters
DMR	Discharge Monitoring Report
DNA	Deoxyribonucleic acid
DOE	U.S. Department of Energy

 https://doi.org/10.5281/zenodo.13971228

Term	Definition
DP	Dynamic Positioning
DPS	Dynamic Positioning System
DR_{pen}	Pocket penetrometer dial reading
DSIM	Discrete Sample Introduction Module
DST	Data Storage Tag
DWOP	Drill-Well-on-Paper
E	East
FAD	First Appearance Datum (evolution)
fbsf	feet below seafloor
fbsl	feet below the sea level or sea surface
FID	Flame Ionization Detector
ft	foot or feet
ft RKB	feet below kelly bushing (rig floor)
g	acceleration due to gravity (m/s2), gallons, or grams, depending on the context
g/cc or g/cm^3	grams per cubic centimeter
g/kg	grams per kilogram
G-APC	Advanced Piston Corer
GC	Gas Chromatography or Green Canyon, depending on context
gDNA	Genomic DNA
GEOM	Geomechanics whole-round sample
GOM2	Nickname for the DOE project Deepwater Methane Hydrate Characterization & Scientific Assessment, DE-FE0023919
gpm	gallons per minute
GR	Gamma Ray
GSL	Grain Size by Laser Particle Analysis discrete split core sample
Gulf	Gulf of America (Gulf of Mexico)
G-XCB	Extended Core Barrel
H	Height
H001, H002, H003	Boreholes at Walker Ridge Block 313 Location H
HDPE	High-density polyethylene
hr or HH	hour
Hrs	hours
Hrz	Horizon
HS	Headspace Gas Sample
IAPSO	International Association for Physical Sciences of the Oceans
IC	Inorganic Carbon
ID	Inner diameter
IN	inch
IODP	Integrated Ocean Drilling Program or International Ocean Discovery Program, depending on the context
IR	Infrared

Term	Definition
ISO	Isotopes of Carbon and Oxygen discrete split core sample
IW	Interstitial Water
IWALK	Interstitial Water Alkalinity sample
IWCLISO	Interstitial Water Chlorine & Boron Isotopes sample
IWDIC	Interstitial Water Dissolved Inorganic Carbon sample
IW13DIC	Interstitial Water $\delta^{13}C$ Dissolved Inorganic Carbon sample
IWDOC	Interstitial Water Dissolved Organic Carbon sample
IWHAL	Interstitial Water Halogens sample
IWH2S	Interstitial Water Hydrogen Sulfide sample
IWLIG	Interstitial Water Ligands sample
IWMAJ	Interstitial Water Major and minor elements sample
IWO	Interstitial Water Organics whole-round sample
IWOH	Interstitial Water Oxygen/Hydrogen isotope ratio sample
IWR	Interstitial Water Regular (or Routine) whole-round sample
IWREE	Interstitial Water Rare Earth Element sample
IWS	Interstitial Water Shipboard analyses sample
IWSO4	Interstitial Water Sulfate sample
IWTRACE	Interstitial Water Trace metals and isotopes sample
JAMSTEC	Japan Agency for Marine-Earth Science and Technology
JIP	Joint Industry Project
JPG	.jpeg image file
K	One Thousand (e.g. 30K = 30,000), Kelvin, or Potassium, depending on context
K_c	Fall Cone Factor
KeV	Kiloelectron volts
klbs	Thousand pounds
Km	Kilometer
kPa	kilo pascals
ksc or kg/cm^2	kilograms per square centimeter
K_v	Vane constant
L	Length
L*	Sediment lightness in spectrophotometry
LAD	Last Appearance Datum (extinction)
lb, lbs	pound, pounds
lb-ft or LB-FT	foot-pounds
L_{cored}	Length of the cored interval
LDNR	Louisiana Department of Natural Resources
LDPE	Low-Density Polyethylene
LFH	Laminar flow hood
LPA	Linear Polyacrylamide
$L_{recovered}$	Length of the recovered core
LWD	Logging While Drilling

 https://doi.org/10.5281/zenodo.13971228

Term	Definition
m	meters
m	Archie tortuosity exponent (Archie, 1942)
M	Molar
M	Total mass of the fall cone plus any additional masses (see text)
MΩ·cm	Megaohm centimeter
MAD	Moisture and Density
MB or MBC	Microbiology whole-round sample
MBq	megabecquerel unit of radioactivity
mbrf	meters below rig floor
mbsf	meters below seafloor
mCi	millicurie unit of radioactivity
MD	Measured Depth
mD	milli-Darcy
MDW	Moisture and Density whole-round sample
MDX	Moisture and Density, X-ray Powered Diffraction, and X-ray Fluorescence discrete spit core sample
MDT	Mass Transport Deposits
m_h	Molecular weight of methane hydrate, 124 g mol-1
MICP	Microbially Induced Carbonate Precipitation
MM	minutes
mM	millimolar
mol	moles
MPa	Megapascal
m/s	meters/second
MSCL	Multi-Sensor Core Logger
N	North
NAD	North American Datum
N_{diss}	Dissolved methane component
NE	Northeast
NETL	National Energy Technology Laboratory
NGHP	Indian National Gas Hydrate Program
n_h	Amount of hydrate methane
n_m	Nanometer
nm	Total moles of methane
nmi	Nautical Mile
ns	nanoseconds
OD	Outer diameter
ODP	Ocean Drilling Program
OSR	Organoclastic Sulfate Reduction
P	Pressure or primary wave, depending on the context
P & A	Plug and Abandonment

Term	Definition
PAL	Biostratigraphy discrete core catcher or split core sample
P_{atm}	Atmospheric pressure
PCATS	Pressure Core Analysis and Transfer System
PCR	Polymerase Chain Reaction
PCTB	Pressure Coring Tool with Ball Valve
PCTB-CS	Pressure Coring Tool with Ball Valve in the Cutting Shoe Configuration
PCTB-FB	Pressure Coring Tool with Ball Valve in the Face Bit Configuration
PEN	Handheld or Pocket Penetrometer
plug DST	Data storage tag with sensors measuring temperature and pressure of the autoclave during and after pressure coring
p-mag	Paleomagnetic
POOH	Pull Out of Hole
ppb	parts per billion
PPE	Personal Protective Equipment
ppf	pounds per foot
ppg	pounds per gallon
ppm	parts per million
psi, psig	pounds per square inch, pounds per square inch by gauge
P-T	pressure and temperature
PYR	Sulfide nodule discrete split core sample
Q4000	Helix *Q4000* deepwater well intervention vessel
QD	Quantitative degassing
rabbit DST	Data storage tag with sensors measuring temperature and pressure of core during and after pressure coring
r_c	Average radius of the recovered core
RES	Resistivity
RFQ	Request for Qualifications
RIH	Run in Hole
RKB	Rotary Kelly Bushing or Rig Floor when no bushing is present
RMG	Paleomagnetic discrete split core sample
R_o	Formation Resistivity assuming 100% water saturation
RO	Reverse Osmosis
ROP	Rate of Penetration
ROV	Remotely Operated Underwater Vehicle
R_{RING}	Ring Resistivity
rRNA	Ribosomal RNA
RW	Reworked
R_w	Water resistivity
S	South or Standard, depending on the context
s	seconds
S_u	Undrained Shear Strength

Term	Definition
SAG	Single-cell Amplified Genomics
SCI	Specular Components Included
SCE	Specular Components Excluded
SED	Particle size settling velocity data
sf	seafloor
S_h	Hydrate saturation (% of pore space)
SI	International System of Units
sl	sea level
SMTZ or SMT	Sulfate-Methane Transition Zone
spud	Initial drilling of a new borehole at the seafloor/mudline
spm	strokes per minute
SS	second
STP	Standard Temperature and Pressure
SUB or Sub	Sub assembly
SW	Southwest
T	Temperature or torque, depending on the context
T2P	Temperature Dual Pressure Penetrometer
TC	Total Carbon
TCD	Thermal Conductivity Detector
TD	Total Depth
TDS	Top Drive System
TIC	Total Inorganic Carbon
TIFF	Tag Image File Format
TN	Total Nitrogen
TOC	Total Organic Carbon
TS	Total Sulfur
TVD	Total Vertical Depth
UHP	Ultra-High Purity
USGS	United States Geological Survey
UT	The University of Texas at Austin
UTM	Universal Transverse Mercator
UT-GOM2-01	UT GOM2 Hydrate Pressure Coring Expedition 1 in Green Canyon 955
UT-GOM2-02	UT GOM2 Deepwater Hydrate Pressure Coring Expedition 2 in Walker Ridge 313
UV	Ultraviolet
VANE	Hand-held vane or table vane shear strength measurement
V_c	Core volume
VCD	Visual Core Description
VF	Vane Factor
V_g	Volume of gas released
Vp	P-wave velocity
V_{pw}	Pore volume

Term	Definition
VPDB	Vienna Pee Dee Belemnite
W	West
WBM	Water-Based Mud
WGS84	World Geodetic System 1984
wireline sinker bar DST	Data storage tag with sensors measuring temperature and pressure of the fluids in the pipe at the wireline tool depth
W/m	Watts per meter
WOB	Weight on Bit
WR	Walker Ridge
WR313	Walker Ridge Block 313
wt.%	percent by weight
X_m	Fraction of methane in sample
XML	Extensible Markup Language file
XRF	X-ray Fluorescence
XRPD	X-ray Powder Diffraction
XT-57	Drill pipe connection specification
XY	X-Y plane through a core or cross-section of a core
XZ	X-Z plane through a core where Z is the direction along the length of the core
YZ	Y-Z plane through a core where Z is the direction along the length of the core

https://doi.org/10.5281/zenodo.13971228

List of conversions

All operations were conducted using US customary units except for some temperature which were collected in °C. Operations and Coring are results are reported in US customary units and can be converted to the International System of Units (S.I.) using the conversion factors listed in the table below. Some conversions are provided in the text. All science, including core logging, was conducted in S.I.

US Customary	Formula	International System of Units
inches (in.)	in x 2.54 = cm	centimeters (cm)
inches (in.)	in x 25.4 = mm	milimeters (mm)
feet (ft.)	fet x 0.305 = m	meters (m)
miles	miles x 1.61 = km	kilomenters (km)
bar	bar x 0.1 = Mpa	MegaPascals (MPa)
pounds per square inch (psi)	psi x 0.00689 = Mpa	MegaPascals (MPa)
pounds (lb or lbs)	lb x 0454 = kg	kilograms (kg)
gallons (g)	g x 3.79 = L	liters (L)
barrels (bbl or bbls)	bbl x 159 = L	liters (L)
Farenheit (°F)	(°F-32) x 0.556 = 0°C	Celcius (°C)
Farenheit (°F)	((°F-32) x 0.556) + 273.15 = K	Kelvin (K)

Vessel banner designating The University of Texas at Austin (UT) as the operator on site. Photo Credit: Camille Sullivan

Introduction

This report provides an overview of the methods used during the University of Texas (UT) Deepwater Hydrate Coring Expedition (UT-GOM2-2). Methods include work done onboard the Helix *Q4000* in the offshore Gulf of America (Gulf of Mexico), herein "the Gulf", "dockside" in Salt Lake City, Utah, and some shore-based work in individual laboratories.

The goal of this report is two-fold: to provide enough detail on the methods so they can be repeated by others; and to provide a reference document for the team to enhance cross-disciplinary understanding and knowledge.

Methods include drilling operations, depth references and depth modification, downhole tool deployment, coring tool performance assessment, core processing, lithostratigraphy, biostratigraphy, as well as physical properties, including core logging and imaging, rock magnetism, dissolved methane concentration, hydrate saturation, microbiology, and geochemistry.

An extensive amount of operational work and planning was required before mobilization of the expedition to permit, build mobile labs, and test downhole tools for deepwater drilling. Detailed plans can be found in the Preliminary Report (Flemings et al., **2024**). The Operational Plan (Flemings et al., **2023b**), and the Prospectus (Flemings et al., **2023a**) also provide more information about sample collection and movement.

 https://doi.org/10.5281/zenodo.13971228

Drilling operations include methods used for gathering rig data (mud logging, See **Rig instrumentation and parameters**), how we located the position of the new boreholes (See **Determining hole locations**), information about the drill string (See **Drill pipe** and **BHAs and bits**), and information about our drilling mud (See **Drilling fluids**).

The **Depth references** section describes the depth units and depth modifications used in these proceedings. The **Depth units** section describes depth terminology and choice of units. **Projection of Hole H001 to Site H measured depth** has information about how depths were modified for borehole deviation. **Compressed depths** provide information about depth modification for core expansion.

The **Downhole tools** section covers the three downhole coring tools, the **Pressure Coring Tool with Ball Valve**, the **Advanced Piston Corer**, and the **Extended Core Barrel**. It also covers two downhole measurement tools, the **Advanced Piston Corer Temperature Tool** and the **Temperature Dual Pressure Penetrometer**. **Coring assessment** covers the coring parameters collected and how the coring tool performance was assessed.

Core processing describes the methods used for processing/curating (e.g., logging, imaging, sampling) cores. Naming conventions are described in **Curation and naming conventions**. Pressure cores are discussed first in **Pressure core processing**, then conventional cores in **Conventional core processing**. Additional processing of cores in College Station, Texas and at Geotek Coring Inc. (Geotek) in Salt Lake City, Utah are discussed in **Core processing in College Station** and **Core processing in Salt Lake City**, respectively.

The **Lithostratigraphy** section covers methods for the determination of the lithofacies and lithologic units of the Terrebonne Basin Site H using a combination of information from macroscopic and microscopic core descriptions (See **Visual core description** and **Smear slide description**), whole-round and Split core logs, grain size determination by a variety of methods (See **Grain size**), and logging while drilling data from the preexisting borehole Hole H001 (See Summary (Flemings et al., **2025a**)). **Split core sampling** methods are also discussed. **Biostratigraphy** provides the method for assessing calcareous nannofossil biostratigraphy.

Physical properties methods for assessing sediment from the Terrebonne Basin Site H include measurements of **Thermal conductivity**; in-situ temperature; core scans and images (See **Pressure core logging and imaging**, **Conventional whole core logging and imaging**, and **Split core logging and imaging**); **Undrained shear strength**; moisture, grain density, porosity, and grain size completed at Tufts University (Tufts, See **Index properties**); and **rock magnetism**.

Dissolved gas and hydrate saturation were determined from **quantitative degassing** stepwise depressurization of pressure cores.

The **Microbiology** section covers onboard sampling for microbiology, dockside sub-coring for microbiology, and DNA extraction and amplification at Oregon State University (Oregon State). The methods discussed preserved samples for (1) 16S rDNA microbial community analysis, (2) single-cell amplified genomics (SAG), (3) assessment of the degradation potential of organic macromolecules by heterotrophs, (4) assessment of microbially-induced carbonate precipitation (MICP), and (5) quantification of microbial cell numbers (CEL).

Geochemistry covers methods for **Pore water geochemistry** sample collection (samples to be analyzed at the University of Washington (UW); **Gas geochemistry**, including gas chromatography at The Ohio State University (Ohio State) and the United States Geological Survey (USGS); and **Sedimentary geochemistry** at the University of New Hampshire (UNH).

Information on our data directory by scientific topic is provided in **Data storage**.

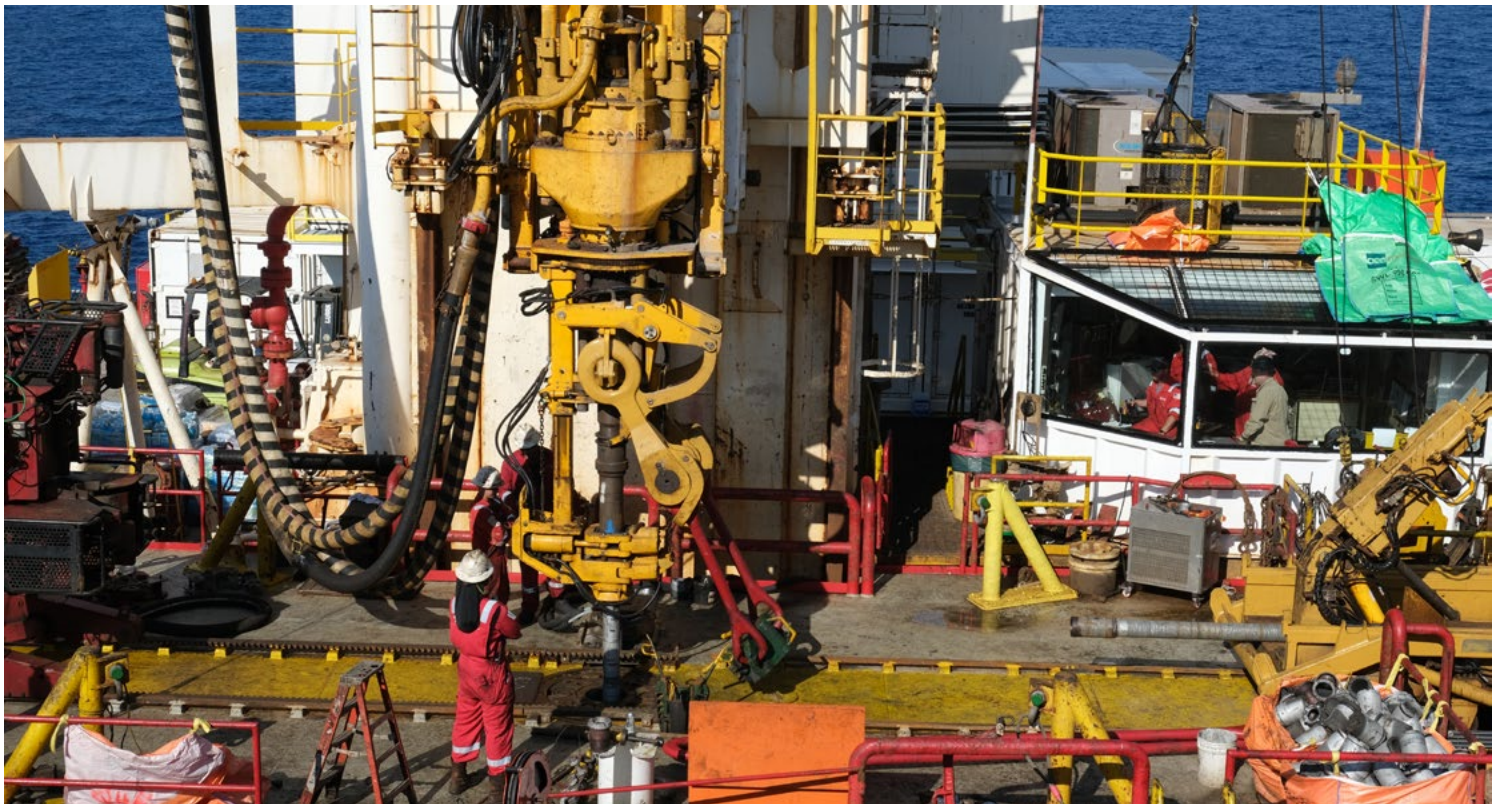

Helix engineers prepare to disconnect drill pipe from the Helix *Q4000* top drive to insert another pipe section.
Photo credit: Peter B. Flemings

Drilling operations

Methods in this section include gathering rig data (mud logging, see **Rig instrumentation and parameters**), how we located the position of the new boreholes (See **Determining hole locations**), information about the drill string (See **Drill pipe** and **BHAs and bits**), and information about our drilling mud (See **Drilling fluids**). Coring operations are discussed in the section on **Downhole tools**.

Rig instrumentation and parameters

This section describes sensor locations, installation, collected data, and how data was transferred to the science party.

We acquired data from different rig locations, including the rig floor, the mud pumps, the cement pumps, and the wireline unit. A summary of data acquired is included in Table **T1**. The rig floor and pump data were acquired by sensors installed by Helix. Wireline data are collected directly by the SLB wireline unit.

All the of the sensors and wiring were installed prior to spudding our first borehole. The data were routed to a central server run by SLB (Geoservices), where it was compiled and synchronized with data from the Helix *Q4000*.

All data were recorded in Universal Coordinated Time minus 5 hours (UTC−5).

Data were collected from different locations and at different times. Thus, some locations report data for a specific time while others report no measurement. To distinguish between a true measurement of zero and a time when no measurement was taken, times with no measurement have recorded values of -999.25. Thus,

 https://doi.org/10.5281/zenodo.13971228

Parameter	Units	Data Channel	Method of data acquisition
Time (YYYY-MM-DD HH-MIN-SEC)	seconds	TIME	
Weight on Hook	lbm	GS_HKLD	Direct measurement via sensor or transducer
Top Drive Speed	1/min	GS_TDRPM	
Top Drive Torque	lbf.ft	GS_TQA	
Stand Pipe Pressure	psi	GS_SPPA	
Hook Height	ft	GS_BPOS	
Flow Pumps (mud Hex pumps)	gpm	GS_TFLO	Sensor on each mud pump, Flow pump gpm is calculated from the combined pump speeds
Mud (Hex) Pump Speed (Pumps 1 & 2)	1/min	GS_SPM1 GS_SPM2	
Cement Unit Density	ppg	GS_CMTMW	Measured with direct recorded output on the cement pumps
Cement Unit Pressure	psi	GS_CMTPPA1	
Cement Unit Flow Rate	gpm	GS_CMTFIA1	
Cement Unit Pit Cumulated Volume	bbl	GS_ CMTTKCUMVOL1	
Instantaneous rate of penetration (ROP)	ft/h	GS_INSROP	Calculated from two or more parameters above
Rate of penetration on depth step	ft/h	GS_DSROP	
Weight on bit (WOB), see **Weight on bit**	lbm	GS_SWOB	
Total Depth	ft	GS_DMEA	
Bit Depth	ft	GS_DBTM	
Wireline Tool Depth	ft	TDEP	Recorded directly by the wireline unit
Cable Tension	lb	TENS	
Cable Velocity	ft/h	CVEL	

Table T1: Parameters acquired as a function of time during drilling and coring operations.

the raw combined data contains entries of -999.25 at different intervals. To plot rig data verses time, or average rig data over time, all entries of -999.25 were first removed and left as null.

On a typical day at ~1 AM local time, SLB provided a data report with plots of the previous 24 hours of data and at approximately 6 AM SLB delivered an ASCII standard log file with digital data from the previous day. All ASCII data were compiled into a single Excel file. Dataset: **http://doi.org/10.5281/zenodo.14680104**.

Weight on bit

The weight on bit (WOB) in the rig data was not directly measured but calculated from Weight on Hook. The calculated WOB was significantly smaller than the true WOB reported verbally from the driller's shack because the calculated WOB did not capture drag while the driller was slacking off or picking up weight. The rig data WOB was also only captured intermittently. The true WOB during pressure coring was received from the drill shack and recorded in the pressure coring run reports (See **PCTB operations**).

Determining hole locations

Fugro personnel identified the location for each borehole position using satellite GPS and Starfix navigation software on the bridge of the *Q4000*. The planned borehole locations for Hole H002 and Hole H003 were established based on their planned direction and distance from the previously drilled borehole, Walker Ridge Block 313 H001 (WR313 H001 or Hole H001).

The process to determine the location of the boreholes was as follows:

1. Fugro provided the official coordinates of Hole H001 in the coordinate system WGS 1984.
2. The *Q4000* moved to the provided location for Hole H001.
3. Work class Remotely Operated Vehicles (ROVs, XLS09 and XLS10) were deployed.
4. The *Q4000* ROV teams searched for the original borehole (~1 day), over a radius of 300 m from the Hole H001 coordinate location. During the ROV search, small mounds and hummocky topography were identified in the area, however, no convincing open hole was located.
5. Because the original Hole H001 was not found, the Fugro official coordinates for Hole H001 location were used to locate the surface location for Holes H002 and H003.
6. The *Q4000* ROVs placed temporary buoys at surveyed locations of Hole H002 and Hole H003.
7. The *Q4000* was moved over the Hole H002 and Hole H003 locations and Fugro obtained the official coordinates from the Fugro Starfix positioning system.
8. After final data processing, Fugro provided the official locations in NAD27 and NAD83 datums.

Drill pipe

A cleaned and certified 5⅞-inch outer diameter, 23.40 ppf (adjusted weight), S-135 drill string pipe with XT-57 connections (minimum internal diameter of 4.125 inches) with internal hardbanding from Workstrings International was used.

BHAs and bits

Two different types of bits were used during UT-GOM2-2, including the Pressure Coring Tool with Ball Valve Cutting Shoe (PCTB-CS) drill bit and the Pressure Coring Tool with Ball Valve Face Bit (PCTB-FB) drill bit (Figure F1). Both bits have an outer diameter of 9⅞ inches (250.8 mm). The PCTB-CS has an inner diameter of 3⅘ inches (96.5 mm), and the PCTB-FB has an inner diameter of 2 inches (50.8 mm). The PCTB-CS bit is compatible with the conventional coring tools and other downhole tools, such as the Temperature Dual Pressure Penetrometer (T2P).

Four different bottom hole assemblies (BHAs) were used during UT-GOM2-2 (Table T2). The first BHA was used for drilling and coring Hole H003 (Figure F2). Two additional BHAs were used for drilling and coring Hole H002 as shown in Figures F3 and F4 and the fourth BHA was used for cementing Hole H002 (Figure F5). Most of the BHA components were the same for the three drilling and coring BHA assemblies. Starting from the bit, these BHAs included one stabilized bit sub, one seal bore drill collar, one landing saver sub, one modified top sub, one modified head sub, one 9⅞ inch stabilizer, one 8½ inch drill collar, one 9⅞ inch stabilizer, four 8½ inch drill collars, and one crossover sub. The only difference between the three assemblies was the bit, either PCTB-CS or PCTB-FB, and the number of drill collars, either four or seven, in the upper section (Table T2). If used, the four additional drill collars increase the weight of the BHA from 24,000 lb to 38,000 lb. The cementing BHA had a slightly different configuration, starting from the bit, the cementing BHA included one stabilized bit sub, one 8½ inch drill collar, one 9⅞ inch stabilizer, another 8½ inch drill collar, one 9⅞ inch stabilizer, six 8½ inch drill collars, and one crossover sub (Figure F5).

Drilling fluids

The UT-GOM2-2 fluids program followed government regulations CFR 30 Section 250 (drilling fluids) and Environmental testing regulations CFR 40.

Water-based mud

On shore, barite was added to fresh water to bring the mud to a weight of 16.0 ppg. Low amounts (ppb) of bulk gel (viscosifier), Duo-Vis (viscosifier), caustic soda (sodium hydroxide), and Poly Pac R (Polyanionic cellulose) were added to form our working water-based mud (WBM).

The WMB was transferred to the *Q4000* from the *Harvey Hermes* and *Harvey Spirit* supply boats. Two

https://doi.org/10.5281/zenodo.13971228

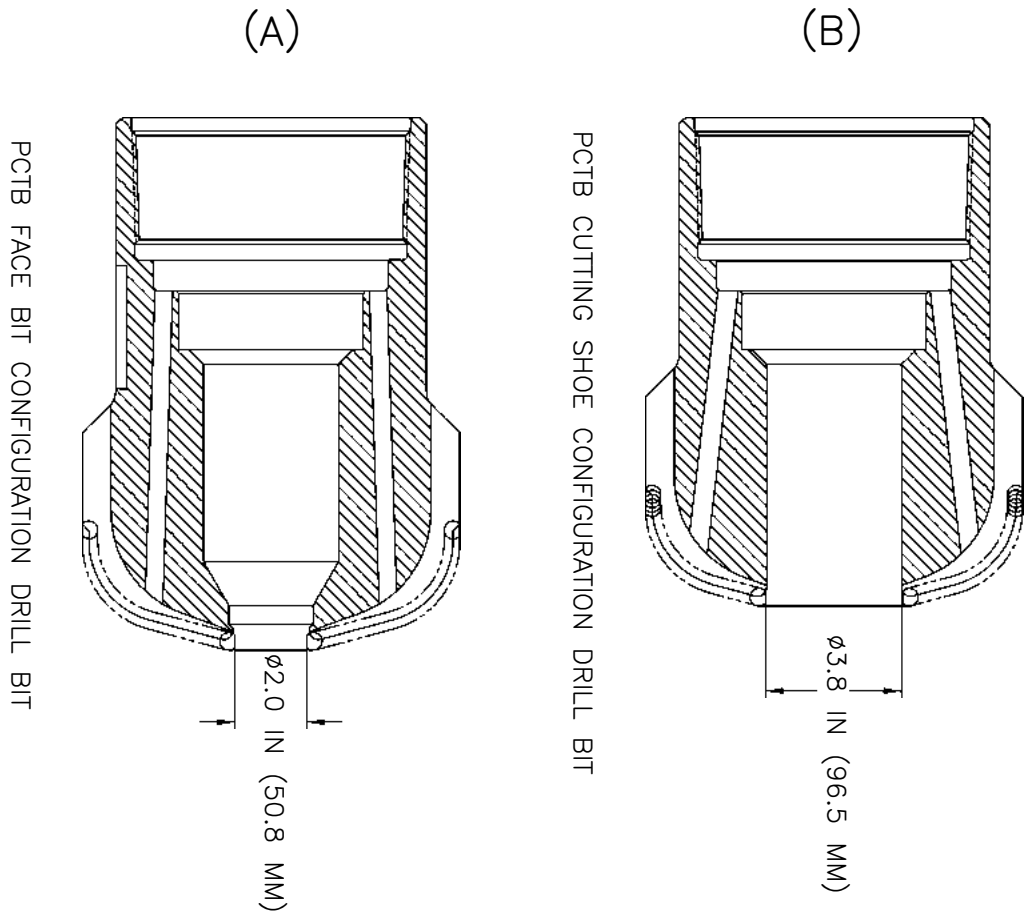

Figure F1: Drill bits used for A) the Pressure Coring Tool with Ball Valve (PCTB) in the Face Bit configuration (PCTB-FB); and B) the Cutting Shoe configuration (PCTB-CS). The larger opening in the PCTB-CS BHA is compatible with conventional coring and other downhole tools.

BHA	Hole H003	Hole H002 to 8,748 ft RKB	Hole H002 Below 8,748 ft RKB	Hole H002 Cementing
Type of bit (Figure F1)	PCTB-CS	PCTB-FB	PCTB-CS	PCTB-CS
# of drill collars in the upper section	4	7	7	6
# of drill collars in the lower section	1	1	1	2
Associated Figure	Figure F2	Figure F3	Figure F4	Figure F5

Table T2: The bottom hole assembly (BHA) variations during UT-GOM2-2.

MI Swaco personnel managed the WBM onboard. The WBM was mixed as needed to create batches of high-viscosity sweep, kill, and pad muds. It was also diluted on the fly with seawater to the desired weight and viscosity for deeper drilling (See **Mud weights with up**) with a mix-on-the-fly unit.

High viscosity sweep mud was created by diluting base mud with seawater to 10.5-11.0 ppg and adding ppb concentrations of Xanthan gum. No Duo-Vis or Poly Plus was used as initially envisioned in the mud program. It was interpreted that Xanthan gum would achieve equally effective results at less cost.

Kill mud was created by diluting base mud to 13.0 ppg.

Several muds were mixed and used for the plug and abandonment program. A 10.5 ppg spacer was created from sacks of dry barite with fresh water. Drilling mud was mixed to 11.0 ppg. Pad mud was created by diluting WBM with fresh water and adding ppb concentrations of Xanthan gum to 11.5 ppg.

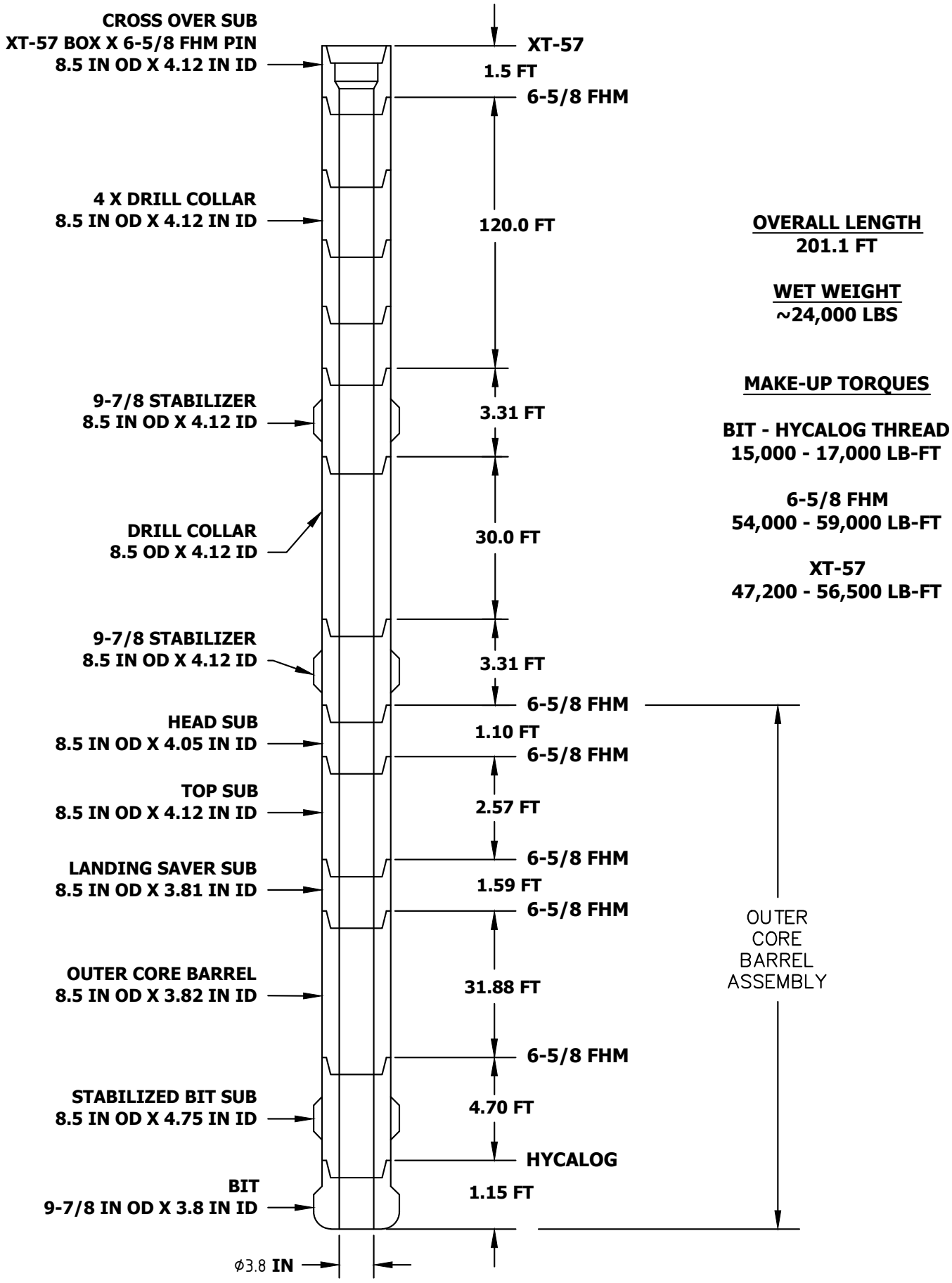

Figure F2: Hole H003 bottom hole assembly (BHA). Box and Pin specifications include XT-57, Full-Hole Modified (FHM), and HYCALOG. Sub assembly (SUB), inch (IN), pounds (LBS), feet (FT), foot-pounds (LB-FT), inner diameter (ID), outer diameter (OD).

https://doi.org/10.5281/zenodo.13971228

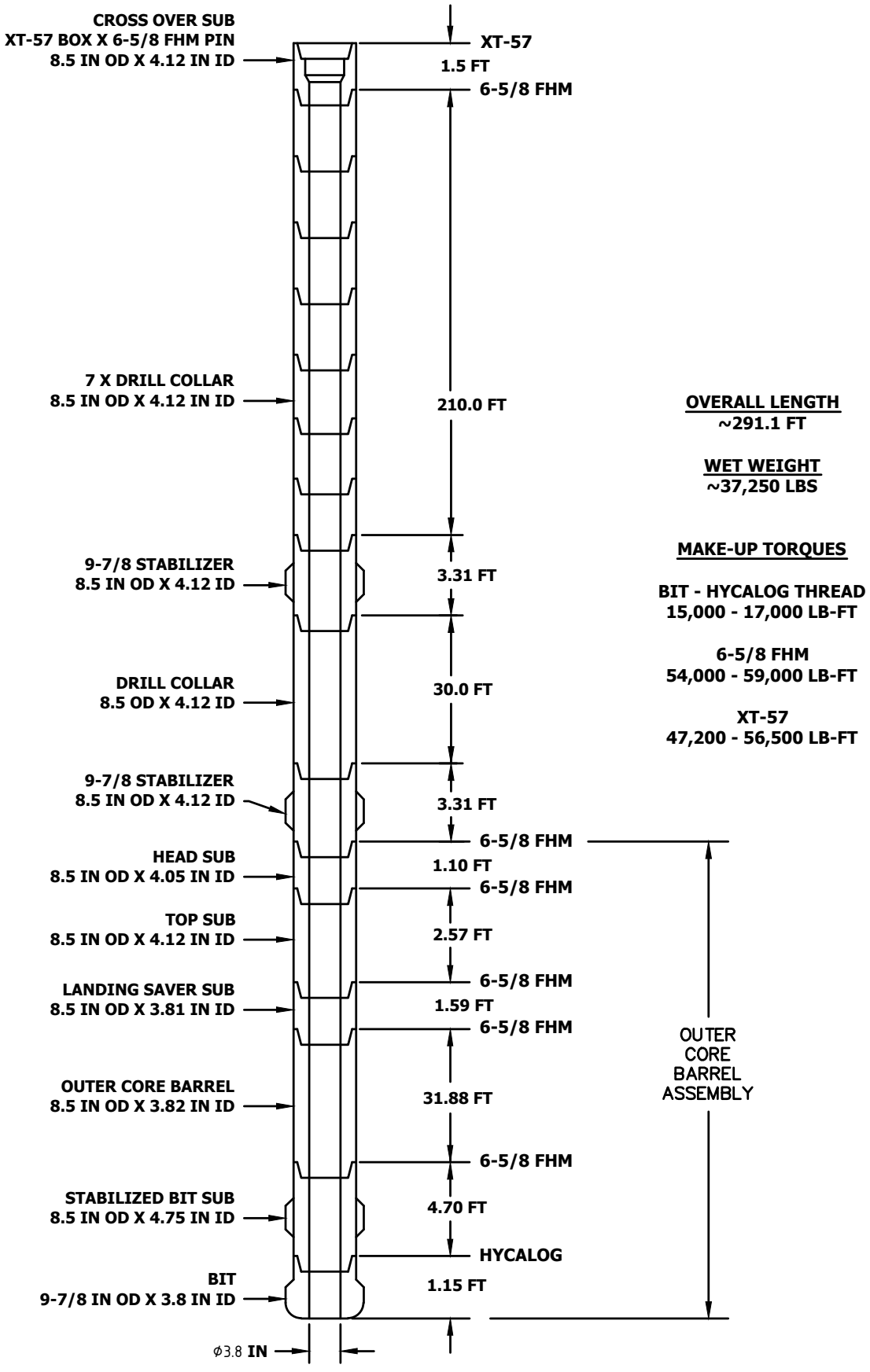

Figure F3: Hole H002 (0-8,748 ft RKB) bottom hole assembly (BHA) in the pressure coring tool with ball valve (PCTB) Face Bit configuration (PCTB-FB) with seven drill collars above the first stabilizer. Box and Pin specifications include XT-57, Full-Hole Modified (FHM), and HYCALOG. Sub assembly (SUB), inch (IN), pounds (LBS), feet (FT), foot-pounds (LB-FT), inner diameter (ID), outer diameter (OD).

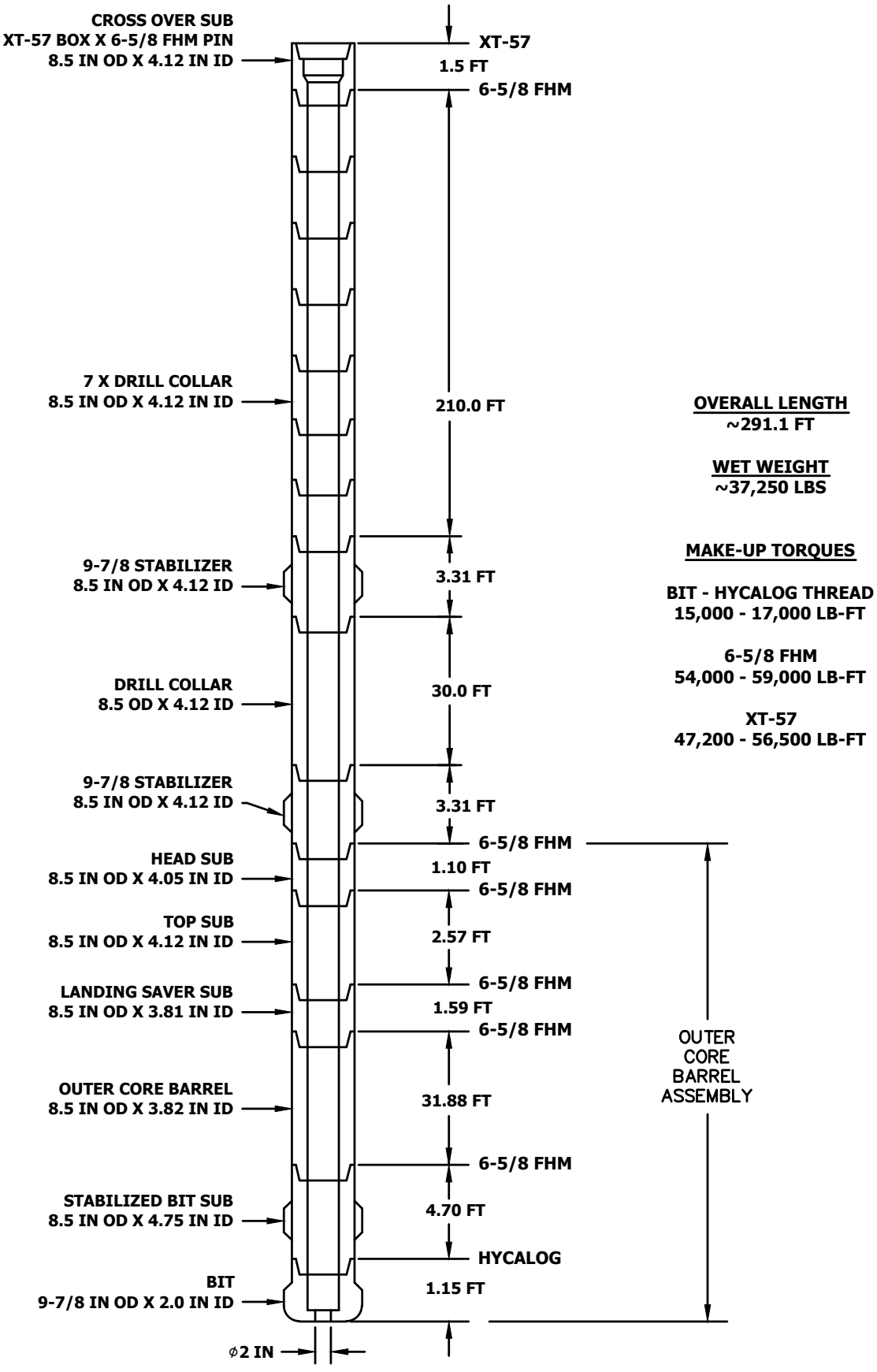

Figure F4: Hole H002 (> 8,748 ft RKB) bottom hole assembly (BHA) in the pressure coring tool with ball valve (PCTB) Cutting Shoe configuration (PCTB-CS) with seven drill collars above the first stabilizer. Box and Pin specifications include XT-57, Full-Hole Modified (FHM), and HYCALOG. Sub assembly (SUB), inch (IN), pounds (LBS), feet (FT), foot-pounds (LB-FT), inner diameter (ID), outer diameter (OD).

 https://doi.org/10.5281/zenodo.13971228

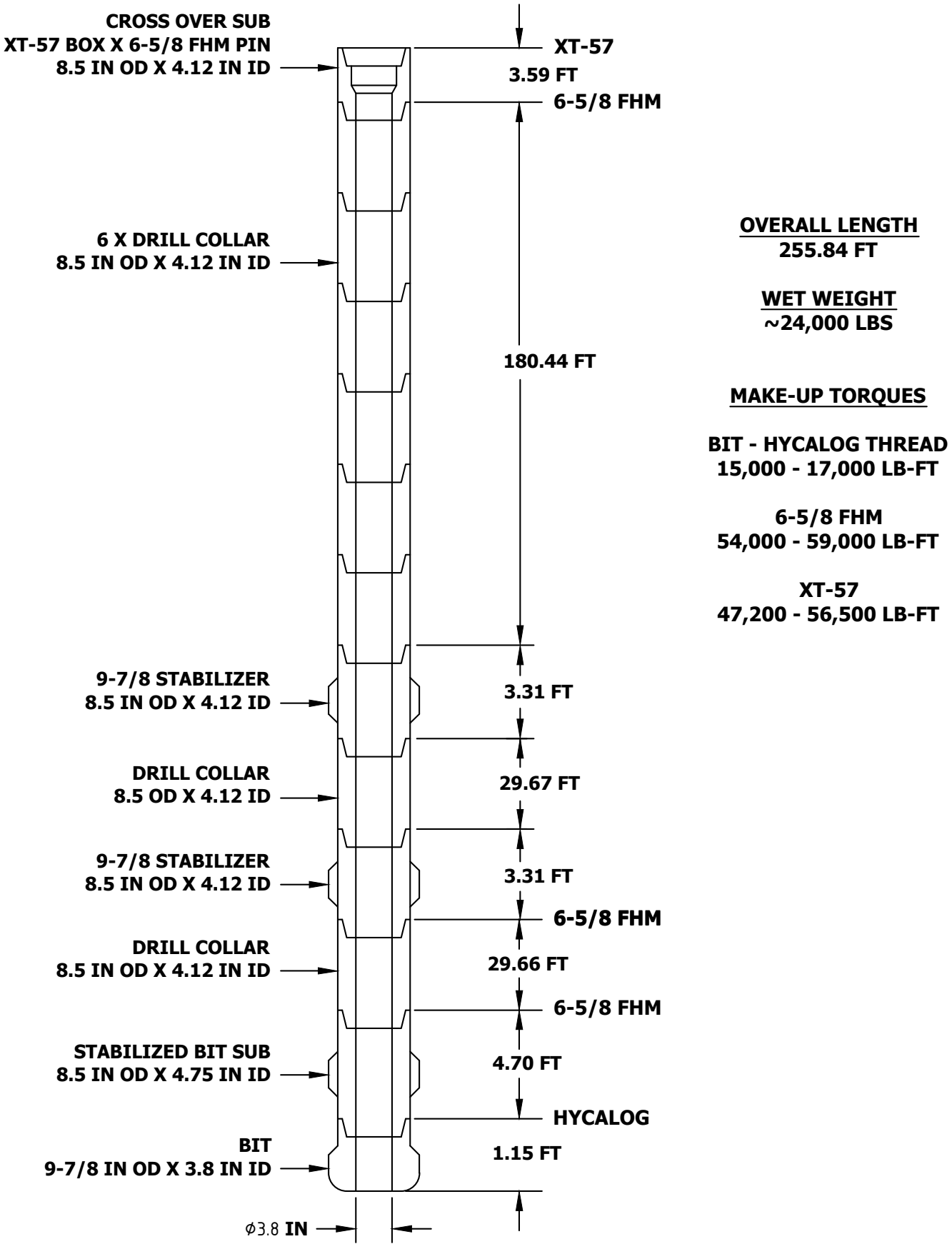

Figure F5: Hole H002 cementing bottom hole assembly (BHA)in the pressure coring tool with ball valve (PCTB) Cutting Shoe configuration (PCTB-CS) with six drill collars above the first stabilizer. Box and Pin specifications include XT-57, Full-Hole Modified (FHM), and HYCALOG. Sub assembly (SUB), inch (IN), pounds (LBS), feet (FT), foot-pounds (LB-FT), inner diameter (ID), outer diameter (OD).

Hex pumps were used to pump the mud into the borehole during piston coring and while circulating, and cement pumps were used to pump the mud during pressure coring.

High viscosity sweeps

Before mobilization, cutting slip velocities were calculated for seawater and 10.5 ppg WBM at 54.5 ft/min and 43.6 ft/min, respectively, using an assumed cutting size of 0.25 inches. Our required minimum flow rates to lift cuttings past the BHA were then calculated for seawater and 10.5 ppg WBM at 62 gpm and 50 gpm, respectively. However, much higher flow rates were utilized to minimize fall-in from the borehole's sandy top.

High-viscosity sweeps were pumped every 4-6 hours while drilling ahead and every 4 hours while waiting for the *Q4000* to be repaired.

During advanced piston coring, when multiple piston cores were taken in succession, we generally pumped a 25 bbl sweep of 10.5 ppg high-viscosity mud after every other core for borehole stability and to remove debris and fall in. Sweeps were pumped at 250-300 gpm, reducing the pump rate as we approached the bottom of the previously cored section. We then continued pumping seawater to ensure the sweep was out of the borehole before the pumps were shut down to start the next piston coring deployment (See Conventional coring tool deployments).

During pressure coring with seawater in H003, we generally followed the practice of pumping a high viscosity sweep before each core while deploying the PCTB core barrel. Sweep volume increased from 15 to 40 bbls as the borehole was deepened. Sweeps were pumped at 100-350 gpm and the BHA was kept slightly off bottom as the high-viscosity sweep was pumped through the BHA and circulated up out of the borehole. Sweep depths are reported for each pressure coring deployment when used (See **Pressure coring tool deployments**). Sweeps were not used in Hole H002 since we were drilling with WBM.

Mud weights with depth

WBM was diluted on the fly with seawater. WBM was introduced at 9.0 ppg at 8,115 ft RKB (490.4 mbsf) and gradually increased to 10.3 ppg to 8,621 ft RKB (644.6 mbsf); occasional high viscosity mud sweeps were also pumped in this interval. From 8,621 to 8,766 ft RKB (644.6 to 688.8 mbsf), 10.3 ppg WBM was used. At depths greater than 8,766 ft RKB (688.8 mbsf), we 10.5 ppg WBM was used.

Plug and abandonment

The method for plugging and abandoning the borehole is discussed in Site H (Flemings et al., **2025b**).

https://doi.org/10.5281/zenodo.13971228

Laboratories from Geotek Coring Inc. are placed on deck. Each lab was supplied with safety monitors, power, water, and air before being set up to receive core. Photo credit: Geotek Ltd.

Depth references

The following sections describe the depth units and depth modifications used in these proceedings. Information about terminology can be found in **Depth units**. Information about how depths were modified for borehole deviation can be found in **Projection of Hole H001 to Site H measured depth**. Information about depth modification for core expansion can be found in **Compressed depths**.

Depth units

Measured Depth is determined by the drill pipe length.

In this report we use three reference points when describing measured depth (Figure **F6**).

The measured depth below the rig floor is the length of pipe below the rig floor. For historical reasons it is referred to as MD_{RKB}. RKB refers to the kelly bushing, which is not present on a top drive rig, such as the *Q4000*. The measured depth below sea level (MD_{BSL}) is MD_{RKB} less the height of the rig floor relative to sea level (52 ft above sea level for this expedition). The measured depth below seafloor MD_{BSF} is MD_{RKB} less the length of pipe when the seafloor was tagged at the onset of the hole.

In this report, MD_{RKB} and MD_{BSL} are reported in feet and expressed as Depth (ft RKB) and Depth (fbsl). MD_{BSF} is reported in meters and expressed as Depth (mbsf) or MD_{MBSF}.

The water depth was determined by subtracting the height of the rig floor from the measured depth of the coring bit as it first touched the seafloor mud line.

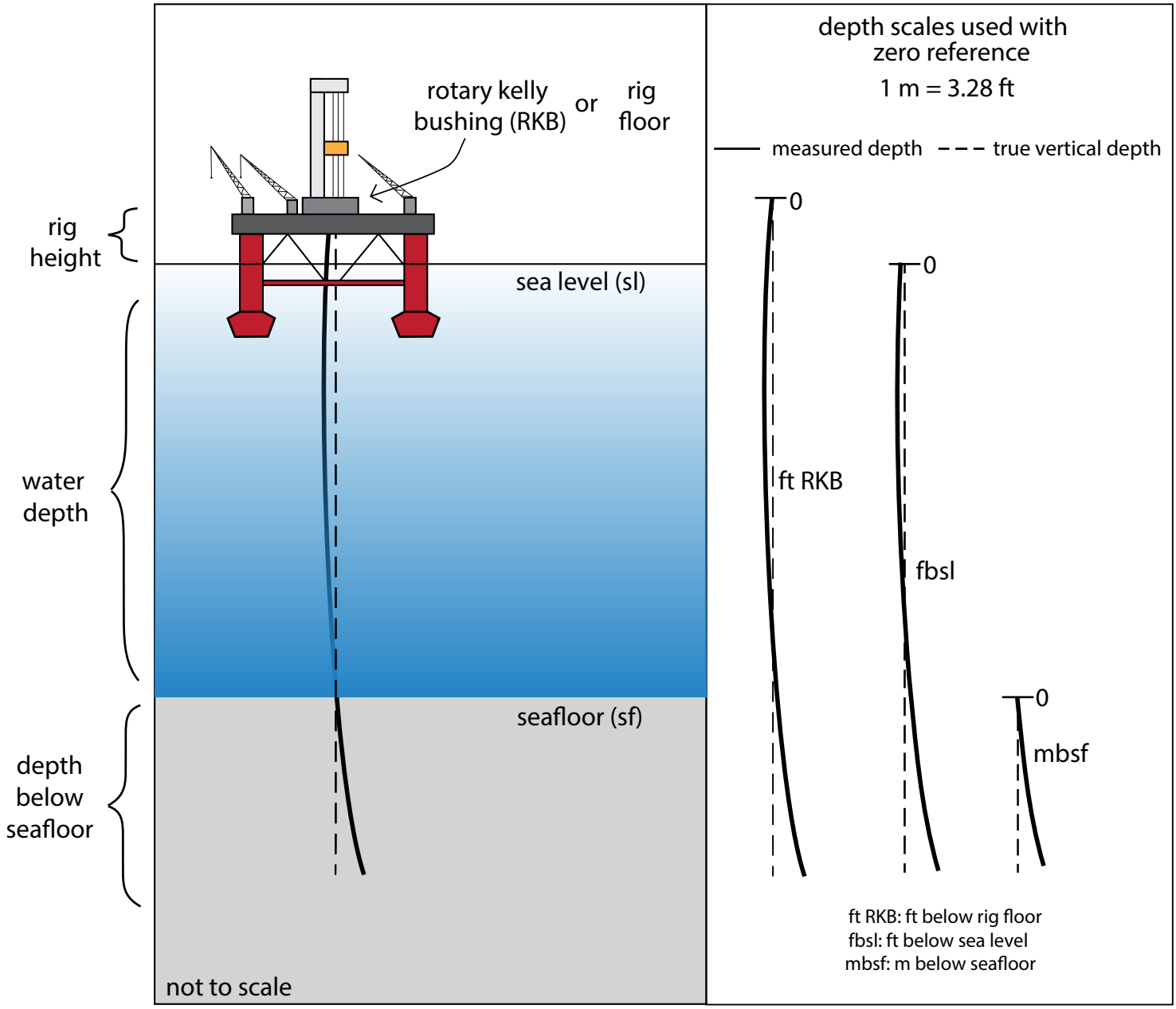

Figure F6: Reference depth relationships and definitions. The measured depth (or archived depth) is shown as a solid back line and is determined from the pipe length. The measured depth is only equal to the true vertical depth if the borehole is not deviated. The true vertical depth is shown as a black dashed line.

Calculation of vertical depth below the seafloor from measured depth

Hole H003 was deviated. We assumed a constant Hole H003 inclination of 7 degrees (See Site H: Borehole deviation survey (Flemings et al., 2025b)). We used simple geometry to calculate Hole H003 vertical depth from the measured depth. We did not account for the slight rise in the seafloor from the location of the top of Hole H003 to the bottom of Hole H003 (Equation E1).

$$Hole\ H003\ True\ Vertical\ Depth = 7^{\circ} * Hole\ H003\ Depth\ (mbsf)$$

Equation E1.

The vertical depth in Hole H002 is the measured depth since Hole H002 was vertical (See Site H: Borehole deviation survey (Flemings et al., 2025b))

https://doi.org/10.5281/zenodo.13971228

Projection of Hole H001 to Site H measured depth

When Hole H001 LWD data and stratigraphic tops are plotted against H002 and H003 downhole data, Hole H001 measured depths to 300 mbsf are first projected to Hole H003 measured depths using Equation E2:

$$Hole\ \ H003\ \ MD_{BSF}\ \ = \\ (C\ \ *\ \ H001\ \ MD_{BSF}) + B$$

Equation E2.

C was determined to be 0.988 and B was determined to be 10.9 ft (3.32 m). See details in Site H report (Flemings et al., 2025b).

The depth conversion is only applied down to 300 mbsf for three reasons. First, Hole H003 was only cored to 7,470 ft RKB (296.9 mbsf). Second, only Hole H003 was deviated. Third, the change in depth from Equation E2 also rounds to zero at 300 mbsf.

Hole H001 measured depths greater than 300 mbsf are not converted using Equation E2 as Hole H002, cored from 8,620 ft RKB (644.3 mbsf) to 8,620 ft RKB (644.3 mbsf), was on strike with Hole H001 and nearly vertical.

Compressed depths

We converted sample and measurement locations in core (measured in cm from the top of each core section) to Depth (mbsf) using two depth scales: 1) archived depth and 2) compressed depth (Figures F7 and F8). See Consolidation of voids and Curation and naming conventions for more information on sediment movement and core, core section, and section piece naming conventions.

The archived depth was calculated by converting the measured depth in section n ($D_{section}$, n) to the depth in core (D_{core}) by adding the depth in section ($D_{section}$, n) to the sum of the lengths of all sections above it in the same core (i=1i=n-1Li) (Equation E3).

$$D_{mbsf}\ = D_{core} + \ \ Top\ \ of\ \ core\ \ mbsf$$

Equation E3.

The depth below the seafloor (Dmbsf) was then calculated by adding the depth in core (Dcore) to the measured depth of the top of the core below the seafloor (Top of corembsf) (Equation E4).

$$D_{core}\ = D_{section},\ n\ \ + \sum_{i=1}^{i=n-1} L_i$$

Equation E4.

Due to the expansive nature of some of the cores, some of the recovered cores were longer than the cored length. In these cases, when results from sequential cores are plotted using archived depth, the results from one core can overlie upon results from the next core (Figure F7, column A). To keep results in stratigraphic order, and to constrain any core data to within its cored interval, results are instead plotted using compressed depth below seafloor (Figure F7, column B and Figure F8, column C, CD_{mbsf}).

The compressed depth below seafloor (CDmbsf) of a specific sample or measurement is calculated in the following way (Equation E5):

First, a compression factor (CF), which is unique to each core, was determined:

$$CF = \frac{L_{cored}}{L_{recovered}}$$

Equation E5.

CF is the ratio of the cored interval (L_{cored}) to the length of the recovered core ($L_{recovered}$). It is the inverse of the core recovery. For example, if the cored interval was 8.53 m and the recovered length was 10.05 m, resulting in compression factor would be 0.849 and the recovery 118%.

In cases where the compression factor was less than 1 (recovery >100%, Figure F7, Coring intervals 2 and 3, Figure F8), the archived sample depth in core was converted (Equation E6) to its compressed depth in core (CD_{core}):

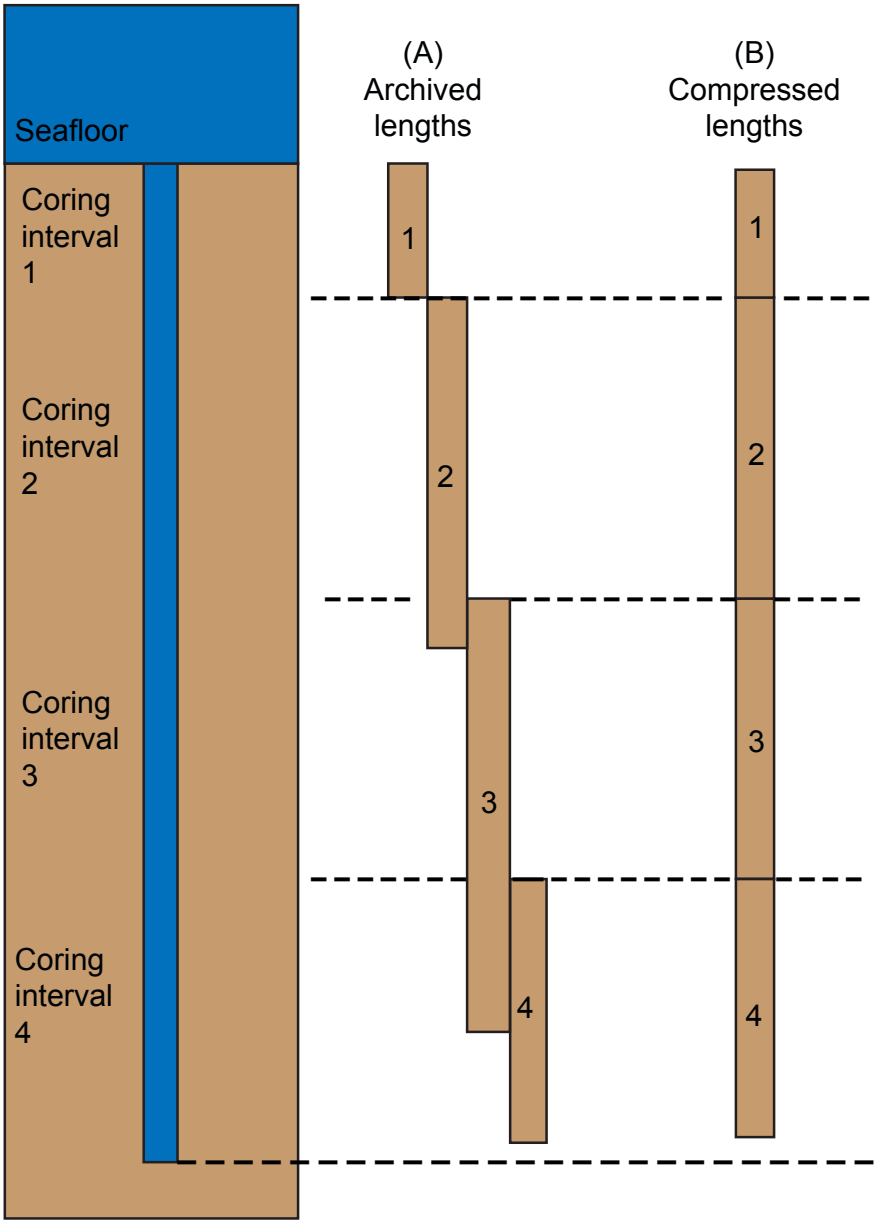

Figure F7: Schematic diagram comparing archived length (left) and compressed depth(right) to the coring interval. Core example 1: Archived length equals the cored interval and no compression was used. Core examples 2 and 3: Archived cores exhibit varying degrees of expansion and are compressed to the length of the cored interval. Core example 4: Archived lengths are less than the cored interval, and no compression was used.

$$CD_{core} = D_{core} * \ CF$$

Equation E6.

In cases where the calculated compression factor is greater than or equal to 1 (recovery ≤100%, Figure F7, Coring intervals 1 and 4), the compression factor was set to 1 and the compressed depth in core (CD_{core}) is equal to the measured depth in core (D_{core}).

The compressed depth below the seafloor (CD_{mbsf}) was then calculated by adding the compressed depth in core (CD_{core}) to the depth of the top of the core below the seafloor (Top of core mbsf) (Equation E7):

$$CD_{mbsf} = CD_{core} + \ Top \ of \ core \ mbsf$$

Equation E7.

This is the same approach used by the Integrated Ocean Drilling Program to determine what they call the core depth below the seafloor in compressed depths or CSF-B scale (IODP Depth Scale Task Force, 2011).

https://doi.org/10.5281/zenodo.13971228

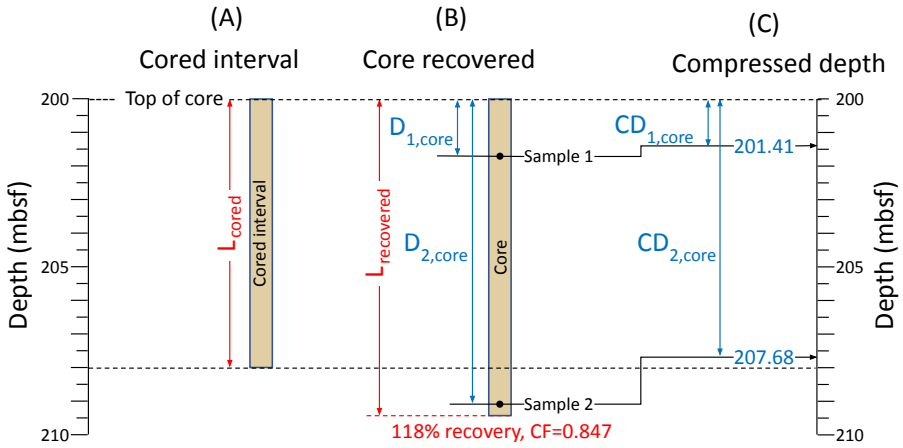

Figure F8: Illustration of how the compressed depth below seafloor (CD_{mbsf}) is calculated. A compression factor (CF) is calculated (Equation **E5**), which is the ratio of the length of the cored interval (L_{cored}) to the recovered interval ($L_{recovered}$). The recovered core in this case is longer than the cored interval and CF is equal to 0.847. The CF is then used to convert depth in the core (D_{core}) to the compressed depth in the core (CD_{core}) (Equation **E6**). The sample compressed depth below the seafloor (CD_{mbsf}) is then calculated as the sum of the compressed depth in core (CD_{core}) plus the depth of the top of the core in meters below seafloor (Top of core mbsf), (Equation **E7**).

Science party members Steve Phillips of the U.S. Geological Survey, Matt Selman of Geotek Coring Inc., Tim Collett of the U.S. Geological Survey, Patrick Riley of Geotek Ltd., and University of Washington professor Evan Solomon onboard the *Q4000*. Photo Credit: Peter B. Flemings

Downhole tools

Three downhole coring tools, the **Pressure Coring Tool with Ball Valve**, the **Advanced Piston Corer**, and the **Extended Core Barrel**; and two downhole measurement tools, the **Advanced Piston Corer Temperature Tool** and the **Temperature Dual Pressure Penetrometer** were mobilized to the vessel. This section describes tool designs, testing, and tool deployment methods.

Pressure Coring Tool with Ball Valve

The PCTB is a wireline coring system designed to recover core samples while maintaining the core at or above in-situ pressure. The PCTB tool collects cores that are cut at 2.0 inches (50.8 mm) in diameter. The cores are contained in a plastic liner with an inner diameter of 2.1 inches (53.6 mm) an outer diameter 2.4 inches (60.3 mm), and up to 10 ft (3.05 m) long. The tool is rated to recover cores at pressures of up to 5,076 psi (35 MPa). There are two PCTB configurations: the Cutting Shoe (PCTB-CS, Figure **F9**, right) and the Face Bit (PCTB-FB, Figure **F9**, left). The PCTB configurations have different BHAs (See **BHAs and bits**). The PCTB-CS has a larger BHA opening that makes it compatible with other wireline tools. The PCTB-CS cutting extends through and past the BHA opening and contributes to the cutting of the core. Different parts of the PCTB-CS and PCTB-FB are designed to rotate with the core (Thomas et al., **2020**) (Figure **F9**, arrows). A more detailed discussion of the tool design can be found in Thomas et al. (**2020**).

Pressure coring tool full function tests

To test the PCTB, the tool was deployed in the drill pipe, latched to the BHA, and unlatched while the BHA was still in the water column. The goal was to test whether the PCTB actuated, the ball valve closed, and the

 https://doi.org/10.5281/zenodo.13971228

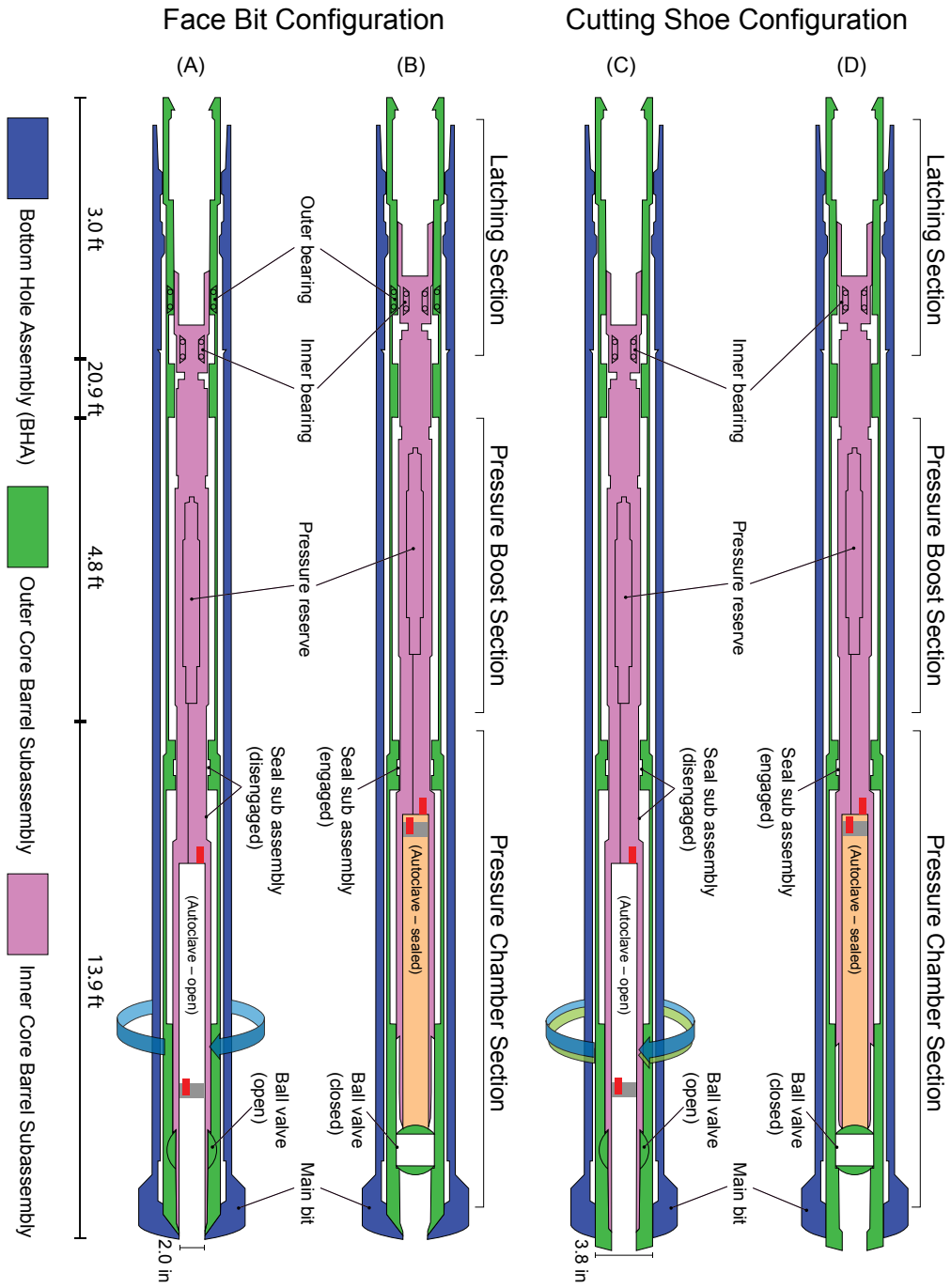

Figure F9: Schematics of the Pressure Coring Tool with Ball Valve in the Face Bit (PCTB-FB) and Cutting Shoe (PCTB-CS) configurations. A) PCTB-FB during coring. In this configuration, the outer (green) and inner (pink) core barrel subassemblies move independently from each other and from the bottom hole assembly (BHA). The blue arrow indicates the direction of BHA rotation. B) PCTB-FB during core retrieval. C) PCTB-CS configuration during coring. In this configuration, only the inner core barrel subassembly moves independently from the BHA. The outer core barrel subassembly is locked to the BHA. The blue arrow indicates the direction of BHA rotation, and the green arrow indicates that the outer core barrel subassembly rotates with the BHA. D) PCTB-CS configuration during core retrieval. To initiate core retrieval, the inner core barrel subassembly (in pink) is pulled up relative to the outer core barrel subassembly (in green). The location of the data storage tags (DST) with pressure and temperature sensors are shown as red boxes. One DST is housed in the inner core barrel at the top of the autoclave in the IT-plug (plug DST) and measures the autoclave pressure and temperature. Another DST is housed inside the autoclave in the rabbit (rabbit DST, gray box) and measures the core temperature and pressure. The rabbit DST moves up the autoclave as the core enters the autoclave during coring. A third DST (not shown) is above the coring tool on the wireline. It is housed in the wireline sinker bar (wireline sinker bar DST) and measures the temperature and pressure of the fluids in the pipe at the wireline tool depth. The ratio of the width and length of the tool is not to scale (see length indicator bars). Figure is modified from Thomas et al. (**2020**).

seawater within the core liner remained pressurized until it was brought back to the surface. The tests were completed before spudding with the BHA.

Pressure coring tool deployments

The method we used for PCTB deployments is best described using an example from the expedition. Deployment and retrieval data for H003-27CS are shown in Figure F10 with an expanded view in Figure F11.

The PCTB core barrel was assembled on the rig floor. The cement pump (Figure F10, row C, solid orange line) pumped a high-viscosity sweep (Figure F10, row A, solid purple line) while the core barrel was run in the hole on the wireline using the PCTB running tool (Figure F10, row A, solid orange line, 18:30-18:55). The wireline sinker bar, plug, and rabbit data storage tags (DSTs, F9, red boxes) recorded the approximate pressure and temperature of the fluids in the pipe at wireline tool depth, the autoclave, and core, respectively (Figure F10, row B and Figure F11, row B). The core barrel was latched into the BHA (Figure F10, row D, ~19:03). The core barrel remained in the BHA while the running tool was pulled back to the rig and replaced with the PCTB pulling tool on the wireline (Figure F10, row A, orange line, 19:03-20:30). The high-viscosity sweep was pumped down and reached total depth before the cement pumps were shut off (Figure F10, row A and D, purple line). The cement pumps were shut off while the running tool was replaced with the pulling tool but otherwise continued to keep the borehole clean (Figure F10, row C, orange line). The pulling tool rested a few hundred feet above the core barrel during and just after coring (Figure F10, row A, orange line, 20:30-20:54). The cement pumps (Figure F10, row C and Figure F11, row C, orange line) pumped 8.6 ppg seawater at an average of 137 gpm during coring (Figure F11, row A, black line hole depth and row C purple line rate of penetration, 20:36-20:50). The standpipe pressure (Figure F10, row D, light blue line) is elevated during coring indicating a partial blockage of flow through the bit. The bit depth (Figure F10, row A, magenta line) does not track with total depth (Figure F10, row A, black line) toward the end of coring (20:45-20:50) and the cause is unknown but may be related to the partial blockage of flow through the bit. Coring ended and the bit was raised 30-50 ft above total depth to break the core from the formation (Figure F11, row A, magenta line, 20:50).

The pulling tool was lowered and latched into the core barrel (Figure F10, row A and D, and Figure F11, row A, 20:54-20:58). The initial pull to unlatch the core barrel from the BHA and actuate the tool was marked by an abrupt increase in the wireline tension (Figure F10, row A and Figure F11, row A, green line, 20:59). This actuated the PCTB by closing the ball valve, setting the inner tube plug seals in the seal sub, opening the sleeve valve of the nitrogen pressure section, and lastly unlatching the PCTB from the BHA to return to surface.

The core barrel was freed from the BHA (Figure F10, row A and Figure F11, row A, green line tension release at 21:00). The autoclave pressure (Figure F11, row B, solid blue line) dropped with the pipe pressure (Figure F11, row B, dashed blue line) until about 21:05 when the autoclave pressure was boosted from 2,919 psi. The pressure was then held (except for small changes in autoclave volume) while the pipe pressure dropped rapidly as the core barrel was raised on the wireline with a few minutes of delay at the seafloor (~6,500 ft RKB). (Figure F10, row B and Figure F11, row B, 21:05-21:45). The pressure boost will not fire unless the sleeve valve is open, and the autoclave pressure is below the pressure boost setting. The pressure boost helped to properly seat the upper seal ring and provided more margin between the core conditions and the hydrate stability boundary as the core was raised up the drill pipe through the warmer water column.

The pipe fluid, autoclave, and approximate core temperatures rose (Figure F10, row B, dashed red, solid red, and pink lines, respectively, 21:05-21:45) as the core barrel was raised through warmer ocean on the wireline. The autoclave temperature increased to 25 °C despite the delay for cooling at the seafloor (which lowered the temperature <1 °C), possibly due to a slower wireline retrieval velocity (286 ft/min)

https://doi.org/10.5281/zenodo.13971228

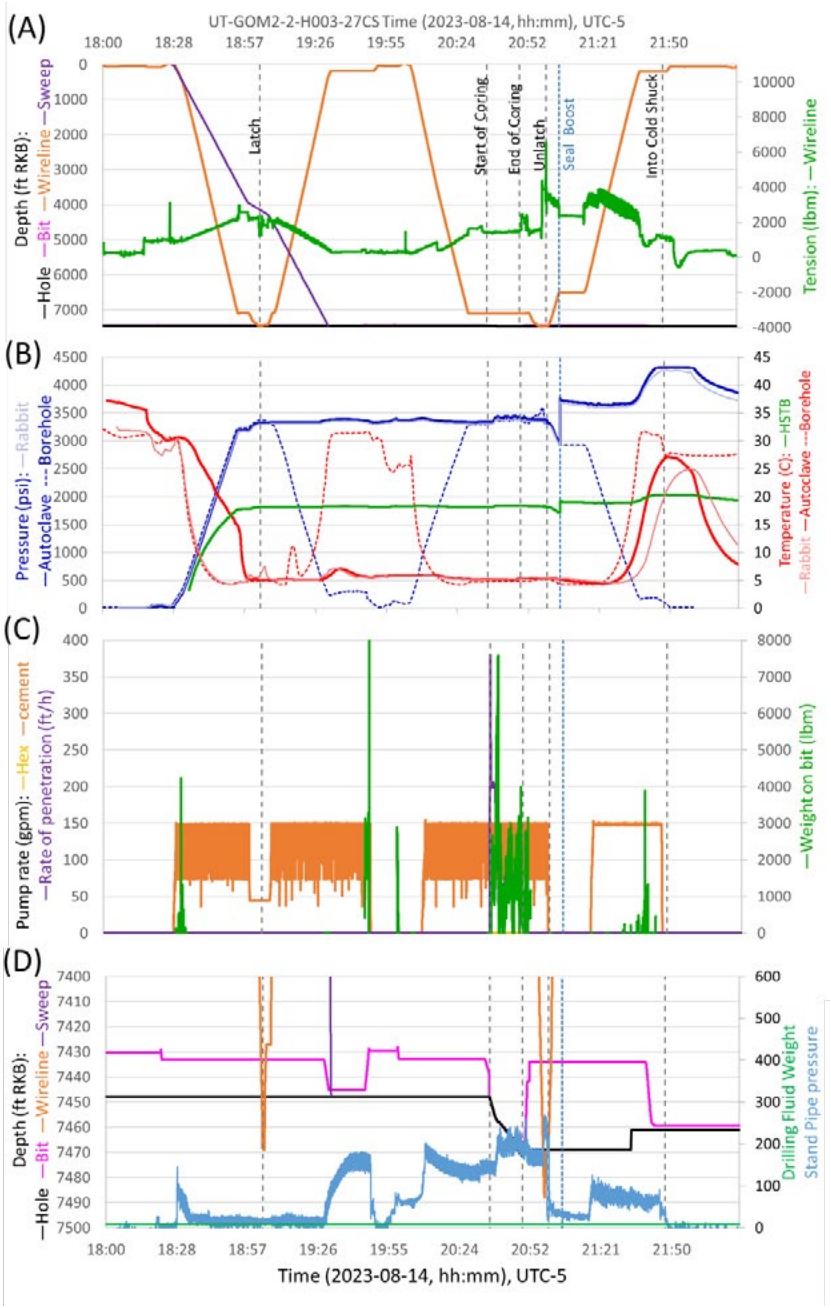

Figure F10: UT-GOM2-2-H003-27CS coring data A) Wireline tension (solid green line), wireline tool depth (solid orange line), bit depth (magenta line), hole depth (solid black line), high-viscosity sweep depth (solid purple line), and seafloor (solid light blue line). We assumed the high-viscosity sweep entered the pipe just as the core barrel was being deployed and calculated the sweep depth from the pump rate. Vertical dashed lines that cut through A, B, C, and D show specific points in the pressure coring deployment. Controlled points including latch, start of coring, end of coring, unlatching, and placing the lower section of the core barrel into the cold shuck are shown as dark gray dashed lines. Resulting points of autoclave sealing and pressure boost are shown as dashed aqua blue lines or a single dashed aqua blue line if concurrent; B) Autoclave pressure (solid blue line), core pressure (solid light blue line), pipe pressure (dashed blue line), autoclave temperature (solid red line), approximate core temperature (solid pink line), and pipe fluid temperature (dashed red line). Measured pressure and temperature values for the core, autoclave, and pipe are from pressure and temperature sensors on data storage tags (DST) in the autoclave IT-plug, autoclave rabbit, and wireline sinker bar, respectively (Figure F9). The hydrate stability temperature boundary (HSTB, solid green line) is the upper limit of the temperature calculated from the autoclave pressure assuming seawater salinity (3.5% NaCl). Any hydrate present in the core will be stable if core temperature stays below the boundary (solid green line) and may remain stable even if it crosses the boundary for several minutes; C) Cement (CMT) pump rate (solid orange line, Hex pumps were not used in this time), weight on bit (WOB, solid green line) is calculated from hook load (See Weight on bit for a discussion WOB), and instantaneous rate of penetration (ROP, solid purple line); D) Zoomed in wireline tool depth (solid orange line), bit depth (magenta line), hole depth (solid black line), high-viscosity sweep depth (solid purple line) from A, plus standpipe pressure (solid light blue line), and drilling fluid weight (solid green line).

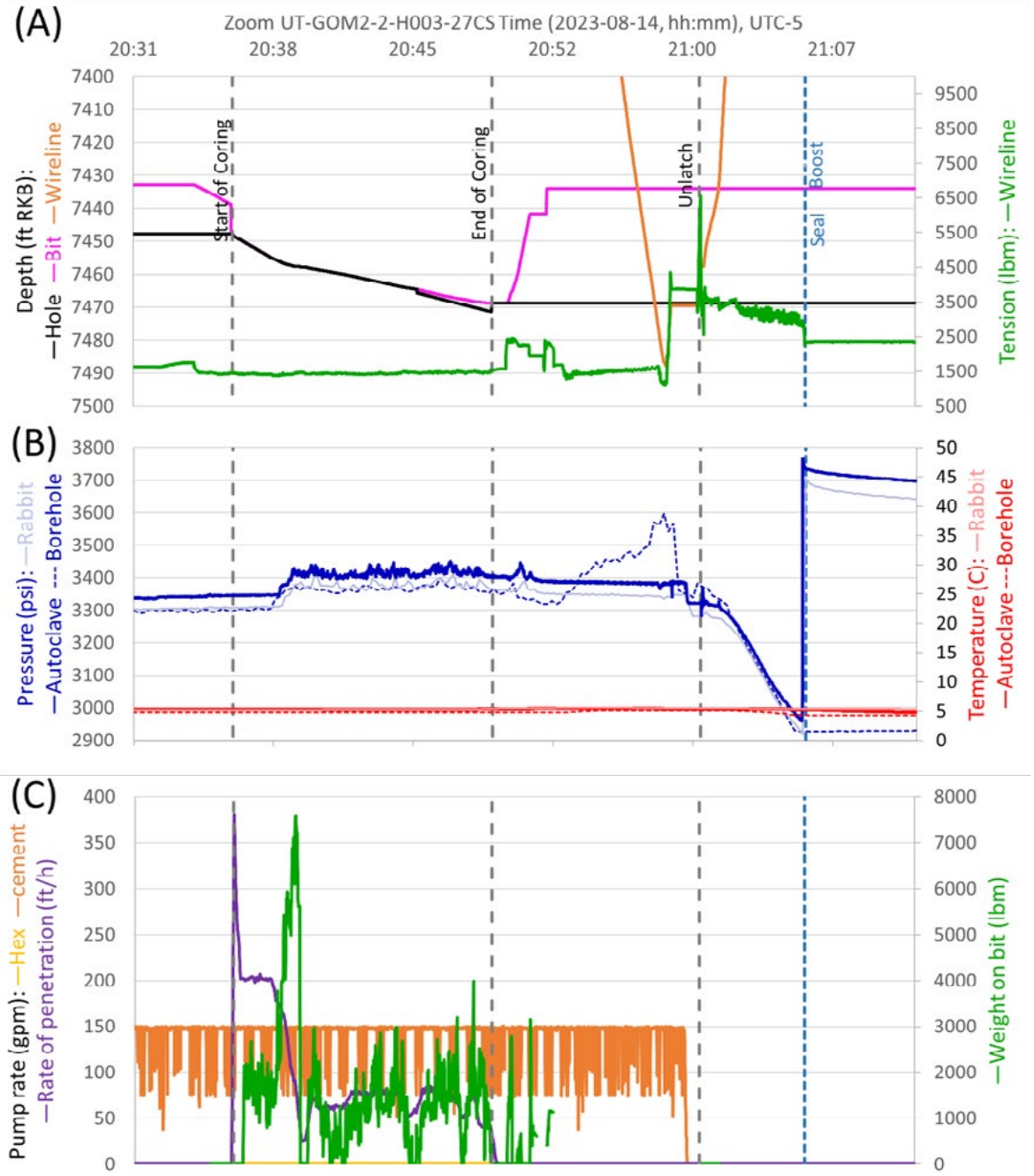

Figure F11: Expanded view of UT-GOM2-2-H003-27CS coring data. A) Wireline tension (solid green line), wireline tool depth (solid orange line), bit depth (magenta line), hole depth (solid black line). A wireline tool depth of 0 ft is above the rig floor and does not correspond to 0 ft RKB of the hole or bit. We assumed the high-viscosity sweep entered the pipe just as the core barrel was being deployed and calculated the sweep depth from the pump rate. Vertical dashed lines that cut through A, B, C, and D show specific points in the pressure coring deployment. Controlled points including latch, start of coring, end of coring, unlatching, and placing the lower section of the core barrel into the cold shuck are shown as dark gray dashed lines. Resulting points of autoclave sealing and pressure boost are shown as dashed aqua blue lines or a single dashed aqua blue line if concurrent; B) Autoclave pressure (solid blue line), core pressure (solid light blue line), pipe pressure (dashed blue line), autoclave temperature (solid red line), approximate core temperature (solid pink line), and pipe fluid temperature (dashed red line). Measured pressure and temperature values for the core, autoclave, and pipe are from pressure and temperature sensors on data storage tags (DST) in the autoclave IT-plug, autoclave rabbit, and wireline sinker bar, respectively (Figure F9). The hydrate stability temperature boundary (HSTB, solid green line) is the upper limit of the temperature calculated from the autoclave pressure assuming seawater salinity (3.5% NaCl). Any hydrate present in the core will be stable if core temperature stays below the boundary (solid green line) and may remain stable even if it crosses the boundary for several minutes; C) Cement (CMT) pump rate (solid orange line, Hex pumps were not used in this time), weight on bit (WOB, solid green line) is calculated from hook load (See H for a discussion WOB), and instantaneous rate of penetration (ROP, solid purple line).

https://doi.org/10.5281/zenodo.13971228

compared to other deployments (See Site H: Pressure coring operations (Flemings et al., **2025b**)). The tool was removed from the pipe and the lower half was placed in a cold shuck on the rig floor. Assuming the rabbit DST was tracking the approximate core temperature, core H003-27CS temporarily rose above the hydrate stability temperature boundary (Figure **F10**, row B solid green line).

After chilling in the cold shuck, the lower half of the core barrel was transported by crane to the PCTB service van, the autoclave was pressure isolated and separated from the core barrel. At this point the pressure in the autoclave was measured for the first time (the recovery pressure) using a pressure gauge at 3,531 psi. Additional pressure boosts may be applied to the autoclave by hand to guarantee the pressure is maintained at this time. The autoclave was prepared for core transfer to PCATS by installing the PCATS adapter onto the autoclave and the autoclave was placed in an ice bath. The autoclave was then moved to the PCATS laboratory (See **Pressure core processing**). A record of each deployment was logged (Figure **F12**). See the methods for assessing Pressure coring results for more information on core recovery, operational setting for each deployment, and assessment of the pressure coring tool performance.

Conventional coring tools

Two conventional downhole coring tools were deployed, the Advanced Piston Corer (G-APC) and the Extended Core Barrel (G-XCB). Both the G-APC and the G-XCB are compatible with the PCTB BHA in the PCTB-CS configuration (See **BHAs and bits**).

Advanced Piston Corer

The G-APC cores relatively undisturbed samples from very soft sediments at the seafloor to sediments of medium stiffness. The G-APC cuts cores that are 2.4 inches (62.0 mm) in diameter. The cores are contained in a plastic liner with an inner diameter of 2.6 inches (66.3 mm) an outer diameter 2.8 inches (71.4 mm), and up to 31 ft (9.5 m) long. The cores are collected using a hydraulically actuated piston corer that is thrust through the Cutting Shoe bit.

During UT-GOM2-2, a temperature tool was often deployed with the piston core to record in situ formation temperature, see **Advanced Piston Corer Temperature Tool** below.

The G-APC consists of an upper and lower section held together by shear pins (Figure **F13**, column A). The upper section has 4 speed control valves. Various configurations of shear pins and speed control valves are used to adjust the velocity in which the tool enters the sediment.

The G-APC Cutting Shoe was adapted by Geotek with the option to install small knife edges or chisels inside the shoe (Figure **F14**). These edges were designed to cut two grooves opposite each other along the outer edge of the core to create a path for expanding gases to escape as a safety mechanism for handling very gassy cores expanding within the core liner.

Extended Core Barrel

The G-XCB is deployed when the sediments become too stiff to piston core, often referred to as piston coring refusal. The G-APC bit cuts cores of 2.3 inches (58.5 mm) diameter. Like the G-APC, cores are contained in a plastic liner with an inner diameter of 2.6 inches (66.3 mm) an outer diameter 2.8 inches (71.4 mm), and up to 31 ft (9.5 m) long. Unlike G-APC, the core is cut with rotation while pumping drilling fluid. Thus, the G-XCB core likely contains more contamination from drilling mud and is often twisted into biscuits surrounded by a slurry of soft sediment, which can make physical property, chemistry, and microbiology sampling more challenging.

The G-XCB is a rotary coring tool consisting of an upper core barrel with latch and compression spring and a lower core barrel with the Cutting Shoe (Figure **F13**, column B).

Conventional coring tool deployments

The number of G-APC shear pins (Figure **F13**, column A, shear pins) and number of closed speed control valves (Figure **F13**, column A, seal vents) are set to achieve the desired speed/force of the tool stroke.

GEOTEK CORING Inc
3350 West Directors Row, Suite 600
Salt Lake City, Utah, 84104 USA
+1 385-528-2536 | info@geotekcoring.com | geotekcoring.com

CORE NO.:		REVISION NO.:	0

CORING RUN REPORT
GOM2-2 2023 CORING PROJECT

DATE:		CORE:	
TOOL ASSEMBLY TEAM:			
EXPECTED BOTTOM CORE DEPTH		APPROXIMATE BOTTOM HOLE PRESSURE:	
PRESSURE SECTION ASSEMBLY NUMBER:		AUTOCLAVE ASSEMBLY NUMBER:	
		CATCHER KIT:	
DST SERIAL NUMBERS:	LINER LENGTH ADJUSTER:	RABBIT:	
NOTES:			

TOOL ASSEMBLY

BUILD CHECKLIST		AUTOCLAVE PRESSURE TEST	
LINER/IT PLUG LENGTH (156.75")		To test, pressurize assembled autoclave to 3000 psi (+/- 100 psi). Record this *INITIAL* pressure below. Wait five minutes to allow for acclimitization. During this time inspect for gross leakage of water or significant pressure drop. If leaks or pressure loss are observed, rectify and retest. At five minutes, record *START* pressure. Wait 10 minutes, then observe and record *END* pressure. If pressure loss >60 psi is observed, the test is considered a failure and should be repeated.	
SET PRESSURE (CONFIRM WITH 3 TESTS):			
RESERVOIR PRESSURE:			
SUPPLY VALVE OPEN			
FILL VALVE CLOSED/PORT PLUGGED		TEST 1	
SET VALVE CLOSED/PORT PLUGGED		DATE:	INITIAL:
DRAIN VALVE CLOSED/PORT PLUGGED		START TIME:	START:
SHUTOFF VALVE OPEN			END:
SAMPLE PORT CLOSED/PORT PLUGGED		TEST 2 (IF REQUIRED)	
BUILD NOTES		DATE:	INITIAL:
		START TIME:	START:
			END:

CORING RUN

DATE:				TOOL DEPLOYMENT TIME:		
START DEPTH:	END DEPTH:			ANTICIPATED RECOVERY:		
CORING START TIME:				CORING END TIME:		
FLOW RATES	RUNNING IN:		DRILL PARAMETERS		WIRELINE PULL	
	CORING:		W.O.B.:	R.P.M.:	MAX PULL:	
	PULLING:				SPEED:	
	P.O.O.H.:		COLD SHUCK:	TIME IN:		TIME OUT:
TOTAL TIME IN HOLE:				TIME ON DECK:		
				TOTAL TIME CORING:		
NOTES:						

CORE TRANSFER & RECOVERY

RECEIVED FROM RIG FLOOR	DATE: TIME:		GAUGE PRESSURE:		
SHUTOFF VALVE CLOSED	PRESSURE DRAINED; DRAIN VALVE AND PORT CLOSED				
PLACED IN ICE BATH	DATE:	N/A	TRANSFERED TO PCATS	DATE:	N/A
	TIME:	N/A		TIME:	N/A
SUCCESSFUL PRESSURIZED TRANSFER?			TOTAL CORE RECOVERY: RECOVERY PERCENTAGE:		
NOTES:					

POST-CORING TOOL ANALYSIS & REBUILD (AS REQUIRED)

Note irregularities, potential problems, or other issues found in the tool after the coring cycle is complete (if any)
NOTES:

Figure F12: Pressure coring run report

 https://doi.org/10.5281/zenodo.13971228

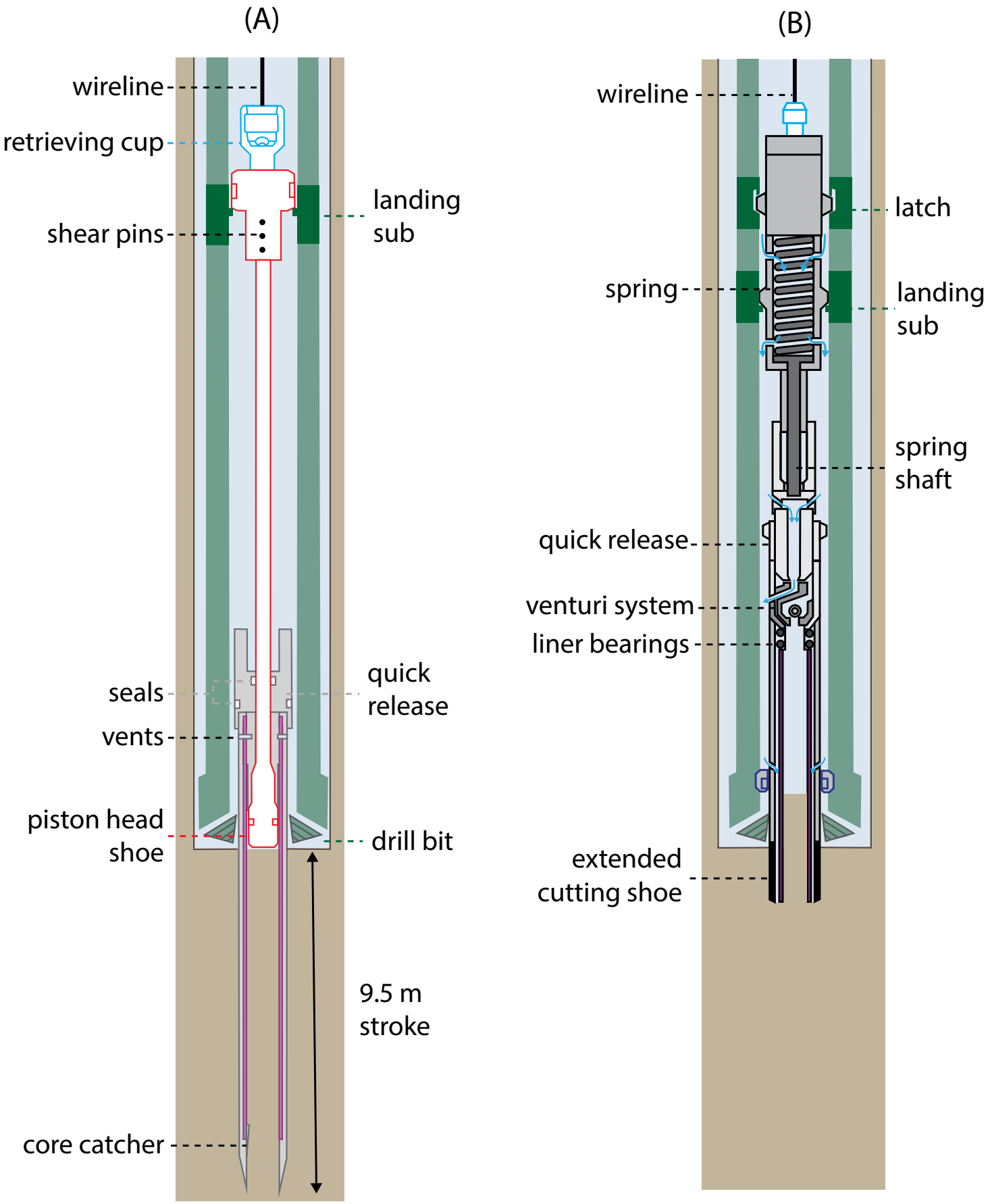

Figure F13: Schematic of conventional coring tools used in expedition UT-GOM2-2: A) Advanced Piston Corer (G-APC) is driven into the formation by compressing the fluid inside the drill string and breaking the shear pins; B) The Extended Core Barrel (G-XCB) is a rotary coring system that locks into the BHA and rotates with the drill string. Sketch is not to scale.

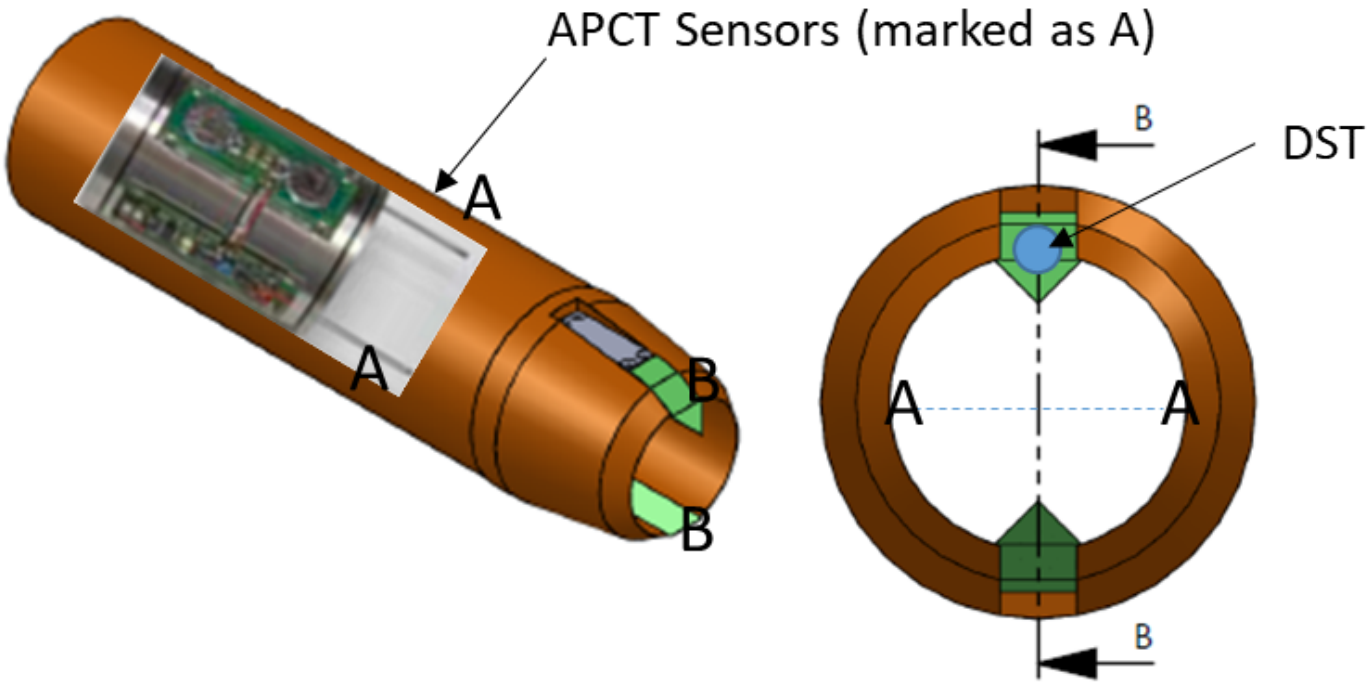

Figure F14: Optional chisels in the G-APC cutting shoe. Sketch is not to scale.

The G-APC is lowered by wireline into the BHA while pumping seawater downhole. Upon landing in the BHA, the speed control valves (seal vents) on the exterior of the tool occlude flow from the BHA causing pressure to build, shearing the shear pins, and firing the tool out of the BHA and into the sediment. When the core barrel reaches the end of its stroke (9.5 m or 31 ft), the core barrel is pulled out of the sediment using the top drive and retrieved from the BHA via wireline.

The G-XCB is deployed by freefall into the drill string and pumped downhole until it latches into the BHA. If adverse conditions exist, the G-XCB can also be deployed via wireline. Upon latching the G-XCB into the BHA the drill string is advanced by rotating the bit (up to 9.5 m). The G-XCB Cutting Shoe protrudes from the BHA and cuts the core ahead of the main bit. This combined with the tool's upper compression spring (Figure F13, column B, spring) reduce disturbance to the core sample during bit advancement. Once the coring interval is completed the G-XCB is retrieved to surface with wireline.

Once the G-APC or G-XCB coring tool is back on deck, the operational processes for the two tools are the same. A tugger is used to lift the coring tool from the drill string and allow the upper part of the tool to be disassembled from the lower part, where the core lies. The lower part of the tool is laid out and transported via crane to the outside of the Geotek van (Figure F15). There, the core catcher and core inside the core catcher are removed. The seal subassembly is then broken, and the core is removed from the metal barrel. See **Conventional coring results** for more information on core recovery, operational setting for each deployment, and assessment of the conventional coring tool performance.

Advanced Piston Corer Temperature Tool

The Advanced Piston Corer Temperature tool (APCT-3) is an instrumented coring shoe owned by and on loan from the International Ocean Discovery Program (IODP) and integrated with the G-APC to measure temperature.

The APCT-3 fits into an internal pocket of the G-APC coring shoe (Figures F16 and F17), and consists of a battery pack, a data logger, and a temperature probe (Figure F17). Detailed descriptions of the tool can be found in Heesemann et al. (2006).

https://doi.org/10.5281/zenodo.13971228

Figure F15: Image of the lower part of the Advanced Piston Corer conventional coring tool being moved from the drill floor to the Geotek Core Receiving mobile lab.

The APTC-3 temperature determination process is described in In-situ temperature.

APTC-3 calibration

We conducted an APCT-3 validation procedure on board in which we compared the APCT-3 values against a digital thermometer. Four comparison points were measured, from ~5 °C inside an ice bucket to an ambient temperature of ~ 30 °C. APCT-3 and thermometer values follow a 1:1 slope (Figure F18) within the expected resolution (APCT-3: 0.02 °C, digital thermometer: 0.1 °C). Discrepancies in the measurement with ice are attributed to the digital thermometer probe directly contacting an ice crystal.

Temperature Dual Pressure Penetrometer

T2P design

The Temperature Dual Pressure Penetrometer (T2P) is a slim penetrometer tool developed by UT to evaluate in situ fluid pressure, hydraulic conductivity, and temperature in silt- and clay-dominated sediment (Flemings et al., 2008a; Flemings et al., 2008b). The T2P is ~2 m long and decreases in diameter from ~69 mm at the top to a narrow tip of 6 mm in diameter (Figure F19). The T2P measures pressure at two different locations using pressure transducers: the tool tip and at 21 cm up-probe from the tip (i.e., the shaft). This allows us to obtain two different dissipation rates with two different tool diameters, which can be used to infer in situ pressure more rapidly than if only one sensor was used. The temperature in the T2P is only measured at the tip (Flemings et al., 2008a; Flemings et al., 2008b; Whittle et al., 2001). The probe is driven into the sediment and left in place while measuring the dissipation of temperature and pressure. During UT-GOM2-2, the

(A)

(B)

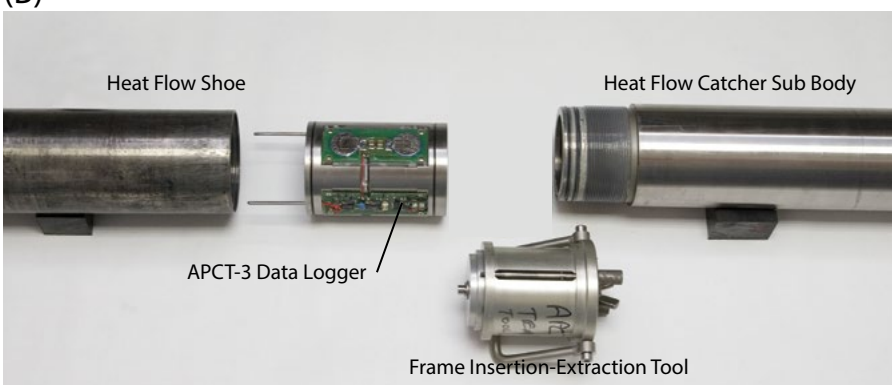

Figure F16: Schematic of the APCT-3 location in the G-APC tool. Figure is not to scale. The temperature sensor is located inside the cutting shoe and measures temperature within the sediment.

T2P was only deployed for a test in the water column and not deployed in the sediment.

Pressure and temperature are recorded internally by the Common Data Acquisition system in the T2P (sampling frequency = 1 Hz). Acceleration (sampling frequency = 12 Hz) in all directions is also measured to monitor tool deployment steps and may help troubleshoot unexpected tool responses based on deployment procedures. In the UT-GOM2-2 expedition, we assembled two identical T2P probes identified as T2P-1 and T2P-2.

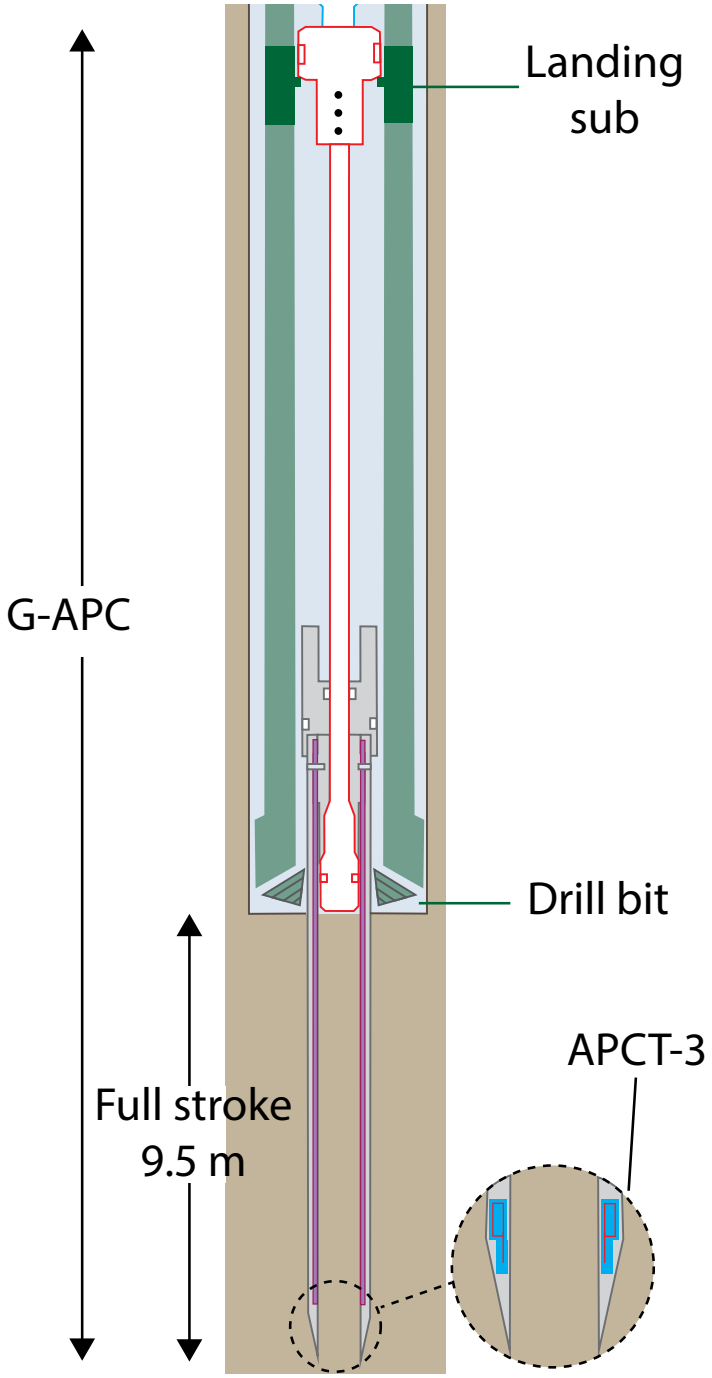

Figure F17: (left) Photos of the APCT-3 and APCT-3 peripherals. A) The APTC-3 is housed within the G-APC cutting shoe (Figure F16); B) APCT-3 with peripherals. The APCT-3 data logger fits into an internal pocket of the G-APC heat flow cutting shoe. The heat flow catcher sub body seals this pocket and prevents water infiltrating the data logger. The frame insertion-extraction tool is used to retrieve and insert the data logger.

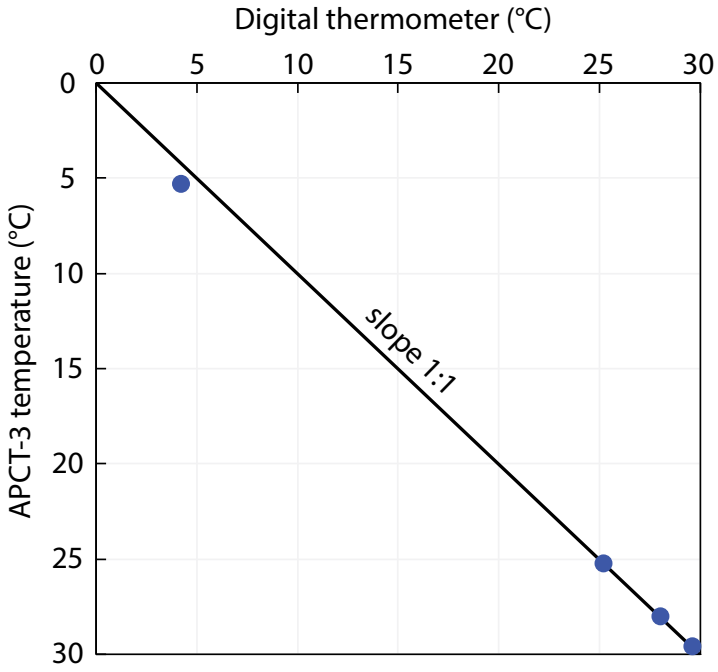

Figure F18: A comparison of the APCT-3 and digital thermometer measurement. The two sensors measure similar temperature values.

T2P-1 pressure test

All pressure transducers were calibrated against a known pressure standard at UT before the expedition. Once deployed, the T2P-1 was assembled, and a pressure test was conducted to ensure the functionality of the probe transducers and data acquisition. These tests were intended to verify transducer readings upon external pressure perturbations and confirm the hydraulic seals within the T2P were performing correctly.

Figure F20 shows the pressure and temperature response during this test. T2P-1 was placed inside a pressure chamber and filled with water (Figure F20, Time 0). The system was allowed to thermally equilibrate for ~2 hours before increasing the pressure with an air pump. At ~124 min, the tip pressure response to the abrupt increase in pressure was captured (Figure F20, Time 124). The shaft pressure

https://doi.org/10.5281/zenodo.13971228

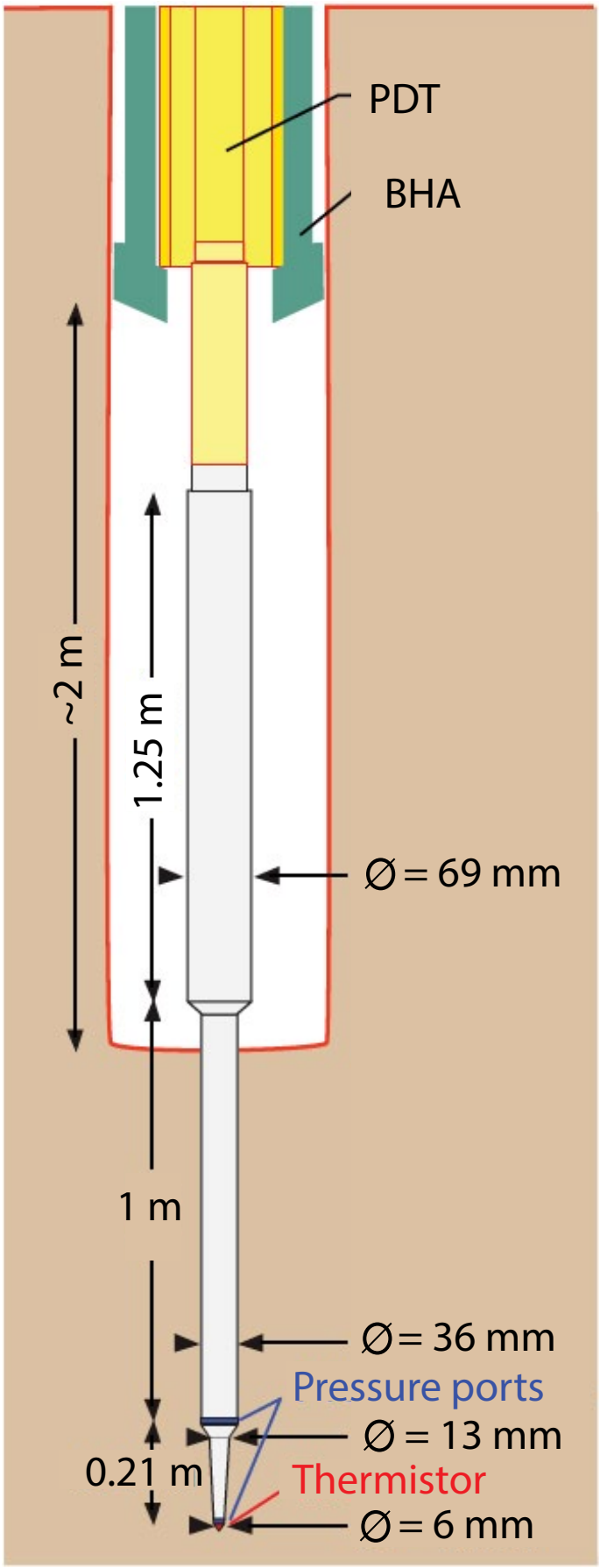

Figure F19: Important components of the Temperature Dual Pressure Penetrometer (T2P) and Penetrometer Deployment Tool (PDT). ϕ = diameter. Sketch is not to scale.

was not captured, indicating a loose connection in the assembly. The tip pressure responded to a gradual decayed in the chamber pressure as trapped air inside chamber dissolved (Figure F20, Time 124-137). At 137 min, the chamber started to leak. Around that time, we also were able to capture data from the shaft again. It is unclear if higher pressures caused the disconnect. Both the shaft and tip pressures return to the original readings.

Despite the failure to properly collect the shaft data, we proceeded with the deployment of the tool for a test in the water column. The tool was never deployed in the formation. See Site H report (Flemings et al., 2025b).

T2P-2 ice bath test

All thermistors were calibrated against a known temperature standard at the International Ocean Discovery Program at Texas A&M University. T2P-2 was assembled onboard and placed in an ice bath to confirm the thermistor's capability to rapidly respond to temperature changes and the correct operation of the data acquisition system. Figure F21 shows the temperature response for the ice bath test. Temperature decreases immediately after the T2P-2 tip and shaft are placed inside the ice bath at time zero. The temperature sharply approached the expected ~0 °C. The pressure in the tip gradually decreases while the temperature in the shaft increases. We interpret these effects are due to the thermal contraction of the tip and shaft system. These changes are small and should not impact any in-situ pressure measurements. We have not determined why the pressure transducers respond in opposite directions. At 25 min, we removed T2P-2 from the ice bath and the temperature increases toward the ambient conditions.

Penetrometer Deployment Tool (PDT)

T2P deployments are run with a wireline using the Penetrometer Deployment Tool (PDT). The PDT decouples the T2P probe from the drill string, minimizes heave effects, and maintains the T2P vertical during deployment. The PDT is an update

of the Motion Decoupled Hydraulic Delivery System previously used to deploy the T2P (Flemings et al., 2013).

T2P-PDT Deployment Protocol

The deployment procedure first involves connecting the T2P to the bottom of the PDT as the final step of the PDT assembly. The T2P-PDT assembly is hung on the top of the drill string on the rig floor with a lifting clamp. The Running Pulling Tool (RPT) is latched into the PDT-T2P assembly. The bit is then raised 2 m above the bottom of the borehole, and the RPT-PDT-T2P assembly is lowered downhole. Hydrostatic reference measurements are made at two locations, approximately 200 m above the seafloor and at the seafloor.

The RPT-PDT-T2P assembly is landed in the BHA. Landing is confirmed by loss of approximately 875 pounds of weight on the wireline as the RPT is then raised up approximately 20 m while the PDT-T2P remains in the BHA. Circulation is then initiated until the drilling string pressure is brought up to approximately 400 psi, the pressure required to advance the T2P into the formation. Once the T2P is in the formation, the bit is raised an additional 2 m above the bottom of the borehole and circulation is stopped. The T2P remains in the formation for 30-90 minutes while maintaining the bit and wireline positions. This time allows measurement of pressure dissipation and thermal pulses created by inserting the probe into the formation. After the waiting period and the measurement is complete, the bit is raised an additional 6m above the bottom of the borehole. The RPT is then lowered via the wireline and latched into the PDT. The full RPT-PDT-T2P assembly is slowly picked up via the wireline as confirmed by the wireline weight, and the full assembly is raised to ~200 m above the seafloor. At ~200 m above the seafloor, another hydrostatic reference check measurement is made (~2 minutes, no circulation). The RPT-PDT-T2P assembly is then pulled back to the rig floor where the RPT is disconnected after the PDT-T2P is landed on top of the drill pipe with the lifting clamp. Then the PDT-T2P is lifted from the drill pipe and laid down on the rig floor to allow the T2P to be disconnected so the probe data can be downloaded.

Gyroscope

Borehole deviation data was acquired by SLB Gyrodata using their Omega Memory Gyro system.

https://doi.org/10.5281/zenodo.13971228

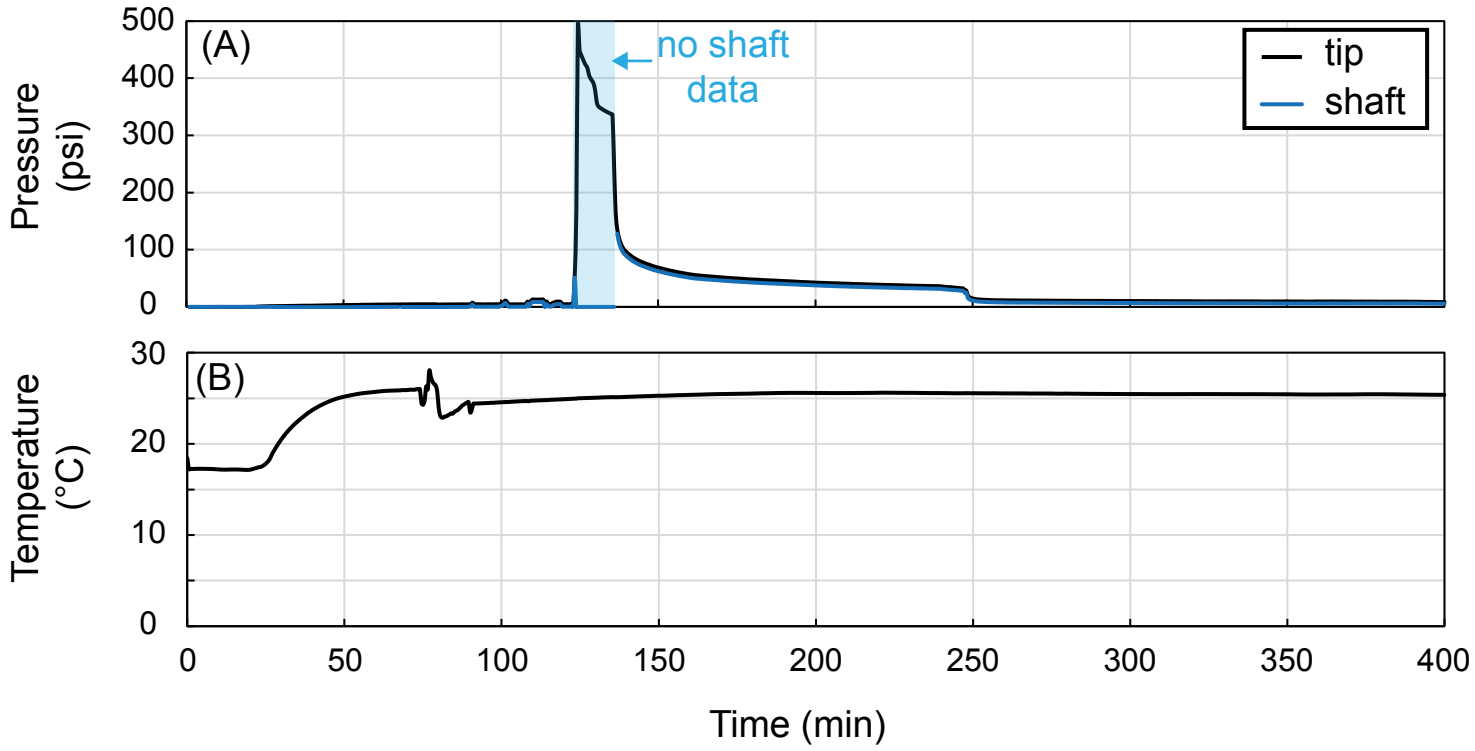

Figure F20: T2P-1 functioning test inside a pressure chamber. The pressure in the shaft (blue) stops responding as the pressure is increased with an external air pump.

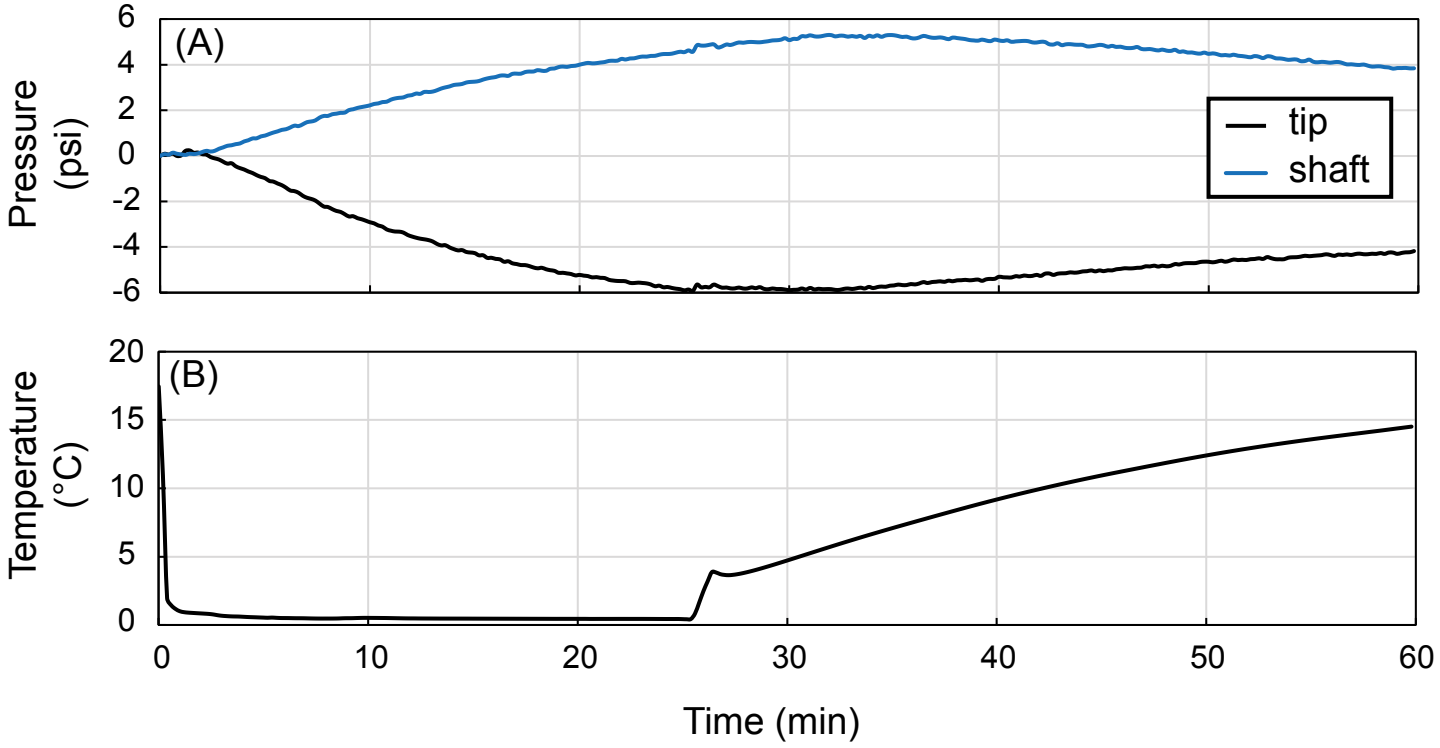

Figure F21: T2P-2 calibration test using an ice bath.

Geotek Ltd. scientist Andrew Goodridge watches several output monitors while the Geotek pressure core and transfer system (PCATS) logs and images a pressure core. Photo credit: Geotek Ltd.

Coring assessment

This section discusses the methods used for coring tool performance assessments. The PCTB is discussed first in **PCTB core recovery**, **PCTB operations**, and **PCTB performance assessment**. Conventional coring tools are discussed in **Conventional coring tool recovery and operations** and **G-APC coring tool performance assessment**.

Coring deployments were tracked using a coring plan worksheet (Figure **F22**). The archived record of the worksheet was marked "as drilled". Core deployments were entered into the Core Log (Figure **F23**).

Pressure coring results

The PCTB tool design is described in **Pressure Coring Tool with Ball Valve**. The PCTB was used during UT-GOM2-2 to collect and maintain cores at or above in situ pressure from hydrate-bearing coarse-grained sediments and bounding and background mud intervals. During pressure coring, the core is ideally sealed inside the coring tool autoclave at the coring depth immediately after the core has been cut. During UT-GOM2-2, pressure cores were collected using both configurations of the tool.

PCTB core recovery

Coring log, PCTB deployment parameters discussed in **Pressure Coring Tool with Ball Valve**, and rig data were used to assess the core recovery for each deployment of the PCTB. The list of parameters reported, and the

 https://doi.org/10.5281/zenodo.13971228

CORING PLAN:	GOM2-2 H002	Aug 2023
DATE		

Notes:
Water Depth -
RKB Height above sea surface -
RKB - Seafloor -

Technical Notes:

CORE Top fbsf	CORE Bottom fbsf	Advance (ft)	Bottom of Hole - RKB ft	Start Coring Bit Depth RKB ft	G-APC Bit Height off hole	No.	Coring Comments	Target Depth ft	Targets Comments	Curated length ft	Recovery (%)	In situ Pressure PSI	Recovery Pressure PSI	Recovery Pressure Bar	curated length (m)	Date/ Time	Results Comments
									TOTALS TO DATE								

Figure F22: Coring plan worksheet/log

(A)

Area	Site	Hole	Core	Core type	Core Name	Depth top of interval (fbsf)	Depth of top interval (mbsf)	Curated (m)	Core throw (m)	% of throw	length of expansion (m)	% expansion	Compression factor
WR313	H	003	1	H	H003-01H	0	0.000	7.690	8.230	0.934	0.000	0.000	N/A
WR313	H	003	2	H	H003-02H	27	8.230	10.050	8.534	1.178	1.516	17.759	0.849
WR313	H	003	3	H	H003-03H	61	18.593	10.220	8.534	1.198	1.686	19.751	0.835
WR313	H	003	4	CS	H003-04CS	89	27.127	3.250	3.048	1.066	0.202	6.627	0.938

(B)

Area	Site	Hole	Core	Core type	Section	Piece	Piece interval top (cm)	Piece interval bottom (cm)	Piece Name	Sample code	Compression factor	Compressed depth in core top piece (m)	Compressed depth in core bottom piece (m)	Archived depth top of piece (mbsf)	Archived depth bottom of piece (mbsf)	Compressed depth top of piece (mbsf)	Compressed depth bottom of piece (mbsf)
WR313	H	003	1	H	1	a	0	95	H003-01H-1a, 0-95 cm,		N/A	0.000	0.950	0.000	0.950	0.000	0.950
WR313	H	003	1	H	1	b	95	115	H003-01H-1b, 95-115 cm, MDW	MDW	N/A	0.950	1.150	0.950	1.150	0.950	1.150
WR313	H	003	1	H	1	c	115	130	H003-01H-1c, 115-130 cm, MB	MB	N/A	1.150	1.300	1.150	1.300	1.150	1.300
WR313	H	003	1	H	1	d	130	140	H003-01H-1d, 130-140 cm, IWR	IWR	N/A	1.300	1.400	1.300	1.400	1.300	1.400
WR313	H	003	1	H	1	e	140	150	H003-01H-1e, 140-150 cm, IWO	IWO	N/A	1.400	1.500	1.400	1.500	1.400	1.500

(C)

Area	Site	Hole	Core	Core type	Section	Piece	Name	Sample code	Sample top (depth in section, cm)	Sample bottom (depth in section, cm)	Section depth in core (m)	Sample top in core (m)	Sample bottom in core (m)	Compression factor	Compressed sample top in core (m)	Compressed sample bottom in core (m)	Archived sample top depth (mbsf)	Archived sample bottom (mbsf)	Compressed sample top depth (mbsf)	Compressed sample bottom (mbsf)
WR313	H	002	1	FB	1	a1	H002-01FB-1a1, 6-7 cm, GSL	GSL	6	7	0	0.06	0.07	N/A	0.060	0.070	644.712	644.722	644.712	644.722
WR313	H	002	1	FB	1	a1	H002-01FB-1a1, 6-8.5 cm, CNS	CNS	6	8.5	0	0.06	0.085	N/A	0.060	0.085	644.712	644.737	644.712	644.737
WR313	H	002	1	FB	1	b	H002-01FB-1b, - cm, CEL	CEL			0	0.47	0.47	N/A	0.470	0.470	645.122	645.122	645.122	645.122
WR313	H	002	1	FB	1	b	H002-01FB-1b, - cm, PEN	PEN			0	0.47	0.47	N/A	0.470	0.470	645.122	645.122	645.122	645.122
WR313	H	002	1	FB	1	b	H002-01FB-1b, - cm, VANE	VANE			0	0.47	0.47	N/A	0.470	0.470	645.122	645.122	645.122	645.122
WR313	H	002	1	FB	1	b	H002-01FB-1b, 20-21 cm, GSL	GSL	20	21	0	0.2	0.21	N/A	0.200	0.210	644.852	644.862	644.852	644.862
WR313	H	002	1	FB	1	b	H002-01FB-1b, 20-22.5 cm, CNS	CNS	20	22.5	0	0.2	0.225	N/A	0.200	0.225	644.852	644.877	644.852	644.877
WR313	H	002	1	FB	1	b	H002-01FB-1b, 31-32 cm, GSL	GSL	31	32	0	0.31	0.32	N/A	0.310	0.320	644.962	644.972	644.962	644.972
WR313	H	002	1	FB	1	b	H002-01FB-1b, 31-33.5 cm, CNS	CNS	31	33.5	0	0.31	0.335	N/A	0.310	0.335	644.962	644.987	644.962	644.987
WR313	H	002	1	FB	1	b	H002-01FB-1b, 35.5-36.5 cm, GSL	GSL	35.5	36.5	0	0.355	0.365	N/A	0.355	0.365	645.007	645.017	645.007	645.017
WR313	H	002	1	FB	1	b	H002-01FB-1b, 35.5-38 cm, CNS	CNS	35.5	38	0	0.355	0.38	N/A	0.355	0.380	645.007	645.032	645.007	645.032

Figure F23: Tabs of the UT-GOM2-2 Core Log; A) Core log; B) Section-piece log; C) Sample-measurement log; Depths are all measured depth. Measured depths are not vertical depths in Hole H003, because the hole was deviated. Measured depths in Hole H002 are equivalent to vertical depths because the hole was vertical. Archived and Compressed mbsf were calculated using Equations **E3** through Equation **E7** (See **Compressed depths**).

Parameter	Method
Core Top	The top of core is the archived depth for each core in MD. Values can be found on the coring run report (Figure F12), in the coring record (Figure F22), and in the core log (Figure F23).
Core Advance	Reported values can be found on the coring run report (Figure F12), in the coring record (Figure F22), and in the core log (Figure F23). Reported values were also compared against changes in the rig bit and total depth during coring. Notations were made if the core advance calculated from the rig data differed from the reported core advance by more than 20%.
Curated Length	Reported values can be found on the coring run report (Figure F12), in the coring record (Figure F22), and in the core log (Figure F23).
Recovery	Reported values can be found in the core log (Figure F23). The values are the ratio of the curated length to the corer advance. Recovery was determined for the eight cores recovered at elevated pressure using log and imaging data from PCATS. Recovery was determined for cores recovered at atmospheric pressure by visual inspection.
In-situ Pressure	Calculated using an assumed pore pressure gradient of 0.465 psi/ft from ambient pressure at the sea surface (using fbsl).
Recovery Pressure	Reported values were measured with a pressure gauge on the rig floor and recorded on the coring run report (Figure F12).

Table T3: Derived PCTB core recovery results/parameters and the method used to determine their values.

Parameter	Method
Core Top	The top of core is the archived depth for each core in MD. Values can be found on the coring run report (Figure F12), in the coring record (Figure F22), and in the core log (Figure F23).
Start of Coring	The start of coring was determined from the rig data as the point during a coring tool deployment at which the bit depth and total depth start increasing (Figure F11, start of coring).
End of Coring	The end of coring was determined from the rig data as the point during a coring tool deployment at which the bit depth and total depth stop increasing (Figure F11, end of coring).
Drilling Fluid	Reported drilling fluid can be found in the Daily Operations Report
Average Flow Rate	The average flow rate is the average of the rig pump combined flow rates from the start of coring to the end of coring.
Average RPM	The average rotation per minute (RPM) is the average of the rig reported RPM from the start of coring to the end of coring.
WOB	The weight on bit during coring was from the coring run report (Figure F12).
Average ROP	The average rate of penetration (ROP) is the average of the rig reported ROP from the start of coring to the end of coring.
Average Wireline Speed	The average wireline speed in feet per minute is the average of the rig reported wireline velocity while pulling the core barrel up the drill pipe from roughly 6,000 to 500 ft RKB.
Sweep Depth	Sweep Depth was calculated by assuming the sweep entered the pipe just as the core barrel was being deployed. The sweep depth was calculated from the pump rate as a function of time.

Table T4: Derived PCTB operational settings/parameters and the method used to determine their values.

method used to derive each value are shown in Table T3.

PCTB operations

The coring log, PCTB deployment parameters discussed in Pressure Coring Tool with Ball Valve, and rig data were used to compile the operational settings for each deployment of the PCTB. The parameters reported with the method used to derive each one are shown in Table T4.

PCTB performance assessment

Coring log, PCTB deployment parameters discussed in Pressure Coring Tool with Ball Valve, and rig data were used to assess the performance of the PCTB. The list of parameters reported for each assessment with the method used to derive each value are shown in Table T5.

Calculation of the hydrate stability temperature boundary

The hydrate stability temperature boundary is the temperature of the hydrate stability boundary for a given pressure. The temperature boundary was calculated from the autoclave DST pressure measurement assuming seawater salinity (3.5% NaCl). Using Equation E8.

$$Upper\ \ limit\ \ of\ \ temperature\ \ in\ \ C\ \ = 8.53\ \ *\ \ In\ \ pressure\ \ in\ \ MPa - 8.58$$

Equation E8.

The equation was derived from Sloan (1998).

Conventional coring results

Conventional coring tools described in Conventional coring tools were used to collect sediments cores to understand the sediments, physical properties, chemistry, and microbiology of the shallow sedimentary and hydrate system at WR313.

Conventional coring tool recovery and operations

Coring log, conventional coring tool deployment parameters discussed in Conventional coring tools, and rig data were used to assess the core recovery for each deployment of the G-APC and G-XCB. The list of parameters reported from the assessment with the method used to derive each value are shown in Table T6.

G-APC coring tool performance assessment

The G-APC has a stroke of 31 ft (9.5 m). If the BHA was placed at the base of the borehole and the increase in standpipe pressure required to fire the G-APC was fully depleted as the tool fired, then we interpret that the tool stroked 31 ft. (9.5m) through the formation. In practice, to limit the amount of core expansion beyond the core liner, the G-APC is set a short distance above the top of the formation (Table T6, BHA offset).

An example of a G-APC deployment with full stroke is illustrated in (Figure F24, column A). A brief pulse of high pressure is created that drives the piston. The maximum standpipe pressure is the reported firing pressure. The piston is stroked fully and the pressure inside the pipe is released. In contrast, Core H003-25H exhibited incomplete stroke (Figure F24, column B). In this case, after the core was fired, some residual pressure was retained (Figure F24, 9:10-9:12 AM), indicating the tool had not fully stroked.

Parameter	Method
Core Top	The top of core is the measured archived depth for each core in MD. Values can be found on the coring run report (Figure F12), in the coring record (Figure F22), and in the core log (Figure F23).
In-situ Pressure	The in-situ pressure is calculated using a pore pressure gradient of 0.465 psi/ft from ambient pressure at the sea surface (using fbsl).
Boost Setting	Recorded on the coring run report (Figure F12) (See **Pressure coring tool deployments** for a description of the boost pressure).
Seal Depth	The assumed seal depth is the wireline tool depth at the point in time just after coring at which the rabbit (or plug DST pressure if the rabbit DST data was not available) stopped dropping/trending with the pipe pressure (if pipe pressure data were available) or stopped trending/dropping like the pipe pressure was expected to change (if pipe pressure data were not available) (see Figure F10, row A and B, "Seal Boost").
Seal Pressure	The assumed seal pressure is the rabbit DST (or plug DST, if the rabbit DST data was not available) pressure at the point in time just after coring at which the rabbit or plug DST pressure stopped dropping/trending with the pipe pressure (if pipe pressure data were available) or stopped trending/dropping like the pipe pressure was expected to change (if pipe pressure data were not available).
Boosted Pressure	The boosted pressure is the pressure recorded at a point in time just after sealing when the rabbit (or plug DST if the rabbit DST data was not available) records a rapid pressure jump (see Figure F11, row B, Boost).
Recovery Pressure	The recovery pressure is measured with a pressure gauge on the rig floor and recorded on the coring run report (Figure F12)
Ball Valve Closed	If the autoclave sealed, then the ball valve was closed. When the autoclave did not seal, notes about the state of the ball valve can be found on the coring run report (Figure F12) and in the coring record (Figure F22).
Upper Seal Triggered	If the autoclave sealed, the upper seal was considered triggered. When the autoclave did not seal but the ball valve was noted as closed, notes about the state of the upper section can be found on the coring run report (Figure F11) and in the coring record (Figure F22).
Autoclave Sealed	The autoclave was assumed to be fully sealed if the pressure just after coring as measured by the rabbit DST (or plug DST if rabbit DST data was not available) no longer dropped/trended with the pipe pressure and only showed pressure variations expected from tool compliance and temperature swings.
Seal Pressure vs In-situ Pressure	The seal pressure is compared to the in-situ pressure to determine if the autoclave sealed close to in-situ pressure.
Core Pressure and Temperature vs. the Hydrate Stability Boundary	The assumed temperature and pressure history of the core is the pressure and temperature recorded by the rabbit DST. The hydrate stability temperature boundary is calculated for each pressure data point (See **Calculation of the hydrate stability temperature boundary**) and plotted in Figure F10 B as a solid green line.

Table T5: Derived PCTB assessment parameters and the method used to determine their valves.

https://doi.org/10.5281/zenodo.13971228

Parameter	Method
Core Top	The top of the core is the measured or archived depth for each core in MD. Values can be found in the coring record (Figure F22) and in the core log (Figure F23).
Cored interval	The cored interval can be found in the coring record (Figure F22) and in the core log (Figure F23).
Recovered Length	The recovered length can be found in the coring record (Figure F22) and in the core log (Figure F23).
Recovery	The recovery is the ratio of the recovered length to the cored interval. The values can be found in the core log (Figure F23).
Firing Pressure	The firing pressure for the G-APC. Values are determined from the maximum standpipe pressure (See G-APC coring tool performance assessment).
BHA offset	The distance the BHA is set above total depth before firing the G-APC. Values can be found in the coring record (Figure F22).
Shear Pins	The number of shear pins in place before firing. The shear pins together with the speed control valves control the speed/force of the stroke. Reported only for the G-APC. Values can be found in the coring record (Figure F22).
Speed Control Valves	The number of closed flow valves in the G-APC. The shear pins together with the speed control valves control the speed/force of the stroke. Valves can be found in the coring record (Figure F22).

Table T6: Derived G-APC and G-XCB operational and recovery parameters, and the method used to determine their values.

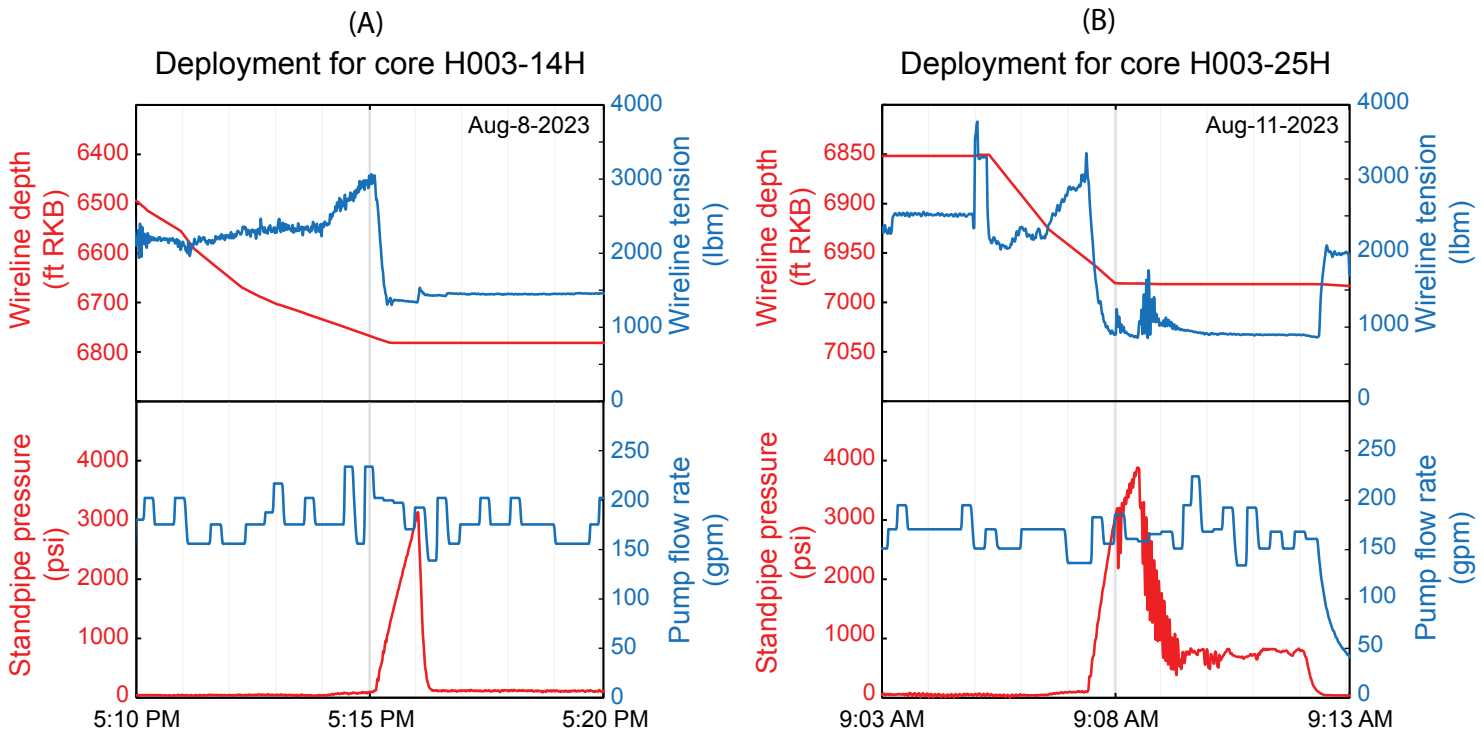

Figure F24: Examples of G-APC deployment recording. (A) a complete stroke in Core H003-14H and (B) an incomplete stroke in Core H003-25H. The top plots show the wireline tool depth (red solid line) and tension (blue solid line) during the deployment of the G-APC. The bottom plots show the corresponding standpipe pressure buildup (red solid line) and the pump flow rate (blue solid line). In A) there is a full stroke and corresponding complete pressure relief. This behavior contrasts with B) where there is incomplete pressure relief after maximum pressure and firing, signaling G-APC refusal and incomplete penetration.

Science party members Melanie Holland of Geotek Ltd., Joel E. Johnson of the University of New Hampshire, and Tim Collett of the U.S. Geological Survey finish processing the first core onboard the Q4000. Photo Credit: Geotek Ltd.

Core processing

This section describes the methods used for processing/curating (e.g., logging, imaging, sampling) cores. Naming conventions are described in **Curation and naming conventions**. PCTB cores are discussed first in **Pressure core processing**, then G-APC and G-XCB cores in **Conventional core processing**. Additional processing of cores in College Station, Texas (but not at Texas A&M University) and at Geotek in Salt Lake City, Utah are discussed in **Core processing in College Station** and **Core processing in Salt Lake City**.

Curation and naming conventions

UT-GOM2-2 adopted conventions similar to IODP for the curation and naming of cores, core sections (Figures **F25** and **F26**), and section pieces.

Cores were numbered sequentially starting at the top of the borehole. Core numbers were suffixed with the coring tool used (CS = PCTB-CS; FB = PCTB-FB; H = G-APC; X = G-XCB). Intervals of drilling without coring were not counted. Thus, Core H003-05CS would be the fifth coring tool deployment and not necessarily the fifth PCTB coring tool deployment, and would not necessarily be just below and adjacent to Core H003-04CS.

If the sediment was expanding beyond the core liner, attempts were made to extend the core liner using core liner extensions. If the core liner could not be extended and sediment spilled out of the top or bottom of the core liner, the sediment was bagged.

The highest retrieved sediment still in the core liner was treated as the core's uppermost point (Figure **F26**, B and C). All sediments and voids recovered in the core liner were regarded as forming a continuous core

 https://doi.org/10.5281/zenodo.13971228

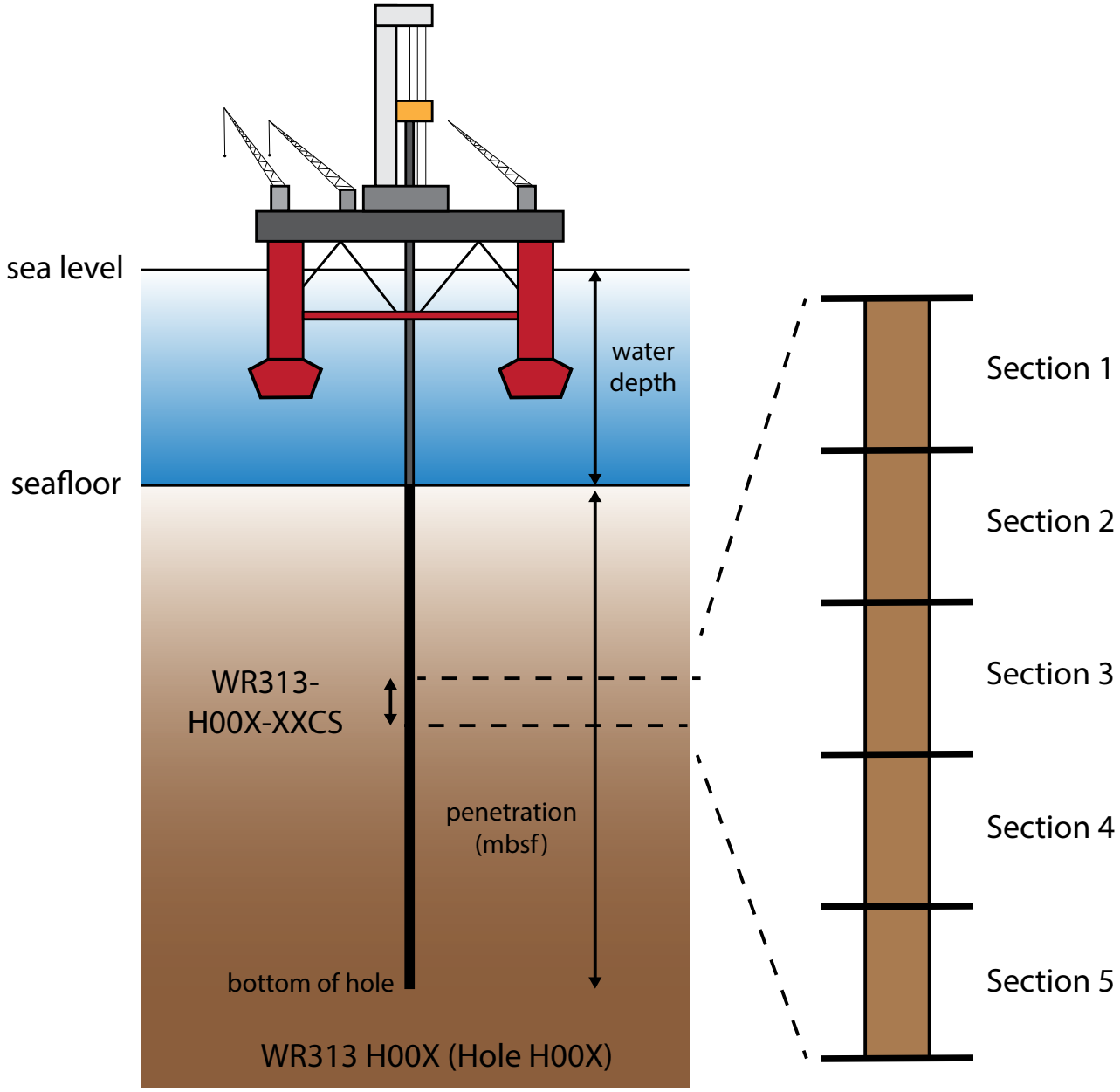

Figure F25: Conventions for naming boreholes, cores, and sections adapted from International Ocean Discovery Program (IODP). The full formal core name includes Walker Ridge Block 313 designation (WR313), hole (H00X), core number (XX), and type of coring tool (CS = PCTB-CS; FB = PCTB-FB; H = G-APC; X = G-XCB) (mbsf, meters below seafloor). Shorter core names without the block designation are used in these proceedings.

(included in the measurement of the core length). This continuous core was sectioned and the sections were numbered sequentially from the top of the core down. To reduce the number of voids, during sectioning, sediment was pushed from the bottom up using pressurized air. Any resulting consolidated void now at the bottom of the section was removed by cutting the core liner into two pieces. Sediment could not always be consolidated, and some voids remained in between intervals of sediment (See **Consolidation of voids**).

If sections were cut into pieces, the pieces were labeled with a letter in alphabetical order from the top of the section down. If any pieces were cut into smaller pieces, these smaller pieces were numbered from the top of the original larger piece down.

Any section, piece, or sample is referenced using all numbers or labels assigned. As an example, consider the sample WR313-H003-29CS-02b, or H003-29CS-02b for short with context. This sample was obtained from the 29th core from Hole H003 in Walker Ridge Block 313. The PCTB-CS tool was used. The core was cut

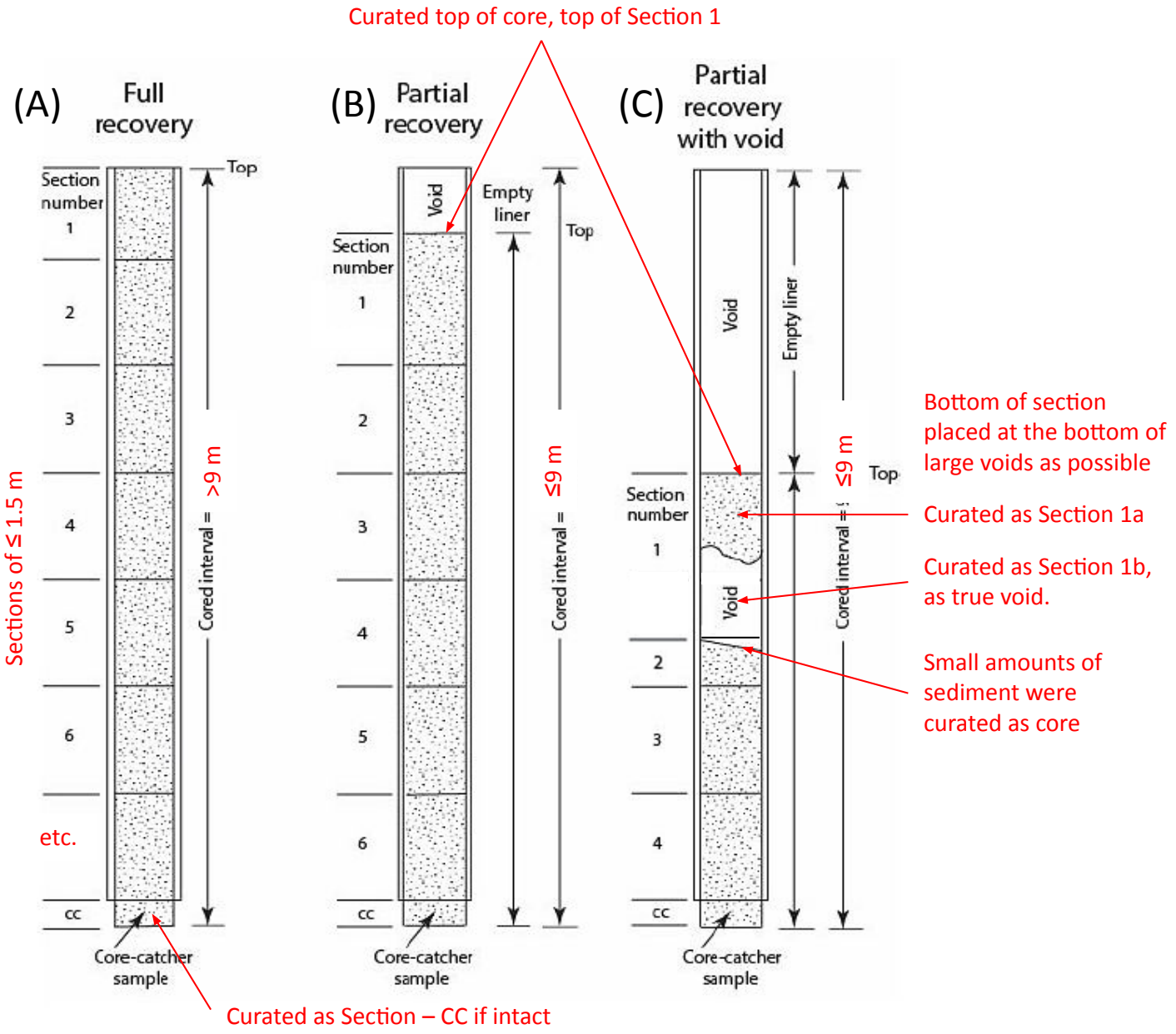

Figure F26: Section numbering and recovery, modified from International Ocean Drilling Program (IODP). Not to scale.

into sections. This sample is from section 2. Section 2 was cut into pieces. The sample is or is from piece b.

Samples and measurements were curated in centimeters measured from the top of each core section. If the sample name is suffixed with a depth interval, the interval is the location of the sample in cm measured from the top of the section down (where 0 cm is the top of the section, archived depth, not compressed depth). If this piece were to be cut into two pieces, they would be labeled H003-29CS-02b1 and -02b2. If no letter occurs after the section number, it can be inferred that the section remains uncut. Similarly, if no number occurs after the piece letter, it can be inferred that the piece was not cut. More examples can be found in **Conventional core processing**.

Pressure core processing

Figure **F27** shows a chart of the PCTB core processing method used during UT-GOM2-2. PCTB core processing was completed onboard the *Q4000* (Figure **F27**, Walker Ridge 313, blue box), in College Station (yellow box), in Salt Lake City (green box), and at UT (Austin, TX, orange box).

PCTB cores recovered above atmospheric pressure (Figure **F27**, pressurized) were kept at their recovered

https://doi.org/10.5281/zenodo.13971228

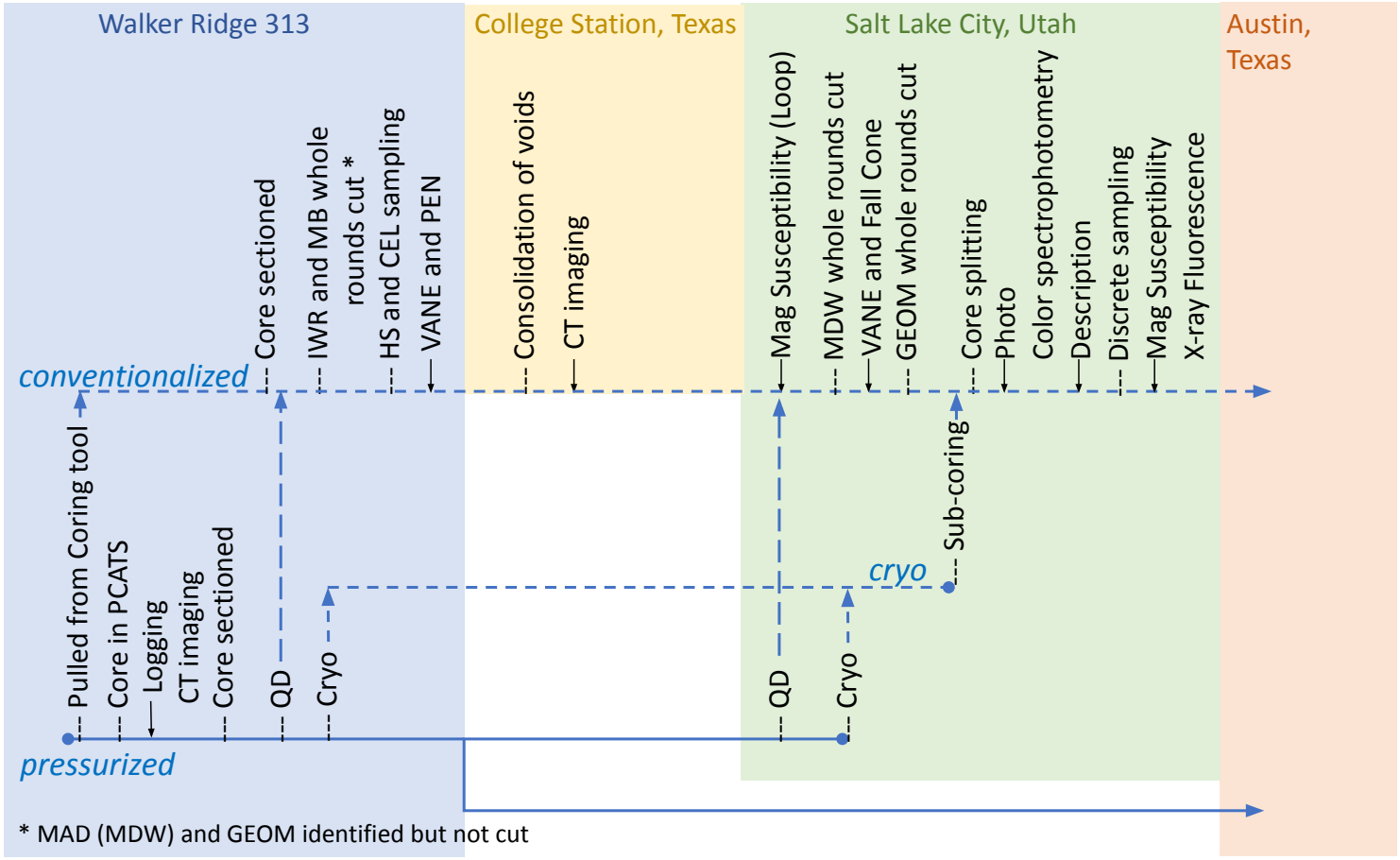

Figure F27: Pressurized, conventionalized (depressurized), and cryo PCTB core processing. Pressurized PCTB cores were logged, imaged using computed tomography (CT), and cut. Conventionalized/ depressurized cores were created when the PCTB did not seal, during quantitative degassing (QD), from rapid depressurization (not shown), or during cryogenic freezing and depressurization (sample code CRYO). These cores were processed, as possible, like conventional cores. Whole-round samples were cut from conventionalized sections for routine pore water (sample code IWR) and microbiology (sample code MB) analysis, and marked for moisture and density (sample code MDW) and geomechanical (sample code GEOM) analysis. Sample were taken from conventionalized sections for headspace gas (sample code HS) and microbial cell counts (sample code CEL). Conventionalized core sections were also measured for undrained strength (measurement code VANE and PEN). In College Station and Salt Lake City, conventionalized core sections were sampled and measured like conventional cores (See **Core processing in College Station** and **Core processing in Salt Lake City**). MDW and GEOM whole-rounds were cut in Salt Lake City.

pressure or higher during storage, logging, and imaging. P-wave velocity and gamma density logs were collected using the Pressure Core Analysis and Transfer System (PCATS) on-board the vessel. Pressurized cores were also imaged using PCATS (See details in **Pressure core logging and imaging**).

PCATS gamma density, P-wave velocity, and computed tomography (CT) data from each pressurized core was used to identify where sections would be cut for rapid depressurization, quantitative degassing, cryogenic depressurization, or transfer to UT. Other factors influencing the cutting plan included the quality of the core, time constraints, lithology, and the availability of storage chambers. Once cut, pressurized sections were stored at elevated pressure (See **Pressure core storage**) until they could be processed further as discussed below.

Pressurized sections, ~1.0 m in length, were cut for transfer to UT (sample code STORE). Chambers for transfer to UT were also equipped with weighted caps above the core liner to prevent the exchange of fluid within the core and between the core and core liner with confining fluid around the liner (See **Pressure core storage**). Sections being transferred to UT were transferred directly to UT and did not go to Salt Lake City.

Pressurized sections, ~1.0 m in length, were cut for quantitative degassing (sample code QD) to

determine the concentration of dissolved methane in muds. Sections of ~ 30 cm sections or less were cut for quantitative degassing to determine the dissolved methane concentration and hydrate saturation in sands (See **Quantitative degassing** and **Dissolved gas and hydrate saturation**). Many, but not all, sections were taken to the Geotek quantitative degassing lab to be quantitatively degassed onboard (Figure **F27**, blue box QD). The rest were transferred to Salt Lake City and quantitatively degassed there (Figure **F27**, green box QD).

Pressurized sections, 20 cm in length were cut and stored for cryogenic freezing before rapid depressurization (sample code CRYO, See **Cryogenically frozen and depressurized whole-rounds** and **Dockside sub-coring for microbiology**). Sections of 5 cm caught in the PCATS grabber were rapidly depressurized and bagged.

PCTB cores recovered at atmospheric pressure and sections depressurized during quantitative degassing were processed as conventional core (Figure **F27**, sometimes called conventionalized or depressurized cores throughout the Proceedings). A few of these cores were put into PCATS and temporarily repressurized with air to try and image them (See **PCATS X-ray imaging**). Whole-rounds were cut from conventionalized sections for routine pore water (IWR) and microbiology (MB) analysis. Whole-round samples were identified for index properties (MAD) and geomechanics (GEOM) but were not cut from the section onboard. Headspace gas (HS) and microbial cell count (CEL) samples were extracted and sediment strength measurements (VANE and PEN, See **Undrained shear strength**) where made (details of the measurement location are shown in **Conventional core processing**). IWR and MB whole-rounds and HS and CEL samples were taken to the appropriate lab (See **Microbiology** for MB and CEL, **Pore water geochemistry** for IWR, and **Headspace gas collection** for HS). The remaining portions of the depressurized sections were stored as conventional core (See **Conventional core storage**) and transferred to College Station.

Pressure core storage

Figure **F28** illustrates the method of pressure core storage. Pressure core sections were stored in Geotek core storage chambers. There are two chamber sizes designed to hold pressurized cores up to 35 cm or up to 120 cm. Most storage chambers were equipped with DST temperature and pressure sensors and solid spacers to minimize the storage fluid volume around the core. Chambers used for longer term storage were also equipped with weighted caps above the core liner to seal (as possible) the fluid in the pore space and between the core and core liner from storage fluid around the core liner.

Cryogenic freezing and depressurization

Onboard the *Q4000* and in Salt Lake City, a unique process developed by Geotek was used to recover whole-rounds for microbiological investigation. The process involves cryogenic freezing of the core sections in liquid nitrogen (sample code CRYO) before depressurization.

The CRYO section was cut in PCATS and then transferred to a specialized 35 cm core storage chamber (Figure **F29**, sample storage chamber and Figure **F30**, column A). This core storage chamber was then attached at the flange to a specialized dewar containing liquid nitrogen (Figure **F29**, LN_2 dewar and Figure **F30**, column B). The water in the core storage chamber was purged at high pressure (10 MPa) with nitrogen gas. The purging process likely only displaces a minimal amount of the pore fluid, leaving most of the pore fluid and associated microbes intact. The ball valve on the core storage chamber was then partially opened to equalize pressures and the sample was allowed to cool (Figure **F30**, column C). After 10-20 min, the ball valve was fully opened. This allowed the sample to drop from the core storage chamber into the Dewar of liquid nitrogen (Figure **F30**, column D). The core sample was immersed in liquid nitrogen and frozen. Once frozen, the chamber was depressurized, and the liquid nitrogen was allowed to boil off. Once the chamber was depressurized, the chamber was opened and the CRYO sample was removed.

https://doi.org/10.5281/zenodo.13971228

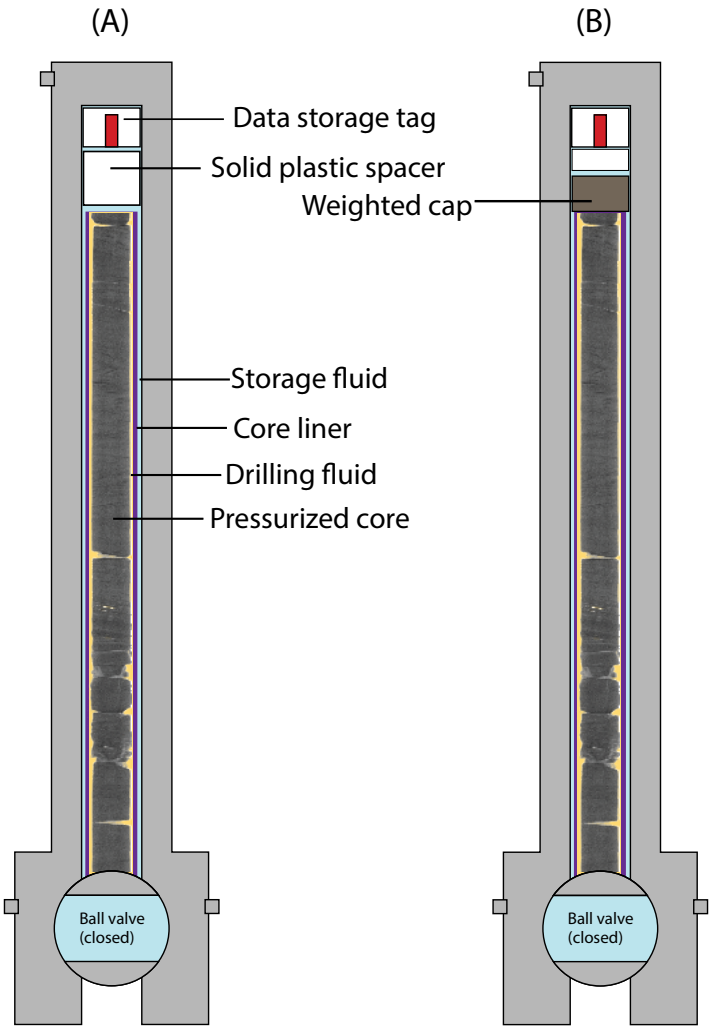

Figure F28: Pressure core storage schematic. A) The core is sealed in the chamber by closing the chamber ball valve before removing the chamber from the Pressure Core Analysis and Transfer System (PCATS). The pressurized core sits inside the core liner (purple) and surrounded by drilling fluid (yellow). Chambers are equipped with data storage tags to track pressure and temperature (red box) and solid plastic spacers of varied length (solid white). B) Chambers used for longer-term storage were also equipped with a weighted cap above the core liner (brown). Storage fluid (light blue) fills the empty space.

CRYO samples were wrapped in multiple sheets of foil (Figure F31), marked with an orientation arrow designating the uppermost part of the core and transferred to a -80 °C freezer to wait for additional microbiological sub-sampling (See **Dockside sub-coring for microbiology**).

Quantitative degassing

Quantitative degassing (QD) samples in core storage chambers were connected to a degassing/gas collection manifold to slowly depressurize/degas the sample and determine the total volume of gas produced. The total volume is used to determine the dissolved methane concentration and hydrate saturation within the core (Dickens et al., 2000) (See **Dissolved gas and hydrate saturation**). In most cases, DSTs placed inside the storage chamber were used to track temperature and pressure during depressurization. Degassing occurred in the degassing lab, which is a temperature-controlled room at ~10 °C. Degassing was conducted over 2.5 to 12 hours depending on the section length, the amount of hydrate present in the section, and scientific goals. For select degassing experiments, depressurization was done in very small steps to estimate the salinity. Multiple degassing experiments were run simultaneously.

During quantitative degassing, the sample pressure was initially at approximately 30 MPa and was quickly depressurized to just above methane hydrate stability zone (about 8 MPa). Pressure was then instantaneously reduced stepwise by ~0.5 MPa and allowed to stabilize during hydrate dissociation. This stabilization was monitored by tracking the pressure in the manifold/core storage chamber. Gas that was forced out of the chamber during depressurization was collected in a gas trap constructed from an inverted 2 L graduated cylinder in a water column, and was measured, recorded, and sampled for compositional analysis. The volume of water forced out of the chamber was also measured and recorded to maintain an accurate mass balance of gas remaining in the chamber. Alternatively, in some instances, the gas was released to a large-volume chamber in which the pressure up to 0.5 MPa was recorded.

The pressure was allowed to return to a stable condition after each pressure drop before the process was repeated until the pressure in the chamber was lowered to atmospheric pressure. At the end of the experiment, the total amount of water forced from the chamber was added to the total volume of gas, as this is an accurate assessment of the gas remaining inside the chamber which could not escape. If possible, the sediment in the chamber was removed intact

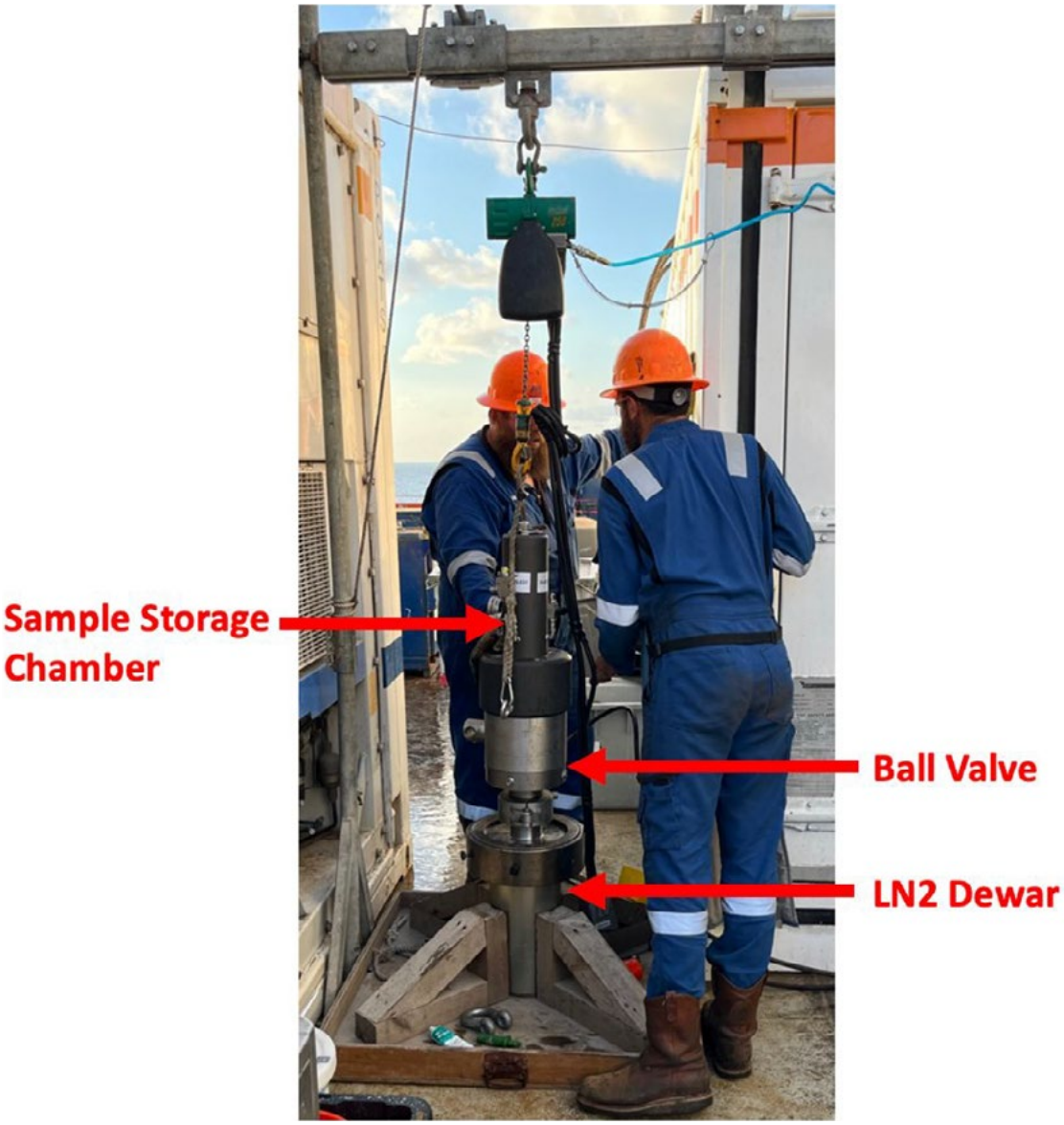

Figure F29: Specialized chamber designed to cryogenically freeze and depressurize cores. LN_2 is liquid nitrogen.

within the liner and the core was entered into the conventional core flow and curation. The remaining sediment or completely disaggregated sediment was collected in plastic storage bags and curated for sediment characterization.

Conventional core processing

Figure F32 shows a chart of the G-APC and G-XCB (conventional) core processing methods used during UT-GOM2-2. Conventional core processing was completed onboard the *Q4000* (Figure F32, Walker Ridge 313, blue box and detailed in Figure F33), in College Station (yellow box), in Salt Lake City (green box), and at UT (Austin, TX, orange box).

After the coring tool was laid out on deck in front of the core receiving lab, the core catcher was removed and carefully transferred the core to a table, where it was properly oriented and labeled before being moved to the core receiving lab for curation. After removal of the core catcher, the core-bearing core liner was removed from the coring tool and inspected (Figure F33, row 1). Small holes were drilled in the liner to relieve pressure as needed. The core was then moved into the core receiving lab, keeping the top of the core oriented to the left.

Conventional cores were then processed in the core receiving lab. A full-length infrared (IR) scan was completed to check for thermal anomalies (Figure F33 row 2). The length of the sediment was measured, and

https://doi.org/10.5281/zenodo.13971228

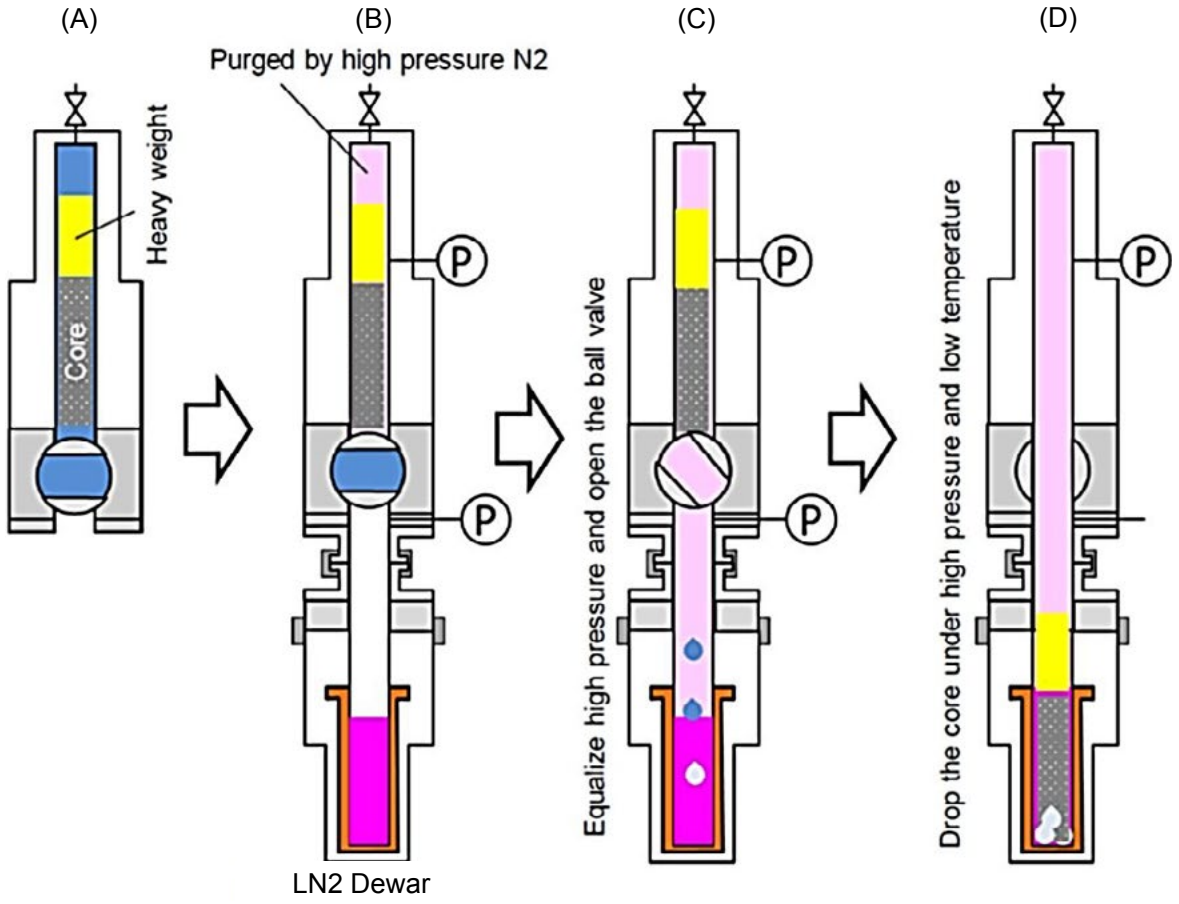

Figure F30: Method for generating cryogenically frozen and depressurized cores. A diagram showing apparatus and steps used to transfer, freeze, and depressurize pressurized core sections (sample code CRYO); A) the special sample chamber with weight, CRYO section, and PCATS water trapped above the closed ball valve (a weight is placed in the sample chamber, the chamber is pressurized with water, a CRYO section is moved at pressure into the sample chamber using PCATS, the chamber is sealed and removed from PCATS); B), the sample chamber is connected to a Dewar filled with liquid nitrogen (LN_2) and the water in the chamber is purged with high pressure nitrogen gas (N_2); C) pressure in the sample chamber is equalized with the LN_2 Dewar and the sample chamber ball valve is partially opened. Water trapped in the ball valve drops into the LN2 and is frozen; D) the sample chamber ball valve is fully opened. The pressure core drops into the LN_2 and is frozen. After freezing the core, the chamber is depressurized, the depressurized frozen core remains in the Dewar, and the sample chamber is removed. Figure modified from Jun Yoneda, National Institute of Advanced Science and Technology, Sapporo, Japan.

Geotek collected void gas samples from larger voids (Figure F33, row 3, See **Void gases**).

The optimal locations for section breaks and whole-round sample sets were determined from visual inspection of the core (Figure F33, row 4). The standard section length was 1.5 meters, but adjustments were made to ensure whole-round samples came from high-quality sections, to avoid foreign material from fall-in, and to work around voids (See **Curation and naming conventions**). Core curation sheets were completed by hand to record the official section lengths and all sample locations (Figure F34). Handwritten curation sheets were photographed, and data was entered into the digital core log spreadsheet (Figure F23, rows B and C).

All sections and whole-round samples were marked and labeled with a permanent black marker with the core name, section, interval, and whole-round sample code. An arrow was also drawn on each section pointing to the core top (Figure F33, row 4). Major voids were also marked and recorded in the core log. Sections, whole-rounds, and major voids were cut. Void sections were discarded.

Whole-rounds were cut from the deeper end of each section (Figure F33, inset B). Whole-rounds for routine and organic pore interstitial water (sample code IWR

Figure F31: A core sample in its frozen state after cryogenic freezing and depressurization (sample code CRYO). The core is still in the core liner. The sample will be wrapped in foil and placed into a -80 °C freezer.

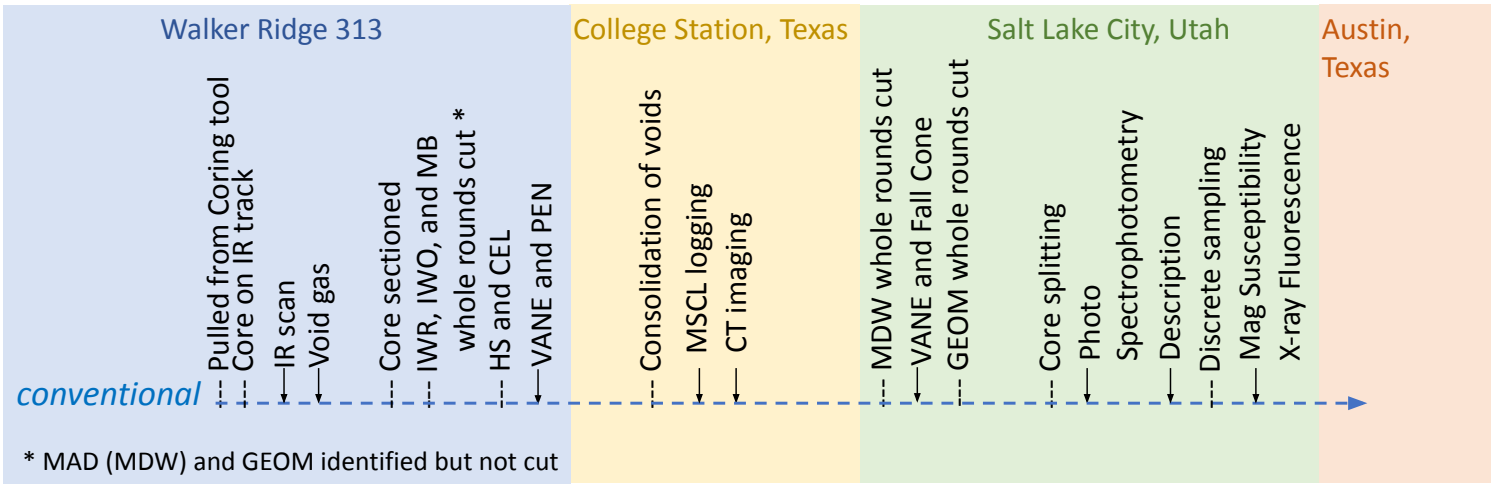

Figure F32: Conventional core processing of G-APC and G-XCB cores Conventional cores were cut for routine pore water (sample code IWR), organic pore water (sample code IWO), and microbiology (sample code MB) analysis. Cores were also marked for moisture and density (sample code MDW) and geomechanics (sample code GEOM) analysis and were cut in Salt Lake City. Samples were taken for headspace gas (sample code HS) and microbial cell counts (sample code CEL) analysis. Conventionalized core sections were also measured for undrained strength (measurement code VANE and PEN). In College Station and Salt Lake City, conventional core sections were sampled and measured (See **Core processing in College Station** and **Core processing in Salt Lake City**).

https://doi.org/10.5281/zenodo.13971228

and IWO, respectively), and microbiology (sample code MB) were cut, capped, and transferred to their respective labs for processing (Figure **F33**, row 5 and inset B, see **Pore water geochemistry** for IWO and IWR, and **Microbiology** for MB processing methods). The top of the moisture and density whole-round (sample code MDW) was not cut from the section so that it would be included in multi-sensor core logging. When voids were consolidated in College Station, some of these MDW whole-round locations were moved (See **Consolidation of voids**). Potential locations for geomechanics whole-rounds (GEOM) were also marked adjacent to MDW whole-rounds but not cut. New optimized GEOM locations were selected in Salt Lake City using conventional core logs (See **Core processing in Salt Lake City**). The new locations were often no longer adjacent to MDW rounds.

After cutting all the whole-round samples, hand shear vane (VANE) and pocket penetrometer (PEN) measurements were made at the bottom end of each section and recorded on the core curation sheet (Figure **F33**, Row 6 and inset B, See **Undrained shear strength** for measurement methods). Headspace gas (HS) and microbial cell count (CEL) samples were collected from the shallow (upper) end of sections, opposite of the IWO (through core 1H-5) or IWR (all cores below 1H-5) whole-round samples (Figure **F33**, row 7 and inset B, See **Headspace gas collection** for HS and **Microbiology** for CEL sampling and processing methods). A sample for biostratigraphic age dating (PAL) was collected from the bottom of each core catcher section (Figure **F33** row 4, See **Biostratigraphy** for the age dating method). All samples were taken to the appropriate labs for further processing.

A second IR scan was originally planned to be made on every core (Figure **F33**, row 8). However, after the first several cores, it was decided that a second IR scan was not necessary unless a thermal anomaly was identified in the first IR scan. No thermal anomalies were identified.

Finally, printed sticker labels were placed and taped to each section with one on the archive half and one on the working half. The core sections were then stored in a cold storage unit (Figure **F33**, row 9).

The core sections were stored in the cold storage unit before being transported to College Station.

Conventional core storage

Whole-round and split core were stored in racks inside a 10 ft mobile refrigerated storage unit chilled to approximately 6 °C. This unit was powered onboard, during transit from the *Q4000* to College Station, TX, from College Station to Salt Lake City, at Salt Lake City, and during transit from Salt Lake City to UT.

Core processing in College Station

Figure **F32** (yellow box) outlines conventional core processing steps and Figure **F27** (yellow box) outlines the similar but less extensive conventionalized PCTB core processing steps competed in College Station, TX (but not at Texas A & M University). G-APC and G-XCB (conventional) and conventionalized PCTB core sections were brought to College Station from the *Q4000*. In College Station, the sediment was moved within the core liner to consolidate sediment and voids (See **Consolidation of voids**). After consolidation of the voids, conventional core sections were logged with a Multi-Sensor Core Logger (MSCL-S) built by Geotek. Logs were collected for natural gamma radiation, bulk magnetic susceptibility, gamma density, and P-wave velocity (See **Conventional whole core logging and imaging**). Conventional and conventionalized core sections were imaged with a specialized computed tomography (CT) scanner built by Geotek. Finally, the cores were restored and shipped to Salt Lake City. Note that surface magnetic susceptibility was also measured after the cores were split in Salt Lake City.

Consolidation of voids

Some smaller voids were consolidated into larger voids where possible at College Station by moving the sediment in the core liner with compressed air (Figure **F35**, compare rows B and C). This consolidation changed the location of sediment where some measurements and discrete samples had been made/taken (Figure **F35**, compare the undrained strength

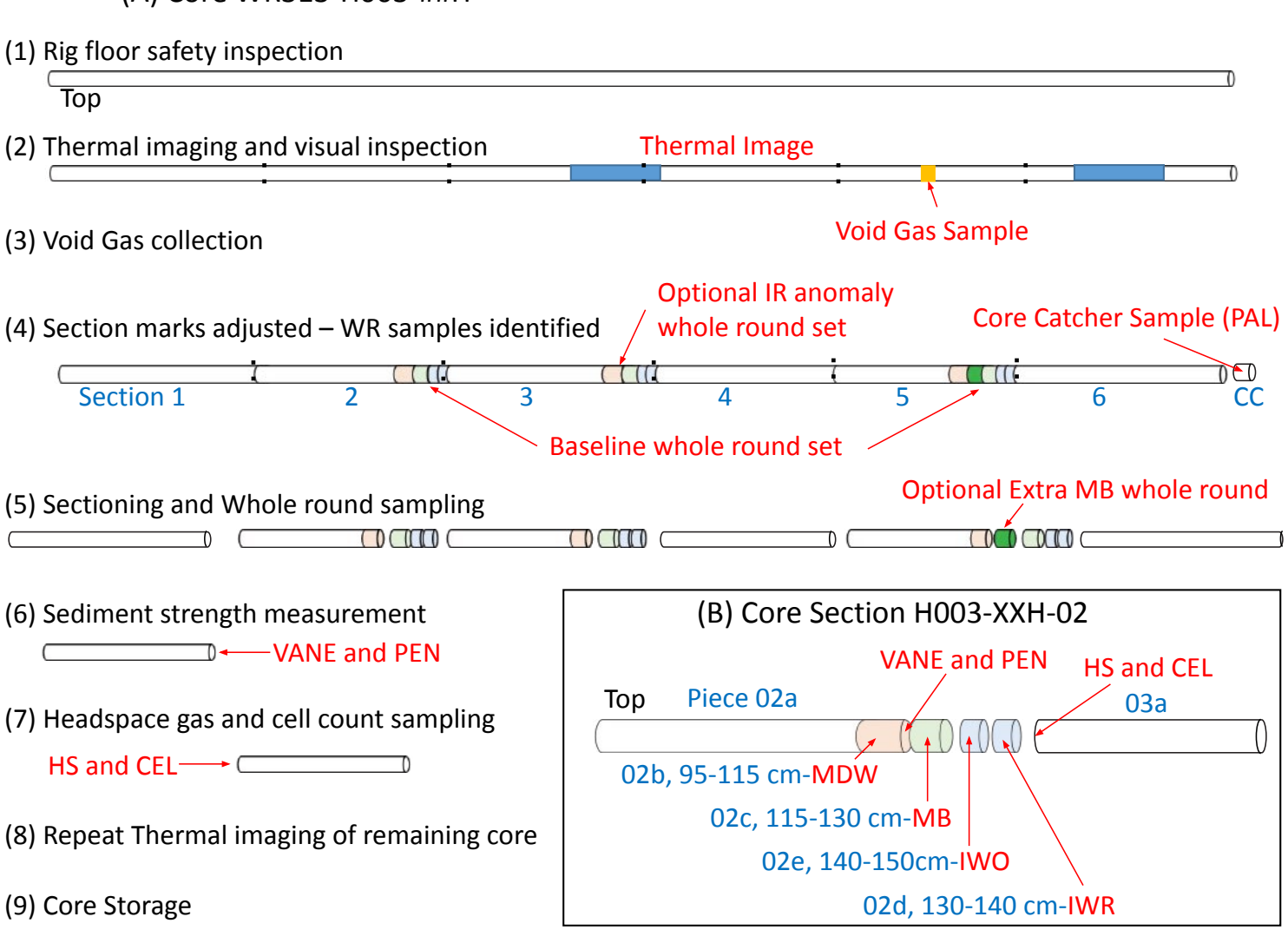

Figure F33: Chart of onboard conventional and conventionalized core processing for a hypothetical full-length G-APC core, H003-##H. Measurements and samples are shown in red text. Measurements included infra-red (IR) imaging, undrained strength tests using a handheld vane (VANE), and pocket penetrometer (PEN). Discrete samples included headspace gas (HS), microbial cell counts (CEL), and biostratigraphy (PAL). Whole-round samples included moisture and density (MDW), microbiology (MB), pore water for organics (IWO), and routine (IWR) analyses. This chart illustrates the standard sampling plan where two whole-round sets were selected per full-length core. An intensive sampling plan was followed in the shallowest cores above and including the sulfur-methane transition zone, Core H003-03H, where whole-round sample sets were collected from every section except the core catcher (CC). Below Core 03H, the standard sampling plan, illustrated above, was applied to all sections in the core, A) Steps from the initial inspection as the core is removed from the coring tool (Step 1) through core storage (Step 9). In row 2, hypothetical IR anomalies are shown within the core liner as a blue box and hypothetical voids filled with free gas are represented as a yellow box, B) Enlarged view of a hypothetical section showing locations of samples that are part of the whole-round set.

measurement, PEN, in rows A and D) and has some impact on the comparison of their associated data with other datasets. Locations of measurements taken onboard were updated in the core log (Figure **F23**, rows B and C).

Sections (or pieces) with any large voids at one end were recorded in the core log as two new pieces, one with sediment, and one as a void. Void pieces were discarded.

Core processing in Salt Lake City

The traditional dockside core processing labs, often used in support of scientific drilling expeditions, are usually established within the port where the acquired cores are transferred from the vessel to land-based facilities. During this expedition, the equivalent

https://doi.org/10.5281/zenodo.13971228

dockside core processing labs were located in Salt Lake City, Utah.

Figure **F27** (green box) outlines the PCTB pressurized and conventionalized core process at Salt Lake City. PCTB pressurized core sections were transported under refrigeration directly to Salt Lake City from Port Fourchon, LA. Some pressurized sections were quantitatively degassed (See **Quantitative degassing**). These sections were processed as PCTB conventionalized whole-round core including cutting whole-round samples, extracting discrete samples, logging and making measurements as described above, as possible. All conventionalized whole-round cores were logged for magnetic susceptibility (See Conventionalized pressure core logging and imaging). Pressure core logs and images were reviewed to select locations for whole-round samples MDW and GEOM. The MDW and GEOM whole-rounds were cut off. The deeper end of all sections was measured for undrained strength using a tabletop vane (code VANE) and Fall Cone. All sections, as well as CRYO whole-rounds that had been subcored (See **Cryogenic freezing and depressurization** and **Dockside sub-coring for microbiology**), were split, described, imaged, sampled, and logged as described in **Visual core descriptions**, **Smear slide descriptions**, **Split core sampling**, and **Split core logging and imaging**.

Figure **F32** (green box) outlines the similar but less extensive conventional core processing steps completed in Salt Lake City. Conventional and PCTB conventionalized core sections were brought to Salt Lake City from College Station.

Conventional core logs and images were used to select final locations for whole-round samples MDW and GEOM. The MDW whole-rounds were cut off. The deeper end of all sections was measured for undrained strength using a tabletop vane (VANE) and Fall Cone. Then, the GEOM whole-round was cut. All sections were split, described, imaged, sampled, and logged as described in **Visual core description**, **Smear slide description**, **Split core sampling**, and **Split core logging and imaging**.

The MDW and GEOM whole-rounds were capped and sealed with electrical tape. The mass of each sealed whole-round was measured to 0.01 g. The whole-round was then heat sealed in a plastic bag and stored in insulated containers in the 4 °C core storage mobile refrigerated van.

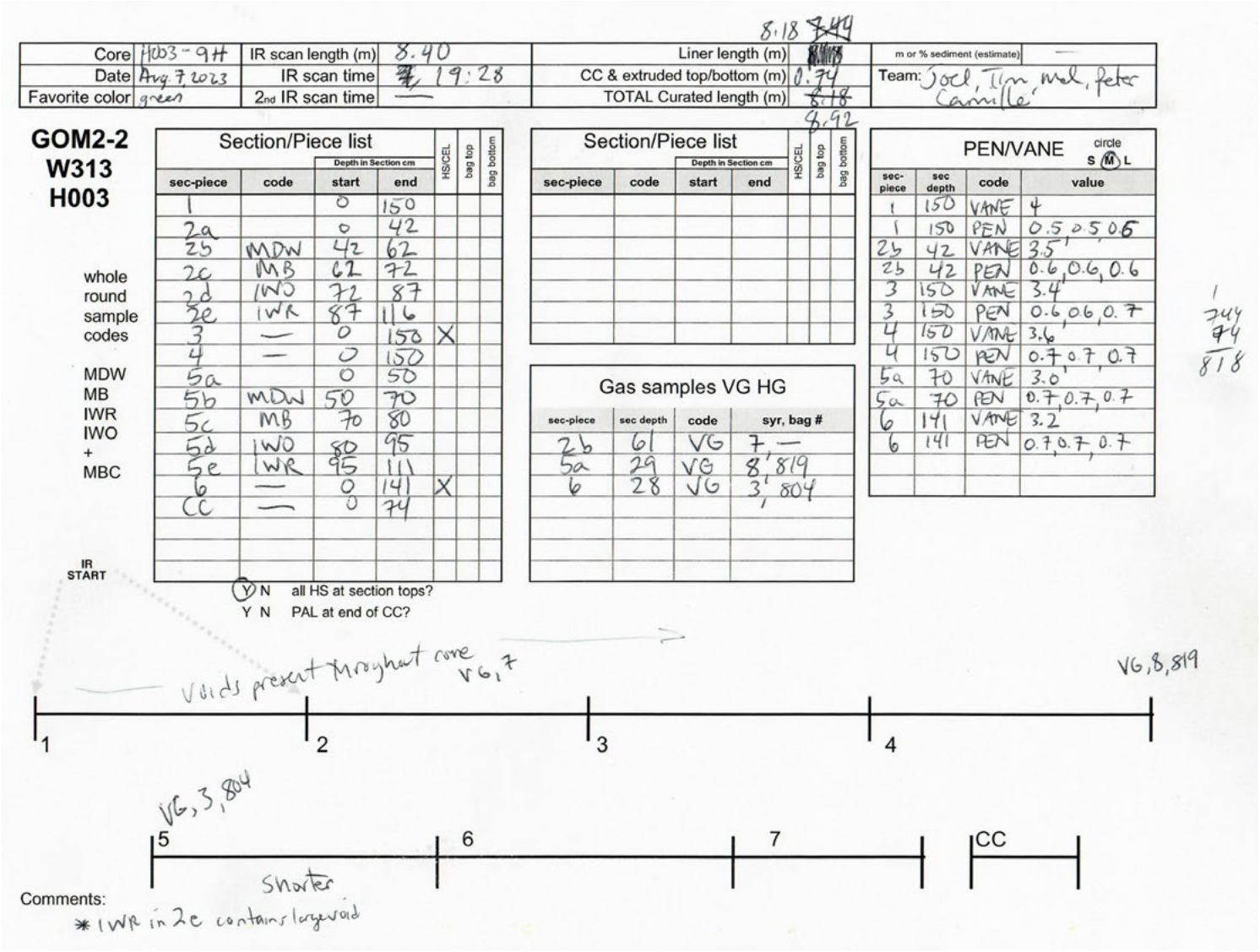

Figure F34: Example onboard core curation sheet

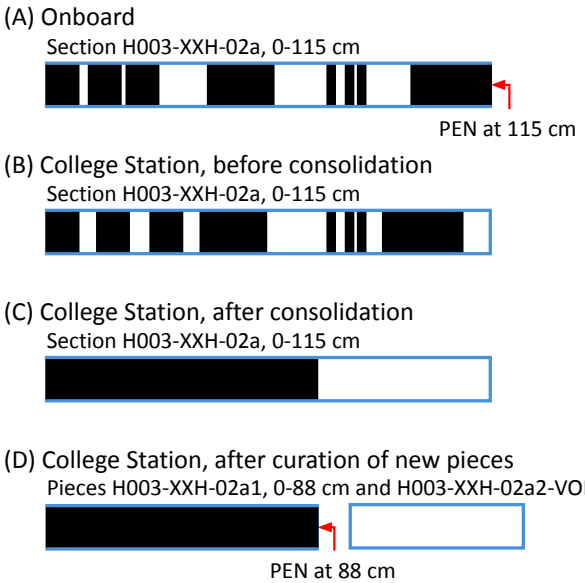

Figure F35: (left) Consolidation of voids for a hypothetical core piece H003-XXH-02a with exaggerated consolidation. Each blue box represents a section of core liner. Voids are represented as white space and sediment as black boxes; A) Hypothetical 115 cm long piece H003-XXH-02a as it was onboard when the section was cut, and undrained strength was measured with a handheld penetrometer at the deeper end of the section (PEN). The measurement was recorded in the core log as being made in section 02a at 115 cm; B) the piece as it was after transport from the *Q4000* to College Station before consolidating voids and sediment; C) hypothetical section as it was after consolidation of voids and sediment; D) new pieces 02a1 and 02a2 after cutting and curation. The section was divided into two entries in the core log, one for each piece. The PEN measurement location in the core log was updated to being in section 02a1 at 88 cm. The new section 02a2 was marked as a void.

https://doi.org/10.5281/zenodo.13971228

Conventional cores prepped and ready for shipping to The University of Texas at Austin (UT). Photo credit: Joel E. Johnson

Lithostratigraphy

The lithofacies and lithologic units of the of Site H were determined using a combination of information from core descriptions (See **Visual core description** and **Smear slide description**), whole-round and split core logs (See **Pressure core logging and imaging**, **Conventional whole core logging and imaging**, and **Split core logging and imaging** under **Physical properties**), grain size determination by a variety of methods (See **Grain size**), and logging while drilling data from the pre-existing borehole Hole H001 (See Summary: Background (Flemings et al., **2025a**)).

Grain size

Table **T7** shows the four different experimental methods for determining the particle size distribution of a material (See **Particle size distribution methods**) and two different definitions of clay, silt, and sand when classifying the grain size of the material from the distribution (See **Grain size classifications**) used in this expedition.

Particle size distribution methods

The four methods for determining the particle size distribution included a qualitative macro-scale determination of the sediment texture (See **Visual core description**), semi-quantitative micro-scale visual determination of the grain size by smear slide description (See **Smear slide description**), as well as two quantitative grain size techniques - laser particle analysis (See **Laser particle analysis**) and hydrometer (See **Hydrometer**). Systematic laser and hydrometer method comparison studies (Di Stefano et al., **2010**; Ferro and Mirabile, **2009**; Wen et al., **2002**) have shown that the laser method typically reports a larger particle size for

Particle size distribution Experimental Method	Size Range	Reported in	Grain Size Classification	
			Geoscience (Udden-Wentworth (Wentworth, 1922))	Geotechnical (ASTM International (2008e))
VCD bulk sediment texture by split core observation (See Visual core description)	≥10 µm	VCD summaries	NA	
VCD grain size by smear slide observation (See Smear slide description)	≥0.2 µm	VCD summaries and Smear slide spreadsheet	X	
Particle size distribution by laser particle analysis (See Laser particle analysis)	0.1 – 1000 µm (Mastersizer spec),	Grain size ternary diagram, cumulative particle size figures		X
		Laser particle analysis data set	X	X
Particle size distribution by Hydrometer method (See Hydrometer)	0.05 to 100 µm	Grain size ternary diagram, cumulative particle size figures		X
		Hydrometer data set	X	X

Table T7: Cross-reference of grain size methods, classifications, and report

plate-shaped clay particles than does the hydrometer method. This is because the laser method reports a value weighted towards the average particle dimension, whereas the hydrometer method reports a value weighed towards the thin (short) dimension. (See Particle size distribution). However, the laser method is much faster to perform and uses less than 1 gram of sediment. The hydrometer method requires days to run each test and requires about 35 grams of sediment.

Grain size classifications

The grain size of the material was named based on relative percentage of clay, silt, and sand within it following Shepard (1954). We used the term clay for both clay minerals and other siliciclastic material. However, two different definitions of what dimensions constitute a clay, silt, or sand particle were used. Thus, the percentage of clay, silt, and sand will differ between the two definitions and the final classification of the grain size of the material (e.g., sandy silt vs silty sand) may differ as well.

Geoscientific classification

These grain size definitions are generally used by geoscientists. These definitions were used for all smear slide descriptions and lithostratigraphic summaries (See Smear slide description).

Particle size (clay, silt, and sand) was classified based on the Udden-Wentworth classification (Wentworth, 1922). The term clay is assumed for material less than 3.9 µm. The term silt is used for material 3.9 µm to 62.5 µm and sand describes grains larger than 62.5 µm and less than 2 mm.

https://doi.org/10.5281/zenodo.13971228

Geotechnical engineering classification

These grain size definitions are commonly used in geotechnical engineering when placing a sample on the grain size ternary diagram (e.g., Figure F36, row A) or plotting the cumulative percent distribution or frequency of a sample measured. Within these proceedings, tables of particle size distributions report results using both definitions.

These grain size assumptions follow the Unified Soil Classification System (ASTM International, 2017). In this system, the term clay is used for particles less than 2.0 microns in size. The term silt is used for material 2.0 µm to 75 µm and sand describes particles larger than 75 µm and less the 2 mm.

Core description laboratory space

The lithostratigraphy program was conducted in one laboratory at Geotek Coring USA, Salt Lake City (Figure F37). The laboratory was air conditioned, and humidity controlled. Tables were available for core layout and split core sampling. A petrographic microscope was set up and a frequency-dependent magnetic susceptibility meter was installed. The lab was fully stocked with split core sampling supplies described in the sections below. A benchtop X-Z Multi-Sensor Core Logger (MSCL-XZ) was also housed in this space. A large screen displayed split core images. Core splitting was done just outside the room.

Visual core description

The techniques and procedures used to describe, analyze, and identify the lithologies in cores recovered during UT-GOM2-2 are described below. They are based on the methodologies employed during previous gas hydrate focused expeditions (Expedition 311 Scientists, 2006; NGHP Expedition 01 Scientists, 2007; Shipboard Scientific Party, 2003) and were adapted to the specific conditions and equipment available during UT-GOM2-2.

UT GOM2-2 cores were split into the working and archival halves. The archival halves were scraped smooth to emphasize sedimentary structures and compositional and/or textural changes in cores and then immediately imaged (See MSCL-XZ linescan split core imaging). Visual core description (VCD) was completed on the archival half by filling in the core description sheets (Figure F38). CT slab images, collected prior to core splitting, were displayed on a large monitor to aid in core description. Working halves were brought to the sampling table and split core samples were collected (See Split core sampling). Archival halves were scanned for x-ray fluorescence (XRF) and magnetic susceptibility after core description (See Split core logging and imaging).

The lithology of each core section is recorded on the core description sheet (Figure F38) and smear slide spreadsheets. In addition to lithology, a wide variety of features that characterize the sediments were recorded, including bedding (See Bedding), core disturbance (See Core disturbance), and primary and secondary sedimentary structures. The primary and secondary structures were characterized by Munsell color (See Sediment color), occurrence of microfossils (See Biogenic content), bioturbation intensity (See Degree of bioturbation), iron monosulfide intensity, diagenetic precipitates (See Accessories), visual grain size from smear slides (See Visual grain size), and composition by smear slides (See Composition).

This information was synthesized for each core in the Golden Software Strater® ver. 5.9.1100 software package, which generates a one-page graphical description of each core (Figure F39). Symbols used in the core description sheets are defined in the legend (Figure F40). These Strater composite lithologic figures are referred to as lithostratigraphic summaries (e.g., Figure F39) in Site H: Lithostratigraphy (Flemings et al., 2025b).

Composition, structure, and texture were used to define lithology for each core. Genetic/interpretative terms such as pelagic, hemipelagic, turbidite, debrite, etc. do not appear in this classification.

The sediment texture was obtained with a hand lens on split cores and is complemented by the description of the composition and grain size of

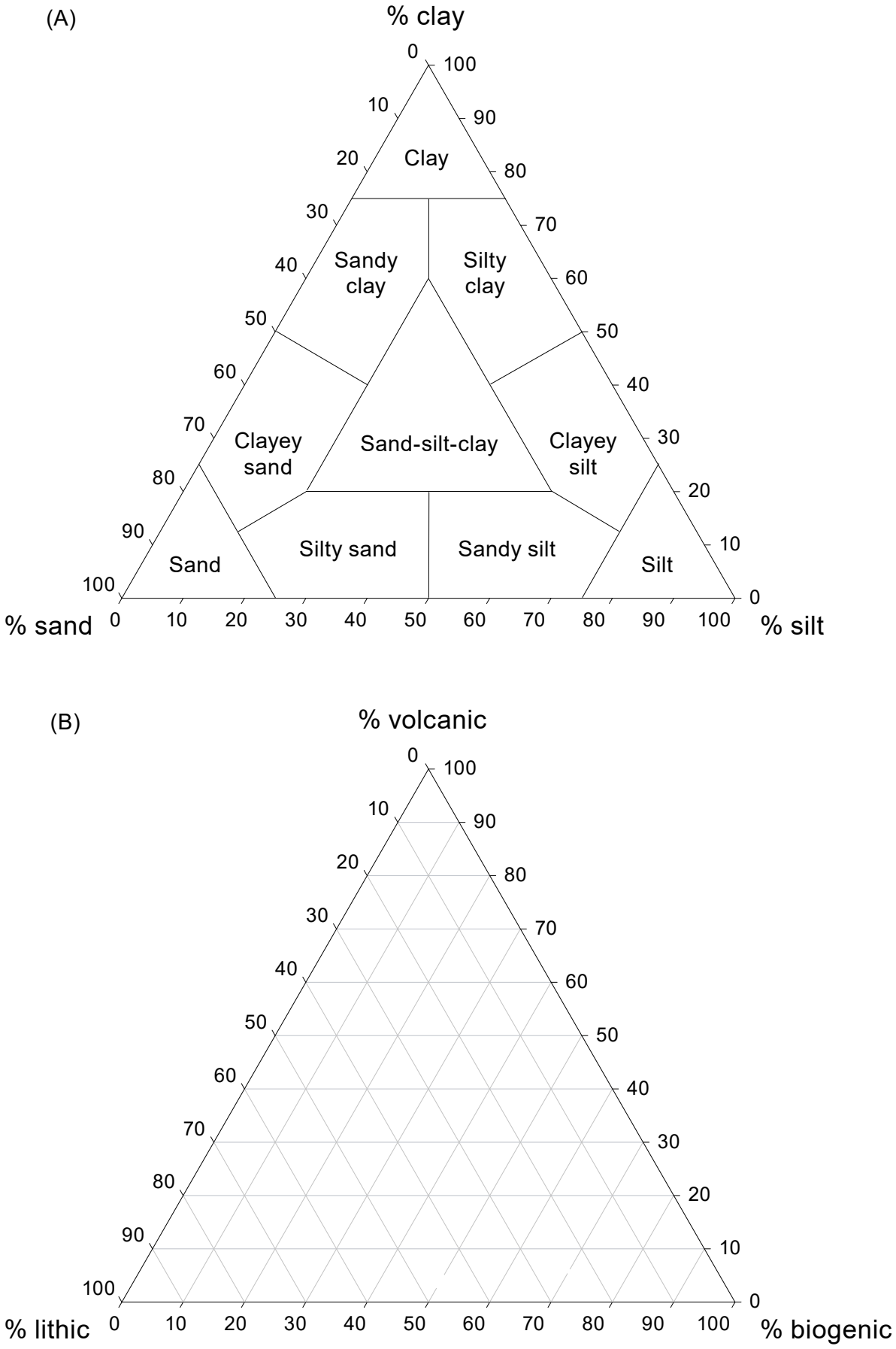

Figure F36: Ternary plots of sediment grain size and composition. A) Ternary diagram modeled after Shepard's diagram (Shepard, 1954); B) Ternary plot of sediment composition derived from smear slide analysis. Variations in the ternary plot apices are a function of the actual bulk composition encountered in the sediment.

 https://doi.org/10.5281/zenodo.13971228

Figure F37: Photos of the split core lab in Salt Lake City.

GOM2-2 VISUAL CORE DESCRIPTION

Exp. GOM2-2	Site	Hole	Core	Type	Section

Date	Time	Observer

Depth (cm)	Core Photo or X-ray	Coring Disturb.	Graphical Lithology	Grain Size: clay	Grain Size: silt	Grain Size: sand: fine	Grain Size: sand: medium	Grain Size: sand: coarse	granules/pebbles	Sedimentary Structures	Bioturb. Intensity 0 1 2 3 4	FeS_x 1 2 3	Munsell Color	Lithologic Description
10														
20														
30														
40														
50														
60														
70														
80														

Figure F38: Hand-drawn VCD core description sheets.

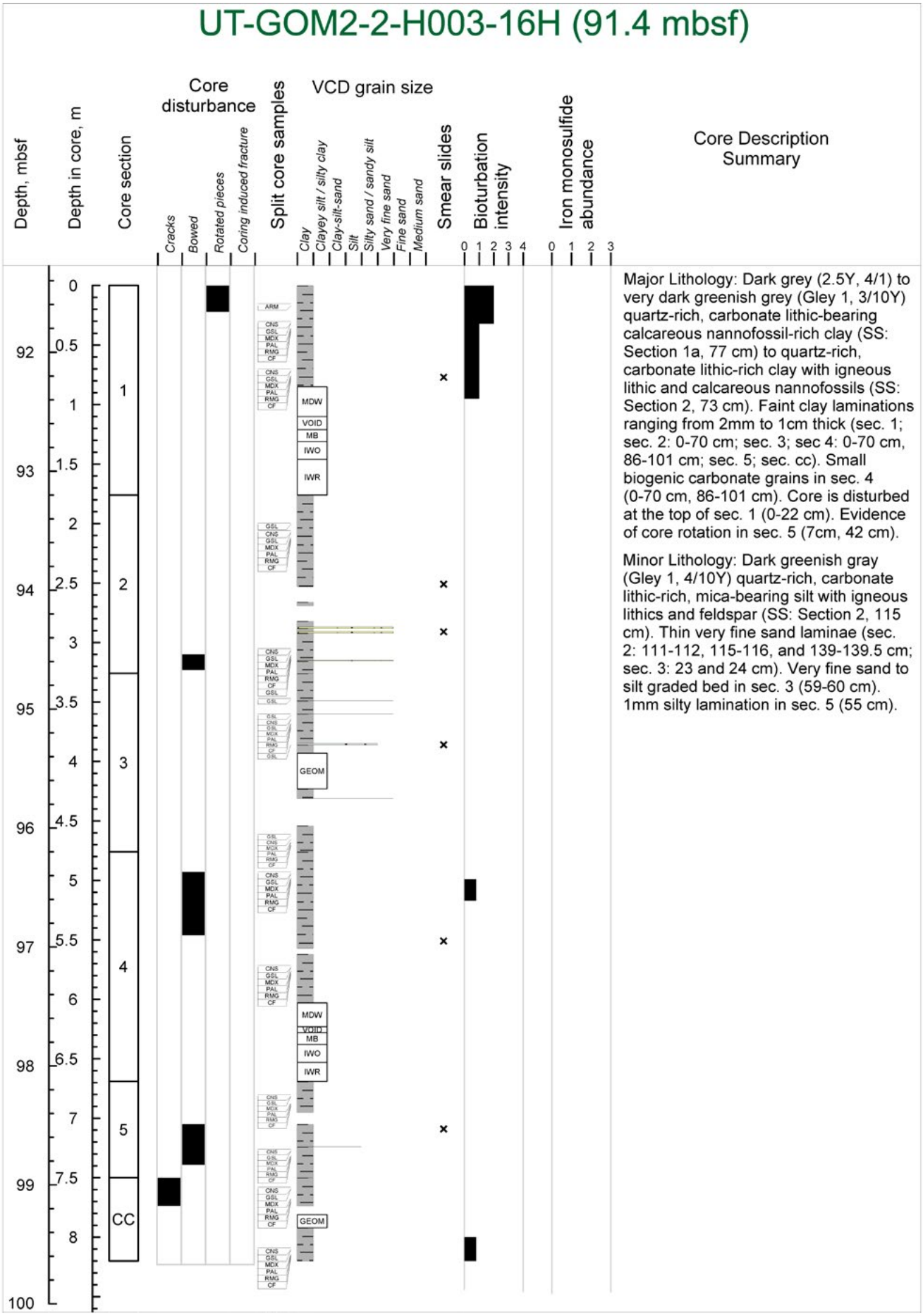

Figure F39: Example of a lithostratigraphic summary produced by uploading information from the hand drawn VCD.

 https://doi.org/10.5281/zenodo.13971228

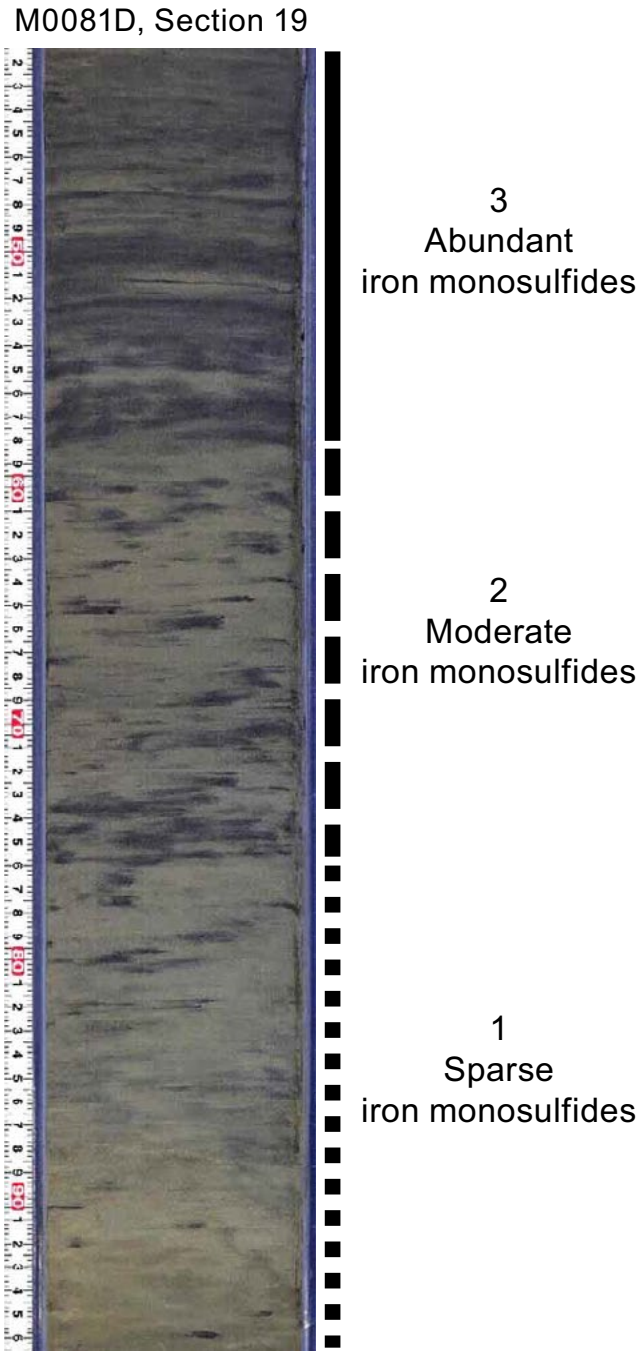

Figure F40: Nomenclature used to classify the intensity of iron monosulfide in cores. Figure is from Expedition 386 (Strasser et al., 2023). This same nomenclature was used for this expedition. The vertical bar on the right shows the relative increase upward in the intensity of monosulfides.

sediment obtained from smear slides observed under a petrographic microscope (See **Smear slide description**). Slight differences in assessment between macro- and microscopic observations may occur in some cases.

Bedding

Bedding terminology used in core description is after McKee and Weir (1953):

- Very thick bed = >100 cm.
- Thick bedded = >30–100 cm.
- Medium bedded = >10–30 cm.
- Thin bedded = >3–10 cm.
- Very thin bedded = 1–3 cm.
- Laminae = <1 cm.

Core disturbance

Coring disturbance that resulted from the coring process are illustrated in the Drilling Disturbance column of the VCD sheets and on the Strater summary plots. Blank regions indicate the absence of apparent disturbance. Disturbance types include gas expansion cracks (these become more abundant with depth in the core and are related to gas expansion upon core recovery), slurry/soupy (water saturated) sediments, fall in materials, and bowed disturbance. Bowed disturbance is evident in sedimentary structures such as lamina. Void is used to document empty spaces related to the coring process. Whole-round core samples are designated with sample codes (e.g. IWO, IWR) and shown on the section log of the Strater summaries.

Primary sedimentary structures

Description of primary sedimentary structures was kept as simple as possible to capture the most frequent observations. Sedimentary features included fining or coarsening upward; parallel-, wavy-, or cross-laminated; chaotic or mottled and in some places exhibit rip-up clasts and soft-sediment deformation such as microfolding. The core description text is located in the free text column on the lithostratigraphic summary plots. The text may contain other descriptions, including faults, fractures, tilted bedding, clastic dikes, flame, dish, water escape, or convolute structures.

Accessories

Accessories (i.e., macroscopically identified authigenic or diagenetic minerals) are minor components of the cores, and the relative abundance of some of them is assessed using the standard visual composition chart of Rothwell (1989). The captured accessories are micas (hand lens scale), rock fragments, authigenic carbonate concretions, iron monosulfides, nodules, and pyritized burrows. The intensity of the presence of iron monosulfides in the cores was assessed using a semiquantitative scale: 0 = not visible, 1 = sparse, 2 = moderate, and 3 = abundant (Figure F40).

Biogenic content

Most of the fauna and flora are represented by microfossils (e.g., diatoms, radiolarians, silicoflagellates, siliceous sponge spicules, foraminifers, and calcareous nannofossils) and were only observed in smear slides, coarse fractions, or in micropaleontology samples. Macroscale wood and plant debris and shell fragments, including visible foraminifera, are reported on the lithostratigraphic summaries when encountered.

Degree of bioturbation

To assess the degree of bioturbation semi quantitatively, a modified version of the Droser and Bottjer (1991) ichnofabric index (ii = 0–4) scheme was employed, where we used Bin 0 as No Bioturbation (Figure F41) The different degrees of bioturbation identified were: (1) slight, (2) moderate, (3) abundant, and (4) homogenized by bioturbation (Figure F41). Slight bioturbation is manifested by discrete burrows and trace fossils covering ~10% of the core surface. Moderate bioturbation includes 10%–50% of the core surface disturbed by burrows or trace fossils. If more than 50% of the core surface is disturbed by burrowing or trace fossils, it is abundant.

Sediment color

Sediment color was determined visually using the Munsell color designation (hue, value, and chroma) of the sediments (Munsell Color Company, 1994).

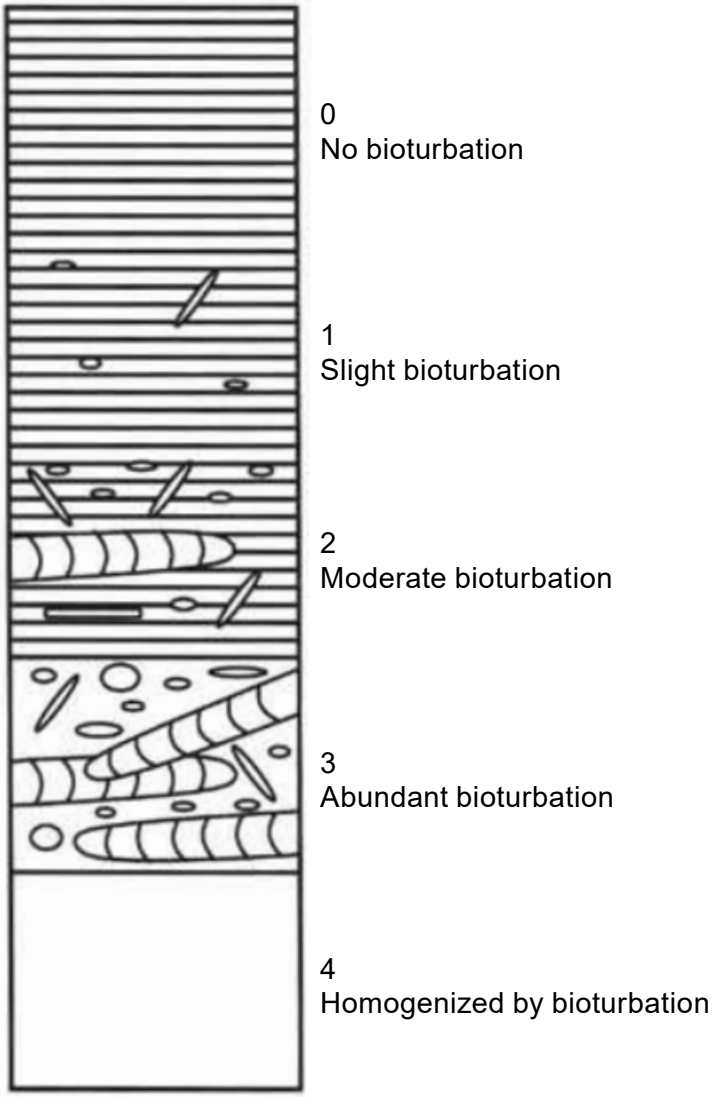

Figure F41: Nomenclature used to classify the degree of bioturbation from no bioturbation to homogenized by bioturbation (modified from Droser and Bottjer (1991)), for the UT-GOM2-2 Expedition. On the core description sheets, the intensity of bioturbation is coded from 0 (no bioturbation) to 4 (homogenized by bioturbation).

Color was coded by a combination of hue, which represents the dominant spectral value (such as red, yellow, green); Value, which represents the relative lightness of color; and chroma, which represents the relative purity or strength of the spectral color. Hue is composed of five major colors—red (R), yellow (Y), green (G), blue (B), and purple (P)—and the respective complement colors–yellow red (YR), green yellow (GY), blue green (BG), purple blue (PB), and red purple (RP). These colors are arranged on a loop, and each of the colors is divided by a decimal system from 0 to 10. Whole hues are assigned values between 1 and 100, R to RP. Value consists of numbers from 0, for absolute

https://doi.org/10.5281/zenodo.13971228

black, to 10 for absolute white, with neutral, which has no depth in color. The colors between 0 and 10 are arranged so that they become successively lighter in visually equal steps. Chroma values of each color gradually change with increases in vividness. When the hue and value are systematically arranged, the chroma value rises with increasing vividness starting at 0 (neutral gray). A color of 7.5Y in hue, 5 in value, and 2 in chroma is noted as 7.5Y 5/2, yellow.

Coarse fractions

Coarse fractions were flagged and sampled in Salt Lake City but were not sieved through a 63 µm sieve and described until the samples were back at the University of New Hampshire. About 5 cm^3 of sediment from the major and minor samples will be sieved using a 63 µ mesh and described as the coarse fraction. In combination with the smear slide results, which are slightly biased toward finer grained components, we used the coarse fractions to identify the relative abundances of the larger species and components (e.g. foraminifera, diatoms, radiolarians, silicoflagellates, pyrite, quartz, mica, feldspar etc.). Together these data will give us the most complete description of the presence and distribution of sedimentary components throughout the core. Detrital and authigenic minerals, as well as major microfossil groups, were estimated as a percent of this fraction and integrated into the lithostratigraphic core description.

Smear slide description

Composition

The grain size and composition of the sediment was determined by observations of smear slides under polarized light using a petrographic microscope (Leica DM 750 P with an ocular micrometer). Smear slides samples were collected every ~3 m to complement visual core description observations. These data help confirm the major lithology and add important compositional information for fine-grained sediments. The smear slide sample locations are shown on the lithostratigraphic summaries (Figure **F39**). The smear slide was prepared by putting a small amount of sediment on a glass slide mixed with distilled water. The water on the slide was evaporated on a hot plate, and the dried sample was covered with a cover slip adhered with Norland Optical Adhesive 61 using ultraviolet light.

The adopted sediment nomenclature was derived from Mazzullo et al. (**1988**). The compositional description is a percentage of individual lithic, biogenic, and diagenetic components which were estimated semi-quantitatively using a standard visual composition chart (Rothwell, **1989**).

Major minerals assessed by this preliminary petrographic analysis of sediments include quartz, feldspar, mica, and pyrite. Lithic fragments were also recognized and dominated by carbonates. Identifiable whole microfossils and fragments included siliceous sponge spicules, foraminifers, and calcareous nannofossils. Smear slide descriptions were recorded in data tables. These tables include a description of where the sample was taken in the core, the estimated percentages of texture (i.e., sand, silt, and clay), and the estimated percentages of composition (i.e., quartz, feldspar, detrital carbonate, foraminifera, diatoms).

The sediment was named in an orderly fashion according to the proportions of its major constituents. The main name is that of the component that represents more than 50% of the sediment, and associated modifiers such as “rich” (25%–50%), “bearing” (10%–25%) and “with” (5%–10%) are added. The sediment composition is named with modifiers organized as follows: Component 1–rich, Component 2–bearing, sediment texture (from sand, silt, clay ternary diagram), with Component 3. Sediment texture composed of 50% or more biogenic components is named “ooze” and sediment texture composed of 50% or more volcaniclastic material is named “ash.”

An example would be (1) foraminifer–rich, quartz-bearing, calcareous nannofossil ooze with pyrite or (2) a quartz-rich, feldspar-bearing silty clay, with foraminifer.

The composition results are summarized in a ternary diagram (e.g., Figure F36 B) with 100% of each chosen component or binned components plotted at each apex.

Visual grain size

The composition of the visual grain size was determined by observations of smear slides under polarized light using a petrographic microscope. The sampling frequency and method for generating and observing the smear slides are described in Composition.

Grain size divisions on the lithostratigraphic summaries for clay, silt (very fine, fine, medium, and coarse), sand (very fine, fine, medium, coarse, and very coarse), gravel (very fine, fine, medium, coarse, and very coarse) and cobble follow Wentworth (1922) and Lane (1947) and were assessed using hand lenses and grain size cards. See **Grain size classifications** for more details.

Split core sampling

Sampling frequency and locations

Figure F42 shows the frequency and locations of discrete samples collected from the split core working halves. Figure F43 is a photo of a working half being sampled.

Discrete sampling methods

The following describes the methods for extracting discrete samples from the split core working half. All holes created from removing the discrete samples were plugged with labelled pieces of foam. When all the samples had been removed, a photograph was taken of the core section with an iPhone.

CNS

One 10 cm^3 sample tube of wet sediment was collected for CHNS, TOC, and isotopic analysis of C and S of major and minor lithology in each core section. The samples were collected as part of the standard set and, when possible, were adjacent to other samples, depending on the thickness of the facies (sample code CNS, Figure F42). CHNS samples were also collected from MDW whole-rounds sent to Tufts University (See **Index properties**) and from Pore Water whole-rounds (See **Pore water geochemistry**).

A clean 10 cm^3 sampling plug was inserted in the working half of the split core as far as it would penetrate (Figure F43, CNS flagged sample). The entire sampling plug, with the sediment inside was placed into a labeled sample bag and the bag was heat sealed.

A labeled piece of foam was used to plug the sample hole.

RMG and ARM

Samples were collected for paleomagnetic (p-mag) studies using 8 cm^3 plastic p-mag sampling cubes. Background (sample code RMG) and magnetic anomaly highs (sample code ARM) were sampled.

One RMG sample was collected from the major and minor lithology in each core section. The samples were collected as part of the standard set and, when possible, were adjacent to other samples, depending on the thickness of the facies (sample code RMG, Figure F42). ARM samples were collected at magnetic anomalies as determined from the whole and split core magnetic susceptibility measurements.

The plastic cover of the sampling cube was removed. The cube was aligned with the open end on the sediment with the cube arrow pointed in the stratigraphic-up direction. The open cube was pressed into the surface of the core until the cube was filled completely with sediment. A clean metal spatula was used to carefully extract the p-mag cube from the sediment. Any excess sediment on the top was trimmed off and the plastic cover was placed back on the cube to encase the extracted sample. The cubes were immediately weighed and measured on the frequency-dependent magnetic susceptibility meter (See **Rock magnetism**).

https://doi.org/10.5281/zenodo.13971228

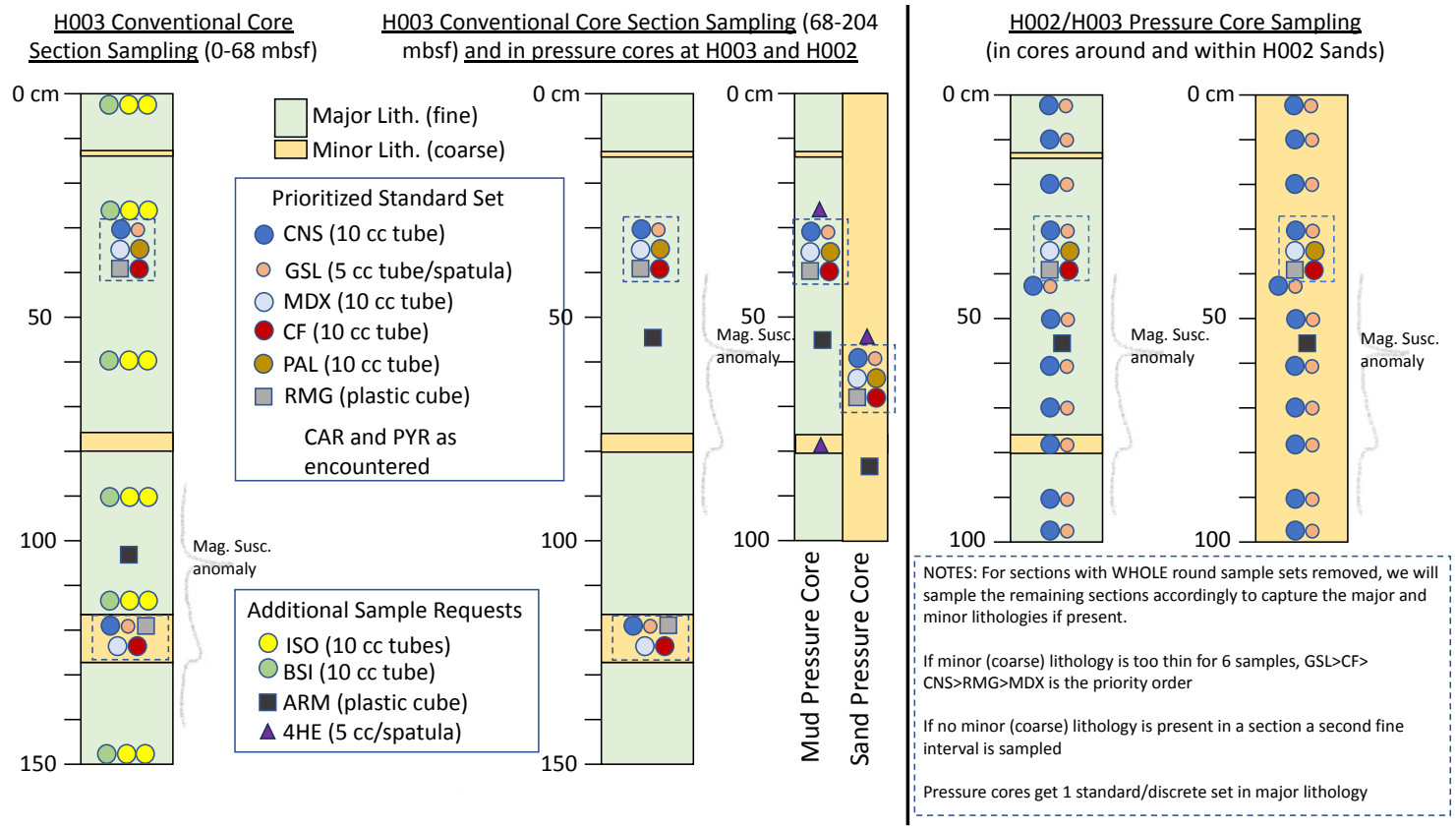

Figure F42: Split core sampling templates. Sample code CNS indicates a sample for CHNS, TOC, and isotopic analysis of C and S. Sample code GSL indicates a sample for grain size analysis using a laser particle analyzer. Sample code MDX indicated a sample for moisture and density, X-ray powered diffraction, and X-ray fluorescence. Sample code CF indicates a sample for coarse fraction analysis. Sample code PAL indicates a sample for biostratigraphy. Sample code RMG indicates a sample for paleomagnetic studies. Sample code CAR and PYR were used to identify samples of authigenic carbonate or sulfide nodules, respectively. Sample code ISO indicates a sample to measure isotopes of carbon and oxygen. Sample code BSI indicates a sample for bulk sediment biogenic silica measurement. Sample code ARM indicates a high magnetic susceptibility (susc) anomaly sampled for paleomagnetic studies. Sample code 4HE indicates a sample for calculating residence times of fluids.

GSL

Approximately 1-2 cm^3 sample of wet sediment was collected for grain size analysis (using a laser particle size analyzer) of the major and minor lithology in each core section. Additional grain size samples were collected from the MDW whole-round (See **Index properties**). The samples were collected as part of the standard set and, when possible, were adjacent to other samples, depending on the thickness of the facies (sample code GSL, Figure **F42**). A 1 cm width metal spatula was used to cut out a 1 cm stratigraphic thickness sample that is 2 cm wide and 2 cm thick. The sample was placed as intact as possible into a labeled sample bag and the bag was heat sealed.

MDX

One 10 cm^3 sample tube of wet sediment was collected for moisture and density, X-ray powered diffraction (XRPD), and X-ray fluorescence (XRF) of major and minor lithology in each core section. The samples were collected as part of the standard set and, when possible, were adjacent to other samples, depending on the thickness of the facies (sample code MDX, Figure **F42**).

The cylindrical plugs were acquired at Salt Lake City from the working half of the split core by pushing a plastic corer or brass cork cutter though the ½ section (Figure **F44**). The plug was cut to a specific length and measured to 0.01 mm using a digital caliper. The diameter was set by the inner diameter of the cutter which was also measured to 0.01 mm with a digital caliper. The plug was extruded into a marked glass container of known mass to 0.001 g. The mass of the wet plug and container (without the cover) were recorded to 0.001 g. The container was then sealed

with a plastic cover and shipped to Tufts. See **Index properties** for the methods used at Tufts.

CF

One 10 cm^3 sample tube of wet sediment was collected for coarse fraction analysis of major and minor lithology in each core section. The samples were collected as part of the standard set and, when possible, were adjacent to other samples, depending on the thickness of the facies (sample code CF, Figure **F42**). A clean 10 cm^3 sampling plug was inserted in the working half of the split core as far as it would penetrate. The entire sampling plug, with the sediment inside was placed into a labeled sample bag and the bag was heat sealed.

PAL

One 10 cm^3 sample tube of wet sediment was collected for calcareous nannofossil biostratigraphy of the major lithology in each core section. The samples were collected as part of the standard set and, when possible, were adjacent to other samples, depending on the thickness of the facies (sample code PAL, Figure **F42**). Samples were also collected from core catchers (See **Conventional core processing**). A clean 10 cm^3 sampling plug was inserted in the working half of the split core as far as it would penetrate. The entire sampling plug, with the sediment inside was placed into a labeled sample bag and the bag was heat sealed.

CAR

No authigenic carbonates were observed.

PYR

Samples of iron sulfide nodules were collected using a clean spatula. Samples were placed into a labeled sample bag and the bag was heat sealed.

ISO

One 10 cm^3 sample tube of wet sediment was collected for determining carbon and oxygen isotope stratigraphy and radiocarbon ages of major lithologies every 30 cm and at the same depths as the BSI sample in each core section in the upper 68 m as per the sampling templates (sample code ISO, Figure **F42**). A clean 10 cm^3 sampling plug was inserted in the working half of the split core as far as it would penetrate. The entire sampling plug, with the sediment inside was placed into a labeled sample bag and the bag was heat sealed.

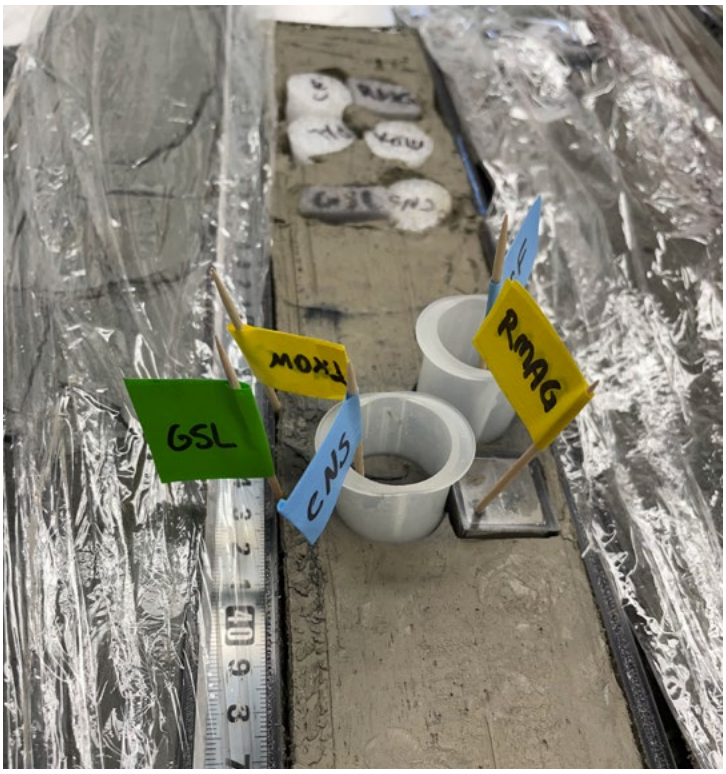

Figure F43: (left) Photo of split core sampling. Flags were used to identify the locations where samples should be collected. The flag labeled CNS inside the 10 cm^3 sample tube indicates a sample for CHNS, TOC, and isotopic analysis of C and S (sample code CNS). The flag labeled RMAG indicates a sample for paleomagnetic studies (sample code RMG). The flag labeled GSL indicates a sample for grain size analysis using a laser particle analyzer (sample code GSL). The flag labeled MDX2 indicated a sample for moisture and density, X-ray powered diffraction (XRPD), and X-ray fluorescence (XRF) (sample code MDX). After sampling, foam plugs with the sample code written on the top were inserted into the hole where the samples were removed.

BSI

One 10 cm^3 sample tube of wet sediment was collected for bulk sediment biogenic silica measurements of major lithologies every 30 cm and at the same depths as the ISO sample in each core section in the upper 68 m per the sampling templates (sample code BSI, Figure **F42**). A clean 10 cm^3 sampling plug was inserted in the working half of the split core as far as it would penetrate. The entire

https://doi.org/10.5281/zenodo.13971228

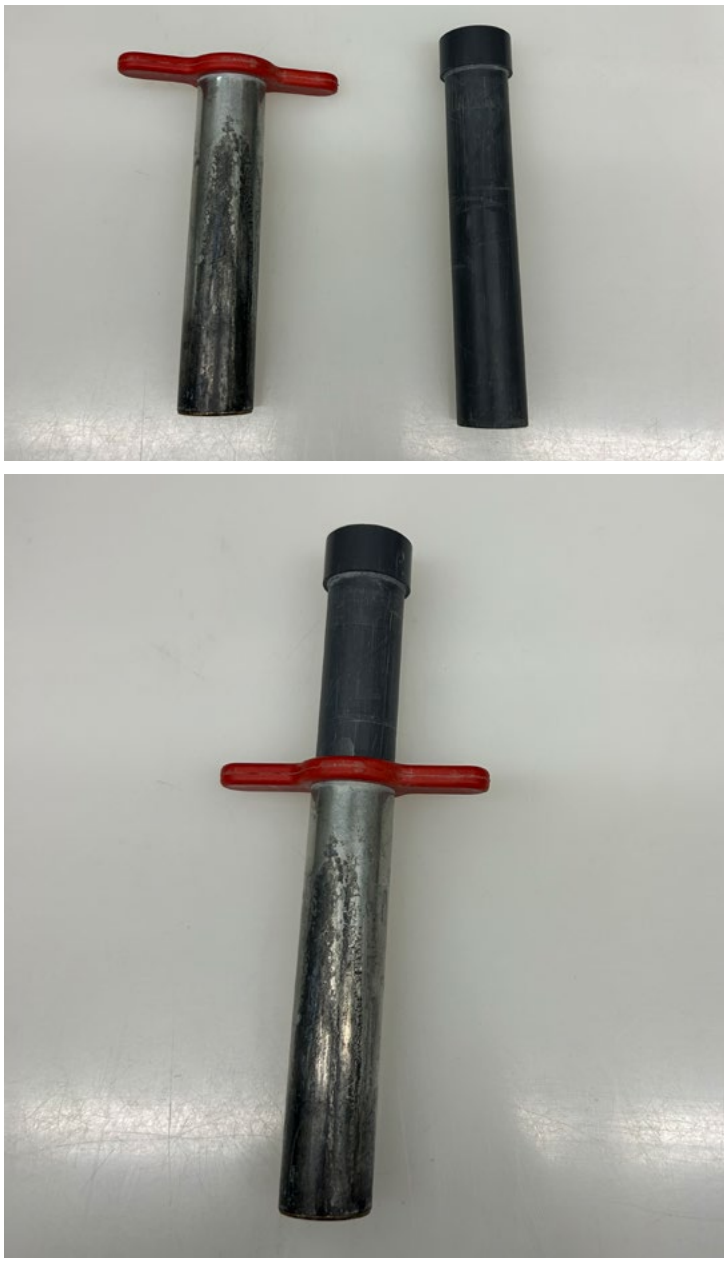

Figure F44: Photos of the brass plug corer and plunger used to extract moisture and density (MAD) samples from the split core working half.

sampling plug, with the sediment inside was placed into a labeled sample bag and the bag was heat sealed.

4HE

One 10 cm^3 sample tube of wet sediment was collected to measure the rate of 4HE release, which is used to calculate residence times of fluids. Samples of major and minor lithologies were collected from pressure cores per the sampling templates (sample code 4HE, Figure F42). A clean 10 cm^3 sampling plug was inserted in the working half of the split core as far as it would penetrate. The entire sampling plug, with the sediment inside was placed into a labeled sample bag and the bag was heat sealed.

Science party members Tim Collett of the U.S. Geological Survey, Joel E. Johnson of the University of New Hampshire, Steve Phillips of the U.S. Geological Survey, and Kelly Shannon of Oregon State University demonstrating the evolution of the expedition scientist onboard the Q4000. Photo Credit: Peter B. Flemings

Biostratigraphy

This section includes the methods for sampling and assessing calcareous nannofossil biostratigraphy.

Biostratigraphy samples and laboratory spaces

Samples collected onboard for calcareous nannofossil biostratigraphic analysis (sample code PAL) were collected from the core catcher of each G-APC and G-XCB conventional core. When possible, biostratigraphy samples were collected from the core catcher of PCTB cores. PAL samples were shipped to the UNH for immediate analysis during the dockside portion of the expedition.

In Salt Lake City, additional PAL samples were collected from every section of split conventional or conventionalized pressure cores to increase the resolution and depth range of the age model. These samples were shipped from Salt Lake City to UNH.

Calcareous nannofossil biostratigraphy

Biostratigraphy samples (sample code PAL) were prepared following standard preparation techniques for sediment smear slides for calcareous nannofossil analysis.

Samples were initially prepared and examined at the industry standard of 30-foot intervals. When a biohorizon or other geologic event was identified, additional samples were prepared and examined, reducing the sample interval to 15-feet or less until the most precise interpretation could be achieved.

Specimens were examined and documented via photomicroscopy in a transmitted light microscope. A modified version of Styzen (**1997**) quantitative counting method of calcareous nannofossils was applied to each sample

examined ensuring precise interpretation of the age and assemblage. Biostratigraphic events, such as First and Last Appearance Datums (FAD and LAD), were determined and known ages for these datums were plotted by depth. Additionally, composite ranges of key taxa were plotted downcore, all of which led to the construction of age-depth models for each borehole that were ultimately combined for a comprehensive biostratigraphic interpretation. Reworked Cretaceous nannofossils are not considered part of the microfossil assemblage when making biostratigraphic age estimations for this project. Instead, they are considered part of the detrital sediment (Constans and Parker, **1986**; Marchitto and Wei, **1995**; Purkey, **2020**).

The biozonations applied to this project to build a site-specific age-depth model are the Quaternary-Neogene Biostratigraphic Chart of the Gulf Basin, USA (Waterman et al., **2017**), which is the product of decades of industry-sourced biostratigraphic data specifically from the Gulf, and the Quaternary-Neogene Calcareous Nannofossil Biochronology (Gradstein et al., **2012**). Both biozonations were further calibrated to the most recent Geologic Time Scale of Gradstein et al. (**2020**).

University of Texas at Austin (UT) science team member Donnie Brooks enjoys the scenery. Photo credit: Peter B. Flemings

Physical properties

The physical properties of sediment from Site H include measurements of thermal conductivity (See **Thermal conductivity**); in-situ temperature (See **In-situ temperature**); core scans and images (See **Pressure core logging and imaging**, **Conventionalized pressure core logging and imaging**, and **Conventional whole core logging and imaging**); undrained strength (See **Undrained shear strength**); moisture, grain density, porosity, and grain size (See **Index properties**); and rock magnetism (See **Rock magnetism**).

Thermal conductivity

Thermal conductivity (k) is the proportionality constant between the temperature gradient (ΔT) and the heat flux (Q), $Q = k \Delta T$. In sediments, the bulk thermal conductivity depends on the mineral composition, porosity, water saturation, and sediment structure. During the UT-GOM2-2 dockside work in Salt Lake City, we conducted one thermal conductivity measurement on each core using the TeKa TK04 unit needle probe set up in the Core Receiving mobile laboratory (Figure **F45**) (Blum, **1997**; Von Herzen and Maxwell, **1959**)

We first transferred cores from storage to the core receiving laboratory and allowed them to thermally equilibrate at room temperature for at least 4 hours. Then, we selected the measurement location based on CT slab visual inspection and avoided measuring near voids, cracks, and disturbed regions. A hole was drilled in the core liner using a 7/64” drill bit. Then the probe was coated with Silicon Warmeleitpaste thermal paste (P12) and was inserted into the sample through the drilled hole.

The TK04 uses the transient line source method to infer thermal conductivity (ASTM International, **2008b**). Constant power is applied to the probe, while the temperature increase is monitored with time. The slower

 https://doi.org/10.5281/zenodo.13971228

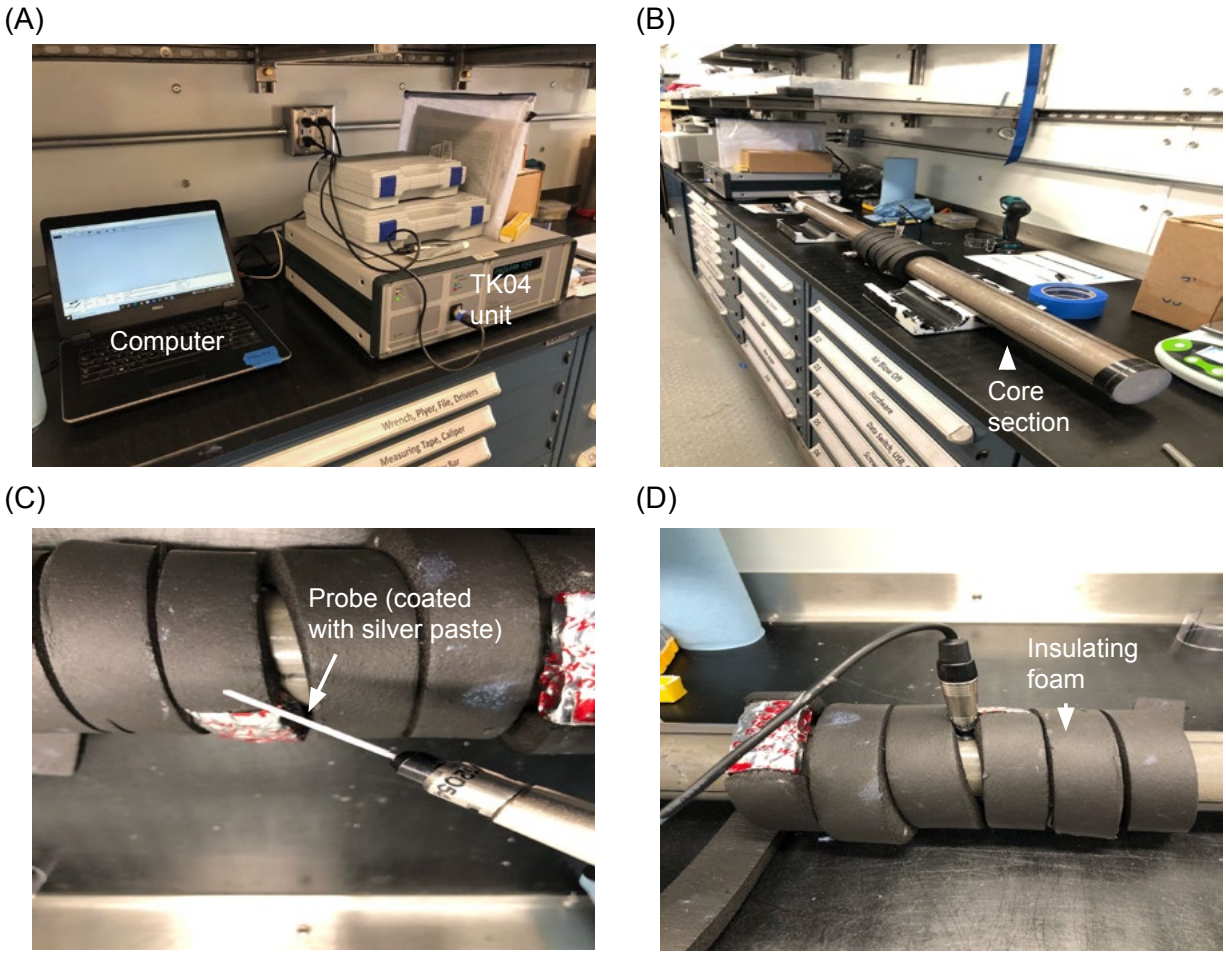

Figure F45: Photos from a thermal conductivity measurement. A) Computer and TK04 unit, B) Core section laid on the table for thermal conductivity measurement, C) needle probe (coated with silicone Warmeleitpaste), and D) after needle probe fully inserted into the sample before starting the measurement.

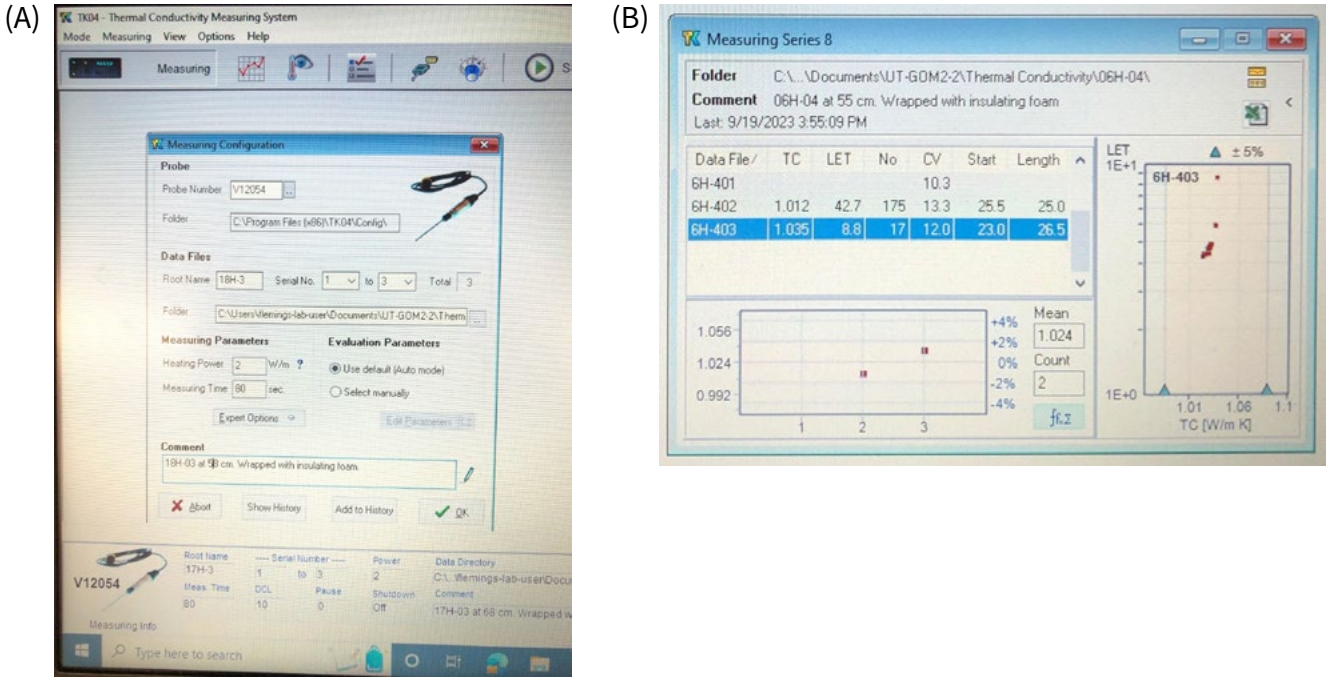

Figure F46: Screen shots from a thermal conductivity measurement. A) Window to set the measuring configuration and evaluation parameters, B) results are added to the results list and diagram and saved to file.

the source temperature rises, the higher the thermal conductivity of the sampled material. For these measurements, we used a heating power 2-3 W/m and a measuring time of 80 seconds (Figure F46).

The thermal conductivity measurement involves a series of steps. First, the TK04 continuously monitors the temperature of the sample until the drift is small and stable. After the background thermal drift is determined, the heater circuit was closed and the increase in the probe temperature was recorded. Thermal conductivity values are automatically determined by the TK04 based on the observed rise in temperature for a given flux of heat. We report the average of three to five measurements conducted at the same location.

The thermal conductivity probe was calibrated before leaving the manufacturer. It was tested on a material of known thermal conductivity prior to use and produced results within acceptable specifications.

In-situ temperature

Discrete measurements of formation temperature at multiple depths in Hole H003 were obtained using the advanced piston corer temperature tool (APCT-3) (Heesemann et al., 2006). We also deployed a penetrometer (See Temperature Dual Pressure Penetrometer) in the water column, but no formation measurement was made.

Extrapolating the APCT-3 temperature measurement

The APCT-3 operation allows us to infer in situ temperature while coring. For example, Figure F47 shows the APCT-3 deployment for core H003-06H on 5 August 2023. First, the G-APC was lowered downhole until reaching the seafloor at a time of 15:55. The tool was stopped for 5 minutes with the pumps turned off to thermally equilibrate with the bottom water before collecting the core (Figure F47, mudline stop). We conducted this equilibration procedure only for the 06H deployment. After equilibration, the pumps were turned on, the tool assembly was run to the bottom of the hole and temperature slightly increases

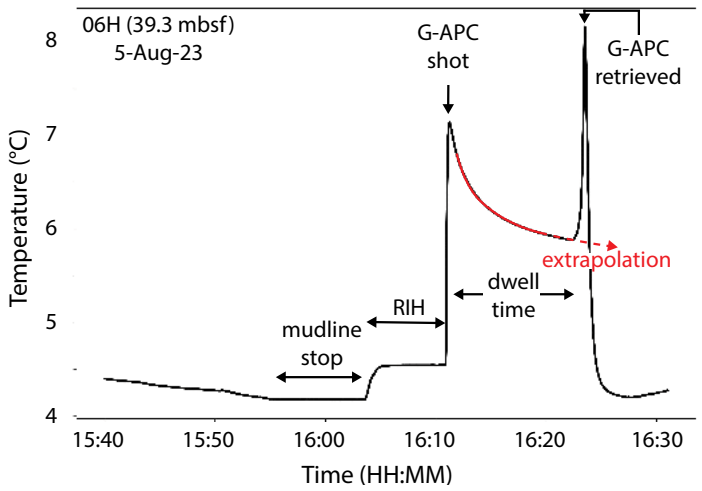

Figure F47: A typical temperature signature, collected during core H003-06H APCT-3 deployment on 5-Aug-23. The tool is lowered to the mudline and held for 5 minutes. Then the tool is run into the hole (RIH) and the G-APC is shot into the formation, which causes the first temperature peak. The second peak corresponds to the retrieval of the coring tool, and the time in between the spikes is referred to as the dwell time. The data shown as red solid line is fitted with the theoretical impulse response of the tool to derive the in-situ temperature.

(Figure F47, RIH). The pressure in the drill string was increased and the G-APC core was shot into the formation. This generated a rapid temperature rise due to frictional heating (Figure F47, peak at 16:11). Heat then dissipated into the surrounding sediment, and the temperature at the APCT-3 decreases toward the formation in situ temperature. To allow for the equilibration of the tool, the G-APC is held in place for ~10 min while the APCT-3 records the temperature (Figure F47, dwell time). Pulling the tool out of the formation also causes frictional heating, and the temperature peaks again (Figure F47, 16:23).

Temperature during the dwell period rarely reaches the equilibrium in-situ temperature. To overcome this limitation, temperature data are fitted with the theoretical impulse response of the tool and extrapolated to “infinite” times (Figure F47, red curves). This thermal decay model depends on the geometry of the probe and thermal properties of the sediments and probe (Bullard, 1954; Davis et al., 1997). We first identify the measured data to be used in the fitting procedure (Figure F47, red solid line). The measured data selection avoids the initial decay affected by tool insertion (approximately the

https://doi.org/10.5281/zenodo.13971228

first minute of data) and typically finishes at the end of the dwell time. Then, we use the software TPFit to extrapolate the downhole temperature measurements (Figure F47, red dashed line). The value at "infinite" time corresponds to the in-situ temperature (Heesemann et al., 2006).

Calculation of the thermal gradient

This measured thermal gradient was obtained by fitting a linear trend of temperature with true vertical depth in meters below the seafloor (See **Calculation of vertical depth below the seafloor from measured depth**). The seafloor temperature was disregarded since it was assumed to be more sensitive to environmental changes (e.g., ocean currents).

Core log plotting

All core logging data, including images, were plotted using Strater, by Golden Software.

Pressure core logging and imaging

Non-destructive measurements were conducted on pressurized core in the PCATS lab (Schultheiss et al., 2014; Schultheiss et al., 2011). These data were obtained at high pressure ~ 30 MPa and low temperature ~ 7-9 °C; thus, measurements were conducted within hydrate stability P-T conditions.

PCATS houses an aluminum pressure section that allows the transmission of gamma and X-ray radiation for gamma density measurement (See **PCATS gamma density**) and X-ray imaging (See **PCATS X-ray imaging**). P-wave velocity was determined by sending 250 kHz ultrasonic pulses between a source and a receiver in the pressure chamber (See **PCATS P-wave velocity**). The pressure core manipulator allowed translation and rotation of the core and the collection of 3D CT data.

PCATS was used to perform initial characterization of the cores onboard. This characterization included compressional wave (P-wave) velocity logs, gamma density logs, 2D and 3D CT scans, and 2D laminography scans. If the core was logged twice, the first scan was used to develop a core cutting plan and the second scan was used as the primary data set for interpretation. Because the P-wave and gamma density were collected separately from the CT data sets, there is the potential for slight offset in depth of these data sets if core physically moved between scans.

PCATS gamma density

Gamma density was logged with a spatial resolution of 10 cm. Gamma density was calculated from the attenuation of a collimated beam of monochromatic gamma photons from a nominal 10 mCi (370 MBq) Cesium-137 (^{137}Cs) source (Schultheiss et al., 2011). This source can penetrate both the core and the aluminum pressure housing (wall thickness of 11 mm) and was shielded in lead with a rotating lead shutter (5 mm diameter collimator).

Calibration of gamma attenuation to gamma density, and from there to bulk density, relied on a set of standards of known average bulk density. The standards of choice for calibration of gamma attenuation to gamma density in standard sediments (water-saturated aluminosilicates) are aluminum and water of known thicknesses inside core liner. This results in a similar electron density in the calibration pieces and the core, allowing gamma density and bulk density to track each other with high precision, though the resultant data were reported as gamma density rather than bulk density.

Gamma counts average near 20000 (total counts) with an integration time of 5 seconds, making the error in the gamma density 1.4% (95% confidence interval).

The calculation of gamma density performed in the field assumed that the core was of a constant diameter, which was not the case. The gamma density could be improved by reprocessing the data, using the X-ray CT data to constrain the diameter.

PCATS P-wave velocity

Ultrasonic P-wave velocity was logged with a spatial resolution of 10 cm. The P-wave velocity was measured with a pulse transmission technique. The two 500 kHz acoustic transducers were

mounted inside the aluminum pressure housing, perpendicular to the core axis (Schultheiss et al., 2011). The transducers were also perpendicular to, but co-located along, the core with the gamma ray beam. The P-wave velocity was calculated from the pulse travel time across the core material and the internal diameter of the core liner ultrasonic velocity with a precision of ±1.5 m s^{-1} and an accuracy of approximately ±5 m s^{-1}. The pulse travel time across the core material is calculated by subtracting the travel time offset, which is the time required for the pulse to transit the core liner as well as the pressurizing fluid between the transducers and the core liner at a given temperature. As with the gamma density, P-wave measurements are also affected by variations in core diameter.

PCATS X-ray imaging

X-ray images were collected using a variable-intensity, microfocal X-ray source and a digital flat-panel detector (Schultheiss et al., 2011). The source energy used was 120 keV at 400 µA. The combination of microfocal source and high-resolution flat-panel detector enabled images to be collected in PCATS with a 112 µm/pixel resolution. All images are positive, meaning denser objects which obscure the X-ray beam appear darker than less dense material.

Radiographs and computed laminography

Linear 2D X-rays were acquired using a continuous scanning technique providing a single line scan image of the complete core. These images are referred to as radiographs and images are labeled with Radiography or Linear Scan and the orientation of the core, either 0 or 90 degrees, in the file name.

Enhanced 2D images were also acquired using a high contrast filter that exaggerates the density variation as described by Geotek (Geotek Ltd., 2023). The method is not the same as classical laminography. These images are referred to as computed laminography (CL) images and the image files are labeled with CL in the file name. CL slabs have lower resolution and different artifacts than computer tomography. CL images should not be used to identify core biscuits.

The 2D X-ray raw data files are 16-bit TIFF and have companion XML files containing information regarding the image collection. Smaller file-sized JPGs of each core were created and mathematically corrected for the variable thickness across the round core.

Computed tomography

Computed tomography (CT) data was collected on all the pressure cores at a voxel resolution of 112 µm per side. We refer to this data as CT data. These data sets were collected using multiple rotations along the length of the core. 3D X-ray CT data are in individual folders as a stack of 16-bit TIFF files with an associated XML file containing information regarding the CT stack. The TIFF images preserve the raw data as collected.

CT slabs

CT slabs are 2D images that were extracted from the CT voxel data. Two CT slabs perpendicular to each other along the axis of the core called the XZ view and the YZ view. The image files are labeled with XZview and YZview in the file name. Pixels in the image are averaged from voxels equivalent to a 5 mm thickness of the core (unless otherwise marked in the associated XML file) and taken slightly off center.

CT slices

CT slices are 2D images that were extracted from the CT voxel data. CT slices are perpendicular to the axis of the core. Pixels in the image are averaged from voxels equivalent to a 0.25 mm thickness of the core (unless otherwise marked in the associated WholeCoreRecon text or index XML file).

X-ray artifacts

X-ray images record the attenuation of a polychromatic X-ray beam as it passes through a sample. Attenuation at any given energy is a function of the thickness, density, and atomic number of a material. Because of this, attenuation of polychromatic X-rays by material of varied atomic number should not be used as a simple proxy for

https://doi.org/10.5281/zenodo.13971228

density. However, with compositional information and application of the proper attenuation coefficients, it is possible to create a high-resolution density profile using CT data.

The correction of the JPG images from the Radiographs assumes a round core of perfect geometry, so any deviation from a cylinder will create a corresponding dark or bright spot on the image. This correction can also create dark vertical lines near the edges of the image.

The X-ray CT data in the initial report data set have several types of artifacts which should not be mistaken for features in the core. Detailed processing of specific volumes could further minimize these artifacts.

Center of rotation artifacts are recognizable as a doubling of features, or an apparent wobble in the image. Center of rotation artifacts appear because a single center point of rotation does not exist (for instance, the core tumbles within the liner or core is not held perfectly in the center of the liner in PCATS).

CT montage artifacts are recognizable as lines in vertical slabs every ~6.7 cm and are a result of the merging of two data sets. These artifacts can be exacerbated if the core moves even slightly in the liner between two rotations.

CT ring artifacts are recognizable as concentric rings in the CT slices, or as vertical lines or repeated patterns in the CT slabs. They are particularly noticeable at the center of rotation (near the center of the core). Some of these ring artifacts were generated as sediment particles accumulated in the X-ray beam during the CT acquisition.

Conventionalized pressure core logging and imaging

Magnetic susceptibility

Bulk or volume magnetic susceptibility was measured on whole-round depressurized pressure core sections in Salt Lake City, Utah using a standalone loop sensor. The same instrument type as was used for the whole-round conventional cores in College Station (See **MSCL-S magnetic susceptibility**). Surface magnetic susceptibility was also measured after core splitting. See **MSCL-XZ magnetic susceptibility**.

X-ray imaging

A few conventionalized cores from Hole H002 were put into PCATS and temporarily repressurized with air to image them before they were sectioned. These images are labeled with AIR in the file name.

X-ray imaging of whole-round depressurized pressure core sections was completed in College Station using the same method as was used for the whole-round conventional cores. See **X-ray imaging**.

Conventional whole core logging and imaging

All whole-rounds were scanned using the MSCL-S after thorough cleaning of the outside of the core liners. The MSCL-S collects simultaneous, co-registered data from multiple sensor systems in an automated fashion on lined sediment or unlined rock samples. Sensors we used included MSCL-S natural gamma radiation, MSCL-S magnetic Susceptibility, MSCL-S gamma density, MSCL-S electrical resistivity, and MSCL-S P-wave velocity. Samples up to 1.5 m long are placed at one end of the MSCL-S track and are pushed past each sensor in turn. Subsequent samples are abutted, making the data acquisition extremely efficient. The accurate core motion (better than 0.01 mm) and laser measurement of sample length allows proper co-registration of all data. The data from all sensors, the cumulative logging depth, and the depth in sample for each data acquisition point are exported together in one file.

MSCL-S natural gamma radiation

Natural gamma radiation is measured using three sodium iodide (NaI) detectors. The detector energy window is set up to measure between 0 to 3000 kiloelectron volts (keV) over a sample length of approximately 10 cm with decreasing sensitivity distal to each one of the three sensors. Calibration

of the natural gamma activity sensors is performed by setting-up the detector channels to output an energy reading. Each gamma sensor comprises 1024 channels. The range of energies viewed by the 1024 channels is determined by the high voltage. Known energies from the chemical elements presented in the table below are used as part of the calibration process. The NaI detectors are calibrated to the 1461 keV peak from the 40K standard, the 2615 keV peak of ^{208}Tl, and the 0.609 peak of ^{214}Bi measured from the ^{238}U standard. Background measurements are also subtracted from each detector. This removes contributions of gamma photons from building materials and the surrounding earth, as well as the gamma density cesium (^{137}Cs) source if it is installed. This background measurement is commonly performed for a duration of twelve hours with an aluminum cylinder piece placed under the natural gamma sensors and a plastic cylinder placed in the path of the open gamma density beam (if installed) to mimic core measurement conditions. The background calibration provides an average count per second measurement of the surrounding natural gamma radiation and is subtracted from all future measurements acquired from samples. Continuous checks are performed on the natural gamma detectors. This is conducted by measuring the 0 ppt MSCL-S check piece at the start and end of each logging file. Should any drift have occurred, the data can be corrected. In addition, temperature is recorded within each logging file.

MSCL-S magnetic susceptibility

Bulk or volume magnetic susceptibility was measured using Bartington Instruments Ltd loop sensors for whole core analysis. The frequency of the low-intensity, non-saturating, alternating magnetic field produced by the sensor is sensitive to changes in the magnetic susceptibility of material within the loop sensor or near the point sensor. Loop sensors are chosen to fit the core diameter. The magnetic susceptibility was measured every 1 cm, however, each magnetic susceptibility measurement represents a core length of approximately 5 cm, with decreasing sensitivity distal to the sensor. The magnetic susceptibility sensor is pre-calibrated by Bartington. Each magnetic susceptibility sensor is paired with a single standard sample (calibration piece) of stable iron oxide provided with each individual sensor. The calibration check pieces state the corrected susceptibility values measured from the sensor's first calibration. These values are used to ensure that the calibration of the magnetic susceptibility sensors is accurate each time a check is performed. Throughout any core logging phase, continuous checks of the live and raw data acquired from the magnetic susceptibility sensor are made before, during, and after individual samples are analyzed. The checks are conducted using the calibration piece and a homogenous rock sample that is logged at the start and end of the logging file. The values of this rock sample are analyzed, and any drift is corrected. The temperature of the core logging environment is also monitored throughout the core logging phase and corrections can be performed for any small variations. Magnetic susceptibility is a dimensionless number and is presented as corrected volume susceptibility (calculated in SI units) with an accuracy of typically ± 4 %. Surface magnetic susceptibility was also measured after core splitting. See **MSCL-XZ magnetic susceptibility**y.

MSCL-S gamma density

MSCL gamma ray attenuation density (gamma density) was measured at 1 cm intervals using a 10 second integration time. Gamma density is measured through the center of a sample using a 10 millicurie (mCi) cesium (^{137}Cs) source and a sodium iodide (NaI) scintillation detector. The gamma ray source and detector are perpendicular and aligned vertically to the sample. The gamma ray detector's energy window is set-up to measure only primary (unscattered) gamma photons (approximately 662 kiloelectron volts (keV)), providing raw gamma attenuation data in counts per second. At this energy, the primary mechanism for the attenuation of gamma rays is by Compton scattering. The gamma beam is collimated through a 5 mm window providing a down-core spatial resolution of approximately 1 cm.

https://doi.org/10.5281/zenodo.13971228

Calibration of the gamma density sensor operating on an MSCL-S is performed prior to core logging. Throughout any core logging phase, continuous checks of the live and raw data acquired from the gamma density sensor are made before, during, and after individual samples are analyzed. A check piece made from a homogenous rock sample is used to check that the calibration and sensor are recording correctly. The temperature of the core logging environment is also monitored throughout the core logging phase and corrections can be performed for any small variations.

Similar to pressure core measurements, conventional core data were reported as gamma density rather than bulk density. Bulk density can be calculated from the gamma density by multiplying the gamma density by an attenuation coefficient equal to the electron density of the aluminum standard over the electron density of the material being measured (Blum, **1997**). This coefficient is approximately 0.979 for marine sediments.

The reported gamma density also assumed that the core was of a constant diameter. Measurements could be improved by reprocessing the data using the X-ray CT data to constrain the diameter.

MSCL-S electrical resistivity

Electrical resistivity was measured using a non-contact resistivity sensor system (NCR) (Jackson et al., **2006**). NCR operates by inducing a high-frequency magnetic field in the core from a transmitter coil, which in turn induces electrical currents in the core which are inversely proportional to resistivity. Very small magnetic fields regenerated by the electrical current are measured by a receiver coil. To measure these very small magnetic fields accurately a technique has been developed which compares the readings generated from the measuring coils to the readings from an identical set of coils operating in air. This technique provides the requisite accuracy and stability required. Resistivities between 0.1 and 10 ohm-meters can be measured at spatial resolutions along the core of approximately 2 cm.

MSCL-S P-wave velocity

Ultrasonic P-wave velocity is measured using a pair of acoustic rolling contact P-wave transducers. A short P-wave pulse is produced at the transmitter; this pulse propagates through the sample and is detected by the receiver. The travel-time for pulse propagation through the sample is measured with a precision of ± 50 nanoseconds (ns). The sample diameter is also measured using a set of laser displacement transducers (coupled to the P-wave transducers) with a precision of ± 0.01 mm. The raw measurement is the outside diameter of the liner. The calculated core diameter assumes that the core liner has a constant wall thickness and that the core material fills the liner. Calibration of the ultrasonic P-wave velocity sensors operating on a Multi-Sensor Core Logger (MSCL-S) is performed prior to core logging. The calibration performed is so that the appropriate conversion factors can be applied to the raw data for interpretation purposes. Throughout any core-logging phase, continuous checks of the live and raw data acquired from the ultrasonic P-wave velocity sensors are made before, during, and after individual samples are analyzed. This is conducted by measuring the P-wave velocity of a piece of core liner filled with 0 ppt salinity water (check piece). The check piece is made from the same sample liner as the core sample. The check piece is logged at the start and end of each logging file. The temperature of the core-logging environment is also monitored throughout the core-logging phase and corrections can be performed for any small variations.

X-ray imaging

X-ray CT scanning was performed on whole-round sections using a stand-alone scanner at College Station, TX. Similar to PCATS, this stand-alone scanner also rotates the core and core liner during CT imaging. X-ray CT images are used to identify 3D sedimentary and structural features that are not easily visible on the split core surface, such as bioturbation, bedding planes, faults, fractures, mineral inclusions, erosion surfaces, and sedimentary laminae successions. X-ray CT scanning collects a series of X-ray images or slices

from a 360° perspective, creating 2D and 3D density-sensitive renderings of the core (Brooks and Di Chiro, 1976; Cnudde and Boone, 2013; McKetty, 1998). The technique can be completed on half- or whole-round core sections, providing 3D images of sediment prior to core splitting. This nondestructive technique allows discrimination between sediment volumes with a different X-ray attenuation, which is a function of the material composition (effective atomic number) and density (Cnudde et al., 2004) and can be used to image subtle changes in the composition of soft sediments. All images are positive meaning denser objects, which obscure the X-ray beam, appear darker than less dense material. Also see **X-ray artifacts**.

Radiographs, both CT slabs and CT slices were acquired from the CT data using the same technique as described in **PCATS X-ray imaging**. Computed laminography was not done on these sections.

Split core logging and imaging

Line scan imaging, color reflectance spectroscopy, magnetic susceptibility, and X-ray fluorescence was measured on all the split core archival halves at the Geotek facility in Salt Lake City using the MSCL-XZ.

MSCL-XZ linescan split core imaging

High-resolution (100 pixels/cm) split core images of the archive half of each core section were obtained. All core sections were imaged using the X-Z digital imaging system (DIS) immediately after being split and scraped. We found it particularly useful to scrape the cores immediately prior to imaging to capture the ephemeral nature of some sedimentary features, particularly iron-bearing minerals, which become oxidized within minutes of splitting the core. All images were acquired at a cross-core and downcore resolution of 100 pixels/cm. To retain the relative variability in core color within each borehole, we found it more expedient to fix the aperture of the camera at a value that would image most cores without the need for further adjustment.

The Geoscan VI color line-scan camera contains a single charge-coupled device (CCD) generating 5340 useable RGB pixels. Each pixel is 4 µm square with a total active array length of 21.3 mm. Dark reference pixels are used to compensate for electrical drift within the sensor due to temperature variations. These reference pixels are electrically identical to the active pixels but have been fabricated with an opaque layer over them. The digitized data from the CCD is 14-bit per color channel and is multiplexed and transmitted in 16-bit streams to the PC via a GigE interface.

The camera control includes automated focus, aperture, and lighting (for visible and ultraviolet light). Two banks of LEDs are used to illuminate the core evenly from both sides of the image line. This provides a flooded illumination that minimizes any shadow effects that could be caused from micro-topographic effects. The camera is arranged directly above the light and “looks” through a slot in the top surface of the light unit. Spurious reflections are reduced by black anodizing on both the camera and light units. There are slots below each LED bank for insertion of diffusing or polarizing filters. The polarizing filters on the lights, in conjunction with a polarizing filter on the camera lens, eliminate reflections from shiny or wet surfaces.

The camera is factory calibrated ahead of core imaging to ensure that the CCD pixels are scaled to the same black (minimum) and white (maximum) values. The high calibration is performed using a standard photographic 18% gray or 90% white flat calibration card, and the low calibration is performed with the lens caps on. This enables images to be qualitatively or quantitatively compared. Calibration files containing the high and low calibrations for each element in the CCD are written into the metadata for each image, along with the CCD convergence data, and acquisition parameters.

Images are collected in one continuous movement, with the images being stitched together live. Images are output as 48-bit RGB TIFF images and converted to JPEG or other formats as required. Each image is accompanied by an XML metadata file containing information of the core sample and acquisition

https://doi.org/10.5281/zenodo.13971228

conditions. In addition, a ruler is generated next to the image presenting either depth in core section or core depth.

A photograph of the split core working half was also taken after sampling. See **Split core sampling**.

MSCL-XZ color reflectance spectroscopy

The Konica Minolta CM-700d spectrophotometer uses a diffused illumination, 8° viewing angle with a pulsed xenon lamp providing the illumination. The instrument detector collects light in 10 nm increments between 400 nm and 700 nm wavelength ranges. The spectrophotometric method utilizes multiple sensors to measure the spectral reflectance of the object at each wavelength or in each narrow wavelength range. The sensor's electronics then calculate the tristimulus values from the spectral reflectance data using integration. The measuring aperture was set to 3 mm (small area of view). For each measurement, data for the specular components included (SCI) and excluded (SCE) are recorded simultaneously to analyze the core surface.

The CM-700d spectrophotometer is electronically calibrated to measure a reference piece provided by Konica. This reference piece is used to check the long-term consistency of the calibration and repeat the calibration measurement when necessary. The reflectance levels of the reference piece are stored internally in the spectrophotometer and are used in conjunction with the zero-calibration data to compute a correction factor to ensure reliable calibrated data are collected.

Data acquired using the CM-700d spectrophotometer requires very little processing as the calibration is applied to the data during acquisition. The data is presented as RGB, L*a*b* and XYZ color spaces along with Munsell color values.

The color of an object depends on both the physics of the object in its environment and the characteristics of the perceiving eye and brain (sensor). Physically, objects can have the color of the light leaving their surfaces; however, some objects not only reflect light, but also transmit light or emit light themselves which also contribute to the color. The L*a*b* color space expresses color as three numerical values: L* for lightness, a* for green to red and b* for blue to yellow. The color space is three dimensions, allowing for an infinite number of colors to be created and is designed to approximate human vision. L* represents black at 0 and white at 100 (grayscale); a* and b* are neutral gray at 0. a* negative values represent green and positive values red. b* negative values represent blue and positive yellow.

MSCL-XZ magnetic susceptibility

Surface magnetic susceptibility is measured using a Bartington MS2E point sensor for surface analysis. The frequency of the low-intensity, non-saturating, alternating magnetic field produced by the sensor is sensitive to changes in the magnetic susceptibility of material within the loop sensor or near the point sensor. Loop sensors vary in diameter and are chosen to fit the core diameter. Magnetic susceptibility measured with the point sensor has a line-shaped field of influence that is oriented horizontally across the sample and is approximately 3 mm wide. Calibration and data processing are carried out in the same manner as the loop sensor described under whole-round scanning.

MSCL-XZ X-ray fluorescence

The Olympus Vanta XRF sensor is a "handheld" XRF core scanner that is installed for automated scanning of cores on a variety of MSCL systems including the MSCL-S, MSCL-XZ and MSCL-XYZ. The unit is robust and versatile, and the associated Olympus software calculates concentration of elements, rather than simple peak intensity. The elemental concentration calibration for the Vanta instrument is a combination of an empirical linear response calibration with the method of fundamental parameters and is performed at the factory. Standardization occurs before each measurement is taken and allows the calibration to be adjusted for variation in X-ray tube output over time. The XRF spectra for each measurement point is processed using the Olympus software and

calibration files to determine the concentration of elements. The quantity of a particular element is greatly affected by the amount of fluorescent X-rays measured. Therefore, poor quality data is recorded close to fractures or irregular core surfaces. The data output is in parts per million but is uncalibrated. Hence, in this report we present XRF data as "uncalibrated instrument units." Each core section was covered with a 4 µm thick Ultralene window film to prevent sediment from accumulating the on the XRF sensor, while allowing for transmission of X-rays.

Summary of all core logging and imaging

Table T8 summarizes the core logging and imaging information available from this expedition. Figure F48 shows an example of all the images and photos collected for all pressure cores that sealed. The first three images are from PCATS and are collected before depressurization. The 2D radiography (radiograph) and computed laminography (CL) images capture the average density throughout the thickness of the core, while the CT slab is a 2D digital extraction from the 3D computed tomography scan. The X-ray attenuation is related to the bulk/wet density; thus, these color contrasts correspond to high- (Figure F48 dark areas) and low-density (Figure F48, light areas) zones. The next two images are 2D and 3D CT images of the core section after depressurization showing created voids from gas expansion (white areas) with faint laminations. The last two images are a gray-scale photo of split core archival half and a color photo of split core working half after discrete samples have been removed. See **PCATS X-ray imaging** for a discussion of radiographs, CL, and CT images.

Undrained shear strength

Undrained shear strength, S_u, of cohesive, mud-dominated sediments was measured in several ways from rapid, basic measurements made onboard the *Q4000*, to intermediate methods dockside in Salt Lake City, to advanced geotechnical experiments planned for post-expedition work. This section describes the methods employed onboard and dockside.

Onboard measurements

While onboard, a handheld shear vane and a pocket penetrometer (Figure F49) were used to estimate the undrained shear strength and aided in evaluating core quality and the consistency of the coring process. Measurements were made rapidly, typically within 1 hour of cutting core sections. Both are standard techniques in a variety of geotechnical engineering applications and are described in several reference texts (e.g., Germaine and Germaine, 2009). ASTM test method D8121 (ASTM International, 2018) provides details relative to the handheld vane equipment and procedures. Measurements were made on conventional and depressurized pressure cores, generally one measurement location per section of core (See **Conventional core processing**).

Measurement locations

Measurements were made on each core section either at the bottom of the section or the bottom of a piece of the section designated as a whole-round sample for moisture and density measurements (sample code MDW, See **Conventional core processing** and **MDW, MAD, and CRS whole-round samples**). Two samples were measured at the top. At each sampling location, a single vane shear measurement was obtained in the center of the circular core section followed by 2-3 pocket penetrometer measurements acquired in the space around the vane shear location (Figure F50). Loose material was removed, and obvious cracks and voids were avoided. Uneven surfaces were gently smoothed with a spatula to achieve a flat testing surface.

Handheld shear vane

The handheld shear vane has three shoes (Figure F50). Each shoe measures a different range of shear strength. The standard shoe is used for soft sediment and can be used on sediment up to 1 kg/cm^2 (98 kPa). The measured shear strength is taken directly from the vane reading (multiplier is 1.0). The large shoe has a larger surface area and a higher resolution. The large shoe can be used on very soft sediments and can measure shear strengths up to 0.2 kg/cm^2

https://doi.org/10.5281/zenodo.13971228

A.Core Type	B. Core Process	C. Sample Code	D. PCATS			E. MSCL-IR	F. MSCL-S and X-ray				G. MSCL-XZ	
			P-wave velocity, gamma density	Radiograph and CL (0- and 90-degree)	CT Slabs (0- and 90-degree), CT slices	Thermal Imaging	P-wave velocity, gamma density, natural gamma, and resistivity	Magnetic susceptibility	Radiograph (0- and 90-degree)	CT Slabs (0- and 90-degree), CT slices	Linescan of archived half and photo of working half after sampling	Color reflectance, magnetic susceptibility, X-ray fluorescence
FB and CS	STORE	STORE	Yes	Yes	Yes							
	QD	IWR, IWO, MB	Yes	Yes	Yes							
		MDW, GEOM	Yes	Yes	Yes			Yes	Yes	Yes		
		A, W	Yes	Yes	Yes			Yes	Yes	Yes	Yes	Yes
	CRYO	CRYO	Yes	Yes	Yes						W half only	
	RD	BAG	Yes	Yes	Yes							
	Conv. (failed pressure core)	IWR, IWO, MB		H002 only								
		MDW, GEOM		H002 only				Yes	Yes	Yes		
		A, W		H002 only				Yes	Yes	Yes	Yes	Yes
		BAG		H002 only								
H and X	Conv.	IWR, IWO, MB				Yes						
		MDW, GEOM				Yes	Yes	Yes	Yes	Yes		
		A, W				Yes	Yes	Yes	Yes	Yes	Yes	Yes

Table T8: Summary of core logging and imaging. A) Core types including the Pressure Coring Tool with Ball Valve in the Face Bit configuration (code FB) and the Cutting Shoe configuration (code CS), Geotek Advanced Piston Corer (code H), Geotek Extended Core Barrel (G-XCB, code X); B) Core process including storing pressure core at high pressure and low temperature (STORE), quantitatively degassing pressure core (QD), cryogenically freezing and depressurizing pressure core (CRYO), rapidly degassing pressure core (RD), and conventional core processing (Conv.). Failed pressure cores (conventionalized cores) were processed as conventional cores; C) Sample codes including regular pore water sample (IWR), organic pore water sample (IWO), microbiology sample (MB), moisture and density (MDW), geomechanics (GEOM), archival half (A), working half (W), and bagged unconsolidated sediment (BAG); D) Pressure Core Analysis and Transfer System (PCATS) logging and imaging. Failed pressure cores from Hole H002 were repressurized with air, logged and imaged in PCATS before conventional core processing; E) Multi-Sensor Core Logger (MSCL) infrared imaging (IR); F) MSCL standard (S) core logging and X-Ray imaging; G) MSCL split core (XZ) logging and imaging.

(20 kPa). Vane readings must be multiplied by 0.2. The small shoe has the smallest surface area and the lowest resolution. The small shoe is used for stiffer sediment and can measure shear strengths up to 2.5 kg/cm^2 (245.16625 kPa). Vane readings must be multiplied by 2.5. Most of the measurements were collected using the standard shoe. The larger vane shoe was used for the first few cores, and the small shoe was used for the deepest cores.

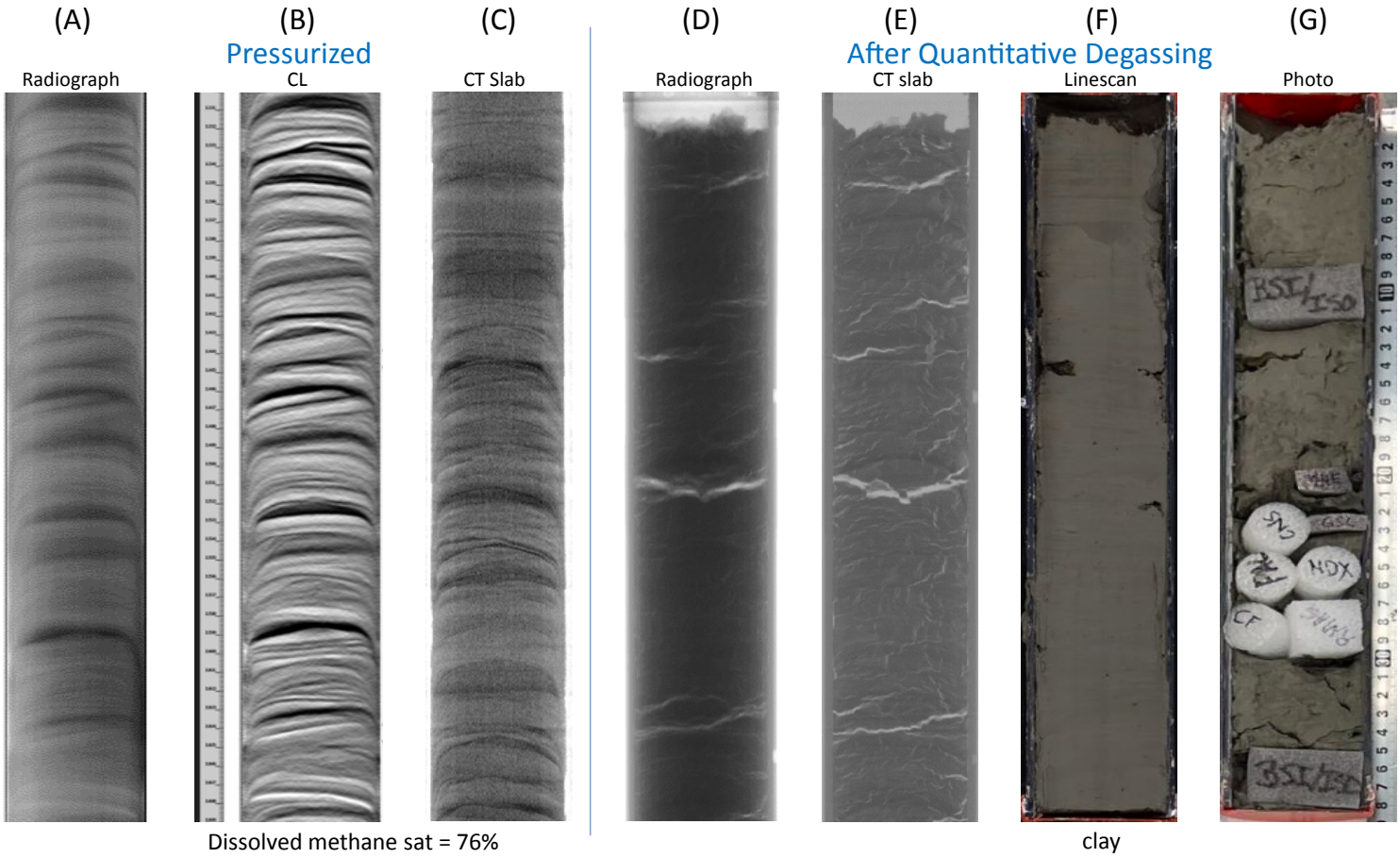

Figure F48: Images and photos of 20 cm intervals of H003-08CS. Image widths are stretched ~2X. From Left to Right; A) Radiograph from the Pressure Core Analysis and Transfer System (PCATS); B) Computed Laminography (CL) from PCATS (high contrast filter exaggerates the density variation); C) Computed tomography (CT) slab image with digitally-enhanced contrast from PCATS; D) Radiograph after depressurization showing voids created from gas expansion (white areas) taken using a stand-alone scanner in College Station, TX; E) CT slab image after depressurization with voids from gas expansion (white areas) taken in College Station; F) LineScan photo of split core archival half taken using the Multi-Sensor Core Logger (MSCL-XZ); G) iPhone photo of split core working half after discrete samples have been removed. See **PCATS X-ray imaging** for a discussion of radiographs, CL, and CT images.

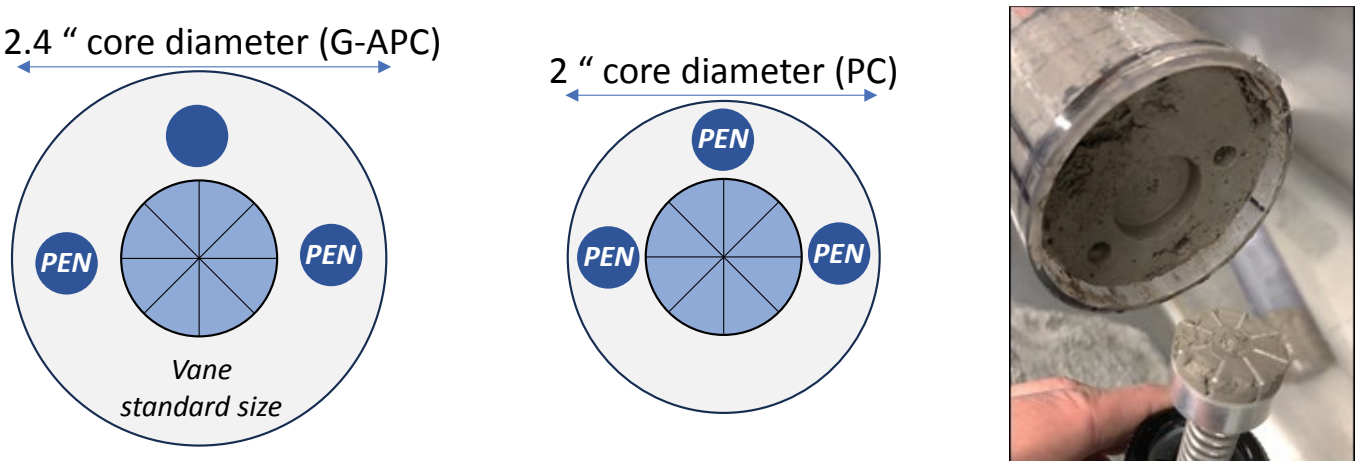

Figure F49: (left) Diagram of testing locations for handheld vane shear and pocket penetrometer made onboard on conventional piston cores (diameter = 2.4 inches (60.9 mm)) and pressure cores (diameter = 2 inches (50.8 mm)). Vane shear was measured first in the center of the core (measurement code VANE). Pocket penetrometer measurements were made in the available space around the vane location and away from core edges (measurement code PEN). Photo shows the vane shear device and an Advanced Piston Core (G-APC) section after VANE and PEN measurements.

https://doi.org/10.5281/zenodo.13971228

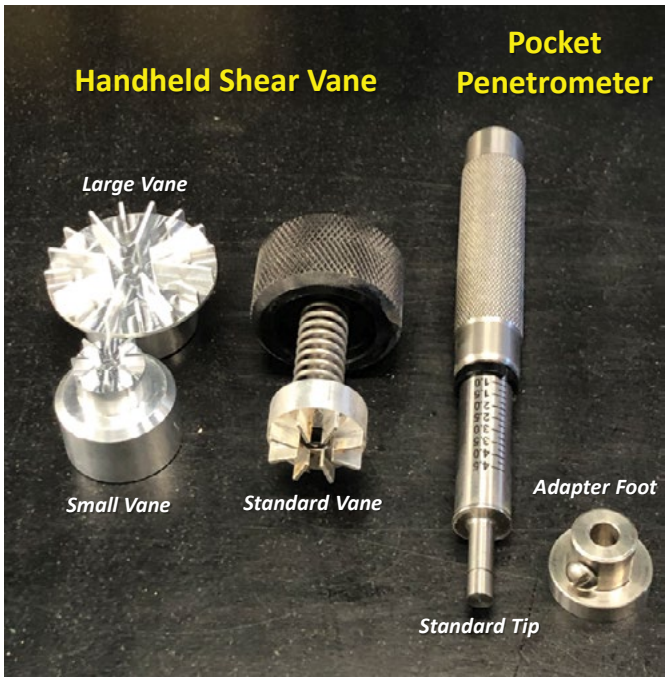

Device	Manufacturer Model No.	Specs	Diameter
Handheld Vane Shear	Humboldt Mfg. H-4212MH	Standard vane	25.4 mm
			1.0-in.
		Large vane	47.6 mm
			1.88-in.
		Small vane	19.0 mm
			0.75-in.
Pocket Penetrometer	Humboldt Mfg. H-4195	Standard tip	6.4 mm 0.25-in.
		Adapter foot	25.4 mm 1.0-in.

Figure F50: Handheld vane and pocket penetrometer devices used for onboard sediment strength measurements. The handheld vane is pictured with a standard shoe attached. The face of the vane, where the meter readings are observed, is not shown. The standard shoe can measure shear strengths of up to 1 kg/cm² (capacity of 1 kg/cm²). Large and small shoes are used for softer and stiffer materials, respectively. All three shoes were used. Pocket penetrometer pictured with standard tip attached. Adapter foot is added when measuring the strength of softer material. Only the standard tip was used.

The testing followed the standard procedure as defined in ASTM D8121/D8121M (ASTM International, 2018). The procedure is summarized here:

1. Mount the desired vane (small, standard, or large) to the device and secure by hand tightening the mounting screw with the hex key.
2. Make sure the vane is clean and dry.
3. Align the "0" on the inner dial on top of the unit with the mark on the outer ring using a counterclockwise rotation while holding the outer ring.
4. The test surface should be relatively flat. Loose material should be removed, and obvious cracks and voids avoided. Uneven surfaces can be gently smoothed with a spatula to achieve a flat testing surface.
5. Press the unit into the sediment sample until the blades are covered. If the sediment is too stiff to press the vanes into the sample, switch to the pocket penetrometer (see below).
6. While maintaining a constant pressure against the sediment, rotate the outer ring of the unit. Turn the outer ring until failure occurs. (The speed of rotation should accomplish failure within 5 to 10 seconds.)
7. Release the outer ring, slowly, once failure has occurred. The mark on the outer ring will remain in place, indicating the shear value at failure. Note one full revolution is 1.0 kg/cm², therefore the dial readings are in tenths of 1 kg/cm².
8. Record the dial reading to 0.01 kg/cm², measurement location depth within section, and additional information required to completely fill one line in the "shipboard strength log."
9. Clean device by removing clay pieces between the vanes on the shoe and brushing while submerged in water.
10. Dry and store device.

Pocket penetrometer

A pocket penetrometer (Figure F50) is a flat-footed, cylindrical probe that provides a measure of the unconfined compressive strength (q_u) of sediment, which is equal to S_u (Germaine and Germaine, 2009). Unconfined compressive strength is a measure of the major principal stress (σ_1) at failure for the condition of zero minor principal stress ($\sigma_3 = 0$) and with no drainage allowed. The method works by pressing the foot into the flat surface at the end of the sample until the indicator line meets the soil surface. The maximum reading is retained by a slip ring. The penetrometer creates an undrained bearing capacity failure in the soil and the scale is calibrated to provide the compressive strength of the material. The scale of the pocket penetrometer reads in kg/cm² and has a range of 0 – 4.5 kg/cm² (equivalent to undrained shear strengths of up to 220 kPa when using the standard tip). When the larger adapter foot is used, which has a diameter of 25.4 mm (1 in.), the results on the scale must be divided by 16. For this expedition, only the standard tip was used.

The testing procedure follows Germaine and Germaine (2009), and was carried out as follows:

1. Select test spots with a smooth surface.
2. Slide the ring down against the handle (knurled portion) of the penetrometer.
3. Hold the pocket penetrometer at right angles to the surface being tested.
4. Grip the handle and push the tip of the penetrometer into the sediment so the groove marked on the tip is even with the level of the soil.
5. Read the scale from the bottom of the ring (side closest to the handle) to determine the unconfined compression strength (q_u) directly from the scale in kg/cm².
6. At each sample location, 3 pocket penetrometer measurements were obtained in the area around the vane shear testing location (Figure F49). If core quality is not sufficient for 3, then 2 were obtained. Each individual measurement is recorded, and the average is calculated and reported.
7. Dry and store device.

Data recording, calculations, and plots

Readings were recorded by hand and then transferred into an Excel workbook "UT-GOM2-2 Shipboard Hand Vane and Pocket Penetration Log" (Figure F51). The master workbook records details including depth in section, depth in meters below sea floor, time and date, vane and penetrometer tip selection, notes, and calculations. Also, there were occasional locations where no penetrometer or vane measurements could be made. There, a comment was given about why a measurement was not measured (NM, i.e., poor core condition, too sandy, too soft/weak).

Dials on both devices are in kilograms per square centimeter (ksc or kg/cm²). Dial readings from the handheld vane and pocket penetrometer are converted to S_u in units of kPa from Equations E9 and E10, respectively.

Calculations of S_u for the handheld vane shear device:

$$S_u(kPa) = \frac{DR_{vane}}{10} \times VF \times 98.0665 \frac{kPa}{ksc}$$

Equation E9.

where,

DR_{vane} = Vane shear dial reading (nearest 0.01 ksc),

VF = Dimensionless vane factor for handheld shear vane device:

- Vane Factor = 1.0 for the standard shoe,
- Vane Factor = 2.5 for the small shoe,
- Vane Factor = 0.2 for the large shoe.

Calculations of S_u for the pocket penetrometer:

$$S_u(kPa) = \frac{q_u}{2} = \frac{DR_{pen} \times TF}{2} \times 980665 \frac{kPa}{ksc}$$

Equation E10.

https://doi.org/10.5281/zenodo.13971228

where,

q_u = unconfined compressive strength,

DR_{pen} = Pocket penetrometer dial reading (nearest 0.05 ksc),

TF = Dimensionless tip factor for pocket penetrometer:

- Tip Factor = 1.0 for the standard tip,
- Tip Factor = 0.0625 for the large adapter (not used).

The calculated undrained shear strength data is plotted versus depth as a scatter plot with distinct symbols to distinguish vane and pocket penetrometer values. The results were plotted as soon as possible to provide supporting information for identifying G-APC refusal depth.

Salt Lake City (Dockside) post expedition lab studies

Approximately 1 month after cores were acquired, measurements of strength were performed with a fall cone penetrometer and an automated table vane shear device at Geotek in Salt Lake City (18-24 September 2023).

We constructed a frame to accommodate core sections of variable length (Figure F52). Both devices were mounted on top of the table frame. Core sections were positioned vertically on an adjustable platform and secured with a vise grip. The table frame allowed for easy and efficient testing.

Figure F52: Two core sections mounted on the adjustable frame being tested with the fall cone penetrometer (right side) and automated vane shear device (left side) with connected computer and display.

Measurement location

Measurements were made on each core section at the bottom of the core section after the MDW whole-round had been removed. At each sampling location, a single fall cone measurement was obtained in the center of the circular core section followed by a single table vane measurement. Loose material was removed, and obvious cracks and voids were avoided. Uneven surfaces were gently smoothed with a spatula to achieve a flat testing surface. The fall cone measurement was made first and the sediment was not smoothed or treated between the fall cone and vane measurement.

SLC Fall Cone and Laboratory Vane Measurement Log

Entry	Location						Who and When			Fall Cone Measurements					Lab Vane Measurements				
No.	Hole	Core	Section	Depth	Depth	Surface	Tester Initial	Date	Time	Cone	Cone Mass	Penetration	Strength (K = 0.4)	Strength (K = 0.29)	Vane Diameter	File Name	Peak Strength	Remolded Strength	Remarks
				(cm)	MBSF	Vert Horiz				(°)	(g)	(mm)	(kPa)	(kPa)	(mm)		(kPa)	(kPa)	
1	H003	1H	4a	95	5.45	Horiz	DS+JTG	9/18/2023	1800	60	80	7.05	6.32	4.58	12.7	LV001	11.93	3.95	
2	H003	1H	5a	81	6.81	Horiz	DS+JTG	9/18/2023	1815	60	80	7.85	5.09	3.69	12.7	LV002	9.90	3.25	
3	H003	2H	1a	100	9.23	Horiz	DS+JTG	9/19/2023	700	60	80	7.00	6.41	4.64	12.7	LV003	12.79	5.23	
4	H003	2H	2a	100	10.73	Horiz	DS+JTG	9/19/2023	710	60	80	4.00	19.62	14.22	12.7	LV004	9.48	3.87	
5	H003	2H	3a	100	12.23	Horiz	DS+JTG	9/19/2023	730	60	80	9.65	3.37	2.44	12.7	LV005	5.58	NM	NM = 2nd shear phase did not start.
6	H003	2H	3a	100	12.23	Horiz	DS+JTG	9/19/2023	745	60	80	9.65	3.37	2.44	12.7	LV005A	5.71	1.51	
7	H003	2H	4a	100	13.73	Horiz	DS+JTG	9/19/2023	800	60	80	5.70	9.66	7.00	12.7	LV006	9.22	2.97	
8	H003	2H	5a	100	15.23	Horiz	DS+JTG	9/19/2023	820	60	80	6.35	7.79	5.64	12.7	LV007	11.32	3.21	
9	H003	2H	6a	100	16.73	Horiz	DS+JTG	9/19/2023	835	60	80	5.10	12.07	8.75	12.7	LV008	11.11	4.23	
10	H003	2H	7a	66	17.89	Horiz	DS+JTG	9/19/2023	850	60	80	6.80	6.79	4.92	12.7	LV009	12.20	3.70	

Figure F51: Screen capture of master log sheet for onboard sediment strength measurements.

Fall cone penetrometer

We used a fall cone penetrometer (ELE model no. 24-0545) with a 30° cone to measure undrained shear strength on whole core rounds prior to core splitting. A fall cone measures the penetration of a cone as it free falls and embeds itself in the sediment (Germaine and Germaine, **2009**). During testing, the cone (pointing downward) is lowered so that it just touches the surface of the split core before it is locked in place. The cone is then released for a total of 5 s to penetrate the sample. The penetration depth is recorded on the log sheet. Undrained shear strength is determined using the empirical formula of Hansbo (**1957**) (Equation **E11**):

$$S_u = K_c \frac{M \times g}{d^2}$$

Equation E11.

where S_u is undrained shear strength (kPa), K_c is an empirical factor related to the cone angle and sediment type, *M* is the total mass of the cone plus any additional masses (in grams), g is acceleration due to gravity (in m/s^2), and d is the penetration depth of cone (in mm).

The mass of the cone is 80 grams, which is suitable for softer sediments. We added an additional 50 grams or 100 grams for stiffer material, for a total mass of 130 g and 180 g.

The cone factor (K_c) depends on the apex angle of the cone. We used a cone factor of 0.83 for a 30° smooth cone (Karlsson, **1961**; Wood, **1985**; Zreik et al., **1995**).

The accuracy of the measurement is dependent on correctly determining the position of the cone above the split surface of the core. The error induced by the initial location of the cone is approximately 0.2 mm. In addition, the analog dial used to read the cone position before and after the release leads to a typical error of 0.05 mm. Hence, the maximum resolution of the measurement of the penetration distance of the cone is estimated to be 0.3 mm. More cohesive and stiff sediment, where cone penetration is less than 2 mm, can result in as much as a 15% error. In addition, the formula of Hansbo (**1957**) may be inadequate for silty sediment, therefore fall cone measurements are best suited for clay-dominated intervals.

Step-by-step procedure for the fall cone test:

1. Secure the sample so that it will not move during the test (Figure **F52**).
2. Clean the cone and make sure the tip is sharp.
3. Lower the cone to be flush with the soil surface.
4. Zero the dial indicator.
5. Release the cone locking mechanism for 5 seconds.
6. Lock the cone.
7. Lower the dial indicator and record the total penetration in mm.

Automated laboratory vane shear

We used a Wille Geotechnik automated vane shear tester (model 10102-A6-001) to determine peak and residual undrained shear strengths. The shear vane apparatus consists of four vanes perpendicular to each other that are inserted in the sediment to their full length while attempting to minimize disturbance to the sediment. The failure surface is a cylinder defined by the length and width of the blades. The procedures are standardized in ASTM D4648 Laboratory Miniature Vane Shear Test for Saturated Fine - Grained Clayey Soil (ASTM International, **2008c**). The laboratory vane is a test that operates on the same principal as the handheld shear device but allows for better control of the testing conditions (Germaine and Germaine, **2009**).

For all experiments, we used a vane ‘type-c’ with dimensions of 12.7 mm (width) and 25.4 mm (height). To perform the laboratory vane test, the vane was inserted into the sediment to a depth equal to twice the vane height (50.8 mm).

We performed two phases of shear per experiment. The first phase determined the peak undrained shear

https://doi.org/10.5281/zenodo.13971228

strength. The second shear phase determined the residual undrained shear strength. The ratio of peak to residual strengths defines the sensitivity. For the first shear phase, the vane was rotated at a constant rate of 60° per minute until the peak strength was reached and allowed to continue beyond the peak value as the resistance dropped. The first shear phase was stopped after the post-peak resistance reached at most 90% of the peak strength. After the first shear phase and before the second shear phase, we performed a fast-shear phase at 1,200° per minute to ensure that the sediment was fully remolded (ASTM International, 2008c). The second shear phase started immediately after the fast-shear and conducted at the same rotation speed as the first shear phase and stopped once the maximum resistance was reached (the residual strength).

For both shear phases, data were recorded to an ASCII file at a sample rate of 0.5 seconds with time, angle, torque, and shear resistance. The data for the fast-shear phase are not recorded by the device.

Undrained shear strength is calculated as (Equation E12):

$$S_u = \frac{T}{K_v}$$

Equation E12.

Where, S_u = undrained shear strength (kPa), T = torque measured (Nm), and K_v = vane constant (m^3) defined by the vane diameter (*D*) and height (*H*) (Equation E13:

$$K = \pi \frac{D^2 H}{2} \left(1 + \frac{D}{3H}\right) \times 10^{-9}$$

Equation E13.

where *D* is the diameter of the vane (mm) and *H* is the height of the vane (mm).

Step-by-step procedure for the laboratory vane shear test:

Define the file name used to store the computer recorded data file. The naming convention was "LV###" where LV refers to lab vane and the numbers increase from 001 to the total number of experiments.

1. Secure the sample so it will not move or rotate during the vane test (Figure F52).
2. Zero the vane position and torque.
3. Lower the vane into the soil to the indicator mark on the vane shaft.
4. Run the computer program.
5. Record the peak strength: this is the maximum value in the first shear phase.
6. Residual strength: this is the peak value of the second shear phase.
7. Extract the vane from the sample.
8. Clean the vane.

Data recording, calculations, and plots

Readings were recorded by hand and then transferred into an Excel workbook "SLC_Fall_Cone_and_Lab_Vane_Log_24Sep23.xlsx." including other testing details and information (Figure F53). All digital data and further details for the onboard and dockside strength testing programs were archived as 'read-me' files on the project database.

Index properties

Table T9 summarizes the sampling, the index properties determined, and where the measurements were made. Accurate moisture and density measurements require precise mass measurements and baking specimens for an extensive time. Neither of these capabilities existed on the *Q4000* and hence initial weights were measured in Salt Lake City and the remaining measurements were made post-cruise at Tufts University.

Sampling, subsampling, and measurements

Samples for determining index properties were collected from split cores and whole-rounds.

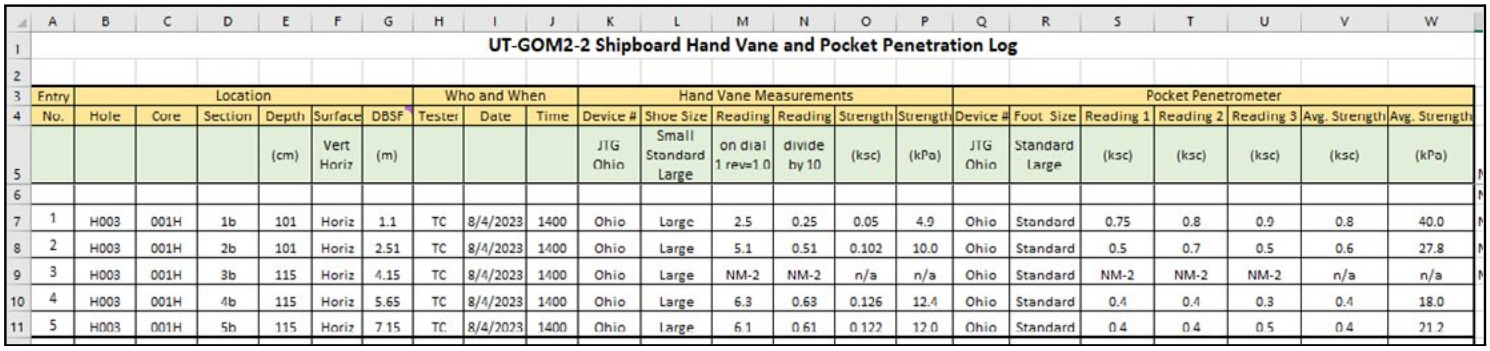

UT-GOM2-2 Shipboard Hand Vane and Pocket Penetration Log

Entry	Location						Who and When			Hand Vane Measurements						Pocket Penetrometer						
No.	Hole	Core	Section	Depth (cm)	Surface Vert Horiz	DBSF (m)	Tester	Date	Time	Device # JTG Ohio	Shoe Size Small Standard Large	Reading on dial 1 rev=1.0	Reading divide by 10	Strength (ksc)	Strength (kPa)	Device # JTG Ohio	Foot Size Standard Large	Reading 1 (ksc)	Reading 2 (ksc)	Reading 3 (ksc)	Avg. Strength (ksc)	Avg. Strength (kPa)
1	H003	001H	1b	101	Horiz	1.1	TC	8/4/2023	1400	Ohio	Large	2.5	0.25	0.05	4.9	Ohio	Standard	0.75	0.8	0.9	0.8	40.0
2	H003	001H	2b	101	Horiz	2.51	TC	8/4/2023	1400	Ohio	Large	5.1	0.51	0.102	10.0	Ohio	Standard	0.5	0.7	0.5	0.6	27.8
3	H003	001H	3b	115	Horiz	4.15	TC	8/4/2023	1400	Ohio	Large	NM-2	NM-2	n/a	n/a	Ohio	Standard	NM-2	NM-2	NM-2	n/a	n/a
4	H003	001H	4b	115	Horiz	5.65	TC	8/4/2023	1400	Ohio	Large	6.3	0.63	0.126	12.4	Ohio	Standard	0.4	0.4	0.3	0.4	18.0
5	H003	001H	5b	115	Horiz	7.15	TC	8/4/2023	1400	Ohio	Large	6.1	0.61	0.122	12.0	Ohio	Standard	0.4	0.4	0.5	0.4	21.2

Figure F53: Screen capture of master log sheet dockside sediment strength measurements via fall cone and laboratory vane shear testing.

Hole and Sample type	Sample Type	Measurement					
		Grain size	Wet density	Water Content	Saturation	Grain Density	Porosity
A. MDX and GSL discrete samples	**GSL Plugs from split cores**	UT - laser particle analysis	-	-	-	-	-
0-859.6 mbsf (Hole H002 and Hole H003)	**MDX Plugs from split cores**	-	Tufts	Tufts	Tufts	Tufts - Gas Pycnometer	Tufts
B. MDW whole-rounds	**MDW 5 cm CRS whole-round**	-	-	-	-	-	-
	MAD whole-round before subsampling	-	Tufts	Tufts	Tufts	-	Tufts
0-296.4 mbsf (Hole H003)	**MAD Plugs**	-	Tufts	Tufts	Tufts	-	Tufts
	MAD Wedges	-	-	Tufts	-	-	-
	MAD Blended material	Tufts - hydrometer	-	Tufts	-	Tufts - Water submersion	-

Table T9: Sampling and index properties for Holes H002 and H003 with location where final measurements were made. A) Discrete sediment samples taken from H002 and H003 split cores including samples for laser grain size (sample code GSL) and moisture and density, X-ray fluorescence, and X-ray (sample code MDX, See **Split core sampling**); B) Whole-round samples (sample code MDW) and subsamples for moisture, density, and constant rate of strain (CRS) measurements.

Split core plugs

Index property plug samples were collected from split cores (Table T9, row A, see **Discrete sampling methods**). They were oriented perpendicular to the axis of the core.

Split core plugs (sample code MDX, Table T9, row A) were acquired for moisture and density (MAD) measurements. The sample wet mass was determined from measurements made in Salt Lake City (See MDX under **Discrete sampling methods**). These MDX plugs were shipped to Tufts, where they were dried at 110 °C to constant mass in a forced draft oven, cooled in a vacuum chamber for at least 10 minutes, and weighed without covers. The mass of the dry plug and container (without the cover) was recorded to 0.001

https://doi.org/10.5281/zenodo.13971228

g. Sample volume was determined from the length of the sample measured in Salt Lake City and the known diameter of the brass corer used to create the sample (Figure F44). After measuring the mass, plugs were stored in sealed glass containers in a 4 °C refrigerator for future analysis of salinity and grain density. MAD properties of wet density, water content, porosity, water saturation, and grain density of the MDX plugs were determined (See **Wet density**, **Water content**, **Porosity**, **Water saturation**, and **Gas pycnometer**).

Split core plugs were also acquired for grain size measurements (sample code GSL, Table T9, row A, see GSL under **Discrete sampling methods**). These samples were shipped to UT for laser particle analysis (See **Laser particle analysis**).

Whole-round samples and whole-round plugs, slices, and blended material

MDW, MAD, and CRS Whole-Round Samples

Index property whole-rounds were cut from whole-round core sections in lengths of up to 20 cm at Salt Lake City (sample code MDW, Table T9 row B). They were collected adjacent to the microbiology whole-rounds as part of the whole-round set (See **Core processing in Salt Lake City**). Wet sample weights of the MDW whole-rounds were measured in Salt Lake City.

MDW whole-rounds were shipped overnight to a Tufts University laboratory in coolers with thermal packs to reduce temperature variations. Each MDW whole-round was processed at Tufts using the methods summarized below. This processing was done quickly to avoid changes in water content, and parchment or wax paper was used on interfaces to prevent sticking and water adsorption during handling.

The MDW whole-round sample was removed from the plastic bag. Caps were removed and the mass of the plastic core liner with the sediment was measured and compared to measurements made in Salt Lake City. The length of sediment in core liner and the length of the core liner were also measured.

Images of the cores were reviewed and a 5 cm length whole-round sample was cut from one end of the whole-round if the sample end was a good candidate for Constant Rate of Strain (sample code CRS) compression tests. If cut, the 5 cm whole-round was labeled, sealed, and stored in a refrigerator at 4 °C.

The remaining sample (sample code MAD) was extruded from the core liner while tracking its orientation in the borehole (top). The mass of the empty core liner was measured. All masses were determined to the nearest 0.01 g and all lengths to the nearest 0.01 mm. The wet density, porosity, and water saturation of the MAD whole-rounds were determined (See **Wet density**, **Porosity**, and **Water saturation**).

The sediment sample was divided according to the following method. The sediment was split in half lengthwise using wire saw or knife depending on sediment stiffness (Figure F54, top). One half of the whole-round (Figure F54, 1) was used to obtain a UNH subsample for sediment geochemistry. This half was placed with the flat side down (Figure F54 middle). Two vertical cuts were made to obtain a center slice that is about 1 cm thick (Figure F54 B and C). Using the center slice, one lengthwise cut was made to obtain a 1 cm slice from the center edge (Figure F54 C). This rectangular slice was transferred to a plastic U channel with the incoming (zero) CT direction on top and the shallow end (top) was labeled on the U channel. The U channel was wrapped in plastic, sealed in a zip-lock bag, labeled, and refrigerated. The wrapped U channels were then transported to UNH.

MAD plugs

The second half of the MAD whole-round was used to obtain a cylindrical plug for measuring MAD (Figure F54 2). This second half was placed with the exterior curved side down. A brass corer (Figure F54) was centered over the thickest part of a clay-rich portion of the sample and used to cut a plug through the half (Figure F54 G). Thus, the cylindrical plugs were oriented perpendicular to the axis of the core.

A small amount was extruded from the brass corer and trimmed off with a wire saw. The remaining plug length was then measured to the nearest 0.01 mm

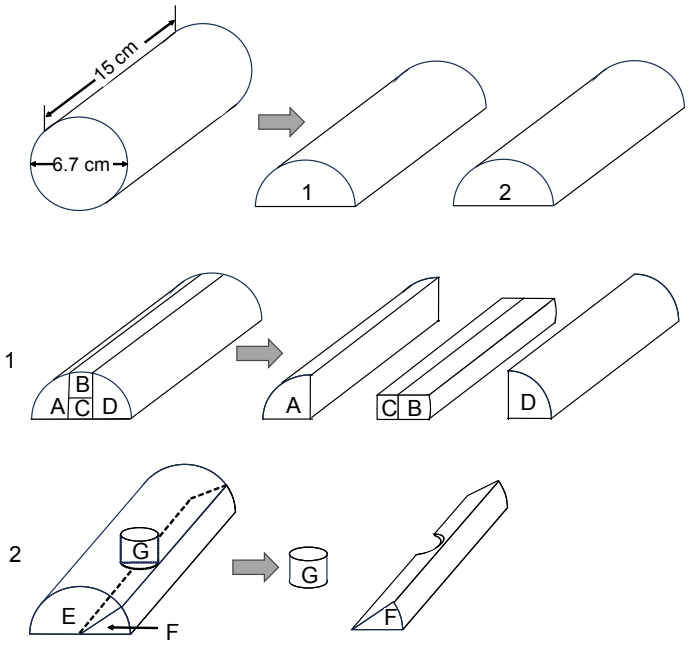

Figure F54: Processing of moisture and density whole-round samples (sample code MDW) into pieces for individual moisture and density measurements. A constant rate of strain sample (sample code CRS) was often cut off at one end and the remaining whole-round (sample code MAD) was split into two halves, 1 and 2. Half 1 was used to extract a clean center channel from the whole-round for UNH (sample C). Half 2 was used to extract a MAD plug (sample G) and, for water content, a wedge of the whole (sample F). The remaining material from half 2 was blended and tested as shown in Table T9.

and extruded into a marked glass container of known mass to the nearest 0.01 g. These plug samples were dried at 110 °C to constant mass in a forced draft oven, cooled in a vacuum chamber for at least 10 minutes, and weighed. The mass of the dry plug and container were recorded to 0.01 g. Sample volume was determined from the length of the sample and the known diameter of the brass corer used to create the sample (Figure F54). After measuring the mass, plugs were stored in sealed glass containers in a 4 °C refrigerator for future analysis of salinity and grain density. MAD properties of wet density, water content, porosity, water saturation, and grain density of the plugs were determined (See **Wet density**, **Water content**, **Porosity**, **Water saturation**, and **Gas pycnometer**).

MAD wedges

MAD wedges were used to determine water content (See **Water content**). A pie shaped slice cut about 15 degrees along the length of the half (Figure F54 F) was used to obtain the average water content of the whole-round. The slice was transferred to an aluminum container of known mass to nearest 0.01 g. The slices were dried at 110 °C to constant mass in a forced draft oven, cooled in a vacuum chamber for at least 10 minutes, and weighed to the nearest 0.01 g. After measuring the mass, the slices were stored in sealed containers for future use in a 4 °C refrigerator.

MAD blended material

All the remaining material from the second half was combined and blended on a glass plate (Figure F54 A, B, D, and E). A representative sample of about 50 g was removed, and the water content was measured for this sample. The rest of the blended material from the whole-round was transferred to a storage container of known mass and labeled. The mass of the container was measured and then stored in a 4 °C refrigerator.

MAD blended material was used to determine water content and grain density (See **Water content** and **Water submersion**)

Particle size distribution

Two different methods were used to measure grain size from the MAD and grain size samples: laser particle analysis and the settling or hydrometer method. Systematic laser and hydrometer method comparison studies (Di Stefano et al., **2010**; Ferro and Mirabile, **2009**; Wen et al., **2002**) have shown that the laser method typically reports a larger particle size for plate-shaped clay particles than does the hydrometer method. This is because the laser method reports a value weighted towards the average particle dimension, whereas the hydrometer method reports a value weighed towards the thin (short) dimension. Thus, some samples may be classified as clayey silt when measured with the laser whereas they will be called silty clay when measured with the hydrometer.

Laser particle analysis

Particle size distribution was measured on subsamples (<1 g) of GSL discrete samples obtained

https://doi.org/10.5281/zenodo.13971228

from split cores from Hole H002 and Hole H003 (See **Discrete sampling methods**). Prior to analyses, subsamples were mixed with a 0.5% solution of sodium hexametaphosphate (dispersant) to create stable slurries where grains could not settle out of suspension, which allowed us to obtain representative subsamples. Samples mixed with excess sodium hexametaphosphate solution (grains settling) were dried in an oven at 40 °C until the desired slurry consistency was reached. Grain size analyses were performed using a Malvern Mastersizer 3000 particle size analyzer with a Hydro LV dispersion unit (600 mL volume). The stable slurries were thoroughly mixed and added individually in a stepwise fashion into the dispersion unit containing fresh water until the laser obscuration was between 10% and 20%. The particle size analyzer settings used a particle refractive index of 1.55, a particle absorption index of 0.1, a dispersant refractive index of 1.33, a stirring/pump speed of 2500 rpm, and sonication at 80% of maximum for 40 seconds prior to measurements. The grain size distributions of sand, silt, and clay were reported for each sample using two classifications (See **Grain size classifications**).

Hydrometer

Particle size distribution was analyzed using a hydrometer method following (ASTM International, **2009a**) on blended material from the moisture and density whole-round samples (sample code MAD, See **Conventional core processing**). The 35–40 g of homogenized sediment was thoroughly mixed with water and 5 g of sodium hexametaphosphate, a dispersing agent. The mixture was then blended for 1 minute in a malt mixer. A suspension was created by transferring the slurry to a cylinder and diluting it to 1 liter. The cylinder was then capped with a rubber stopper and allowed to come to equilibrium overnight at room temperature. A specific gravity hydrometer was used to measure the suspension density as a function of settling time. After the test, the slurry was separated using a 75 µm sieve to observe the sand sized fraction. The dry mass of the sediment was measured at the end of the test by oven drying to constant mass at 110 °C. Since the separation was not done using 62.5 µm sieve, the half minute hydrometer reading was used to approximate the 62.5 µm cutoff for the geoscience classification. The grain size distributions of sand, silt, and clay were reported for each sample using the two classifications (see **Grain size classifications**).

Moisture and density

MAD measurements were made on five types of specimens: cylindrical plugs removed from split cores (see **Split core plugs**), whole-round sections, and plugs, slices, and blended material removed from those whole-round sections (See **Whole-round samples and whole-round plugs, slices, and blended material**).

Wet density

Wet density, sometimes called bulk or total density (ASTM International, **2009b**), determinations require measurements of the wet mass and wet volume. Mass measurements were straight forward but the volume determination for the whole-rounds was a challenge, depending on the stiffness of the material. This leads to the use of several methods for the determination of volume. If the sample is regular shaped, the physical dimensions of the sample were measured. Otherwise, the mass measurements are used with the additional measurements of the grain density and the salt content of the pore fluid were needed; this method was more applicable for soft and swelling materials. In either case, the volume was calculated based on the assumption of 100% water saturation.

The average wet density was determined for the MDX plugs, the MAD whole-rounds and the MAD plugs using Equation **E14**.

$$Wet\ \ density = \frac{Wet\ \ mass}{Wet\ \ volume}$$

Equation E14.

Water content

Water or moisture content determinations require measurements of the wet and dry mass. The water content of a material is the ratio of the mass of water

contained in the pore spaces (removed at 110 °C) to the solid mass of particles, expressed as a percentage (ASTM International, 2005).

The average water content was determined for the MDX plugs, the MAD wedges, MAD plugs, and MAD blended material using Equation E15.

$$Water\ \ Content = \frac{(Wet\ \ mass - Dry\ \ mass)}{Dry\ \ mass}$$

Equation E15.

Water saturation

The water saturation is the ratio of the volume of water to the volume of the pore space.

Water saturation was determined for the MDX plugs, the MAD whole-rounds, and the MAD plugs using Equation E16.

$$Water\ \ Saturation = \frac{Volumne\ \ of\ \ pore\ \ fluid}{Volumne\ \ of\ \ pore\ \ space}$$

Equation E16.

Porosity

The porosity is the ratio of the volume of the pore space to the total volume. The porosity was determined assuming a grain density of 2.7 g/cc, a typical value for silty clay mixtures. The porosity was determined using the density of fresh water, 1 g/cc, and was not corrected for salinity.

The porosity was determined using an assumed water saturation of 100% and using the measured water saturation for the MDX plugs, the MAD whole-rounds, and the MAD plugs using Equation E17:

$$Porosity = \frac{(Total\ \ volume - Volume\ \ of\ \ solids)}{Total\ \ volume}$$

Equation E17.

Grain density

Grain density was measured on a few samples using two methods: 1) water submersion, and 2) gas pycnometer.

Water submersion

Grain density was measured on MAD blended material using the water submersion method according to ASTM D854 (ASTM International, 2008d). A subsample of the blended material was diluted with distilled water and blended with an electric hand blender for 1 minute. The slurry was transferred to an iodine flask and evacuated until no bubbles appeared. The flask was filled with distilled water and located in a covered cooler overnight. The volume was set using the matched stopper. The mass of the container was determined to the nearest 0.01 g. The stopper was removed and the temperature measured to the nearest 0.1 °C. Distilled water was added to fill the flask, and it was returned to the cooler. After 15 minutes, the process was repeated to obtain 5 sets of readings. The slurry was then oven dried at 110 °C to constant mass. The final dry mass was measured to the nearest 0.01 g. The volume of the final dry mass was measured to the nearest 0.04 mL (Equation E18).

$$Density = \frac{Final\ \ dry\ \ mass}{Volume\ \ of\ \ final\ \ dry\ \ mass}$$

Equation E18.

Gas pycnometer

Grain density was measured on MDX split core plug samples using the gas pycnometer method according to ASTM D5550 (ASTM International, 2008a). The device was a 10 cm^3 capacity Micromeritics Accupyc III gas pycnometer. The dried material was ground to a fine powder using a mortar and pestle. The powder was dried in an oven at 110 °C for at least one day. The powder was cooled in a sealed container. The mass of the container and powder was determined to the nearest 0.001 g. The powder was transferred to the gas pycnometer for volume determination. The pycnometer was supplied with helium gas. The chamber was purged 3 times and then the volume measured using three pressure cycles. The software reported the average volume of solids and standard deviation to 0.0001 cc (Equation E19).

$$Density = \frac{Final\ \ dry\ \ mass}{Volume\ \ of\ \ final\ \ dry\ \ mass}$$

Equation E19.

https://doi.org/10.5281/zenodo.13971228

Rock magnetism

Samples for rock magnetic analyses were collected at a relatively high resolution throughout the recovered conventional cores and conventionalized pressure cores. These samples were collected from split core sections at a resolution of one per section (sample codes RMG, see **Discrete sampling methods**), plus additional sampling to characterize major changes in volume-normalized magnetic susceptibility (κ) observed in the whole-round MSCL scans (sample code ARM, see **Conventional whole core logging and imaging** for MSCL information). Additional samples were collected from every pore water squeeze cake.

All samples were collected in 8 cm^3 paleomagnetic cubes and measured for mass-normalized, frequency-dependent magnetic susceptibility using the following method. The mass of each sample was measured prior to magnetic susceptibility analysis. Magnetic susceptibility is a ratio of a material's magnetization relative to a weak applied field. Examples of magnetic susceptibility values of minerals commonly comprising marine sediments are shown in Table **T10**. Each of our samples was measured using a Bartington MS3 Magnetic Susceptibility Meter with a MS2B Dual-Frequency Sensor. Each sample was measured for mass-normalized magnetic susceptibility (χ) at low (465 Hz) and high (4650 Hz) frequencies. Each sample was measured over 10 seconds and was corrected by air measurements before and after each sample. Check standards over the range of 10^{-8} to 10^{-3} m^3kg^{-1} were run and measured within the long-term average of ±1%. The frequency dependence of magnetic susceptibility (χ_{fd}) was calculated as a percentage of the decrease in χ in response to a 10-fold increase in frequency (Equation **E20**):

$$\chi_{fd} = \frac{(\chi_{465Hz} - \chi_{4650Hx})}{\chi_{465Hz}} \times 100$$

Equation E20.

where χ_{465Hz} is the low-frequency measurement of χ and χ_{4650Hx} is the high frequency measurement of χ (Dearing et al., **1996**). Higher values of χ_{fd} (10 to 15% or more) indicate an increase in fine superparamagnetic particles (< 300 nm) (Dearing et al., **1996**; Worm and Jackson, **1999**).

Mineral	Mass-normalized magnetic susceptibility (χ) (10^{-8} m^3kg^{-1})
Quartz	-0.5 to -0.6
Illite	15
Montmorillonite	13 to 14
Calcite	-0.3 to -1.4
Orthoclase	-0.49 to -0.67
Biotite	52 to 98
Pyroxene	43 to 50
Magnetite	20,000 to 110,000
Hematite	10 to 760
Pyrrhotite	69,000

Table T10: Magnetic susceptibility values of minerals commonly observed in marine sediments. Values from (Hunt et al., **1995**).

After measurement of χ, samples were vacuum sealed and frozen for additional post-expedition rock magnetic analyses.

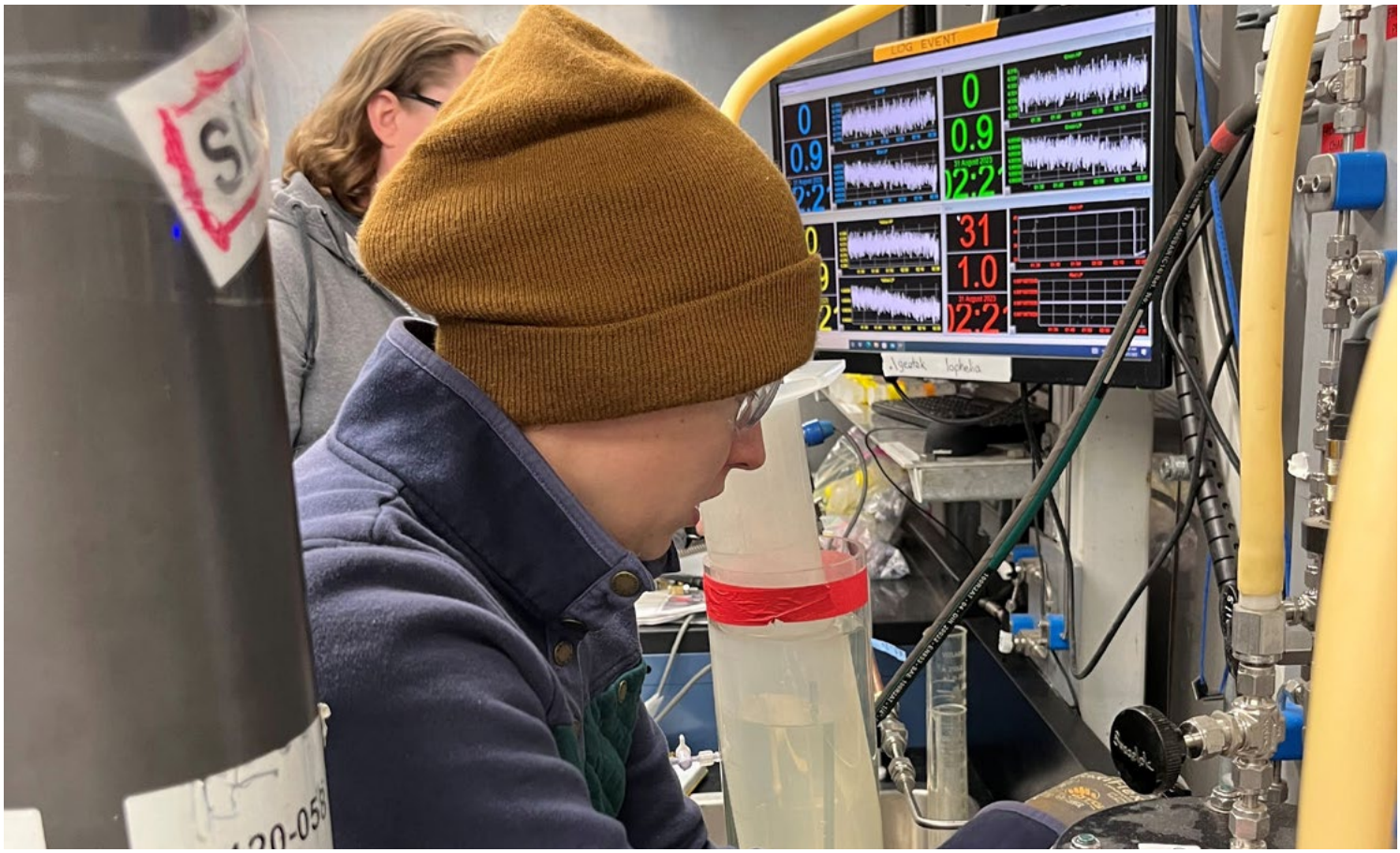

Science party member Rachel Coyte of The Ohio State University collects gas samples while degassing a pressure core.
Photo Credit: Carla Thomas

Dissolved gas and hydrate saturation

PCATS was used to transfer the sample into a 0.35 or 1.2 m core storage chambers. The storage chambers were then connected to a degassing/gas collection manifold that is pressurized to the same pressure as the core storage chamber to determine the total extracted gas volume and the concentration of hydrate within the core (See **Quantitative degassing**).

Dissolved methane concentration

The dissolved methane concentration was calculated based on the total amount of methane produced during degassing. Using the total moles of methane from degassing and a calculated pore volume, we calculated a concentration of methane in mol L^{-1} of the pore fluids. The total moles of methane (n_m) were calculated using the ideal gas law based on the volume of methane produced and the ambient conditions of the degassing van (Equation **E21**):

$$n_m = \chi_m \times P_{atm} \times \frac{V_g}{(R \times T)}$$

Equation E21.

where V_g is the volume of gas released, mis the fraction of methane present in the samples. *T* is the temperature of the laboratory space, P_{atm} is atmospheric pressure, and *R* is the gas constant (8.314 J $(mol\ K)^{-1}$). The gas volume is measured from the amount of gas released to the bubbling chamber and the amount of gas

 https://doi.org/10.5281/zenodo.13971228

remaining in the chamber (as indicated by the volume of water expelled to the bubbling chamber.)

Core volume (V_c) was calculated based on the average radius (r_c) of the recovered core and the length (*L*) of the sample (Equation E22).

$$V_c = \pi r \frac{2}{c} L$$

Equation E22.

The average radius of the core was determined by measuring the diameter of the 3D CT data using ImageJ every 5 cm.

The porosity (ϕ) was estimated from the gamma density (ρ_b) from the PCATS core log, a grain density (ρ_{gr}) of 2.70 g cm^3 and the fluid density (ρ_f) (density of seawater) (Equation E23):

$$\phi = \frac{(\rho_{gr} - \rho_b)}{(\rho_{gr} - \rho_f)}$$

Equation E23.

We calculate fluid density at each depth based on the temperature gradient (See **In-situ temperature**), salinity (See **Pore water geochemistry**), and pressure using the equations of state for seawater (Gill, 1982, pg 599). Pore volume (V_{pw}) was calculated by multiplying V_c by ϕ (Equation E24):

$$V_{pw} = V_c \times \phi$$

Equation E24.

The concentration of dissolved methane was calculated as the moles of dissolved methane per L of porewater (Equation E25):

$$[CH_4] = \frac{n_m}{V_{pw}}$$

Equation E25.

The solubility of methane was calculated using the equations of Tishchenko et al. (2005) applicable within the hydrate stability field. From this comparison, we can determine whether the methane concentration is high enough to form gas hydrate.

If the methane concentration exceeds solubility, we calculate hydrate saturation using the equations below.

Methane hydrate saturation

When the amount of methane from the core section exceeds the amount that can be held in solution in the pore space, that excess amount is assumed to be in hydrate. This excess amount is then used to calculate the saturation of methane hydrate as a percentage of the pore space. In hydrate bearing cores, total amount of methane (as hydrate), core volume, and porosity are calculated as described in Equations E21, E22, and E23. The amount of hydrate methane (n_h) is calculated from the difference of n_m and the amount of dissolved methane (Equation E26):

$$n_h = n_m - n_{diss}$$

Equation E26.

where n_{diss} is the dissolved methane component, calculated as the solubility of methane at the section's in-situ conditions, which were calculated based on the thermal gradient, hydrostatic pressure, and the salinity profile. Given the hydrate stability conditions, all methane exceeding n_{diss} was assumed to be in the hydrate. The volume of methane hydrate was calculated using the molecular weight of methane hydrate (m_h = 124 g mol^{-1}) (Circone et al., 2005) and the density of methane hydrate (ρ_h = 0.91 g cm^{-1}) (Kiefte et al., 2002) (Equation E27):

$$V_h = n_h \times \frac{m_h}{\rho_h}$$

Equation E27.

Hydrate saturation (S_h) was calculated from the ratio of V_h to V_{pw} (Equation E28):

$$S_h = \frac{V_h}{V_{pw}} \times 100$$

Equation E28.

Pod of dolphins on site at Walker Ridge monitoring pipe being pulled out of the hole. Photo Credit: Geotek Ltd.

Microbiology

We preserved samples for (1) 16S rDNA microbial community analysis, (2) single-cell amplified genomics (SAG), (3) assessment of the degradation potential of organic macromolecules by heterotrophs, (4) assessment of microbially-induced carbonate precipitation (MICP), and (5) quantification of microbial cell numbers (CEL). These samples were taken from three types of cores during the expedition: 1) conventional cores, 2) quantitatively depressurized pressure cores (conventionalized cores), and 3) cryogenically frozen and then depressurized pressure cores (Sample code CRYO). This section covers **onboard sampling for microbiology**, **dockside sub-coring for microbiology**, and **DNA extraction and amplification** at Oregon State University.

Onboard sampling for microbiology

Microbiological sampling generally followed the procedures used by the IODP during expeditions that include a microbiology science component (Sylvan et al., **2021**).

Cryogenically frozen and depressurized whole-rounds

Onboard sections of pressure core were cryogenically frozen and depressurized (sample code CRYO), using the method described in **Cryogenic freezing and depressurization**., and then placed in the -80 °C freezer.

 https://doi.org/10.5281/zenodo.13971228

Conventional and conventionalized sediment plugs

Syringes containing sediment plugs were collected by forcing a syringe (with its Luer Lock end cut off) into the exposed core face (sample code CEL, see **Core processing**). Two cm3 of sediment from each of these plugs (as determined using the gradations on the side of the syringe) was aseptically added to 8 mL of zinc acetate preservative in a 15 cm3 Falcon tube. These samples were placed in Whirlpak bags and stored at -80 °C for quantification of microbial cell numbers (cell counts).

Conventional and conventionalized whole-rounds

Between five and seven 10 cm-long whole-round core sections (sample code MB, see Core processing) were collected from the first three ~9-m conventional cores, which were assumed to be above and just below the SMT. Below this, sampling decreased to two to three 10 cm-long MBs per nine-meter core. Following cutting, MBs were immediately transferred to the microbiology core processing lab and held at 4 °C until they could be sub-sampled.

All sub-sampling of MBs occurred in a PCR workstation (FisherBrand Inc., Model no. FB-PCR2) under ISO Class 5 conditions with HEPA filtered air to protect from particulate contaminants. The workstation was sterilized with 10% bleach and 70% ethanol. All sampling tools and the gloves of workers were sterilized with 70% ethanol prior to being brought into the PCR workstation to maintain sterile conditions. After opening, the exposed surface of each sub-core was scraped with a sterile spatula to remove the upper 1-3 mm of contaminated sediment (known as core pairings) that had touched the unsterile plastic core liner.

The following methods were used to take microbiology samples from this interior pristine sediment:

1. 16S rDNA microbial community analysis: Samples for 16S rDNA microbial community analyses were collected by scooping approximately 10 g of sediment with a sterile stainless-steel scoopula into sterile 50-mL Falcon tubes, placing the Falcon tubes in Whirlpak bags, and storing the bags at -80 °C.
2. Single-cell amplified genomics (SAG): Five cm^3 of sediment were collected for SAGs with 10 cm^3 sterile syringes, with the Luer Lock end removed, by pushing the syringe into sediments and extracting the syringe to remove sediment plugs. These were performed in duplicates, and each was sealed with Parafilm, put into Whirlpak bags, and stored at 4 °C.
3. Assessment of the degradation potential of organic macromolecules by heterotrophs: About 50 cm^3 of sediment was extruded from the centermost portion of the core using a sterile spatula. Aliquots of the sediment were then added to a sterile glass bottle to bring the total volume to 50 cm^3. Bottles were sealed and stored at 4 °C.
4. Assessment of microbially-induced carbonate precipitation (MICP): Carbonate precipitation samples were taken by scooping 10 g of sediment with a sterile stainless-steel scoopula into 50 mL Falcon tubes filled with tryptic soy broth/urea media, which were allowed to overflow to exclude the intrusion of air. These were stored at 4 °C.

The remainder of MB sediments were preserved to analyze the presence of foraminifera.

Contamination control

Many different types of fluids and air were sampled to assess the presence of contaminant microbes, including samples of drilling fluid, seawater (make-up water), PCATS water, core pairings, air in the Geotek core container, the microbiology lab stack trailer, and in the PCR workstation adjacent to where microbiology sampling was aseptically performed.

Drilling fluid and seawater samples were obtained once per day by the M-I Swaco engineer into sterile 50-mL screw-top, Falcon tubes. Nitrile gloves were used when the tube was filled from a stream or

from a cup or dipper that was rinsed once with the fluid. Aseptic techniques were observed to prevent contamination of the sample. The two samples were delivered to the microbiology lab immediately after being collected and the samples were frozen at -80 °C for future analysis. PCATS water was collected periodically from the PCATS instrument to be used for microbial community analysis to determine the degree to which microbial communities in PCATS fluids may change the communities in the pressure cores. Core parings (the rind of a core that has been sub-cored, see above) were collected daily, then matched to a particular core and recorded as a paring sample from a specific core section.

Lab air samples were collected to check the types of microbes in the microbiology lab stack trailer on the *Q4000*. At minimum, lab air samples were taken three times during active coring/core processing to allow a useful measure of lab air contaminants on the ship. Sampling was conducted by unwrapping each of three autoclaved sections of an SKC BioSampler (SKC Inc.) in the microbiology lab stack trailer. The BioSampler was then filled with approximately 20 mL of autoclaved 1x phosphate-buffered saline collection fluid. A Gilian abatement air sample pump (Sensidyne Industrial Health and Safety Instrumentation) was then calibrated to a flow rate of 4 L/min with a Dwyer (Dwyer Instruments Inc.) flowmeter. After calibration, the air sampler was attached with autoclaved Tygon tubing to the BioSampler and operated for 4 h + 10 mins to sample approximately 1 m^3 of air. The BioSampler was refilled to the 20 mL mark twice during sampling. Following sampling, the collection fluid was poured into a sterile 50 mL Falcon tube and frozen at -80 °C.

Salt Lake City (Dockside) sub-coring for microbiology

Additional sections of pressure core were cryogenically frozen and depressurized (sample code CRYO) using the method described in **Cryogenic freezing and depressurization**.All CRYO whole-rounds were sub-cored using a specialized mini coring system designed and operated by JAMSTEC to acquire samples needed for microbial community characterization and enumeration (Figure **F55**). This allowed us to obtain samples with little exterior contamination (Shiraishi et al., **2016**). The sub-coring method was as follows. X-ray scans, as well as P-wave velocity and gamma density data, acquired while the samples were still in PCATS were used to guide the sub-coring process. CRYO whole-rounds were moved to the drill press from the -80 °C freezer and pre-chilled in liquid nitrogen for 10 min. After chilling, the whole-rounds were vertically placed in a vice and a sterilized, hollow, diamond-tipped drill bit was used to core 1-5 cm long cores in a four-spot array. Sub-cores (still frozen) were extruded from the hollow bit into 50-ml sterile Falcon tubes using a retrofitted caulking gun and the tubes were then immediately chilled using cold packs before placing these samples in the -80 °C freezer. For each CRYO whole-round, one set of sub-cores was obtained from the upper end and a second set of sub-cores was obtained from the lower/opposite end. Sub-coring a single 20 cm long cryo-core took approximately one hour.

Following sub-coring, the remaining rinds of the cryo-cores were transferred to the core description team for splitting.

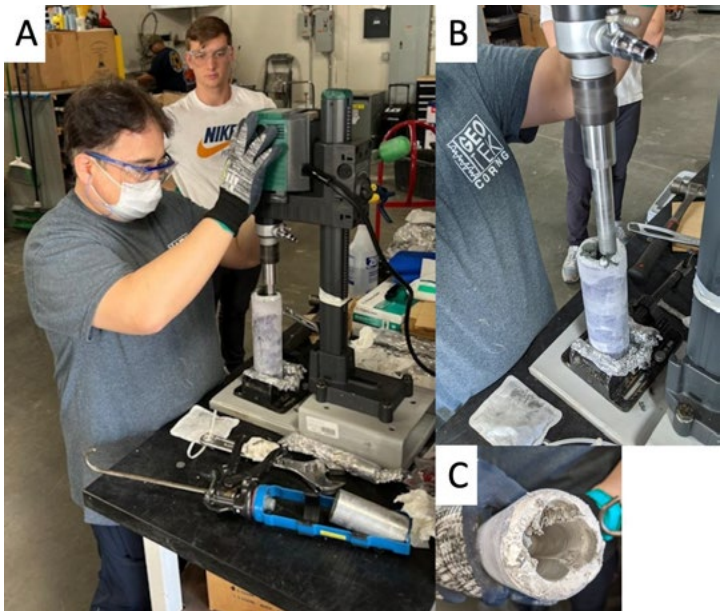

Figure F55: Photos of the drill press and vise for holding cryo-cores during sub-coring. (A), close-up of same (B), and completed sub-coring of one end of a 20 cm cryo-core showing cavities remaining after coring (C).

https://doi.org/10.5281/zenodo.13971228

DNA extraction and amplification

UT-GOM2-2 samples were prepared for microbiological analyses by the team at Oregon State University using a low-biomass DNA extraction protocol developed for deep marine sediments, as these samples typically have exceedingly low levels of microbial biomass. Methods that improve recovery of low levels of extracted DNA yield more complete assessments of the community. Also, free-DNA tends to bind to clay-rich materials, so methods that reduce or account for this phenomenon help to improve yields of DNA released from native microbes such that it can subsequently be sequenced. The following section describes our approach for maintaining clean lab conditions and obtaining high quality DNA where minimal DNA is present in fine-grained, clay-rich materials.

Laboratory cleaning and disinfection

Daily disinfection

Prior to starting disinfection, hands were washed with soap and warm water for 60 seconds. Estashoes were donned as well as sterile coveralls over a designated UT-GOM2-2 short lab coat. Hair (including facial hair) was covered by a bouffant cap. A mask, face shield, and sterile gloves, in this order, were donned. This order was reversed when doffing personal protective equipment (PPE). The sterile shell (the "greenhouse", Figure F56) was entered and shoes and gloves were surface sterilized using diluted detergent (Alconox). Surfaces and the inside of the greenhouse were then disinfected with the diluted detergent (Table T11).

Trash, waste, and expired reagents were removed and disposed of appropriately. Entering and exiting the greenhouse was minimized. Absorbent pads and/or blankets from PIG were removed as necessary and discarded. Detergents and cleaning solutions were refilled. Bottles were only opened in the greenhouse. All hard, non-porous work surfaces were cleaned with diluted detergent (Alconox) in warm water using a sterile wipe and deliberate movements to avoid aerosolizing particles. The detergent was

Figure F56: "Greenhouse" enclosure in Geomicrobiology lab at Oregon State University designed to minimize lab-borne contaminants during processing of GOM2-2 samples.

rinsed away with a new, wet sterile wipe then the work surface was allowed to air dry. The floor was mopped with a sterile, lint free mop and the diluted detergent solution. Once dry, all surfaces were wiped with a disinfectant solution using a sterile wipe or lint free mop. The manufacturer's instructions were followed regarding surface contact time. Disinfectants (isopropyl alcohol, ethyl alcohol, or bleach) were alternated daily to avoid incomplete sterilization. Absorbent pads and/or PIG blankets were replaced, as necessary. The daily cleaning and disinfection log was updated. Gloves were changed prior to working with samples. This cleanup protocol was repeated after working with samples each day.

Weekly cleaning protocols

The designated UT-GOM2-2 lab coat was discarded into a Caroeas Excellent Laundry Basket Hamper and a clean coat was obtained. The inside and outside

Disinfectant	Removing Nucleic acid	Removing cells	Removing dust / abiotic origin
Ultraviolet light	●		
100% DNA Away (NaOH)	●		
100% Obliterase (Na citrate dihydrate, Steol CS-330, Biosoft D-40, 45% KOH)	●		
Flame sterilization	●	●	●
70% isopropyl alcohol		●	●
70% ethyl alcohol		●	●
10% bleach or equivalent quaternary ammonium product (NaOCl)		●	●
Alconox detergent		●	
2.5% Savlon (0.5% w/v cetrimide, 0.1% w/v chlorhexidine digluconate)			●
2.5% Dettol (4.9% Chloroxylenol)			●
Autoclave 30 minutes, dry			●

Table T11: Microbiology lab disinfectants used and their ideal application.

of Estashoes were washed with detergent and warm water. Disinfectant solution (isopropyl alcohol, ethyl alcohol, or bleach) were applied with a new, sterile wipe, following recommended contact time and manufacturer's instructions. A sterile lint-free mop was used to wipe the walls, floor, and all plastic liners with detergent and warm water. Once dry, a disinfectant solution was applied with a new mop head, following the manufacturer's instructions. Disinfectant solutions were rotated to take advantage of different bactericidal actions of the respective disinfectants. PPE and supplies for the following week's work were inventoried.

Hard, non-porous surfaces (floor, benchtops, light switches, handles, cabinets, seats, reagent containers, hard analytical equipment, plastic wall liners, micropipettes, pens/writing utensils, pipet tip containers, and trash cans) were cleaned with diluted detergent.

DNA extraction

On the night prior to DNA sample extraction, the preparation for each sample is as follows: one rock crusher and two small palette knives and any other preferred tools (i.e., tweezers and chisels) were wrapped securely in foil and run in an autoclave for 45 min on the "Dry" setting. Insulated gloves and a lab coat were used when removing anything from the autoclave. Tools were allowed to cool on the benchtop (foil wrapping was left in place).

A total of 500 µL of G2 reagent (mutagenized S. salar double-stranded DNA, Jacobsen et al. (**2018**)) was added to PowerSoil bead-beating tubes (Qiagen, Hilden, Germany). This solution was incubated overnight at 5 °C and was vortexed before use.

Immediately prior to working with a sample, working surfaces were disinfected with 70% ethanol and 10% bleach. Cleaners that use enzymes to sterilize surfaces were not irradiated by UV light.

The general use rotor was removed from the centrifuge and the centrifuge was surface sterilized, allowed to air dry, and then turned on. The large laminar flow hood was opened and all hard surfaces in the UT-GOM2-2 section were surface sterilized. Subsequently, the hood was cleaned with 2% Dettol, the sash drawn down, and sterilized with UV light. A styrofoam box was disinfected with Alconox detergent and filled with ice. One sediment sample was collected from the -80 °C chest freezer and placed deep into the styrofoam box. The required PPE was donned and the greenhouse was decontaminated, as described above. Pens and paper pads already in the greenhouse were used. Outside lab notebooks

 https://doi.org/10.5281/zenodo.13971228

were not brought into the greenhouse to prevent contamination. The sample ice box was brought into the greenhouse. Decontamination steps were repeated if contamination was suspected. The benchtop was sterilized and allowed to dry. The laminar flow hood was turned on and the interior of the hood and the contact surfaces of other items (balance, pipette tip boxes, micropipettes, waste containers, pens, and any reagents which do not contain DNA) were sterilized. The hood sash was pulled down and the UV light was turned on while samples were protected from incidental exposure to UV. Two sterile wipes, one drenched in DNAway and the other in a germicide such as Dettol or Savlon, were prepared for use on all materials moving to and from the sterile hood. These wipes were wetted, as necessary.

If the sample was soft enough to be disaggregated with a spatula, then a rock crusher was not needed. The Whirlpak sample bag was opened and laid down on the foil, with the bag open and facing to the side. The Falcon tube containing the sample was removed and uncapped carefully. The tube was shaken to dislodge the frozen sediments from the tube and using the small pallet knife, 0.5-1.0 g of sediment was collected and placed into the overnight-prepared (500 µL G2) Qiagen PowerSoil bead-beating tube. Typically, five preps were made for a single sample, then they were combined on the same filter, although, due to the low-biomass extraction practice, the number of preps per unique samples sometimes differed. Any unused sediment was returned to the -80 °C chest freezer. Only one unique sample was processed between each sterile hood deep cleanings. If more than one sample per day was extracted, then laboratory cleaning and disinfection was repeated during that day.

If the sample was indurated and could not be disaggregated with a spatula, then a rock crusher was used. One sterile rock crusher and one set of tools were unwrapped and placed into the sterile hood. If necessary, any rust in the interior of the crusher was wiped with 70% ethanol and allowed to dry. The Whirlpak sample bag was opened and laid on the foil, with the bag opening facing to the side. The Falcon tube was removed, and a portion of the sediment was deposited into the rock crusher. The rock crusher piston was inserted into the cylinder, and any remaining sediment in the Falcon tube was then placed in the ice box. The rock crushing system was moved out of the hood and onto the benchtop prepared with sterile aluminum foil. The frozen sediment was disaggregated using the rock crusher. The lab balances were tared and re-calibrated, as necessary. The whole rock crushing system was moved back into the sterile hood and the piston removed. The pallet knife was used to release compacted sediments and the piston was replaced. Rock crushing steps were repeated, as needed to obtain an adequate amount of pulverized sediment for DNA extraction.

A small pallet knife was used to add 0.5-1.0 g of disaggregated sediment into the overnight-prepared (500 µL G2) Qiagen PowerSoil bead-beating tube. Sometimes the number of preps per sample was repeated, assuming low-biomass volumes. All sediment contents from the rock crusher were collected and returned to the original sample bag (or a new, relabeled one if the original bag is damaged), and the bag placed it back on ice. Any unused sediment was returned to the -80 °C chest freezer. Only ONE unique sample was processed between each sterile hood deep cleanings. If more than one sample per day was extracted, then laboratory cleaning and disinfection was repeated each day.

DNA concentration, quantification, and visualization protocols

DNA concentration

For all samples, sediment extraction continued as outlined in the Qiagen PowerSoil Kit, with elution to 100 µL in the final step. The number of spin columns used per unique sample varied as required for the low-biomass extraction practice. Once the PowerSoil protocol was complete, Linear Polyacrylamide (LPA) and a SpeedVac were used to concentrate all DNA 10-fold to a final volume of 10 µL as explained below.

All concentration and cleaning of total extracted DNA or PCR-amplified amplicons was carried out in the biosafety hood.

For the concentration steps, 20 µL sterile sodium acetate, 0.1x (times sample volume) GenElute LPA, and 2.5x (times sample volume) 100% ethanol were added to each tube. The solution was vortexed on mid-high setting for 10s to thoroughly mix the samples, then the samples were centrifuged on maximum speed for 5 min. The location of the visible pellet was marked with a permanent marker and most (~90%) of the supernatant was gently removed with a 100 µL pipette leaving ~20-50 µL. If the pellet was accidentally disturbed, then it was ejected back into the tube and re-centrifuged. The remainder of the supernatant was evaporated in a SpeedVac (the pellet does not need to be dry) at 50 °C for 30 min. After the evaporative step, 100 µL 70% ethanol was added to each tube. Without vortexing, the centrifuged steps were repeated while ensuring that the pellet (indicated by mark made by permanent marker) was facing outward in the centrifuge so it would settle in the same location as before. After this centrifugation step, the supernatant was again removed as described above, and the remaining supernatant was evaporated in the SpeedVac. This time, all the solution was removed, leaving the pellet entirely dry to avoid ethanol inhibition of PCR or any other downstream processes. The dried pellet was resuspended in elution buffer using 10 µL for low biomass samples (10x initial DNA concentration of extraction). The same volume of solution was used as originally extracted if this concentration step was just being used to remove PCR inhibitors. The resuspended solution was gently mixed up and down using a pipette then vortexed on medium setting for 5 s to homogenize the DNA. Finally, tubes were spun (not centrifuged) to settle all DNA in the solution at the bottom.

DNA quantification

After concentrating sample DNA, the quantity of extracted DNA was determined using a Qubit Fluorometer (Thermo Fisher, USA). Using solutions provided in a Qubit dsDNA kit, a 1:200 dye to solvent (Qubit dsDNA HS Assay solution) ratio solution was prepared for samples and standards. An appropriate volume of dye to solvent mixture was aliquoted for each preparation (190 µL for standards, 198 µL for samples) into the 0.5 mL PCR tubes. 10 µL standards were added to two 190 µL tubes, with only the top labeled (to prevent interference with fluorescence measurements). 2 µL samples were added to each 198 µL tube and labeled. All tubes were briefly vortexed and then incubated at room temperature for 5 min and returned to the freezer.

dsDNA HS Assay measurement was selected on the Qubit Fluorometer and the sample volume set as 2 µL. Run Standards was selected. If the standards were deemed to be acceptable, then sample DNA was measured. All values were recorded in the lab notebook. When the assay was complete, the 0.5 mL PCR tubes were discarded and the laminar flow hood was cleaned.

DNA visualization

In the PCR room, a 1% agarose solution dissolved in 1X TAE buffer was prepared. To dissolve the agarose, the solution was microwaved in short (< 20 second) rounds, while gently mixing and avoiding boiling. Insulated gloves were used to handle this hot solution. Once the solution was fully dissolved and allowed to cool, 5 µL of agarose gel dye was added and swirled to mix. The gel electrophoresis tray was oriented long-ways in the electrophoresis box to create a water-tight seal. The agarose-dye solution was poured into the tray, and the appropriate gel comb was inserted. The whole apparatus was covered with a small cardboard box, as the dye is photosensitive.

Once the gel hardened (~30 min), the comb was removed and the tray was placed short ways in the instrument. The gel was then covered by ~1 cm of 1X Tris-acetate-EDTA. Samples were loaded into wells left by the comb. An appropriate ladder (one with large DNA fragments for genomic DNA, one with small DNA fragments for amplicon DNA) was loaded on one or both sides of the gel. The lid was

 https://doi.org/10.5281/zenodo.13971228

placed onto the electrophoresis instrument, with the cathode farthest away from the wells. Voltage was applied for 20-40 min and the distance the ladder had traveled was checked periodically. After completing the electrophoresis run, the gel tray was placed into the carrier and a transilluminator was used to visualize the gel by sliding the gel out of its tray onto the surface of the transilluminator. The software on the adjacent computer was used to visualize the DNA and capture an image. The gel was discarded once the imagining was completed and the surface of the transilluminator was cleaned with nanopore water and Kimwipes.

DNA amplification

After concentrating, quantifying, and visualizing, the template DNA was diluted 1:10 to decrease the effect of environmental inhibitors (Schrader et al., **2012**). The microbial community structure was assessed using DNA amplification (samples run in triplicate) of the V4 region of the 16S rRNA gene using universal 515 forward and 806 reverse primers (Apprill et al., **2015**). PCR amplification followed the Earth Microbiome Project protocol without modifications (Caporaso et al., **2011**). Triplicate samples were pooled and gel electrophoresis was used to verify the anticipated size of amplicons (300–350 base pairs) and identify any potential problems.

Cleanup

Specific cleanup instructions were followed at the end of the extraction protocol. Rock crushers were rinsed with 70% ethanol, securely wrapped in foil, and autoclaved for 45 min on the dry cycle. Use of bleach on the rock crushers was avoided because it causes rust to form. All materials were sterilized and the cleaning log in the “greenhouse” was updated.

Members of the science party gather beneath the vessel banner designating The University of Texas at Austin (UT) as the operator on site. Photo credit: Monica Kortsha

Geochemistry

This section covers methods for **Pore water geochemistry** sample collection (samples to be analyzed at UW; **Gas geochemistry**, including gas chromatography at Ohio State and the USGS; and **Sedimentary geochemistry** at UNH.

Pore water geochemistry

The pore water subsampling plan based on the volume of water recovered is detailed below. All pore water subsamples were shipped to the University of Washington for post-expedition analyses, except those for rare earth element analyses (IWREE), which were shipped to UT.

Pore water laboratory spaces

The pore water geochemistry program was conducted in two laboratory vans aboard the *Q4000* (Figure **F57**). The air-conditioned laboratory was fabricated by Pro-Log Inc. and housed 3 hydraulic presses, a Dosimat titrator, pH meter and electrode, a sub-sampling station, a sink with sediment trap, compressed air gun, label maker, a Milli-Q Direct water purification system for ultrapure water, and space for storing lab consumables and reagents. The air-conditioned laboratory was maintained at a temperature of approximately 20 °C throughout the expedition. Temperature fluctuations were observed, however, with lab temperatures as low as 19 °C and as high as 23 °C. The refrigerated laboratory was mobilized to store the sediment whole-round samples, prepare the samples for pore water extraction at in situ sediment temperatures, and for storing pore water samples. The refrigerated laboratory was fabricated by Geotek Coring USA and housed 3 nitrogen glove bags, racks for 3

 https://doi.org/10.5281/zenodo.13971228

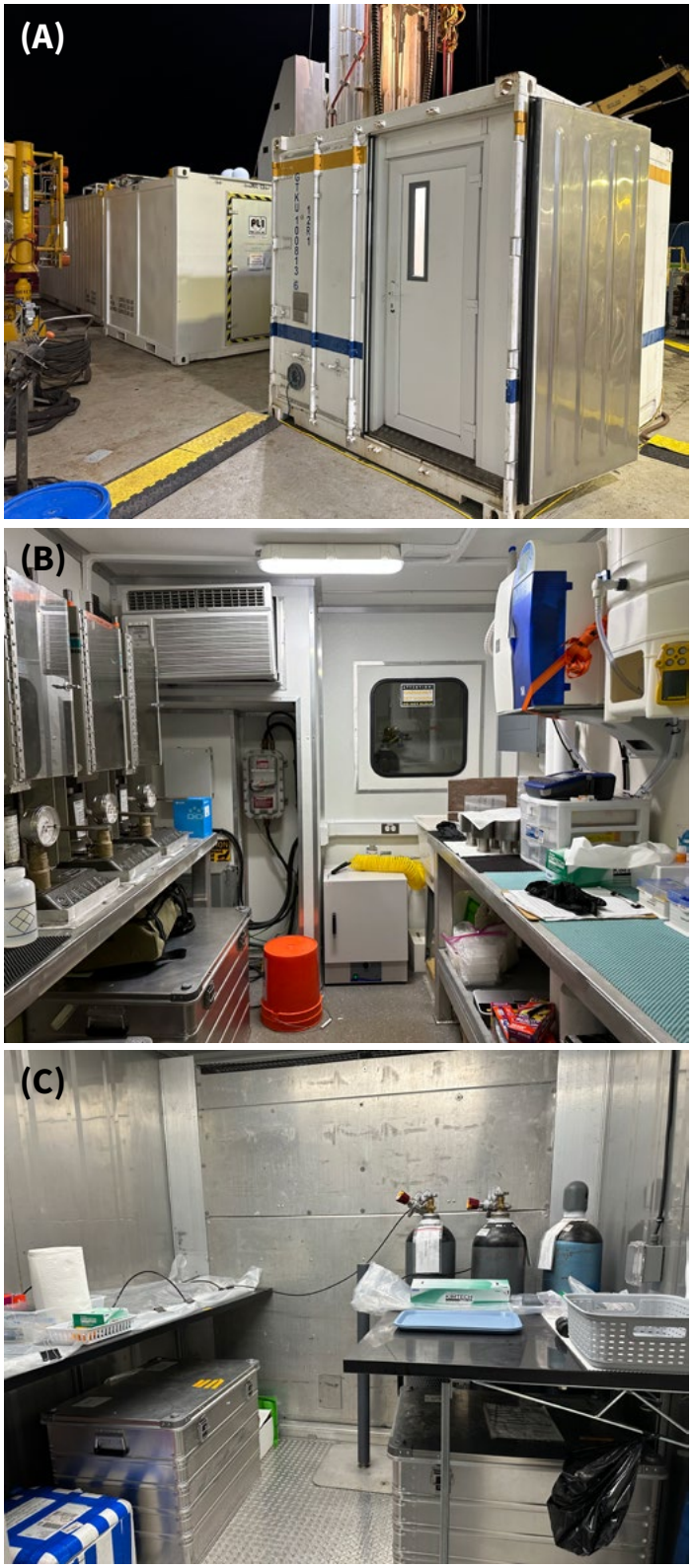

Figure F57: Shipboard pore water geochemistry laboratories. A) Picture taken from the rig floor of the refrigerated laboratory (front right) and air-conditioned laboratory (back left); B) Inside the air conditioned laboratory showing hydraulic presses (left), Milli-Q water purification system, and sub-sampling station (right); C) Inside the refrigerated laboratory showing ultra-high purity nitrogen tanks (back), glove bags for storing samples (left), and table for cleaning whole-round samples (right).

ultra-high purity (UHP) nitrogen tanks, and space for cleaning sediment samples for pore water extraction. The temperature of the refrigerated laboratory kept at 6 °C for the duration of the expedition.

Ultrapure water

During mobilization on the *Q4000*, we discovered the potable feedwater available to the air-conditioned laboratory on the rig floor contained extremely high concentrations of iron oxides and was of very poor quality (Figure **F58**). As such, feedwater was first passed through an Everpure Model RT-3 water filter, then through a 0.4 µm General Ecology Seagull IV water filter before introduction to the Milli-Q Direct water purification system. The two pre-filters were changed several times during the expedition. The Milli-Q Direct provides both reverse osmosis (RO, Type 3), and ultrapure (Type 1) water directly from potable water in a single device. To obtain ultrapure water, the feedwater is purified to RO water then irradiated by a bactericidal ultraviolet (UV) lamp. The RO water is stored in a 30 L polyethylene tank. The RO water is then passed through a dual wavelength UV lamp and a QPAK purification cartridge to reach a resistivity of 18.2 MΩ·cm. The Milli-Q system delivered 18.2 MΩ·cm water throughout the expedition, which was used for rinsing equipment, tools, labware, and for sample dilutions for onboard analyses.

Routine pore water sampling

In Hole H003, routine whole-round samples (sample code IWR) were collected for pore water geochemistry at a resolution of 1 whole-round sample per section for Cores 1H to 3H and 2 whole-round samples per core for cores 6H to 26X (see **Conventional core processing**). In Holes H003 and H002, 1 whole-round sample was collected per pressure core. Whole-round samples were selected, labeled, cut, and capped in the core receiving van. The caps were sealed with electrical tape. The samples were then immediately taken to the refrigerated laboratory for processing. During high-resolution sampling, when there were too many interstitial water whole-round samples to process immediately, capped and taped whole-

round samples were stored in a glove bag filled with ultra-high purity nitrogen (UHP N_2) in the refrigerated laboratory at 6 °C until they were squeezed. Squeezing occurred no later than 36 hr after core retrieval. When possible, extrusion from the core liner was done by hand using a cylindrical extruding post. Deeper in the section (starting at H003-17H), sediment was often too stiff to extrude by hand and the core liner was sliced using an oscillating tool and round blade. Care was taken to only cut the core liner and to not touch the sediment with the saw blade. After extrusion from the core liner, the surface of each whole-round sample was carefully scraped with a spatula or sliced with fishing line to remove potential contamination from seawater and sediment smearing during core collection. Approximately 1 cm from the outer diameter, top, and bottom faces were removed for G-APC cores. G-XCB and PCTB samples required more cleaning due to additional contamination from rotary coring. The remaining sediment (~50–300 cm^3) was placed into a titanium squeezer, modified after the stainless-steel squeezer of Manheim and Sayles (**1974**).

Pressures up to 17 MPa (defined as the applied load over the cross-sectional area of the titanium squeezer) were applied using a laboratory hydraulic press to extract pore water. Pore water was passed through a pre-washed Whatman No. 1 filter fitted above a titanium screen and extruded into a pre-cleaned (10% HNO_3) plastic syringe attached to the bottom of the squeezer assembly. Pore water was then dispensed from the syringe through a 0.2 µm Whatman Puradisc polyether sulfone disposable filter into sample containers and preserved for various analyses (Tables **T12** and **T13**). The residual squeezed sediment (squeezed cake) was then cut into pieces and stored in vacuum-sealed bags. Half of each squeeze cake was stored at 6 °C for analysis of physical properties at UT-Austin, ¼ was stored at -20 °C for rock magnetism, inorganic carbon, total organic carbon, total nitrogen, and total sulfur analyses at the USGS and University of New Hampshire, and ¼ was stored at -20 °C for bulk digestions and sequential leaching experiments at the University of Washington.

Figure F58: Pictures of the potable feedwater to the rig floor laboratory spaces on the Helix *Q4000*. A. Vessel full of feedwater direct from the line on the rig floor. B. Picture of the 0.4 mm General Ecology Seagull IV water filter after 1 week of use. This is one of 2 inline filters before the feedwater is fed into the Milli-Q direct RO system.

All pieces of the titanium squeezer assembly were washed in ultrapure Milli-Q water and dried completely using an air hose and Kimwipes before use. The compressed air was passed through two

https://doi.org/10.5281/zenodo.13971228

Subsample Description	O/H	Halogens	DIC Isotopes	DIC	Majors, Minors, Isotopes	SO4/H2S	Cl+B Isotopes	REEs	Alkalinity	Alkalinity residue
Code	IWOH	IWHAL	IW13DIC	IWDIC	IWMAJ	IWSO4	IWCLISO	IWREE	IWS	IWALK
Container	glass					plastic			shipboard	
	2 ml glass vial	2ml glass vial	2 ml agilent vials	2 ml agilent vials	4-15 ml Acid-Cleaned Nalgene Bottles	15 ml Corning Centristar Tubes	4-15 ml Acid-Cleaned Nalgene Bottles	8 ml LDPE bottles	14 ml Falcon tubes	5 ml cryovials
Treatment	Nothing	Nothing	HgCl2 10 ul	HgCl2 10 ul	Acidified to pH2 with Optima HNO3	0.1 ml sample in 10 ml of 0.5 mM Zn-Acetate	Nothing	Acidified to pH2 with Optima HNO3	Nothing	Nothing
Total volume	Allocation									
45 ml	2.0	2.0	2.0	2.0	15.0	0.1	10.0	8.0	3.5	3.0
40 ml	2.0	2.0	2.0	2.0	12.0	0.1	8.0	8.0	3.5	3.0
35 ml	2.0	2.0	2.0	2.0	8.0	0.1	8.0	8.0	3.5	3.0
30 ml	2.0	2.0	2.0	2.0	8.0	0.1	4.0	6.0	3.5	3.0
25 ml	2.0	2.0	2.0	2.0	4.0	0.1	4.0	5.0	3.5	3.0
20 ml	2.0	2.0	2.0	1.0	4.0	0.1	2.0	4.0	3.5	3.0
15 ml	2.0	1.0	2.0		4.0	0.1	2.0		3.5	3.0
10 ml	2.0	1.0	1.0		4.0	0.1	2.0			
5 ml	2.0				3.0	0.1				
3 ml	1.0				2.0	0.1				
1 ml	1.0									

Table T12: Allocation and treatment of pore water from G-APC routine whole-round samples (sample code IWR).

Subsample Description	O/H	Halogens	DIC Isotopes	DIC	DOC/VFAs	Majors, Minors, Isotopes	SO4/H2S	Cl+B Isotopes	REEs	Alkalinity	Alkalinity residue
Code	IWOH	IWHAL	IWDI13C	IWDIC	IWDOC	IWMAJ	IWSO4	IWCLISO	IWREE	IWS	IWALK
Container	glass						plastic			shipboard	
	2 ml glass vial	2ml glass vial	2 ml agilent vials	2 ml agilent vials	5 ml amber bottles, pre-combusted	4-15 ml Acid-Cleaned Nalgene Bottles	15 ml Corning Centristar Tubes	4-8 ml Acid-Cleaned Nalgene Bottles	8 ml LDPE bottles	14 ml Falcon tubes	5 ml cryovials
Treatment	Nothing	Nothing	HgCl2 10 ul	HgCl2 10 ul	Frozen -20C	Acidified to pH2 with Optima HNO3	0.1 ml sample in 10 ml of 0.5 mM Zn-Acetate	Nothing	Acidified to pH2 with Optima HNO3	Nothing	Nothing
Total Volume	Allocation										
45 ml	2.0	2.0	2.0	2.0	5.0	12.0	0.1	8.0	8.0	3.5	3.0
40 ml	2.0	2.0	2.0	2.0	5.0	12.0	0.1	4.0	8.0	3.5	3.0
35 ml	2.0	2.0	2.0	2.0	5.0	8.0	0.1	4.0	7.0	3.5	3.0
30 ml	2.0	2.0	2.0	2.0	5.0	5.0	0.1	4.0	5.0	3.5	3.0
25 ml	2.0	2.0	2.0	2.0	2.0	4.0	0.1	4.0	4.0	3.5	3.0
20 ml	2.0	2.0	2.0	1.0	2.0	4.0	0.1	4.0		3.5	3.0
15 ml	2.0	1.0	2.0		1.0	4.0	0.1	2.0		3.5	3.0
10 ml	2.0	1.0	1.0			4.0	0.1	2.0			
5 ml	2.0					3.0	0.1				
3 ml	1.0					2.0	0.1				
1 ml	1.0										
Note - DOC samples are collected with APC Organic Geochem Whole-Round, Only Collect DOC Samples for XCB and PCTB Cores											

Table T13: Allocation and treatment of pore water from G-XCB and PCTB whole-round samples (sample code IWR).

filters in series to prevent contamination while drying the squeezers.

Salinity and alkalinity were measured within 12 hr after squeezing. Salinity was determined using a Reichert temperature-compensated handheld refractometer. The refractometer was calibrated using International Association for the Physical Sciences of the Oceans (IAPSO) standard seawater. Alkalinity was determined by Gran titration with 0.1 N trace metal grade HCl following the procedure described in Gieskes et al. (**1991**). Acid was added using a Metrohm 876 Dosimat Plus and potential was measured with a Metrohm combination glass electrode and a Metrohm 780 pH meter. Potential/pH was calibrated using Orion ThermoFischer pH buffers. IAPSO standard seawater was used as the calibration standard for the alkalinity determinations, and IAPSO was analyzed at the beginning of each analysis period and after approximately every 2-5 samples. The average accuracy and precision of the alkalinity measurements based on repeat analysis of IAPSO standard seawater was <3.5% and <4%, respectively. The residual titrated solution was stored in 5 mL cryovials (Tables **T12** and **T13**).

All remaining pore water was allocated into vials and bottles, preserved for a variety of shore-based chemical analyses, and stored at 6 °C (Tables **T12** and **T13**). Sample allocation was determined by the pore water volume recovered and analytical priorities based on the expedition objectives (Tables **T12** and **T13**). For each G-APC, G-XCB, and pressure core whole-round samples, up to 2 mL of pore water was stored in glass vials for O/H isotope ratio and halogen concentration analyses. Up to 2 mL of pore water was treated with 10 µL of mercuric chloride and stored in glass vials for dissolved inorganic carbon (DIC) and δ^{13}C-DIC analyses. Up to 15 mL of pore water was acidified with optima HNO_3 to reach a pH of 2 and stored in acid-washed high-density polyethylene (HDPE) and low-density polyethylene (LDPE) bottles for analysis of major, minor, and rare earth elements. First, 0.1 mL of pore water was pipetted into 15 mL Corning Centristar centrifuge tubes along with 10 mL of 0.495 mM Zn-Acetate solution for SO_4 analysis. Up to 10 mL of pore water was stored in acid-washed HDPE bottles for Cl and B isotopic analysis. In G-XCB and pressure core samples, an additional aliquot of up to 5 mL of pore water was stored at -20 °C in pre-combusted amber glass bottles for dissolved organic carbon and volatile fatty acid analysis (Table **T13**).

Organic pore water sampling

In the borehole section cored by G-APC, additional whole-round samples (sample code IWO) were squeezed for shore-based pore water analyses of trace metal concentrations, trace metal isotope ratios, and dissolved organic carbon characterization. These whole-round samples were 10 to 20 cm in length and collected immediately adjacent to the IWR. In Hole H003, IWO sections were collected at a resolution of 1 whole-round samples per section for Cores 1H to 3H and 2 whole-round samples per core for cores 6H to 25H. Due to potential contamination with drilling fluid, IWO whole-round samples were not collected from G-XCB cores or pressure cores.

IWO samples from G-APC cores were selected, labeled, cut, and capped in the core receiving van. The caps were sealed with electrical tape. The sections were then immediately taken to the refrigerated laboratory and stored in a glove bag filled with UHP N_2 and kept at 6 °C until they could be cleaned and squeezed for pore water. Extrusion from the core liner was done by hand using a cylindrical extruding post. After extrusion from the core liner, the surface of each whole-round sample was carefully scraped with a plastic knife or fishing line to remove potential contamination from drilling fluid. Cleaning of the IWO whole-round samples was done rapidly to prevent oxidation. Approximately 1 to 2 centimeters from the outer diameter, top, and bottom faces were removed for IWO whole-round samples. The cleaned whole-round sample was then placed in a titanium squeezer assembly that was fully flushed and purged with UHP N_2. This was done by connecting a N_2 line to the sample port at the base of the squeezer and purging the sampling port and cylinder with approximately 5 volumes of UHP nitrogen. The sample was then placed in the squeezer, and the unit was then purged

https://doi.org/10.5281/zenodo.13971228

again for approximately 1 to 2 minutes. After the squeezer assembly was fully sealed (by capping with a Teflon disk, polyurethane disk, and the piston), an acid-cleaned syringe flushed 5 times with UHP N_2 was inserted into the sample port.

At this stage, the squeezer assembly is a closed system and filled with N_2, maintaining anoxic conditions. The whole-round sample was then squeezed in a hydraulic laboratory press. Once enough pore water was collected for the trace metal concentration sample (Table T14), the pore water was immediately transferred to an LDPE bottle that was flushed with at least 5 volumes of UHP N_2 containing enough Optima nitric acid to fix the subsample at a pH of 2. During transfer of the subsample into the LDPE bottle, it was passed through a 0.2 µm Whatman Puradisc polyether sulfone disposable filter that was pre-flushed with UHP N_2 for approximately one minute. When dispensing, the sample is immediately mixed with the Optima nitric acid, reaching a pH of 2 and preventing the oxidation of reduced trace metals.

After collecting the subsample for trace metal concentrations, the syringe was returned to the squeezer, and pore water was extracted for the remaining IWO subsamples (Table T14). After a sufficient volume of pore water was collected, up to 15 ml was added to an LDPE bottle for characterization of the DOC pool and stored at -20 °C, up to 8 ml was added to a pre-combusted amber glass vial for dissolved organic carbon and volatile fatty acid concentrations and stored at -20 °C, and 2 ml was added to a microcentrifuge tube, fixed with 50 µL of a 1230 mM zinc-acetate solution, and stored at 6 °C for shore-based analyses of H_2S concentrations (Table T14). Next, 100 µL of sample was pipetted into a 15 ml Corning Centristar tube with 10 ml of 0.495 mM zinc-acetate solution for shore-based analysis of sulfate concentrations. Similar to the routine pore water samples, the IWO squeezed cakes were then cut into pieces and stored in vacuum-sealed bags for shore-based analysis. Half of each squeeze cake was stored at 6 °C for analysis of physical properties at UT, ¼ was stored at -20 °C for rock magnetism, inorganic carbon, total organic carbon, total nitrogen, and total sulfur analyses at the USGS and University of New Hampshire, and ¼ was stored at -20 °C for bulk digestions and sequential leaching experiments at the University of Washington.

Subsample Description	DOC/VFAs	Ligands	Trace Metals and Isotopes	SO4	H2S
Code	IWDOC	IWLIG	IWTRACE	IWSO4	IWH2S
Container	glass: 5 ml Amber Glass Bottle (pre-combusted)	plastic: 4-15 ml Acid-Cleaned LDPE Bottle	plastic: 4-20 ml Acid-Cleaned LDPE Bottle	plastic: 15 ml Corning Centristar Tubes	plastic: 2 ml centrifuge tube
Treatment	Frozen -20C	Frozen -20C	Acidified with Optima Nitric to pH 2	0.1 ml sample in 10 ml of 0.5 mM Zn-Acetate	Add 50 uL of 1230 mM Zn-Acetate
Total Volume	Allocation				
40 ml	5.0	15.0	18.0	0.1	2
35 ml	5.0	15.0	12.0	0.1	2
30 ml	5.0	12.0	12.0	0.1	2
25 ml	3.0	12.0	8.0	0.1	2
20 ml	3.0	10.0	6.0	0.1	1
15 ml		10.0	5.0	0.1	
10 ml		6.0	4.0	0.1	
5 ml		2.0	3.0	0.1	

Table T14: Allocation and treatment of pore water from G-APC organic whole-round samples (sample code IWO).

Dockside sampling in Salt Lake City

Due to time limitations onboard the Helix Q4000, whole-round samples from Hole H002 Cores H002-05CS to H002-15CS were processed dockside at Geotek in Salt Lake City. The whole-round samples from these pressure cores were stabilized onboard before being shipped to Geotek. The top and bottom of the sections were purged with UHP N_2 in the refrigerated pore water laboratory immediately after being cut from the core section. Both core caps were also purged with nitrogen and placed securely on the core liner, then sealed with electrical tape. The capped and taped sections were then placed in a large plastic bag that was purged with UHP N_2. The bag was sealed while still purging with nitrogen at a low flow rate to ensure it was completely anoxic. The bagged sections were shipped at 4 °C to Salt Lake City for dockside processing.

The air-conditioned and refrigerated pore water laboratories were shipped from Port Fourchon, LA to

Geotek in Salt Lake City. The layout of the two pore water laboratories at Geotek was identical to the set-up onboard the *Q4000*, except the Milli-Q did not need pre-filtration of the higher quality feedwater in Salt Lake City. Sample processing occurred from 20-26 September 2023. The methods for cleaning/squeezing the pore water sections, pore water filtration and sample subdivision, and the salinity and alkalinity determinations were identical to the shipboard methods described above. All the pore water samples and portions of the sediment squeezed cakes were shipped overnight from Salt Lake City to the University of Washington on 27 September 2023, then immediately transferred to a cold room and freezer at UW for long-term storage.

Contamination tracking

Daily samples of drilling seawater and drilling mud were collected to be used as tracers for sample contamination due to drilling. Drilling seawater was filtered through a 0.2 µm Whatman polyether sulfone disposable filter and aliquoted into vials/bottles for shore-based analyses in the same manner as described above for pore water subsamples. Salinity and alkalinity were measured onboard.

Drilling mud was sampled at approximately daily resolution and stored in acid-washed HDPE bottles. Drilling mud samples collected on 8 August 2023 and 20 August 2023 were filtered through a 0.2 µm Whatman polyether sulfone disposable filter and aliquoted into vials/bottles for shore-based analyses in the same manner as described above for pore water subsamples. Drilling mud samples collected after 20 August 2023 were filtered and preserved in Salt Lake City. The salinity and alkalinity of the samples processed shipboard and in Salt Lake City were measured within 12 hours of sample filtration. The rest of the drilling mud samples were filtered through 0.1 µm Rhizon samplers connected to acid cleaned (10% nitric acid) 10 ml syringes, then preserved for later analyses at the University of Washington in September 2023. Drilling mud samples processed at the University of Washington were only analyzed for salinity.

For pressure cores, samples were taken of the PCATS fluid, which was spiked with 10 ppm cesium chloride as a tracer for contamination. Approximately 20 mL of PCATS fluid was filtered through a 0.2 µm Whatman polyether sulfone disposable filter and aliquoted into sample containers similar to the drilling seawater and drilling mud samples. All the PCATS fluid samples from Hole H003 and Hole H002 Core 3 FB were processed shipboard. Due to time limitations onboard the *Q4000*, PCATS fluid samples from Hole H002 5CS to 15CS were filtered and preserved in Salt Lake City. Salinity and alkalinity were measured within 12 hours of filtering the samples both onboard and in the Salt Lake City dockside laboratory.

Gas geochemistry

Pressure core produced gases

During every quantitative degassing (see Dissolved gas and hydrate saturation) onboard and at Salt Lake City, we collected 60 mL of produced gas via syringe (Figure **F59**) after each depressurization step for immediate gas chromatography analysis using the Geotek gas chromatograph (See **Geotek gas analysis**). We also collected 160 mL of gas from every 1-2 depressurization steps in Cali-5 Bond gas bags (Figure **F60**) for onshore analysis at the U.S. Geological Survey (See **USGS gas analysis**) and Ohio State (See **Ohio State gas analysis**). Syringes and gas bag samples were collected from the top of the bubbling chamber of the degassing apparatus (Figure **F61**). From select quantitative degassing experiments, we collected up to 3 samples in refrigeration-grade

Figure F59: Transfer syringe with three-way Luer valve and Whatman filter.

https://doi.org/10.5281/zenodo.13971228

Figure F60: Calibrated Instruments, Inc. Cali-5 Bond gas bag.

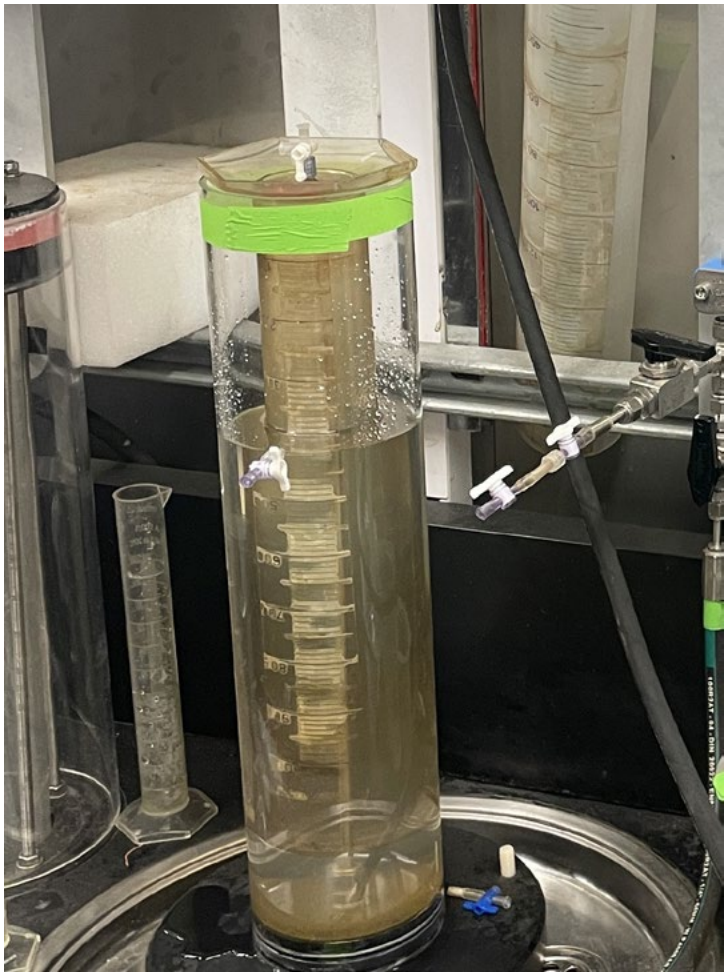

Figure F61: Bubbling chamber to measure gas volume during quantitative degassing. Syringe and gas bag samples were collected from the three-way Luer valve at the top of the bubbling chamber.

copper tubes (0.95 cm outside diameter, 40 cm long, Figure F62) using a modified quantitative degassing technique first reported by Moore et al., 2020. The copper tubes were evacuated below 65 millitorr (mtorr) prior to sample collection (Figure F63). Gases were expanded from the degassing manifold into the copper tube from a valve connected to the syringe port upstream of the bubbling chamber to minimize contact with air-saturated water. After sample collection, the copper tube was cold welded on each end using clamps to create a tight seal. These samples were collected for noble gas analysis at Ohio State (See Ohio State gas analysis).

Void gases

Void gases were extracted using a stainless-steel puncture sampler that was pushed through the core liner shortly after the core was collected onboard the *Q4000*. The sampler contains a three-way Luer valve that can be attached to a syringe for gas sampling (Figure F64). One 60 mL syringe was used to collect void gas samples for onboard gas chromatography analysis (See Geotek gas analysis). Another 120 mL syringe was then used to extract up to 160 mL from the void and transfer it to a Cali-5 Bond gas bag for molecular and isotopic analysis at the U.S. Geological Survey (See USGS gas analysis) and the Ohio State (See Ohio State gas analysis). Each syringe was fitted with 3-way Luer valves and 0.45 µm Whatman filters for connection to the puncture sampler and extraction of void gas. Up to 2 void gas samples were collected for each conventional core after being marked on the core liner. The valve was flushed with the void gas before transferring to the syringe or gas bag.

Headspace gas collection

Headspace gas was collected from an exposed core cut adjacent to the standard whole-round sampling set onboard the *Q4000*. If possible, this sample was always collected at the top of section. In standard conventional core sampling, headspace was collected from 2 to 5 sections and from one section in the select pressure cores. Three 5 cm^3 sediment plugs were collected from a freshly exposed core cut using a cut-off syringe. Two of the sediment plugs were extruded into a 30 mL glass serum vial with 10 mL of 1M potassium chloride (KCl) (Figure F65 A). One sediment plug was plunged into a 20 mL glass serum vial with 10 mL of 1 M KCl (Figure F65 B). Each vial

Figure F62: Copper tube with Swagelok valves for noble gas sampling.

Figure F63: Evacuation of a copper tube before gas sampling.

was then plugged with a butyl septum and crimped with a 20 mm aluminum cap. The vials were shaken to create a sediment slurry and stored upside down for post-expedition analysis at The Ohio State University. There, an aliquot of the headspace gas was extracted from the vials via a gas-tight syringe. Once extracted, the headspace gas was then transferred to the quadrupole mass spectrometer and GC by injection

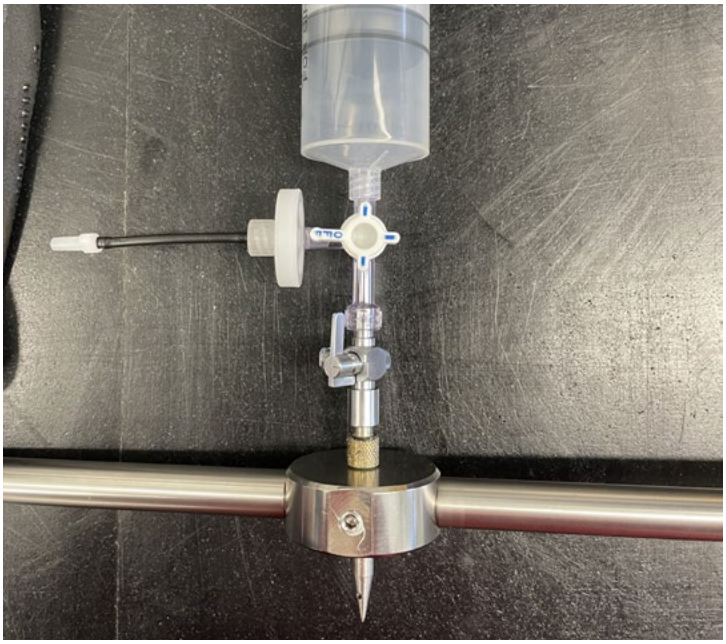

Figure F64: Puncture tool for collecting void gas samples. A transfer syringe is attached.

through a gas-tight septum (See **Ohio State gas analysis**).

Hydrate-bearing sediment dissociation gases

Where solid hydrate or hydrate-bearing sediment was encountered in a conventionalized core, the hydrate or sediment chunk was placed into the back of a 120 mL transfer syringe. The plunger was replaced and used to evacuate the syringe. The syringe was closed off and gas was allowed to expand. The gas was then transferred to a Cali-5 Bond gas bag. Hydrate-bearing sediment was only sampled from cryo core microbiology sections during subsampling.

https://doi.org/10.5281/zenodo.13971228

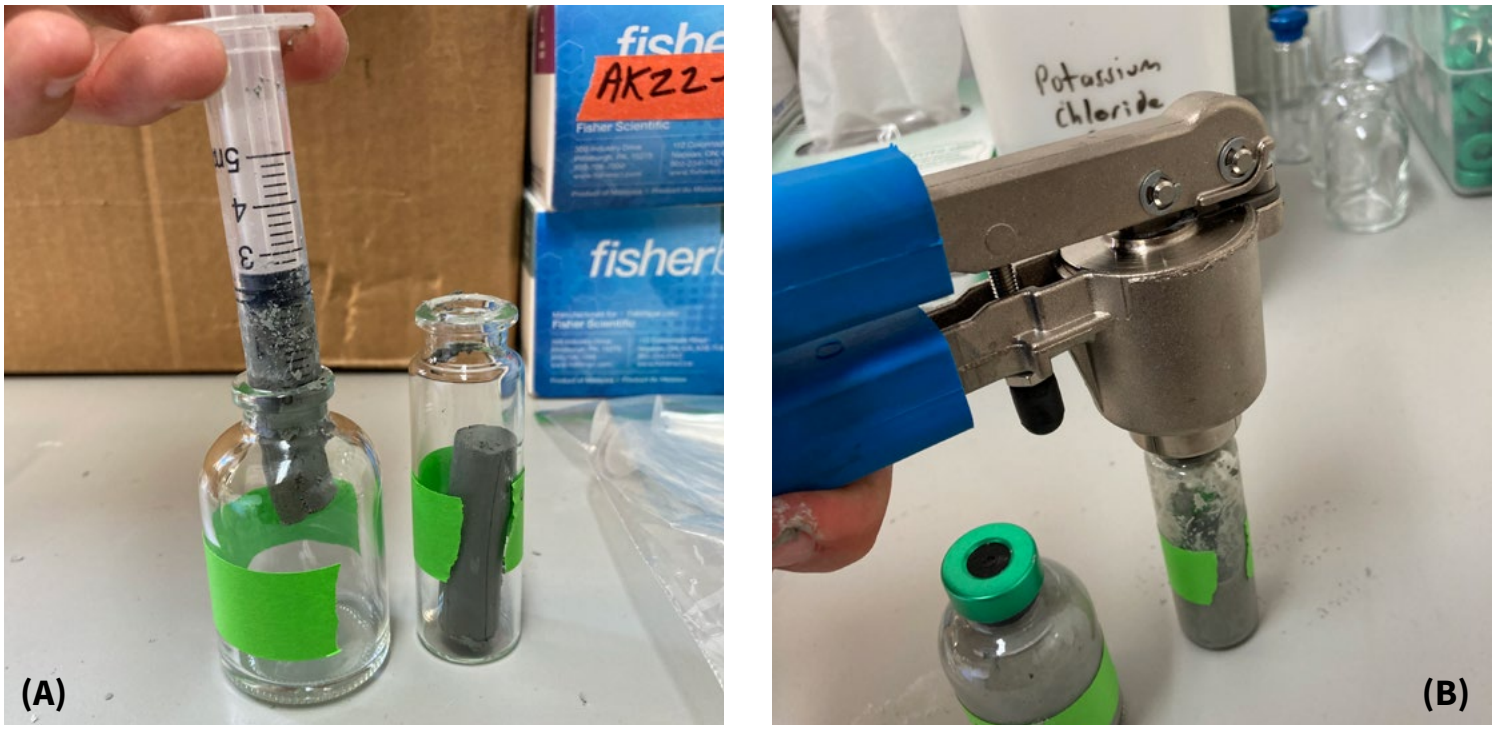

Figure F65: Extrusion of 5 mL headspace sediment plugs from cut-off syringes into serum vials for headspace gas analysis.

Gas chromatography

Geotek gas analysis

An Inficon Fusion MicroGC chromatograph with molecular sieve, PLOT Q columns, and thermal conductivity detectors were used to measure carbon dioxide, oxygen, nitrogen, methane, ethane, propane, butane, isobutane, and pentane. The Inficon Fusion MicroGC chromatograph has a detection limit of 10 ppm and a quantification limit of 30 ppm for all gases.

USGS gas analysis

Void gas, pressure core gas, and hydrate gas collected in Cali-5 Bond gas bags were analyzed for gas composition and methane stable carbon isotopes at the U.S. Geological Survey Woods Hole Coastal and Marine Science Center using their Automated Sample Introduction Module (Auto-SIM) Gas Chromatography/Cavity Ring-Down Spectroscopy System (Auto-SIM GC/CRDS) (Figure F66). Analysis was performed from Jan 4-9, 2024.

Gas samples in Cali-5 Bond bags were attached to the 16-port Auto-SIM that automatically transfers a portion of each sample to a series of samples loops of the Auto-SIM GC/CRDS that includes the USGS

Figure F66: USGS Auto-SIM GC/CRDS System with attached Cali-5 gas bags. The Auto-SIM distributes gas to the USGS DSIM and GC. Gas composition is measured by the SRI MG#5 GC. Methane/CO_2 stable carbon isotopes are measured by the Picarro G2201-i CRDS.

Discrete Sample Introduction Module (DSIM) with a cavity ring-down spectrometer and a Scientific Research Instruments (SRI) MultipleGas#5 (MG5) gas chromatograph (GC) equipped with sample loops and injection valves for parallel analysis by flame ionization detection (FID) and thermal conductivity detection (TCD). Gas separation by the FID is achieved with a 2 m x 1/8" o.d. Haysep D column. Gas

separation by TCD is achieved with a 1 m x 1/8" o.d. MS-5A column.

The DSIM contains a fixed (low-volume) internal sample loop and a replaceable external sample loop (larger-volume) that allows the user to properly dilute gases so they're within the ideal analytical range of a Picarro G2201-I CRDS (100-600 ppm). The CRDS measures methane and CO^2 concentrations and stable carbon isotopes of each (See Pohlman et al., **2021**) for additional details). For this study, the small volume (~100 µl) internal loop in combination with an expansion volume that enhances dilution by increasing system volume yielded a dilution factor of 1700.13. Diluted samples are introduced to the CRDS via a closed loop circulation path.

Isotope ratios measured by the CRDS are reported in the δ-notation ($\delta^{13}C$) relative to a Vienna Pee Dee Belemnite (VPDB) standard. Measurement precision of the $\delta^{13}C$ of methane carbon isotope ratios improves from 1‰ at 10 ppm to < 0.2‰ at 30 ppm and remains constant through the range of measurements made. The average sample precision for this project was 0.18‰ for methane.

Methane concentrations measured by DSIM-CRDS were converted to sample concentration by multiplying the measured and calibrated concentration by the dilution factor (1700.13) described above. The precision of methane concentration measurements was determined based on calibration using two 94% methane standards from Mesa Specialty Gas and Equipment, **www.mesagas.com**. The standards were included in each run and results had a relative standard deviation (RSD) of 1.3%, which was significantly better than the 4.8% RSD (and less accurate) gas chromatograph (GC) described below.

The CO_2 concentration measured by the DSIM-CRDS was too low for all of samples to obtain reliable stable carbon isotope ratio measurements. The low CO_2 concentrations measured by DSIM-CRDS also had a relatively high 24.7% RSD. Thus, CO_2 concentrations reported were from flame ionization detection (FID) with the SRI GC5. The relative standard deviation of the column was methane (4.9% RSD), n-alkanes ethane (1.9% RSD), propane (4.2% RSD), i-butane (5.8% RSD), n-butane (7.6% RSD), neo-pentane (46.8% RSD), iso-pentane (18% RSD), and n-pentane (22.1% RSD), which were all measured with the SRI MG5 GC FID detection system. The RSDs reported for each n-alkane are based on duplicate analysis of the Mesa gas standard during each of the six runs performed in this study. The limit of detection for CO_2 and then n-alkanes by FID is 2 ppm based on the visual inspection and analysis of sample chromatograms that were quantified using calibration curves generated from four gas standards containing all the compounds reported herein.

Percent nitrogen and oxygen are reported relative to the response of atmospheric air (21% O_2, 79% N_2) as measured by SRI MG5 GC thermal conductivity detection (TCD) following separation with a 1 m MS-5A packed column. The RSD for N_2 and O_2 is less than 5%.

Ohio State gas analysis

The molecular compositions of major non-hydrocarbon gases (e.g., N_2, O_2, CO_2, H_2) and hydrocarbon gases (C_1–C_5) were measured using a Thermo Fisher Trace 1310 Gas Chromatograph (GC) equipped with a thermal conductivity detector (TCD) and flame ionization detector (FID), as well as a Standard Research Systems (SRS) quadrupole mass spectrometer, following previously reported methods (Moore et al., **2018**; Whyte et al., **2021**). Average analytical uncertainties for these components are based on repeated measurements of natural gas reference materials from DCG and Praxair, as well as a cross-calibrated atmospheric air reference material (i.e., Lake Erie air, Ohio air). Long-run uncertainties are as follows: N_2 (± 2.03%), CO_2 (± 2.06%), Ar (± 2.01%), CH_4 (± 2.26%), C_2H_6 (± 2.05%), C_3H_8 (± 0.36%), i-C_4H_{10} (± 0.13%), n-C_4H_{10} (± 0.15%), i-C_5H_{12} (± 0.21%), and n-C_5H_{12} (± 0.24%). The method detection limits are typically as follows: CH_4 (3.5×10^{-6} ccSTP/cc or 3.5 ppmv), C_2H_6 (1.05×10^{-6} ccSTP/cc), C_3H_8 (7.34×10^{-7} ccSTP/cc), i-C_4H_{10} (4.01×10^{-7} ccSTP/cc), n-C_4H_{10} (5.27×10^{-7} ccSTP/cc), i-C_5H_{12} (7.12×10^{-7} ccSTP/cc), and n-C_5H_{12} (4.14×10^{-7} ccSTP/cc), N_2 (8.6×10^{-3} ccSTP/cc), and CO_2 (2.1×10^{-4} ccSTP/cc).

https://doi.org/10.5281/zenodo.13971228

Sedimentary geochemistry

During UT-GOM2-2 shipboard operations on the Q4000, IWR and IWO sections were collected adjacent to each other for pore water geochemistry (see Pore water geochemistry). Squeeze cakes from the IWR set were subdivided and a portion from the p-Mag sample was used for sediment geochemistry (see Pore water geochemistry). These squeeze cake samples represent 10-25 cm of stratigraphic thickness (depending on the length of the IWR section) and are thus considered an average value across that interval. A subsample of each squeeze cake was subsampled for carbon, nitrogen, and sulfur (CNS) elemental analysis. Approximately 5 g of material was transferred to a vial, dried at 40 °C for two days, and crushed using an agate mortar and pestle.

Bulk sediment total carbon (TC), total nitrogen (TN), total sulfur (TS), and carbonate free total organic carbon (TOC) were measured at the University of New Hampshire using an Elementar Unicube CHNS elemental analyzer. Bulk sediment total inorganic carbon (TIC) was calculated by difference where TIC (total inorganic carbon) = TC-TOC. The weight percent of calcium carbonate ($CaCO_3$) was calculated by multiplying the TIC weight percentages (TIC = TC-TOC) by 8.33 to account for the non-carbon mass fraction. Bulk sediment samples were dried, powdered, and weighed (10 mg) into tin capsules. Prior to TOC analysis, inorganic carbon (IC) was dissolved using 6% sulfurous acid applied to weighed samples in amounts and steps optimized for carbonate-rich sediments (Phillips et al., **2011**). A total of 780 µL of 6% sulfurous acid was added to each 10 mg powdered, dry, sediment sample used for TOC analysis. The calculated bulk $CaCO_3$ fraction represents biogenic, authigenic, and any detrital carbonate phases. In addition to instrument standards and blanks, Elemental Microanalysis Soil Standard (peaty) TC 0.83 (B2180), Soil Standard (silty) TC 2.19 (B2182), and Soil Standard (chalky) TC 5.39 (B2188) were analyzed as unknowns and used to assess analytical precision and accuracy. Average values of carbon and nitrogen agree within the uncertainty of the certified values. Atomic TOC/TN ratios were calculated as (TOC/12.011)/(TN/14.007) using the TN from the bulk sediment (non-acidified) sample runs.

The Elementar Unicube CHNS has both a thermal conductivity detector and an infrared (IR) sensor available for sulfur measurements. The IR sensor is optimized to measure samples with very low TS content (<0.5 wt.%). All TS measurements presented in this work are from the IR sensor. Elementar's sulfanilic acid standard (18.5 wt.% S) was used to calculate a daily factor and to condition the instrument, followed by three soil standards – Elemental Microanalysis Soil Standard (chalky) TC 5.39 (B2188), Elemental Microanalysis Soil Standard (silty) TC 2.19 (B2182), and Elementar Soil Standard Ah (0.052 wt.% S). Replicates of every tenth sample run were used to confirm sample reproducibility. The reproducibility error was established by analyzing the measurements of the replicates and calculating the standard deviation.

Data storage

All raw and processed data from the expedition is stored in a web accessible data directory. Data files can be found in the data directory. All data plots in this and other reports reference the file(s) containing the data shown. Specific data set locations are also referenced in the text.

https://doi.org/10.5281/zenodo.13971228

References

Apprill, A., McNally, S., Parsons, R., and Weber, L., 2015, Minor revision to V4 region SSU rRNA 806R gene primer greatly increases detection of SAR11 bacterioplankton: Aquatic Microbial Ecology, v. 75, no. 2, p. 129-137, https://doi.org/10.3354/ame01753.

ASTM International, 2005, ASTM D2216-05: Standard Test Methods for Laboratory Determination of Water (Moisture) Content of Soil and Rock by Mass, Annual Book of ASTM Standards, https://doi.org/10.1520/D2216-05.

ASTM International, 2008a, ASTM D5550-14: Standard Test Method for Specific Gravity of Soil Solids by Gas Pycnometer, Annual Book of ASTM Standards, Volume 04.08, https://doi.org/10.1520/D5550-14.

ASTM International, 2008b, ASTM D5334-08: Standard Test Method for Determination of Thermal Conductivity of Soil and Soft Rock by Thermal Needle Probe Procedure, Annual Book of ASTM Standards, Volume 04.08, https://doi.org/10.1520/D5334-08.

ASTM International, 2008c, ASTM D4648/D4648M-16: Standard Test Methods for Laboratory Miniature Vane Shear Test for Saturated Fine-Grained Clayey Soil, Annual Book of ASTM Standards, Volume 04.08: West Conshohocken, PA, American Society for Testing and Materials, https://doi.org/10.1520/D4648_D4648M-16.

ASTM International, 2008d, ASTM D854-23: Standard Test Methods for Specific Gravity of Soil Solids by the Water Displacement Method, Annual Book of ASTM Standards, Volume 04.08, https://doi.org/10.1520/D0854-23.

ASTM International, 2008e, ASTM D0422-63R07: Standard test method for particle-size analysis of soils, Annual Book of ASTM Standards, Volume 04.08: West Conshohocken, PA, American Society for Testing and Materials, p. 10-17, https://doi.org/10.1520/D0422-63R07.

ASTM International, 2009a, ASTM D7928-21e1: Standard Test Method for Particle-Size Distribution (Gradation) of Fine-Grained Soils Using the Sedimentation (Hydrometer) Analysis, Annual Book of ASTM Standards, Volume 04.09, https://doi.org/10.1520/D7928-21E01.

ASTM International, 2009b, ASTM D7263-21: Standard Test Methods for Laboratory Determination of Density and Unit Weight of Soil Specimens, Annual Book of ASTM Standards, Volume 04.09, https://doi.org/10.1520/D7263-21.

ASTM International, 2017, ASTM D2487-17e1: Standard Practice for Classification of Soils for Engineering Purposes (Unified Soil Classification System): Annual Book of ASTM Standards, https://doi.org/10.1520/D2487-17E01.

ASTM International, 2018, ASTM D8121/D8121M–19: Standard Test Method for Approximating the Shear Strength of Cohesive Soils by the Handheld Vane Shear Device: Annual Book of ASTM Standards, v. 04.09, https://doi.org/10.1520/D8121_D8121M-19.

Blum, P., 1997, Physical Properties Handbook: A guide to the shipboard measurement of physical properties of deep-sea cores, https://doi.org/10.2973/odp.tn.26.1997.

Brooks, R. A., and Di Chiro, G., 1976, Principles of computer assisted tomography (CAT) in radiographic and radioisotopic imaging: Phys Med Biol, v. 21, no. 5, p. 689-732, https://doi.org/10.1088/0031-9155/21/5/001.

Bullard, E. C., 1954, The flow of heat through the floor of the Atlantic Ocean: Proc. R. Soc. London, Ser. A, v. 222, p. 408-429, https://doi.org/10.1098/rspa.1954.0085.

Caporaso, J. G., Lauber, C. L., Costello, E. K., Berg-Lyons, D., Gonzalez, A., Stombaugh, J., Knights, D., Gajer, P., Ravel, J., Fierer, N., Gordon, J. I., and Knight, R., 2011, Moving pictures of the human microbiome: Genome Biol, v. 12, no. 5, p. R50, https://doi.org/10.1186/gb-2011-12-5-r50.

Circone, S., Kirby, S. H., and Stern, L. A., 2005, Direct Measurement of Methane Hydrate Composition along the Hydrate Equilibrium Boundary: The Journal of Physical Chemistry B, v. 109, no. 19, p. 9468-9475, https://doi.org/10.1021/jp0504874.

Cnudde, V., Cnudde, J. P., Dupuis, C., and Jacobs, P. J. S., 2004, X-ray micro-CT used for the localization of water repellents and consolidants inside natural building stones: Materials Characterization, v. 53, no. 2-4, p. 259-271, https://doi.org/10.1016/j.matchar.2004.08.011.

Cnudde, V., and Boone, M. N., 2013, High-resolution X-ray computed tomography in geosciences: A review of the current technology and applications: Earth-Science Reviews, v. 123, p. 1-17, https://doi.org/10.1016/j.earscirev.2013.04.003.

Constans, R. E., and Parker, M. E., 1986, Calcareous nannofossil biostratigraphy and paleoclimatic indices for the late Quaternary, Deep Sea Drilling Project, Leg 96, Gulf of Mexico, Initial Reports of the Deep Sea Drilling Project, 96, p. 601–630, https://doi.org/10.2973/dsdp.proc.96.132.1986.

Davis, E. E., Villinger, H., Macdonald, R. D., Meldrum, R. D., and Grigel, J., 1997, A robust rapid-response probe for measuring bottom-hole temperatures in deep-ocean boreholes: Marine Geophysical Researches, v. 19, p. 267-281, https://doi.org/10.1023/A:1004292930361.

Dearing, J. A., Dann, R. J. L., Hay, K., Lees, J. A., Loveland, P. J., Maher, B. A., and O'Grady, K., 1996, Frequency-dependent susceptibility measurements of environmental materials:

Geophysical Journal International, v. 124, no. 1, p. 228-240, https://doi.org/10.1111/j.1365-246X.1996.tb06366.x.

Di Stefano, C., Ferro, V., and Mirabile, S., 2010, Comparison between grain-size analyses using laser diffraction and sedimentation methods: Biosystems Engineering, v. 106, no. 2, p. 205-215, https://doi.org/10.1016/j.biosystemseng.2010.03.013.

Dickens, G. R., Wallace, P. J., Paull, C. K., and Borowski, W. S., 2000, Detection of methane gas hydrate in the pressure core sampler (PCS): volume-pressure-time relations during controlled degassing experiments: Proceedings of the Ocean Drilling Program Scientific Results, v. 164, p. 113-117, https://doi.org/10.2973/odp.proc.sr.164.210.2000.

Droser, M. L., and Bottjer, D. J., 1991, Trace fossils and ichnofabric in Leg 119 cores, in Barron, J., Larsen, B., and al., e., eds., Proceedings of the Ocean Drilling Program, Science Results, Volume 119: College Station, TX, Ocean Drilling Program, p. 635-641, https://doi.org/doi:10.2973/odp.proc.sr.119.206.1991.

Expedition 311 Scientists, 2006, Site U1328, in Riedel, M., Collett, T. S., Malone, M. J., and Expedition 311 Scientists, eds., Proceedings of the Integrated Ocean Drilling Program, Volume 311: Washington, DC (Integrated Ocean Drilling Program Management International, Inc.), https://doi.org/10.2204/iodp.proc.311.106.2006.

Ferro, V., and Mirabile, S., 2009, Comparing Particle Size Distribution Analysis by Sedimentation and Laser Diffraction Method: Journal of Agricultural Engineering, v. 40, no. 2, https://doi.org/10.4081/jae.2009.2.35.

Flemings, P. B., Long, H., Dugan, B., Germaine, J. T., John, C. M., Behrmann, J. H., Sawyer, D., and IODP Expedition 308 Scientists, 2008a, Pore pressure penetrometers document high overpressure near the seafloor where multiple submarine landslides have occurred on the continental slope, offshore Louisiana, Gulf of Mexico: Earth and Planetary Science Letters, v. 269, no. 3–4, p. 309-325, https://doi.org/10.1016/j.epsl.2007.12.005.

Flemings, P. B., Long, H., Dugan, B., Germaine, J., John, C. M., Behrmann, J. H., and Sawyer, D., 2008b, Erratum to "Pore pressure penetrometers document high overpressure near the seafloor where multiple submarine landslides have occurred on the continental slope, offshore Louisiana, Gulf of Mexico" [Earth and Planetary Science Letters 269/3-4 (2008) 309-32]: Earth and Planetary Science Letters, v. 274, no. 1-2, p. 269-283, https://doi.org/10.1016/j.epsl.2008.06.027.

Flemings, P. B., Polito, P. J., Pettigrew, T. L., Iturrino, G. J., Meissner, E., Aduddell, R., Brooks, D., Hetmaniak, C., Huey, D., Germaine, J. T., and IODP Expedition 342 Scientists, 2013, The Motion Decoupled Delivery System: A new deployment system for downhole tools is tested at Site U1402, New Jersey Margin: Scientific Drilling, v. 15, https://doi.org/10.2204/iodp.sd.15.07.2013.

Flemings, P. B., Thomas, C., Collett, T. S., Colwell, F., Cook, A. E., Germaine, J., Holland, M., Houghton, J., Johnson, J. E., Malinverno, A., Meazell, K., Pettigrew, T., Phillips, S. C., Portnov, A., Price, A., Santra, M., Schultheiss, P., Solomon, E., and You, K., 2023a, UT-GOM2-2 Prospectus: Science and Sample Distribution Plan, https://doi.org/10.5281/zenodo.13694088.

Flemings, P. B., Cook, A. E., Houghton, J., Morrison, J., Portnov, A., Pettigrew, T., Phillips, S. C., Polito, P., Santra, M., and Thomas, C., 2023b, UT-GOM2-2 Operations Plan, https://ig.utexas.edu/wp-content/uploads/2023/06/OperationsPlan_Rev2.3.pdf.

Flemings, P. B., Thomas, C., Phillips, S. C., Collett, T. S., Cook, A. E., Solomon, E., Colwell, F. S., Johnson, J. E., Awwiller, D., Aylward, I., Bhandari, A. R., Brooks, D., Cardona, A., Casso, M., Coyte, R., Darrah, T., Davis, M., Dugan, B., Duncan, D., Germaine, J. T., Holland, M., Houghton, J., Mills, N. T., Mimitz, M., Minarich, D., Morono, Y., Murphy, Z., O'Connell, J., Petrou, E., Pettigrew, T., Pohlman, J. W., Portnov, A., Phillips, M. P., Redd, T., Sawyer, D. E., Schultheiss, P., Shannon, K., Sullivan, C., Small, C., Tozier, K., Tsang, M.-Y., Maal, C. V. D., Waite, W. F., and Walton, T., 2024, UT-GOM2-2 Preliminary Report Terrebonne Basin Northern Gulf of Mexico, University of Texas Institute for Geophysics, https://doi.org/10.5281/zenodo.13648253.

Flemings, P. B., Thomas, C., Phillips, S. C., Collett, T. S., Cook, A. E., Solomon, E., Colwell, F. S., Johnson, J. E., Awwiller, D., Aylward, I., Bhandari, A. R., Brooks, D., Buser-Young, J. Z., Cardona, A., Casso, M., Coyte, R., Darrah, T., Davis, M., Dugan, B., Duncan, D., Germaine, J. T., Holland, M., Houghton, J., Martin, S., Mills, N. T., Mimitz, M., Minarich, D., Morono, Y., Murphy, Z., O'Connell, J., Petrou, E., Pettigrew, T., Pohlman, J. W., Portnov, A., Phillips, M. P., Redd, T., Sawyer, D. E., Schultheiss, P., Shannon, K., Sullivan, C., Small, C., Tozier, K., Tsang, M.-Y., Maal, C. V. D., Waite, W. F., and Walton, T., 2025a, Expedition UT-GOM2-2 Summary, in Flemings, P. B., ed., Proceedings of the Deepwater Hydrate Coring Expedition UT-GOM2-2: The University of Texas at Austin, University of Texas Institute for Geophysics, https://doi.org/10.5281/zenodo.13971076.

Flemings, P. B., Thomas, C., Phillips, S. C., Collett, T. S., Cook, A. E., Solomon, E., Colwell, F. S., Johnson, J. E., Awwiller, D., Aylward, I., Bhandari, A. R., Brooks, D., Buser-Young, J. Z., Cardona, A., Casso, M., Coyte, R., Darrah, T., Davis, M., Dugan, B., Duncan, D., Germaine, J. T., Holland, M., Houghton, J., Martin, S., Mills, N. T., Mimitz, M., Minarich, D., Morono, Y., Murphy, Z., O'Connell, J., Petrou, E., Pettigrew, T., Pohlman, J. W., Portnov, A., Phillips, M. P., Redd, T., Sawyer, D. E., Schultheiss, P., Shannon, K., Sullivan, C., Small, C., Tozier,

K., Tsang, M.-Y., Maal, C. V. D., Waite, W. F., and Walton, T., 2025b, Expedition UT-GOM2-2 Site H, in Flemings, P. B., ed., Proceedings of the Deepwater Hydrate Coring Expedition UT-GOM2-2: The University of Texas as Austin, University of Texas Institute for Geophysics, https://doi.org/10.5281/zenodo.13971276.

Geotek Ltd., 2023, Laminography Imaging, https://www.geotek.co.uk/x-ray-ct-system/laminography/.

Germaine, J. T., and Germaine, A. V., 2009, Geotechnical Laboratory Measurements for Engineers, John Wiley & Sons, https://doi.org/10.1002/9780470548790.

Gieskes, J. M., Gamo, T., and Brumsack, H., 1991, Technical Note 15: Chemical Methods for Interstitial Water Analysis aboard JOIDES Resolution, https://doi.org/10.2973/odp.tn.15.1991.

Gill, A. E., 1982, Atmosphere—Ocean Dynamics, New York, NY, Academic Press, International Geophysics, https://www.sciencedirect.com/bookseries/international-geophysics/vol/30/suppl/C.

Gradstein, F. M., Ogg, J. G., Schmitz, M. D., and Ogg, G. M., 2012, Geologic Time Scale 2012 -- 2 volume book, https://www.sciencedirect.com/book/9780444594259/the-geologic-time-scale.

Gradstein, F. M., Ogg, J. G., Schmitz, M. D., and Ogg, G. M., 2020, Geologic Time Scale 2020, https://doi.org/10.1016/C2020-1-02369-3.

Hansbo, S., A New approach to the determination of the shear strength of clay by the fall-cone test, Stockholm, Royal Swedish Geotechnical Institute, p. 47.

Heesemann, M., Villinger, H., Fisher, A. T., Tréhu, A. M., and White, S., 2006, Data report: testing and deployment of the new APCT-3 tool to determine in situ temperatures while piston coring: Integrated Ocean Drilling Program Management International, Inc., https://doi.org/10.2204/iodp.proc.311.108.2006.

Hunt, C. P., Moskowitz, B. M., and Banerjee, S. K., 1995, Magnetic Properties of Rocks and Minerals, in Ahrens, T. J., ed., Rock Physics & Phase Relations: A Handbook of Physical Constants, Volume 3, AGU, https://doi.org/10.1029/RF003p0189.

IODP Depth Scale Task Force, 2011, IODP Depth Scale Terminology, https://www.iodp.org/policies-and-guidelines/142-iodp-depth-scales-terminology-april-2011/file.

Jackson, P. D., Lovell, M. A., Roberts, J. A., Schultheiss, P. J., Gunn, D., Flint, R. C., Wood, A., Holmes, R., and Frederichs, T., 2006, Rapid non-contacting resistivity logging of core, in Rothwell, R. G., and Rack, F. R., eds., New techniques in sediment core analysis: an introduction, Geological Society of London, p. 209-217, https://doi.org/10.1144/GSL.SP.2006.267.01.01.

Jacobsen, C. S., Nielsen, T. K., Vester, J. K., Stougaard, P., Nielsen, J. L., Voriskova, J., Winding, A., Baldrian, P., Liu, B., Frostegard, A., Pedersen, D., Tveit, A. T., Svenning, M. M., Tebbe, C. C., Ovreas, L., Jakobsen, P. B., Blazewicz, S. J., Hubablek, V., Bertilsson, S., Hansen, L. H., Cary, S. C., Holben, W. E., Ekelund, F., and Baelum, J., 2018, Inter-laboratory testing of the effect of DNA blocking reagent G2 on DNA extraction from low-biomass clay samples: Sci Rep, v. 8, no. 1, p. 5711, https://doi.org/10.1038/s41598-018-24082-y.

Karlsson, R., Suggested improvements in the liquid limit test, with reference to flow properties of remoulded clays, in Proceedings 5th International Conference on Soil Mechanics and Foundation Engineering, Paris, France, International Society for Soil Mechanics and Geotechnical Engineering, p. 171–184, https://www.issmge.org/uploads/publications/1/40/1961_01_0029.pdf.

Kiefte, H., Clouter, M. J., and Gagnon, R. E., 2002, Determination of acoustic velocities of clathrate hydrates by Brillouin spectroscopy: The Journal of Physical Chemistry, v. 89, no. 14, p. 3103-3108, https://doi.org/10.1021/j100260a031.

Lane, E. W., 1947, Report of the Subcommittee on Sediment Terminology: Eos, Transactions American Geophysical Union, v. 28, no. 6, p. 936-938, https://doi.org/10.1029/TR028i006p00936.

Manheim, F. T., and Sayles, F. L., 1974, Composition and origin of interstitial waters of marine sediments, based on deep sea drill cores, in Goldberg, E. D., ed., Marine Geochemistry: New York, Wiley, p. 527–568, https://doi.org/10.1146/annurev.pc.12.100161.000333.

Marchitto, T. M., and Wei, K.-Y., 1995, History of Laurentide meltwater flow to the Gulf of Mexico during the last deglaciation, as revealed by reworked calcareous nannofossils: Geology, v. 23, no. 9, p. 779–782, https://doi.org/10.1130/0091-7613(1995)023%3C0779:HOLMFT%3E2.3.CO;2.

Mazzullo, J. M., Meyer, A., and Kidd, R. B., 1988, New sediment classification scheme for the Ocean Drilling Program, Handbook for shipboard sedimentologists, Technical Note No. 8, p. 45–67, https://doi.org/10.2973/odp.tn.8.1988.

McKee, E. D., and Weir, G. W., 1953, Terminology for Stratification and Cross-Stratification in Sedimentary Rocks: Geological Society of America Bulletin, v. 64, no. 4, https://doi.org/10.1130/0016-7606(1953)64[381:Tfsaci]2.0.Co;2.

McKetty, M. H., 1998, The AAPM/RSNA physics tutorial for residents. X-ray attenuation: Radiographics, v. 18,

no. 1, p. 151-163; quiz 149, https://doi.org/10.1148/radiographics.18.1.9460114.

Moore, M. T., Vinson, D. S., Whyte, C. J., Eymold, W. K., Walsh, T. B., and Darrah, T. H., 2018, Differentiating between biogenic and thermogenic sources of natural gas in coalbed methane reservoirs from the Illinois Basin using noble gas and hydrocarbon geochemistry: Geological Society, London, Special Publications, v. 468, no. 1, p. 151-188, https://doi.org/10.1144/sp468.8.

Moore, M. T., Phillips, S. C., Cook, A. E., and Darrah, T. H., 2020, Improved sampling technique to collect natural gas from hydrate-bearing pressure cores: Applied Geochemistry, v. 122, https://doi.org/10.1016/j.apgeochem.2020.104773.

Munsell Color Company, I., 1994, Munsell Soil Color Chart (revised edition).

NGHP Expedition 01 Scientists, 2007, Sites NGHP-01-10, 12, and 13, in Collett, T. S., Reidel, M., Cochran, J., Boswell, R., Presley, J., Kumar, P., Sathe, A., Sethi, A., Lall, M., and the NGHP Expedition 01 Scientists, eds., National Gas Hydrate Program Expedition 01 Initial Reports, Directorate General of Hydrocarbon, Ministry of Petroleum and Natural Gas (India), p. 150, https://doi.org/10.3133/sir20125054.

Phillips, S. C., Johnson, J. E., Miranda, E., and Disenhof, C., 2011, Improving CHN measurements in carbonate-rich marine sediments: Limnology and Oceanography: Methods, v. 9, no. 5, p. 194-203, https://doi.org/10.4319/lom.2011.9.194.

Pohlman, J. W., Casso, M., Magen, C., and Bergeron, E., 2021, Discrete Sample Introduction Module for Quantitative and Isotopic Analysis of Methane and Other Gases by Cavity Ring-Down Spectroscopy: Environ Sci Technol, v. 55, no. 17, p. 12066-12074, https://doi.org/10.1021/acs.est.1c01386.

Purkey, M., 2020, Data Report: UT-GOM2-1 Biostratigraphy Report Green Canyon Block 955, Gulf of Mexico, in Flemings, P. B., Phillips, S. C., Collett, T. S., Cook, A. E., and Boswell, R., eds., Proceedings of the UT-GOM2-1 Hydrate Pressure Coring Expedition: Austin, TX, University of Texas Institute for Geophysics, https://doi.org/10.2172/1823039.

Rothwell, R. G., 1989, Minerals and Mineraloids in Marine Sediments, Springer Dordrecht, 282 p, https://doi.org/10.1007/978-94-009-1133-8.

Schrader, C., Schielke, A., Ellerbroek, L., and Johne, R., 2012, PCR inhibitors - occurrence, properties and removal: J Appl Microbiol, v. 113, no. 5, p. 1014-1026, https://doi.org/10.1111/j.1365-2672.2012.05384.x.

Schultheiss, P., Roberts, J., Druce, M., Priest, J. A., Holland, M., Yamamoto, K., and Yang, S., 2014, PCATS and PCATS Triaxial: Further Development and Recent Field Experience Making Core Measurements Under Pressure, in Proceedings Proceedings of the 8th International Conference on Gas Hydrates, Beijing, China, July 29-Aug 2, 2014, p. 10.

Schultheiss, P. J., Holland, M., Roberts, J., Huggett, Q., Druce, M., and Fox, P., 2011, PCATS: Pressure Core Analysis and Transfer System, in Proceedings 7th International Conference on Gas Hydrates, Edinburgh, Scotland, United Kingdom, July 17- 21, 2011, p. 10.

Shepard, F. P., 1954, Nomenclature based on sand-silt-clay ratios: Journal of Sedimentary Petrology, v. Vol. 24, p. 151-158, https://doi.org/10.1306/D4269774-2B26-11D7-8648000102C1865D.

Shipboard Scientific Party, 2003, Site 1249, in Trehu, A. M., Bohrmann, G., Rack, F. R., Torres, M. E., and et al., eds., Proceedings of the Ocean Drilling Program, Initial Reports, Volume 204: College Station, Ocean Drilling Program, https://doi.org/doi:10.2973/odp.proc.ir.204.108.2003.

Shiraishi, F., Mitsunobu, S., Suzuki, K., Hoshino, T., Morono, Y., and Inagaki, F., 2016, Dense microbial community on a ferromanganese nodule from the ultra-oligotrophic South Pacific Gyre: Implications for biogeochemical cycles: Earth and Planetary Science Letters, v. 447, p. 10-20, https://doi.org/10.1016/j.epsl.2016.04.021.

Sloan, E. D., 1998, Clathrate Hydrates of Natural Gases, Third Edition, New York, NY, Marcel Dekker, http://books.google.com/books?id=T7LC8ldaVR4C.

Strasser, M., Ikehara, K., Everest, J., and Expedition 386 Scientists, 2023, Expedition 386 Methods: Proceedings of the International Ocean Discovery Program, v. Volume 386, https://doi.org/10.14379/iodp.proc.386.102.2023.

Styzen, M. J., 1997, Cascading Counts of Nannofossil Abundance: Journal of Nannoplankton Research, v. 19, no. 1, p. 49, https://doi.org/10.58998/jnr2235.

Sylvan, J. B., Estes, E. R., Bogus, K., Colwell, E. S., Orcutt, B. N., and Smith, D. C., 2021, IODP Technical Note 4: Recommendations for microbiological sampling and contamination tracer use aboard the JOIDES Resolution following 20 years of IODP deep biosphere research, https://doi.org/10.14379/iodp.tn.4.2021.

Thomas, C., Phillips, S. C., Flemings, P. B., Santra, M., Hammon, H., Collett, T. S., Cook, A. E., Pettigrew, T., Mimitz, M., Holland, M., and Schultheiss, P., 2020, Pressure coring operations during The University of Texas-Gulf of Mexico 2-1 (UT-GOM2-1) Hydrate Pressure Coring Expedition in Green Canyon Block 955, northern Gulf of Mexico: AAPG Bulletin, v. 104, no. 9, p. 1877-1901, https://doi.org/10.1306/02262019036.

Tishchenko, P., Hensen, C., Wallmann, K., and Wong, C. S., 2005, Calculation of the stability and solubility of methane hydrate

in seawater: Chemical Geology, v. 219, no. 1-4, p. 37-52, https://doi.org/10.1016/j.chemgeo.2005.02.008.

Von Herzen, R. P., and Maxwell, A. E., 1959, The measurement of thermal conductivity of deep-sea sediments by a needle probe method: Journal of Geophysical Research, v. 64, p. 1557-1563, https://doi.org/10.1029/JZ064i010p01557.

Waterman, A. S., Weber, R. D., Lu, Y., Smith, V. E., George, R. A., Reilly, T. M., Roederer, R. V., Edmunds, J. A., Parker, B. W., Myers, N. R., and Avery, A. J., 2017, Biostratigraphic Chart - Gulf Basin, USA, Quaternary and Neogene: Paleo-Data, Inc., https://www.paleodata.com/chart/.

Wen, B., Aydin, A., and Duzgoren-Aydin, N. S., 2002, A comparative study of particle size analyses by sieve-hydrometer and laser diffraction methods: Geotechnical Testing Journal, v. 25, no. 4, https://doi.org/10.1520/GTJ11289J.

Wentworth, C. K., 1922, A scale of grade and class terms of clastic sediments: Journal of Geology, v. 30, p. 377-392.

Whittle, A. J., Sutabutr, T., Berg, C. F., Haley, A. V., and Aldrich Inc., 2001, Prediction and Measurement of Pore Pressure Dissipation for a Tapered Piezoprobe, Offshore Technology Conference: Houston, Texas, p. 7, https://doi.org/10.4043/13155-MS.

Whyte, C. J., Vengosh, A., Warner, N. R., Jackson, R. B., Muehlenbachs, K., Schwartz, F. W., and Darrah, T. H., 2021, Geochemical evidence for fugitive gas contamination and associated water quality changes in drinking-water wells from Parker County, Texas: Sci Total Environ, v. 780, p. 146555, https://doi.org/10.1016/j.scitotenv.2021.146555.

Wood, D. M., 1985, Some fall-cone tests: Géotechnique, v. 35, no. 1, p. 64-68, https://doi.org/10.1680/geot.1985.35.1.64.

Worm, H. U., and Jackson, M., 1999, The superparamagnetism of Yucca Mountain Tuff: Journal of Geophysical Research: Solid Earth, v. 104, no. B11, p. 25415-25425, https://doi.org/10.1029/1999JB900285.

Zreik, D. A., Ladd, C. C., and Germaine, J. T., 1995, A New Fall Cone Device for Measuring the Undrained Strength of Very Weak Cohesive Soils: Geotechnical Testing Journal, v. 18, no. 4, p. 472-482, https://doi.org/10.1520/GTJ11022J.

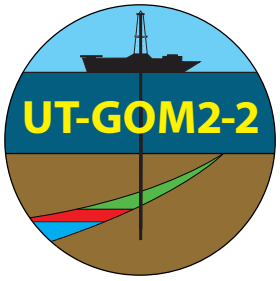

Expedition UT-GOM2-2 Methods

Proceedings of the UT-GOM2-2 Deepwater Hydrate Coring Expedition

Terrebonne Basin (Walker Ridge Block 313)

WR313 H002 (API 608124014800) and WR313 H003 (API 608124014900)

July 30–September 28, 2023 | Expedition UT-GOM2-2 Scientists

University of Texas Institute for Geophysics | 2025

https://doi.org/10.5281/zenodo.13971228